Lawrence Berkeley Laboratory
UNIVERSITY OF CALIFORNIA

EARTH SCIENCES DIVISION

Characterization of Leaky Faults

C. Shan
(Ph.D. Thesis)

May 1990

Prepared for the U.S. Department of Energy under Contract Number DE-AC03-76SF00098.

DISCLAIMER

LBL-29235

Characterization of Leaky Faults

Chao Shan

(Ph.D. Thesis)

Department of Materials Science and Mineral Engineering
University of California

and

Earth Sciences Division
Lawrence Berkeley Laboratory
University of California
Berkeley, California 94720

May 1990

This work was supported by the Director, Office of Civilian Radioactive Waste Management, Office of Facilities Siting and Development, Siting and Facilities Technology Division, of the U.S. Department of Energy under Contract No. DE-AC03-76SF00098.

CHARACTERIZATION OF LEAKY FAULTS

Chao Shan

Department of Materials Science and Mineral Engineering
University of California, Berkeley
Berkeley, California 94720

ABSTRACT

Leaky faults provide a flow path for fluids to move underground. It is very important to characterize such faults in various engineering projects. The purpose of this work is to develop mathematical solutions for this characterization. The flow of water in an aquifer-fault-aquifer system and the flow of air in the unsaturated fault-rock system were studied.

If the leaky fault cuts through two aquifers, characterization of the fault can be achieved by pumping water from one of the aquifers, which are assumed to be horizontal and of uniform thickness. Analytical solutions have been developed for two cases of either a negligibly small or a significantly large drawdown in the unpumped aquifer. Some practical methods for using these solutions are presented.

If one is interested in characterization of a fault in the unsaturated zone, measurement of air pressure changes in this zone could provide a means to achieve such a task. By assuming that the water phase is immobile, it has been possible to develop analytical solutions for the effects of transient air pressures in the fault on pressures in the adjacent rock. One set of solutions assumes that the fault/rock system is infinitely deep, and another set of solutions assumes that the unsaturated zone has closed boundary at the water table. For each set of solutions, two different boundary conditions were used at the land surface: a step function change in the atmospheric pressure and a

sinusoidal variation in pressure. In developing these solutions, it was assumed that the transient behavior is one-dimensional in the leaky fault and two-dimensional in the surrounding rocks. Once the flow parameters of the surrounding rocks are known, these solutions can be used to determine the parameters of the leaky fault.

Numerical verification of these analytical solutions was obtained using the well-known computer program, TRUMP. There was an excellent agreement between the results. The TRUMP code was then used to extend this approach to a multi-layered unsaturated zone, and examples of the application to the Ghost Dance and Solitario Canyon faults at Yucca Mountain were investigated.

P. A. Witherspoon

Thesis Committee Chairman

Table of Contents

List of Figures

List of Tables

Notation

(*I*) *CHAPTER* 2

Symbol	Description	Dimension
A	introduced parameter, equal to $\sqrt{p/\alpha_a + \rho^2}$	L^{-1}
a	distance from the pumping well to the fault	L
a_D	dimensionless distance, equal to a/r	
a, b	x, y coordinates of the pumping well	L
c	modified transmissivity ratio, equal to $\frac{1}{2L}\cdot\frac{T_f}{T_a}$	L^{-1}
c'	parameter, $c' = c\cdot(\frac{1}{T_D}+1)$	L^{-1}
c_D	dimensionless c, equal to $c\cdot r$	
$\overline{d}$	dimensionless parameter, equal to $a_D - 1/2$	
$\overline{d'}$	dimensionless parameter, equal to $a_D + 1/2$	
$\overline{d_1}, \overline{d_2}$	dimensionless parameters	
$-Ei(-u)$	exponential integral, equal to $\int_u^\infty \frac{e^{-x}}{x}dx$	
$erf(x)$	error function, equal to $\frac{2}{\sqrt{\pi}}\int_0^x e^{-t^2}dt$	
$erfc(x)$	complementary error function, equal to $1-erf(x)$	
H	thickness	L
K	hydraulic conductivity	L/T

k	dimensionless parameter, defined by $1/T_D + 1$	
L	length of flow path in the fault	L
p	transform variable in Laplace domain	T^{-1}
Q	volumetric pumping rate	L^3/T
Q_r	overall recharge rate from the fault to the aquifer	L^3/T
$\overline{Q_r}$	dimensionless overall recharge rate, equal to Q_r/Q	
q_r	recharge flux from the fault to the aquifer	L^2/T
r	distance from the observation well to the pumping well	L
S_s	specific storage	L^{-1}
s	drawdown of hydraulic head	L
s_D	dimensionless drawdown, defined as $s/(\frac{Q}{4\pi T_a})$	
s_F	dimensionless drawdown component due to fault recharge	
s_{F_1}	s_F at Point #1	
s_T	dimensionless drawdown component of Theis solution	
T	transmissivity, defined as $K \cdot H$	L^2/T
T_D	aquifers' transmissivity ratio, equals to T_u/T_a	
t	time	T
t_D	dimensionless time, defined as $\frac{\alpha t}{r^2}$	
u	parameter, equal to $\overline{d}^2/t_D$, dimensionless	
v	s after Laplace transform	

w	v after exponential Fourier transform	
x, y, z	three dimensional Cartesian coordinates	L
α	diffusivity, defined as K/S_s	L^2/T
$\delta(x)\cdot\delta(y)$	Dirac δ-function of second degree	
ρ	transform variable in the exponential Fourier domain	L^{-1}
θ	polar angle of the observation well, dimensionless	
τ	integral variable of t	T
τ_D	dimensionless τ	

Subscripts:

a	aquifer
f	fault
u	unpumped aquifer
1	variables in Region I (pumping-well side)
2	variables in Region II (the other side)

(*II*) *CHAPTER* 3

Symbol	Description	Dimension
b'	half width of the fault	L
B_1, B_2	parameters defined by (3-37) and (3-38), dimensionless	
d	a function of n, $d = d(n) = (n - \frac{1}{2})\frac{\pi}{h}$, dimensionless	
D_1, D_2, D_3	dimensionless parameters defined by (3-85)	
$erf(x)$	error function, equal to $\frac{2}{\sqrt{\pi}}\int_0^x e^{-t^2}dt$	
$erfc(x)$	complementary error function, equal to $1 - erf(x)$	
h'	thickness of rock layer	L
h	dimensionless thickness, $h = \frac{h'}{b'}$	
k_a	permeability to air	L^2
k	permeability ratio, $k = \frac{k_r}{k_f}$	
K_a	pneumatic conductivity, $K_a = \frac{k_a \rho_a g}{\mu_a}$	L/T
n	generalized finite Fourier transform variable, positive integer	
n_a	interconnected air filled porosity, dimensionless	
p	air pressure	F/L^2
$\bar{p}$	mean air pressure	F/L^2
p_0	initial air pressure	F/L^2

p_b	air pressure constant	F/L^2
s	transform variable in Laplace domain	
S_a	pneumatic specific storage, $S_a = \frac{n_a \rho_a g}{\bar{p}}$	L^{-1}
t'	time	T
t	dimensionless time, $t = \frac{\alpha'_f t'}{b'^2}$	
v	ϕ after Laplace transform	
w	v after Fourier transform	
x'	horizontal coordinate	L
x	dimensionless x', $x = \frac{x'}{b'}$	
z'	vertical coordinate	L
z	dimensionless z', $z = \frac{z'}{b'}$	
α'	diffusivity to air, $\alpha' = \frac{k_a \bar{p}}{n_a \mu_a}$	L^2/T
α	diffusivity ratio, $\alpha = \frac{\alpha'_r}{\alpha'_f}$	
β	ratio of dimensionless frequency and diffusivity ratio, $\beta = \omega/\alpha$	
ϕ'	square pressure, $\phi' = p^2$	F^2/L^4
ϕ	dimensionless ϕ', defined by either (3-12) or (3-73)	
μ_a	viscosity of air	$M/L/T$
ρ	variable of Fourier sine transform	

ρ_0	critical value of ρ	
ρ_a	density of air	M/L^3
ω'	frequency	T^{-1}
ω	dimensionless frequency, $\omega = \frac{b'^2}{\alpha_f'} \cdot \omega'$	
Δ	determinant, $\Delta = \frac{k^2}{\alpha} + 4(\alpha - 1)\rho^2$	
Δp	pressure increment at certain point	F/L^2
δ	pressure difference between two points	F/L^2

Subscripts:

f	fault
r	rock

Acknowledgements

My first and most sincere thanks go to Professor Paul A. Witherspoon, who has given me such a good opportunity of doing research in this respect. Any progress in my research is always related to his advice and encouragement. I am deeply grateful to Dr. Iraj Javandel for providing the interesting problem and for offering his invaluable advice. His support and friendship have greatly helped me working happily and efficiently. I would like to thank Professor Neville G. W. Cook and Professor Kent S. Udell for their critical review of this work. I would like to acknowledge the use of the atmospheric pressure data collected by the Sandia National Laboratory at the Yucca Mountain.

Most of my thanks owes to my dear brother and sister-in-law. They constantly attach great importance to my degree study and scientific research. My dear wife Xiaoxia, who has always been patient and understanding can undoubtly deserve my thanks and share the joy of the completion of the dissertation.

My beloved parents have provided me with their greatest love and support. I wish they are happy to know my success in heaven.

This work was supported by the Director, Office of Civilian Radioactive Waste Management, Office of Facilities Siting and Development, Siting and Facilities Technology Division of the U.S. Department of Energy under Contract No. DE-AC03-76SF00098.

CHAPTER 1

INTRODUCTION

1.1 Problems and Motivations

Faults are fractures along which significant movement has occurred. During this movement, the rocks adjacent to the fault are often pulverized or ground to bits forming a clayey, soft material called 'fault gouge'. In some instances the rocks in the fault zone may be broken and sheared, creating a 'fault-zone breccia'. Fault gouge is usually highly impermeable. On the contrary, the fault-zone breccia is highly permeable (Birkeland and Larson, 1978).

In geology, faults are classified into three categories according to the direction of movement: a normal fault, a reverse fault or a strike-slip fault. In groundwater hydrology and petroleum engineering, faults are classified into three categories according to their hydraulic response during a field pumping test: (1) tight faults ($K = 0$); (2) constant head faults ($K = \infty$); and (3) non-constant head leaky faults ($0 < K < \infty$); where K is the hydraulic conductivity of the fault (Witherspoon, et al., 1967). For purposes of simplification, faults in the third category will frequently be referred to as 'leaky faults' in this study.

Because a fault is a kind of discontinuity and inhomogeneity it can cause many unusual phenomena in nature. Research on faults is thus very important in various fields of engineering. From the point of view of rock mechanics and geotechnical engineering, the potential danger of faults is that two blocks of rock separated by a fault may slide on one another and thus cause an earthquake (Jaeger and Cook, 1979).

From the point of view of groundwater hydrology and petroleum engineering, the big differences in geometry and porous structure between faults and their surrounding rocks can strongly affect the underground fluid flow; the variation of fluid pressure in faults may in turn induce further tectonic movement along the fault surfaces.

For a very long time, deep well injection has been considered as a cheaper and safer way of managing waste liquid in industry. It is estimated that 423 million gal. (1.3 million m^3) of nonaqueous hazardous waste with about 10 billion gal. (38 million m^3) of water were injected through 181 wells in 1983 (U. S. Environmental Protection Agency, 1985). However, if there is a leaky fault nearby, the hazardous wastes can easily migrate up the fault to shallow aquifers, resulting in serious groundwater contamination.

It is well-known that storing natural gas in underground aquifers is an effective way to accommodate the great seasonal difference in natural gas consumption. A thorough geological investigation is very important before the construction of storage. If there is a leaky fault near the site, any leakage of natural gas through the fault can cause both financial loss and environmental pollution.

Since World War II, nuclear weapons have been developed to enhance military strength, and nuclear power plants have been utilized to generate electricity. However, the management of the large amount of high level radioactive waste is still a serious problem. Several ways have been proposed to solve this urgent problem. Among them, building huge repositories in the less permeable unsaturated zone in some arid region is thought to be a practical safe way. For example, Yucca Mountain in Nevada is being studied as a possible candidate for construction site in the United States. The

hydrogeological criterion for selecting the potential site is to guarantee the repository to be as dry as possible. Geological studies have revealed that there are some faults in Yucca Mountain. Obviously, it is very important to carefully study these faults before making the final decision. For every single fault, the question is not just simply 'is it leaky?' but 'how leaky it is?'.

Depending on the properties of local geologic materials, the amount of relative displacement of layers and the state of stress, a fault can provide a conductive pathway or it may be almost impermeable. The above examples show that the capability of locating and characterizing faults is very important for various engineering projects such as underground injection of hazardous liquids, underground storage of natural gas and radioactive waste isolation. A study on pressure variations in the fault zone could also be useful in earthquake research. It is therefore necessary and worthwhile to find some practical methods for characterizing leaky faults.

1.2 Previous Studies

The theoretical basis for study of the first two categories of faults (i.e. tight faults and constant head faults) has been available in the groundwater literature for over three decades. When a confined aquifer is bounded on one side by an impermeable boundary (a tight fault), it is conceivable that drawdowns near such a boundary due to pumping will be greater than those that would be predicted on the basis of the Theis equation for an aquifer of infinite areal extent. On the contrary, when a confined aquifer is bounded on one side by a constant-head boundary (a constant-head fault), drawdowns will be smaller due to the recharge from the boundary. In order to predict head drawdowns in such kind of systems, the method of images, which is widely

applied in heat-transfer theory, has been adapted in the field of groundwater hydrology (Ferris, et al., 1962). With this approach, the real bounded system is replaced by an imaginary system of infinite areal extent. In this imaginary system, the effect of the real boundary is identically given by an imaginary well located at an equal distance from the boundary. If the real well is a pumping well, the image well would pump (for tight faults) or inject (for constant-head faults) at the same rate as that of the real well. The solution for drawdowns in the real systems is simply the sum of two drawdown components due to the disturbance at the two wells in the imaginary system. Problems with parallel boundaries have also been discussed (Ferris, et al., 1962).

The similar problem has been studied in petroleum engineering for quite a long time. Among those researchers, it was Horner (1951) who first presented the idea of using the image solution to detect and locate a reservoir boundary. Dolan et al. (1957) applied this technique to drillstem tests. Davis and Hawkins (1963) derived a formula to determine the distance from the well to the fault using drawdown data. Some other studies were given to problems considering two parallel sealing faults around a well (Tiab and Kumar, 1980), a well between two sealing faults intersecting at any angle (Prasad, 1975), and the effect of reservoir anisotropy on fault detection (Overpeck and Holden, 1970).

There are serious limitations given by these previous studies. First, aside from predicting drawdowns, the solution can be used only for detecting and locating the linear boundary. Secondly, to use this solution, the linear boundary should be either absolutely impermeable or infinitely leaky. However, a natural fault can be neither absolutely impermeable nor infinitely leaky. On the contrary, it will have some finite

values of properties such as hydraulic conductivity (K) and specific storage (S_s). As a consequence, the solutions developed for such cases may not be applicable to the problems being investigated.

The effect of a non-constant head leaky fault was studied by Yaxley in 1987. Developed from the previous study of an aquifer with linear discontinuity (Bixel et al., 1963), Yaxley presented a mathematical model that described the effect of a partially communicating fault on transient pressure behavior. In that model, the two parts of the aquifer and the fault have different hydrologic properties in finite values. Analytical solution was obtained based on the assumption of a linear pressure distribution crossing the fault zone. The result can be used to determine the horizontal transmissivity of the fault section inside the aquifer. However, the fault zone is usually inhomogeneous and anisotropic. Its permeability in vertical direction is usually larger than that in horizontal direction. Therefore, it is still necessary to obtain new solutions for problems being investigated.

1.3 Objective and Approaches

As implied by the title of the thesis, the objective of this study is to find new methods of determining the hydrogeological properties of leaky faults in both saturated and partially saturated systems. Recalling that there are basicly two ways (i.e. the laboratory test and the pumping test) to determine the hydrogeological properties of an aquifer, it is conceivable that these methods can also be used to characterize the leaky faults. However, because the fault zone itself is highly heterogeneous, it is probably very difficult to determine the hydrogeologic properties of the fault zone by means of laboratory tests. From this point of view, it is extremely important for this problem to

develop methods based on field tests. Two different approaches will be considered in determining the hydrogeologic properties of the fault zone. A conventional pumping test will be employed for the characterization of leaky faults in saturated systems. For the vadose zone, the possibility of the application of transient responses of air pressure in the rocks due to barometric fluctuation will be investigated. Therefore, the study will contain two major parts, i.e., the flow of water in the confined-aquifer and the flow of air in the unsaturated zone.

In the first part, a pumping test is performed in a confined horizontal aquifer of uniform thickness, which is cut by a fault located at a distance from the pumping well. Both the aquifer and the fault are assumed to extend to infinity on the plan view. It is also assumed that there is no flow in the system initially. The aquifer is cut by the fault into two regions. In previous studies, one only needed to consider the draw-downs in the region of aquifer on the side where the water is pumped or injected, while for the other side, the head variation is absolutely zero. In the present study, we shall take both regions of the aquifer into consideration. This is because there is flow between the two regions of the aquifer as well as between the fault and the aquifer.

Two possible cases will be studied in this part. The one is to assume a constant head at the other end of the fault. The other is to study an aquifer-fault-aquifer system with only one of the aquifers being pumped (or injected). In both cases, the head in the fault varies with both space and time. Although the second case sounds more realistic, the study of the first case is also very important. The reason is that this case can easily be found in nature. The constant head case can exist due to a very good hydraulic connection between the fault and some large sources such as rivers and

lakes. It could also be a result of the connection with another aquifer (unpumped), which has such a large transmissivity that the drawdown at that aquifer is negligibly small. Analytical solutions will be derived for both cases, in which the drawdown in the aquifer(s) will always be the dependent variables. The development of these solutions can provide a series of formulae for determining the recharge rate from the fault and other characteristic values of interest. More importantly, one can develop a practical method to characterize the fault zone.

In the second part, the air flow in the unsaturated zone due to certain atmospheric fluctuations at the ground surface will be studied. In this rock-fault system, by assuming the water is immobile and the pressure variations are small, the governing equation for the air flow can be simplified to a diffusion equation (Weeks, 1978).

Analytical solutions will be worked out for simple single-layer problems with different boundary conditions. The single rock layer can be either semi-infinite in thickness or bounded by an impermeable boundary such as the groundwater table at a certain depth. Corresponding to each of these lower boundary conditions, two different boundary conditions at the ground surface will be studied. The first one assumes a step function variation for atmospheric pressure, while the second assumes that the fluctuation in atmospheric pressure is a sinusoidal function of time. These analytical solutions can be used directly in the characterization of faults in the vadose zone consisted of a single layer. In addition, they can provide a vehicle for verification of numerical codes which are useful in the study of multi-layer systems.

For multi-layer problems with complex initial and boundary conditions, solutions can be obtained by means of numerical methods. A well developed code, TRUMP

(Edwards, 1972) will be used to solve these problems. The program will be first verified against the analytical solutions for single-layer problems. Then it will be used to evaluate the validities of some assumptions which have been given in deriving the analytical solutions. Finally, examples of calculations will be given for the purpose of practical applications.

1.4 Solution Strategies

Most efforts in this study are to obtain solutions analytically. For this kind of problem with composite-materials, the whole system is first divided into several regions. The governing equations are then set up for each region separately. A uniform initial condition is assumed for all regions in all problems. The external boundary conditions are limited to some typical cases for the purpose of simplification; while the inner boundary conditions play the role of keeping the separate regions together. Some reasonable assumptions are employed for simplifying the solution process.

The mathematical tool for solving the governing equations is basicly the method of integral transforms. There are several kinds of integral transforms which will be used in this thesis. Among them are the Laplace transform, the exponential Fourier transform, the Fourier sine and cosine transforms, and the finite Fourier transforms. During the inverse process, the Laplace inversion is usually performed first so that the final solution can be derived in a closed form with at most a real integral. In some cases, the technique of series expansion will be used to get a form which can be inverted in the Laplace domain. Some mathematical manipulations such as variation of variables will also be frequently used in obtaining and simplifying solutions.

Every time a solution is obtained, some detailed analyses and studies will be given to obtain more useful expressions from the solution. In this way, practical methods for characterizing leaky faults can be fully developed, which is the goal of this investigation.

CHAPTER 2

CHARACTERIZATION OF LEAKY FAULTS IN SATURATED SYSTEMS

2.1 Review

It is Theis (1935) who first established the theoretical basis of transient fluid flow in an aquifer. The well-known Theis solution was obtained by using an analogy to heat-flow theory. In deriving this solution analytically, Theis used the simplest possible aquifer configuration, which is: (1) horizontal, (2) confined between impermeable formations on top and bottom, (3) infinite in horizontal extent, (4) of constant thickness, and (5) homogeneous and isotropic with respect to its hydrogeological parameters. He further gave another five limitations to this ideal system: (6) there is only a single pumping (or injection) well in the aquifer, (7) the pumping (or injection) rate is constant with time, (8) the well diameter is infinitesimally small, (9) the well penetrates the entire aquifer, and (10) the hydraulic head in the aquifer prior to pumping (or injection) is uniform throughout the aquifer (Freeze and Cherry, 1979).

This is a radial flow problem and the final solution written in terms of drawdown, s, is $s = \frac{Q}{4\pi T} W(u)$, where Q is the constant pumping (or injection) rate, T is the transmissivity of the aquifer and $W(u)$ is known as the " well function ", which is in fact the exponential integral defined as $W(u) = \int_u^\infty \frac{e^{-x}dx}{x}$. The independent variable of the well function is related to the radial distance, r, the storativity of the aquifer, S, the transmissivity of the aquifer, T and time, t by: $u = \frac{r^2 S}{4Tt}$.

The Theis solution can be used both for predicting the transient drawdown in the aquifer and for determining the hydrogeological parameters of the aquifer. The latter application is called "inverse problem ". Several methods have been developed for this application. Two of them, namely the log-log method and the semilog method, are still useful tools in analyzing field tests.

Theis started a new era in the study of transient problems in the field of groundwater hydrology. All studies since then have been basically directed at removing the assumptions listed above. For example, the study of leaky aquifers is for the purpose of cancelling out the second assumption; the study of a bounded aquifer is for obtaining the solution without the third assumption; the study on the effect of well diameter is for the purpose of evaluating the error caused by the eighth assumption; and the study on partial penetration is related to removing the restriction imposed by the ninth assumption.

In some sense, the work in this chapter can be thought to be a continuous effort on the study of a bounded aquifer. However, the main interest is not the aquifer but the boundary (the leaky fault). For the case of an aquifer bounded by a linear boundary, the previous solutions which are obtained by superposition of Theis solutions can only treat the simplest problems containing either a constant-head boundary or a no-flow boundary. A non-constant head leaky fault is one in which the fault acts as a conduit for fluid movement into the aquifer during the pumping test. In this case, however, there is resistance to movement within the fault zone, and consequently, at the point where the fault intersects the aquifer the hydraulic head does not stay constant. Solutions to the non-constant head leaky fault case are not available (Witherspoon, et

al., 1967).

For purpose of characterizing leaky faults, this study will first develop solutions to the general leaky fault case and then discuss the applications. The leaky fault under consideration will be assumed to have finite values of hydrogeological properties. The methodology to be employed in this study will be totally different from those applied in previous studies for solving constant-head and tight faults problems.

2.2 Theory

Figure 2.1 illustrates a schematic picture of the fault-aquifer system to be studied. The confined aquifer is pumped with a constant rate of Q through the well W. The aquifer and the overlying aquitard are cut by a near vertical fault with the effective thickness of H_f. To be able to characterize the fault, one has to obtain a solution that provides drawdowns within the aquifer as a function of time and space. As shown in Figure 2.1, the three-dimensional Cartesian coordinates are oriented in such a way that the $x-y$ plane rests on the top of the pumped aquifer (the x axis through the pumping well is vertical to the fault plane) and the z axis extends vertically up on the axial plane of the fault.

With such coordinates, the whole flow system is divided into two interconnecting plane flow fields, that is, the aquifer flow on the $x-y$ plane and the fault flow on the $y-z$ plane. To distinguish all variables (for example, the drawdown, s) and parameters (for example, the hydraulic conductivity, K and the specific storage, S_s), the subscripts a and f will frequently be used in this chapter to represent aquifer and fault, respectively.

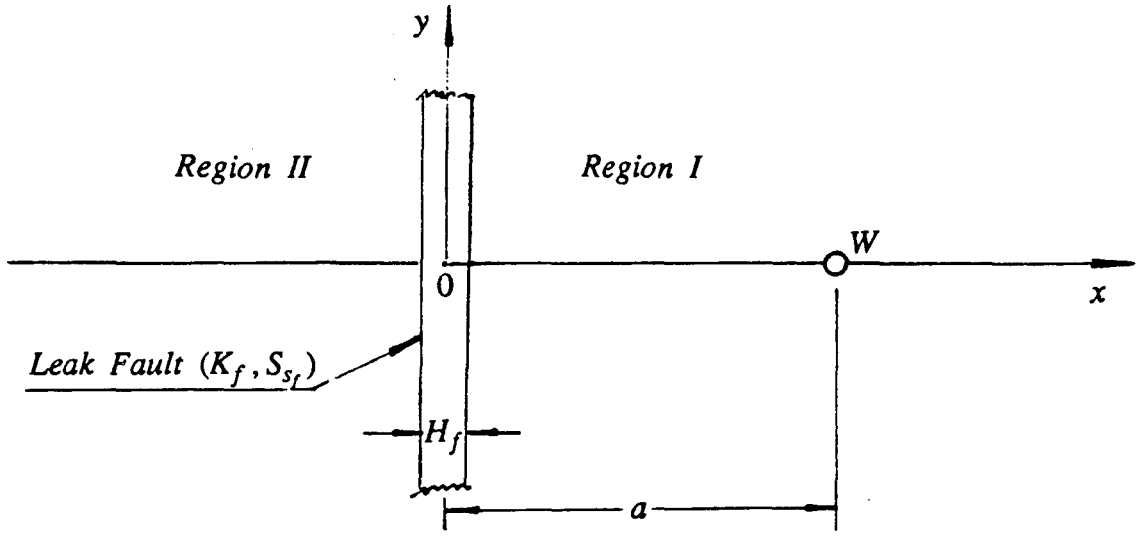

(a) Plan View

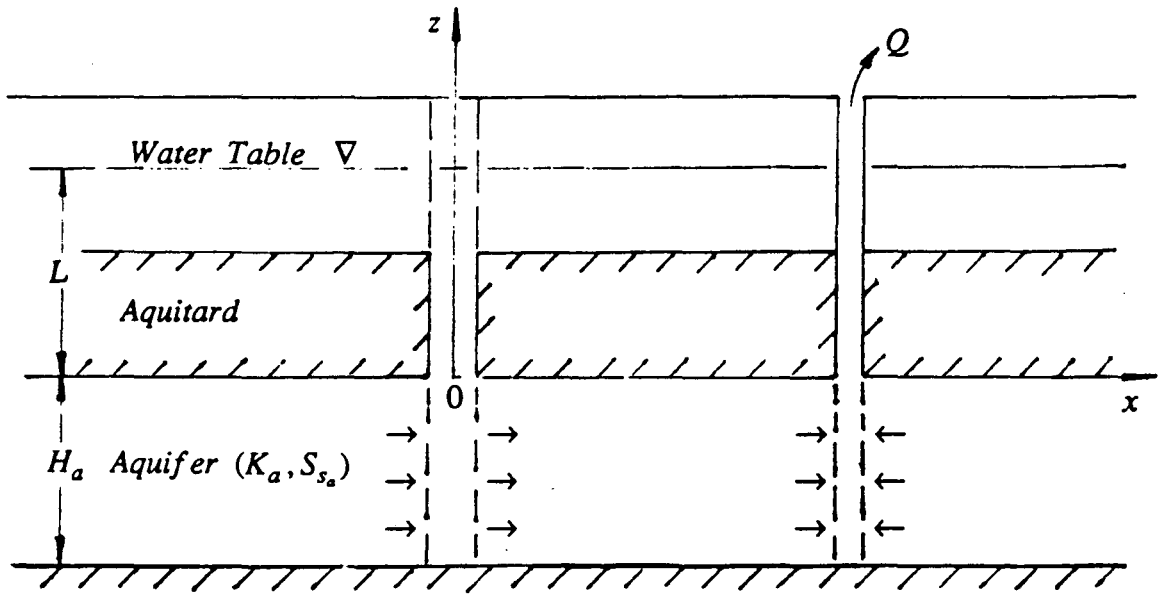

(b) Sectional View

Figure 2.1 Schematic view of a fault-aquifer system.

To work out a solution analytically, it is necessary to adopt some reasonable assumptions to simplify the problem. As it is treated conventionally, the aquifer is still assumed to be homogeneous, isotropic, uniform in thickness and infinite in areal extent. In addition, if there is a vertical displacement due to faulting, it is assumed that the displacement is much smaller than the aquifer thickness. Similarly, the vertical fault is assumed to be homogeneous, uniform in thickness and infinite in length. Again, this study is restricted to conditions where the pumping well (or injection well) fully penetrates the aquifer and where the pumping (or injection) rate is constant, Q.

This configuration for the aquifer is convenient in that flow in the aquifer can be treated as a kind of transient planar flow where drawdown is a function of horizontal coordinates x, y and time, t. A new condition is that the aquifer is cut by the fault into two sides, i.e., the side with the pumping well which is called " Region I " ($x \geq 0$) and the side without the well which can be called " Region II " ($x \leq 0$). If the governing equation for drawdown in the aquifer, s_a, is written separately for the two regions, they are (Bixel, et al., 1963):

$$\frac{\partial s_{a_1}}{\partial t} = \alpha_a \left[\frac{\partial^2 s_{a_1}}{\partial x^2} + \frac{\partial^2 s_{a_1}}{\partial y^2} \right] + \frac{\alpha_a Q}{T_a} \cdot \delta(x-a) \cdot \delta(y) \qquad (x \geq 0) \qquad (2\text{-}1)$$

$$\frac{\partial s_{a_2}}{\partial t} = \alpha_a \left[\frac{\partial^2 s_{a_2}}{\partial x^2} + \frac{\partial^2 s_{a_2}}{\partial y^2} \right] \qquad (x \leq 0) \qquad (2\text{-}2)$$

where $\delta(x-a) \cdot \delta(y)$ is the Dirac δ-function; α and T are diffusivity and transmissivity, respectively, defined as:

$$\alpha = K/S_s \qquad T = K \cdot H \qquad (2\text{-}3)$$

In this study, the faults of interest will have a large hydraulic conductivity but a small specific storage. Based on these conditions, we can reasonably assume that the

recharge rate from the fault to the aquifer is proportional to the head difference between the two ends of the vertical fault. This assumption is valid in most cases of interest and the verification is given in Appendix A. The following work in this chapter will be based on this simplification.

In general, the fault may cut through several aquifers. However, this study will consider two horizontal aquifers, one of which is penetrated and screened by the pumping well. The other aquifer can be located either above or below the aquifer that is being pumped. To distinguish the two aquifers, they will be referred to as the " pumped aquifer " and the " unpumped aquifer " in this study.

It is assumed that flow is induced only by pumping. In other words, the drawdown at the very beginning is zero everywhere. Therefore, the initial condition can be written as:

$$s_{a_1} = s_{a_2} = 0 \quad at \quad t = 0 \tag{2-4}$$

The boundary conditions in this case are:

$$s_{a_1} = 0 \quad at \quad x \to +\infty \ \ or \ \ y \to \pm\infty \tag{2-5}$$

$$s_{a_2} = 0 \quad at \quad x \to -\infty \ \ or \ \ y \to \pm\infty \tag{2-6}$$

$$s_{a_1}|_{x=0} = s_{a_2}|_{x=0} \tag{2-7}$$

$$T_a \left[\frac{\partial s_{a_1}}{\partial x}\right]_{x=0} = T_a \left[\frac{\partial s_{a_2}}{\partial x}\right]_{x=0} + q_r \tag{2-8}$$

where q_r is the recharge flux from the fault to the aquifer and is defined by:

$$q_r = T_f \frac{s_{a_1}|_{x=0} - s_u|_{x=0}}{L} \tag{2-9}$$

where L is the length of flow path in the fault.

There are two possibilities for the boundary condition in the fault: (1) Case 1, there is a " big source " at the other end of the fault or drawdown in the unpumped

aquifer is negligible, i.e., $s_u = 0$; and (2) Case 2, the drawdown in the unpumped aquifer is nonnegligible, i.e, $s_u \neq 0$.

2.3 Case 1: Constant-Head at the Other End of the Fault

This kind of situation can be found in nature where there is a significant source (for example, a river, a lake, etc.) that is well connected to the leaky fault at the other end, or if the unpumped aquifer has a much larger transmissivity than the pumped aquifer such that drawdown in the unpumped aquifer is negligibly small. Under this condition, an analytical solution in closed form can be obtained as following.

2.3.1 Analytical Solution

For governing equations (2-1) and (2-2), if the Laplace transform

$$v(p) = L\{s(t)\} = \int_0^{\infty} s(t) \cdot e^{-pt}\, dt \tag{2-10}$$

and the exponential Fourier transform

$$w(\rho) = F\{v(y)\} = \int_{-\infty}^{+\infty} v(y) \cdot e^{i\rho y}\, dy \tag{2-11}$$

are applied one after another, and the following theorems

$$L\{\frac{ds}{dt}\} = p \cdot v - s\,|_{t=0} \tag{2-12}$$

$$F\{\frac{d^2v}{dy^2}\} = -\rho^2 \cdot w \tag{2-13}$$

are used sequentially, the transformed equations will be:

$$\frac{d^2 w_{a_1}}{dx^2} - A^2 w_{a_1} = -\frac{Q \cdot \delta(x-a)}{pT_a} \qquad (x \geq 0) \tag{2-14}$$

$$\frac{d^2 w_{a_2}}{dx^2} - A^2 w_{a_2} = 0 \qquad (x \leq 0) \tag{2-15}$$

where A is a temporarily introduced parameter defined as:

$$A = \sqrt{p/\alpha_a + \rho^2} \tag{2-16}$$

During the above process, the initial condition (2-4) and part of the boundary conditions (2-5) and (2-6) have been used. The remaining boundary conditions to be satisfied in the transformed domain are:

$$w_{a_1} = 0 \quad at \quad x \to +\infty \tag{2-17}$$

$$w_{a_2} = 0 \quad at \quad x \to -\infty \tag{2-18}$$

$$w_{a_1}|_{x=0} = w_{a_2}|_{x=0} \tag{2-19}$$

$$T_a \left[\frac{dw_{a_1}}{dx}\right]_{x=0} = T_a \left[\frac{dw_{a_2}}{dx}\right]_{x=0} + T_f \frac{w_{a_1}|_{x=0}}{L} \tag{2-20}$$

Applying the method of variation of parameters and determining all integral constants by using the above boundary conditions, the solutions for (2-14) and (2-15) have the final forms as follows (the process of derivation is given in Appendix B).

$$w_{a_1} = \frac{Q}{2T_a}\left[\frac{e^{-|x-a|A}}{pA} - \frac{ce^{-(x+a)A}}{pA(A+c)}\right] \quad (x \geq 0) \tag{2-21}$$

$$w_{a_2} = \frac{Q}{2T_a}\cdot\frac{e^{-(a-x)A}}{p(A+c)} \quad (x \leq 0) \tag{2-22}$$

where the newly defined c is a very important parameter with a dimension of reciprocal length:

$$c = \frac{1}{2L}\cdot\frac{T_f}{T_a} \tag{2-23}$$

For the purpose of an easier inversion, it is necessary to divide the second term in equation (2-21) into two parts and rewrite the solution as:

$$w_{a_1} = \frac{Q}{2T_a}\left[\frac{e^{-|x-a|A}}{pA} - \frac{e^{-(x+a)A}}{pA} + \frac{e^{-(x+a)A}}{p(A+c)}\right] \quad (x \geq 0) \tag{2-24}$$

It is fortunate that the second term is similar to the first one in (2-24), while the third term in (2-24) is similar to the term in (2-22), which means that we need to do

the inversion for only two terms. Since it does not matter which inversion is done first, there are two possible inversion orders, that is:

$$s = L^{-1}\{F^{-1}\{w\}\} = F^{-1}\{L^{-1}\{w\}\} \tag{2-25}$$

The book of " Tables of integral transforms " (Erdelyi, 1954) will be frequently used in this study and will be referred to as " the tables ". To get full use of the tables, we shall now introduce a formula for the relationship between the inverse exponential Fourier transform of an even function and its Fourier cosine transform. For any arbitrary even function, $w(\rho^2)$, its inverse exponential Fourier transform with respect to ρ is equal to its Fourier cosine transform with respect to ρ multiplied by a factor of $1/\pi$. This can be proved in the following:

$$\begin{aligned} F^{-1}\{w(\rho^2)\} &= \frac{1}{2\pi}\int_{-\infty}^{+\infty} w(\rho^2)\, e^{-i\rho y}\, d\rho \\ &= \frac{1}{\pi}\int_{0}^{+\infty} w(\rho^2)\cos(\rho y)\, d\rho \\ &= \frac{1}{\pi} F_c\{w(\rho^2)\} \end{aligned} \tag{2-26}$$

(Note: since $w(\rho^2)\sin(\rho y)$ is an odd function of ρ, and its integration with respect to ρ from $-\infty$ to $+\infty$ is definitely zero.)

For convenience, the Laplace inversion will be performed first. Two Laplace inversion theorems will be used in the following process:

$$L^{-1}\{f(p+k)\} = e^{-kt}\cdot L^{-1}\{f(p)\} \tag{2-27}$$

$$L^{-1}\{f(p)/p\} = \int_0^t L^{-1}\{f(p)\}dt \tag{2-28}$$

From the tables, two Laplace inversion formulae will be applied.

$$L^{-1}\left\{\frac{e^{-k\sqrt{p}}}{\sqrt{p}}\right\} = \frac{e^{-k^2/(4t)}}{\sqrt{\pi t}} \tag{2-29}$$

$$L^{-1}\left\{\frac{e^{-k\sqrt{p}}}{\sqrt{p}+l}\right\} = \frac{e^{-k^2/(4t)}}{\sqrt{\pi t}} - le^{kl+l^2t}\cdot erfc\left(\frac{k}{2\sqrt{t}}+l\sqrt{t}\right) \tag{2-30}$$

where $erfc(x)$ is the complementary error function.

Also from the tables, there is a Fourier cosine transform formula which is useful to this problem.

$$F_c\{e^{-k\rho^2}\} = \frac{1}{2}\sqrt{\frac{\pi}{k}}e^{-\frac{y^2}{4k}} \tag{2-31}$$

With all these formulae, the inversion for the two basic terms can be derived without difficulty. The derivation process is given in the following steps:

$$F^{-1}\left\{L^{-1}\left\{\frac{e^{-(x+a)A}}{pA}\right\}\right\} = \sqrt{\alpha_a}\,F^{-1}\left\{L^{-1}\left\{\frac{e^{-[(x+a)/\sqrt{\alpha_a}]\sqrt{p+\alpha_a\rho^2}}}{p\sqrt{p+\alpha_a\rho^2}}\right\}\right\}$$

$$= \sqrt{\alpha_a}F^{-1}\left\{\int_0^t e^{-\alpha_a\rho^2\tau}\cdot\frac{e^{-(x+a)^2/(4\alpha_a\tau)}}{\sqrt{\pi\tau}}d\tau\right\}$$

$$= \frac{\sqrt{\alpha_a}}{\pi\sqrt{\pi}}\int_0^t F_c\{e^{-\alpha_a\tau\rho^2}\}\cdot\frac{e^{-(x+a)^2/(4\alpha_a\tau)}}{\sqrt{\tau}}d\tau$$

$$= \frac{1}{2\pi}\int_0^t \frac{e^{-[(x+a)^2+y^2]/(4\alpha_a\tau)}}{\tau}d\tau$$

$$= \frac{1}{2\pi}W\left[\frac{(x+a)^2+y^2}{4\alpha_a t}\right] \tag{2-32}$$

where $W(u)$ is called the " well function " in the groundwater hydrology literature. This is equal to the exponential integral function, $-Ei[-u]$ in mathematics, and is defined as:

$$W(u) = -Ei[-u] = \int_u^{\infty} \frac{e^{-x}}{x} dx \tag{2-33}$$

The last step towards the final solution of (2-32) is achieved by means of a change of the variable: $u = [(x+a)^2+y^2]/(4\alpha_a \tau)$.

To get the inversion of the second basic term, the prepared formulae are applied in the sequence of (2-27), (2-30), (2-28) and (2-31). The derivation process can be shown as follows:

$$F^{-1}\left\{L^{-1}\left\{\frac{e^{-(x+a)A}}{p(A+c)}\right\}\right\} = \sqrt{\alpha_a} F^{-1}\left\{L^{-1}\left\{\frac{e^{-[(x+a)/\sqrt{\alpha_a}]\sqrt{p+\alpha_a \rho^2}}}{p(\sqrt{p+\alpha_a \rho^2}+c\sqrt{\alpha_a})}\right\}\right\}$$

$$= \sqrt{\alpha_a} F^{-1}\left\{\int_0^t e^{-\alpha_a \rho^2 \tau} \cdot \left[\frac{e^{-(x+a)^2/(4\alpha_a \tau)}}{\sqrt{\pi\tau}} - c\sqrt{\alpha_a} e^{c(x+a)} \cdot f(\tau)\right] d\tau\right\}$$

$$= \frac{\sqrt{\alpha_a}}{\pi} \int_0^t F_c\{e^{-\alpha_a \tau \rho^2}\} \cdot \left[\frac{e^{-(x+a)^2/(4\alpha_a \tau)}}{\sqrt{\pi\tau}} - c\sqrt{\alpha_a} e^{c(x+a)} \cdot f(\tau)\right] d\tau$$

$$= \frac{1}{2\pi} \cdot W\left[\frac{(x+a)^2+y^2}{4\alpha_a t}\right] - \frac{c\sqrt{\alpha_a} e^{c(x+a)}}{2\sqrt{\pi}} \int_0^t g_1(\tau) d\tau \tag{2-34}$$

where the function $g_1(\tau)$ is introduced during the inversion process and is defined as:

$$g_1(\tau) = \frac{e^{-y^2/(4\alpha_a \tau)}}{\sqrt{\tau}} \cdot f(\tau)$$

$$= \frac{e^{c^2 \alpha_a \tau - y^2/(4\alpha_a \tau)}}{\sqrt{\tau}} \cdot erfc\left[\frac{x+a}{2\sqrt{\alpha_a \tau}} + c\sqrt{\alpha_a \tau}\right] \tag{2-35}$$

Applying (2-25) to (2-24) and collecting all results from (2-32) and (2-34), the expression of drawdown in Region I is:

$$s_{a_1} = \frac{Q}{4\pi T_a} W\left[\frac{(x-a)^2+y^2}{4\alpha_a t}\right] - \frac{Qc\sqrt{\alpha_a} e^{c(a+x)}}{4\sqrt{\pi} T_a} \int_0^t g_1(\tau) d\tau$$

$$(x \geq 0) \tag{2-36}$$

Applying (2-25) to (2-22) and using the result of (2-34), the expression of drawdown in Region II is:

$$s_{a_2} = \frac{Q}{4\pi T_a} W\left[\frac{(x-a)^2+y^2}{4\alpha_a t}\right] - \frac{Qc\sqrt{\alpha_a}e^{c(a-x)}}{4\sqrt{\pi}T_a}\int_0^t g_2(\tau)d\tau$$
$$(x \leq 0) \tag{2-37}$$

It is unnecessary to give the expression for $g_2(\tau)$ because one can write it down by simply replacing $(x+a)$ in (2-35) by $(a-x)$. Comparing (2-37) with (2-36), it is easy to construct an unified form for drawdowns on the whole $x-y$ plane. Furthermore, if the x axis is not chosen to pass through the pumping well, the coordinates of the pumping well will be (a,b), $(b \neq 0)$. A general unified formula for drawdowns is:

$$s_a = \frac{Q}{4\pi T_a} W\left[\frac{(x-a)^2+(y-b)^2}{4\alpha_a t}\right] - \frac{Qc\sqrt{\alpha_a}e^{c(|x|+a)}}{4\sqrt{\pi}T_a}\int_0^t g(\tau)d\tau \tag{2-38}$$

where $g(\tau)$ is similar to $g_1(\tau)$ as follows:

$$g(\tau) = \frac{e^{c^2\alpha_a\tau-(y-b)^2/(4\alpha_a\tau)}}{\sqrt{\tau}} \cdot erfc\left[\frac{|x|+a}{2\sqrt{\alpha_a\tau}} + c\sqrt{\alpha_a\tau}\right] \tag{2-39}$$

To demonstrate how the new solutions behave, examples of computed results for some practical problems are given in Figures 2.2A through 2.2D.

In Figure 2.2A, three sets of aquifer drawdown curves along the symmetric plane $(y=0)$ offer a clear comparison between the new solution and the conventional solutions. With a finite value for transmissivity, a non-constant head leaky fault has a drawdown curve between the Theis curve and the curve corresponding to the solution for the constant head fault case.

Figure 2.2B shows the drawdown curve in the aquifer along the leaky fault

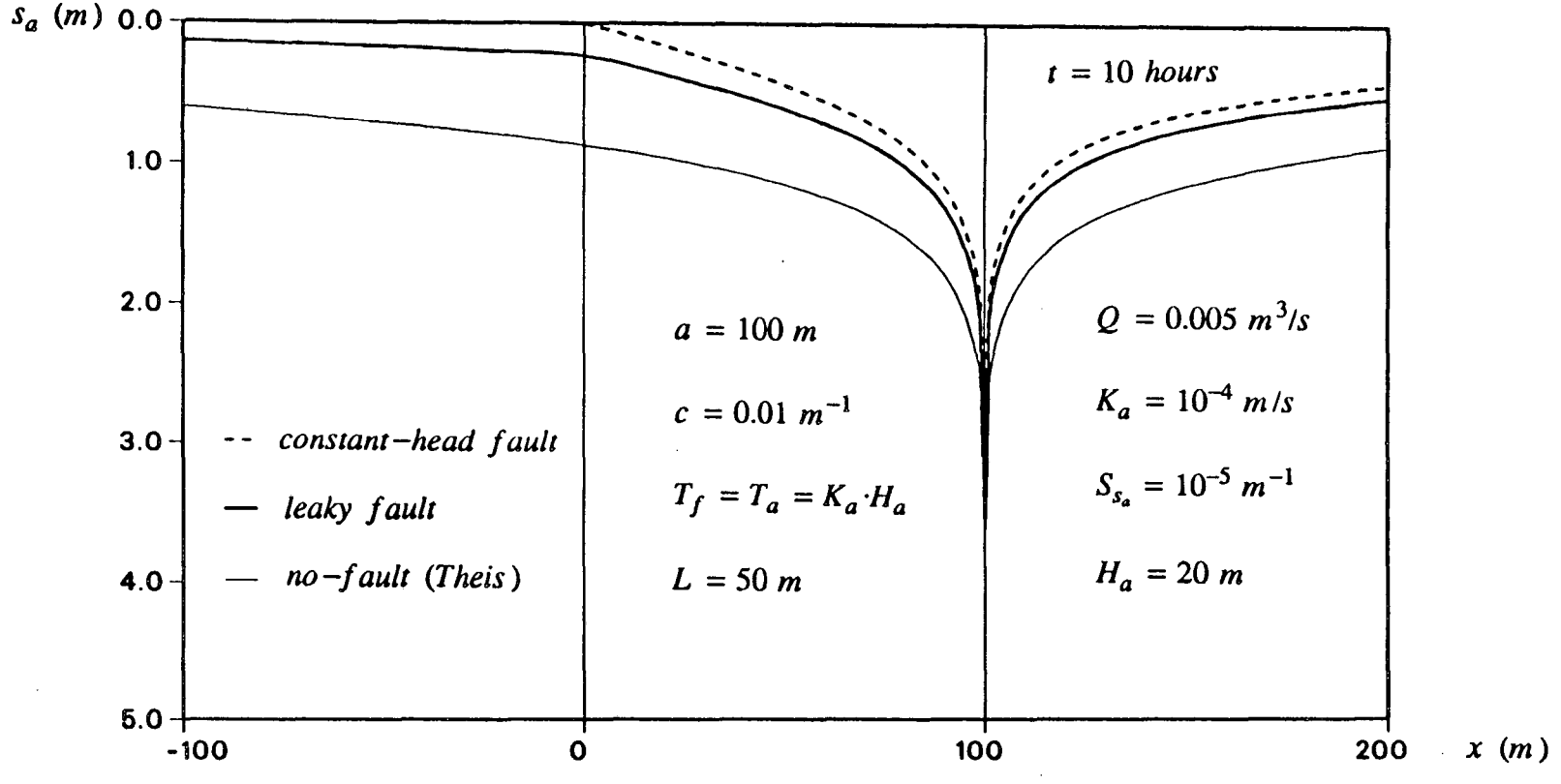

Figure 2.2A Aquifer depletion curves at the symmetric plane (y=0): a comparison of the leaky fault solution with the constant-head fault solution and the Theis solution.

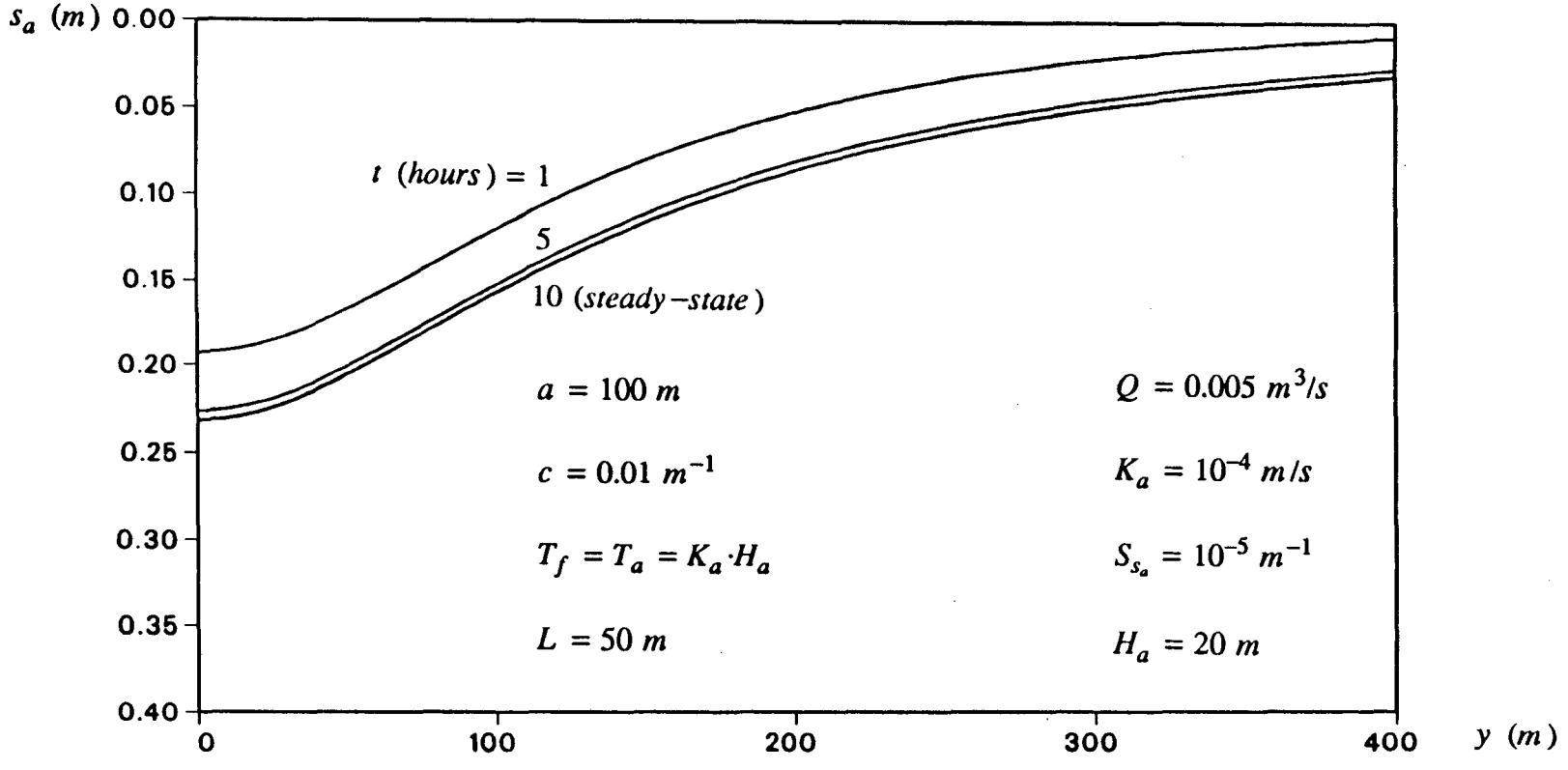

Figure 2.2B Aquifer depletion curves along the fault (x=0) at three different times.

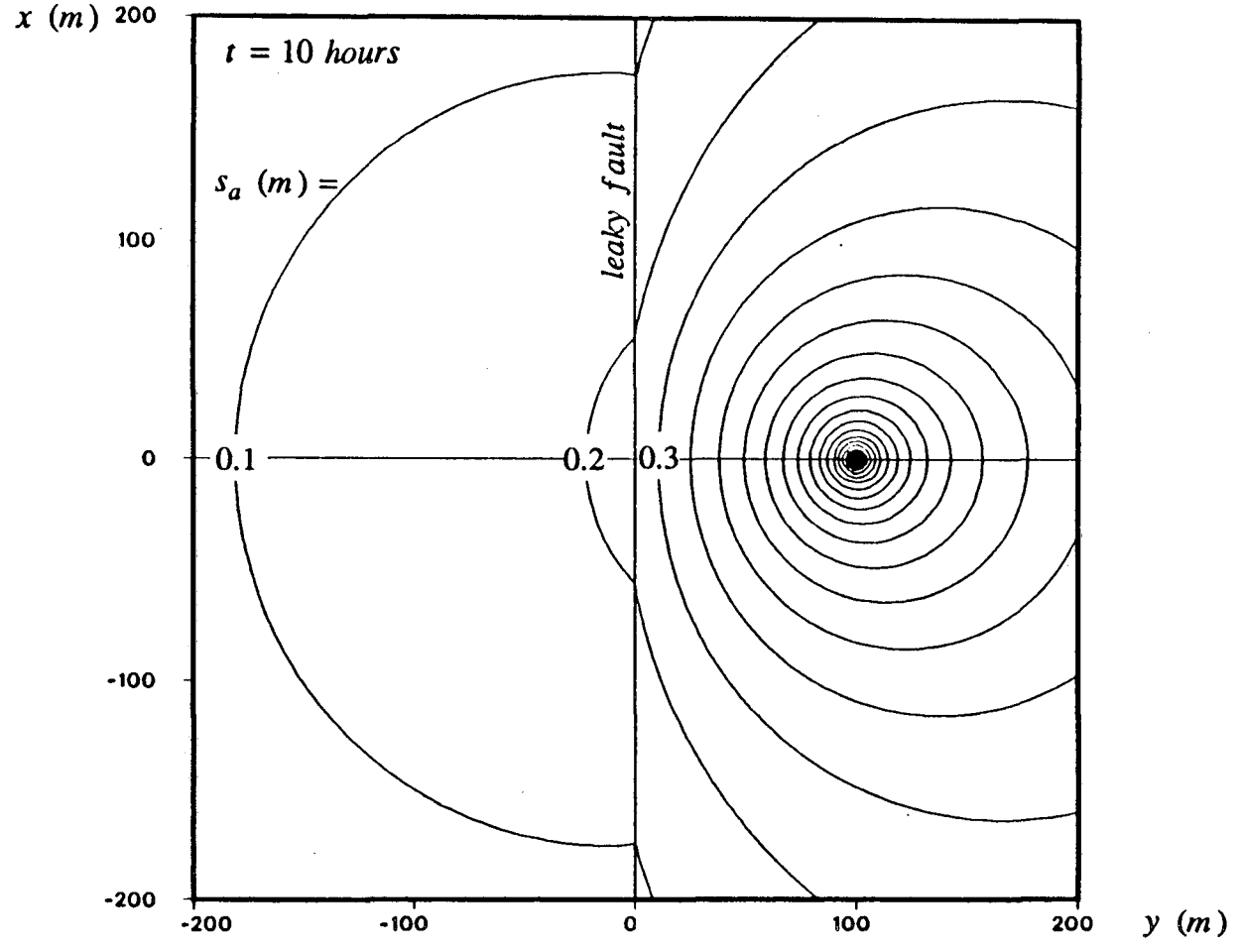

Figure 2.2C Steady-state lines of equidrawdown in the aquifer.

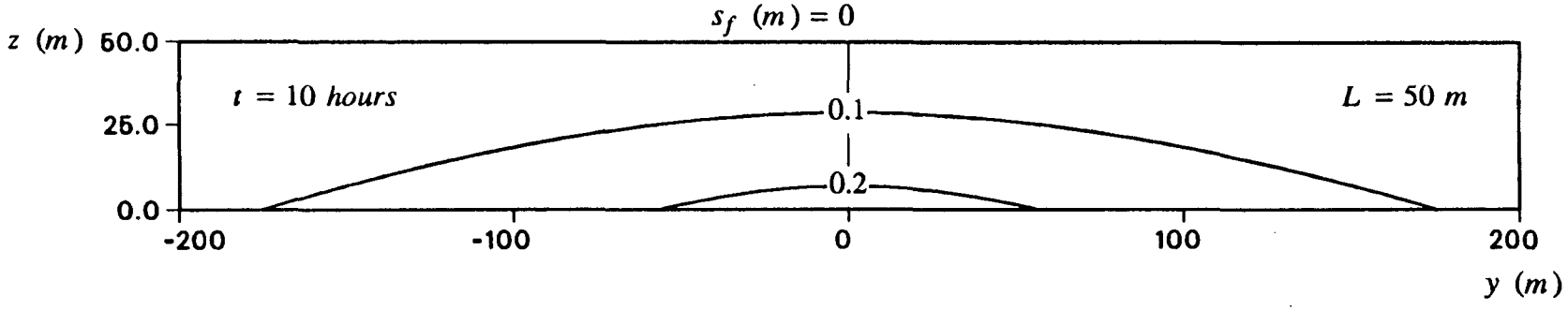

Figure 2.2D Steady-state lines of equidrawdown in the fault.

($x = 0$) as time advances. This figure shows that the system can eventually reach steady state; the mechanism will be discussed later.

The contours of equi-drawdowns at quasi-steady state are plotted on Figure 2.2C and Figure 2.2D, where the former is for the aquifer while the latter is for the fault. The drawdowns in the fault zone are obtained by means of linear interponation using the drawdowns in the aquifer along the fault. Note that because of the leakage from the fault, the contours of equi-drawdown (or the isopotentials) in the aquifer have deflection points at the fault-aquifer intersection ($x = 0$).

2.3.2 Dimensionless Solution

Although (2-38) is a general solution, (2-36) is of most interest in practice. This is because the observation wells are usually drilled on the side of the pumping well (Region I) and for a single pumping well problem the x axis is usually chosen to pass through the pumping well. For this reason, only (2-36) will be discussed in detail in the following.

The analytical solution is derived in a Cartesian coordinate system. In practice, it will be more convenient to develop the solution in polar coordinates because the distance between the observation well and the pumping well is always a known value. To make the solution applicable, the following coordinate transformation is introduced.

$$x - a = r \cdot \cos\theta \qquad y - b = r \cdot \sin\theta \tag{2-40}$$

where r and θ are the polar coordinates of the observation well.

This transform, in fact, moves the origin to the pumping well while keeping the polar axis along the direction of the x axis. Noting that $b \equiv 0$ in (2-36) and (2-35), the solution in polar coordinates is:

$$s_{a_1} = \frac{Q}{4\pi T_a} W\left[\frac{r^2}{4\alpha_a t}\right] - \frac{Qc\sqrt{\alpha_a}\, e^{c(2a+r\cos\theta)}}{4\sqrt{\pi}T_a} \int_0^t g_1(\tau) d\tau \qquad (2\text{-}41)$$

where

$$g_1(\tau) = \frac{e^{c^2\alpha_a\tau - r^2\sin^2\theta/(4\alpha_a\tau)}}{\sqrt{\tau}} \cdot erfc\left[\frac{2a + r\cos\theta}{2\sqrt{\alpha_a\tau}} + c\sqrt{\alpha_a\tau}\right] \qquad (2\text{-}42)$$

As mentioned above, r is a known value so that it can be taken as the characteristic length in this non-dimensionalization. The dimensionless drawdown, s_D and the dimensionless time, t_D are defined in the usual way as:

$$s_D = s/(\frac{Q}{4\pi T_a}) \qquad t_D = \frac{\alpha_a t}{r^2} \qquad (2\text{-}43)$$

Two new dimensionless parameters are defined by:

$$a_D = a/r \qquad c_D = c \cdot r \qquad (2\text{-}44)$$

This reduces the solution to the final dimensionless form:

$$\begin{aligned} s_D &= s_T - s_F \\ &= W\left[\frac{1}{4t_D}\right] - \sqrt{\pi}\, c_D\, e^{c_D(2a_D+\cos\theta)} \int_0^{t_D} G_1(\tau) d\tau \end{aligned} \qquad (2\text{-}45)$$

where

$$G_1(\tau) = \frac{e^{c_D{}^2\tau - \sin^2\theta/(4\tau)}}{\sqrt{\tau}} \cdot erfc\left[\frac{2a_D + \cos\theta}{2\sqrt{\tau}} + c_D\sqrt{\tau}\right] \qquad (2\text{-}46)$$

2.3.3 Type Curve Studies

In dimensionless solution (2-45), the drawdown is equal to the difference of two drawdown components. The first component, s_T, is exactly the Theis solution for simple radial flow, while the second is the drawdown component due to the fault recharge. In the Theis solution, the dimensionless drawdown is a function of dimensionless time, t_D only. However, the second drawdown component is a function of t_D, θ, a_D and

c_D. It may be seen that due to the connection with a leaky fault, three additional parameters are needed to determine dimensionless drawdown in the aquifer.

Among the three additional parameters, the polar angle, θ determines the location (direction) of the observation well; a_D represents the relative distance between the fault and the pumping well; and c_D is a parameter of most interest. From definitions (2-44) and (2-23), c_D can also be written as $(T_f r)/(2T_a L)$. Apparently, if the transmissivity of the fault, T_f, is relatively large and the " height " of the fault, L, is relatively short, a larger value of c_D will result, which implies a larger amount of recharge from the fault to the aquifer. The expression for s_F in (2-45) agrees with this interpretation. More detailed studies on the drawdown component, s_F will be given later. Of the three new parameters, the first two, θ and a_D, can be classified as geometric factors while the third one, c_D, includes physical parameters which characterize the hydrogeologic properties of the leaky fault. The integral in (2-45) can be evaluated by means of numerical integration. A simple program is written based on (2-45) and (2-46) to calculate s_D, in which the integral is calculated by calling a subroutine in the computer math-library. The integral in (2-45) can also be evaluated by approximation method, which will be studied in section 2.3.5 and Appendix C.

With this dimensionless solution available, many sets of type curves can be generated for different combinations of the three parameters. Proposed ranges for these parameters and related parameters can be found in Table 2.1.

Table 2.1 Ranges of System Parameters

Classifications	*Parameters*	*Ranges*
Fault	*Thickness*, H_f (m)	0.1 — 5
	Height, L (m)	10 — 100
	Distance, a (m)	50 — 1000
	Hydraulic Conductivity, K_f $(m \cdot \sec^{-1})$	10^{-5} — 10^{-2}
Aquifer	*Thickness*, H_a (m)	10 — 100
	Hydraulic Conductivity, K_a $(m \cdot \sec^{-1})$	10^{-4} — 10^{-3}
	Specific Storage, S_s (m^{-1})	10^{-5} — 10^{-3}
Well	*Pumping Rate*, Q $(m^3 \cdot \sec^{-1})$	0.01 — 0.1
	Radial Distance, r (m)	30 — 50
	Polar Angle, θ	0 — π
Calculated	*Dimensionless Distance*, a_D	2 — 33
	Dimensionless Transmissivity, c_D	1.5×10^{-6} — 125

Note: a_D and c_D are calculated from (2-44) and (2-23).

Three sets of them are given in Figures 2.3A through 2.3C, as examples. In all three figures, a_D is fixed to be 2.0; in other words, the observation wells are drilled on a circle with the pumping well at its center and with half of the distance between the fault and the pumping well as its radius. The type curves on Figure 2.3A represent drawdowns at the observation well when $\theta = \pi$; Figure 2.3B corresponds to $\theta = \pi/2$ and Figure 2.3C, $\theta = 0$. The three observation wells will be referred to as Point #1, Point #2 and Point #3, respectively. Because c_D is the most important parameter, its effect on the type curves has been shown on every figure.

It can be seen that as c_D increases from 0 to ∞, the type curve departs from the Theis curve to a line corresponding to the solution for an aquifer with a linear constant-head boundary. The limiting solutions for $c_D = 0$ and ∞ have been available in the literature for a long time; the curves in between are worked out in this study. One question may arise for the limiting case of $c_D = 0$, that is, the curve is reduced not to the curve corresponding to an aquifer with a linear impermeable boundary but to the curve of the Theis solution. Why? To answer this question, we need to look at inner boundary condition (2-8). The condition of $c_D = 0$ implies that $\frac{T_f}{L} = 0$, which then reduces the problem to that of a simple radial flow. Instead of cutting through the aquifer, the leaky fault represented by Equation (2-8) is actually " connected " to the top of the aquifer. This simplification, however, will not limit the applicability of the analytical solution.

Theoretically speaking, there is no such fault which is " infinitely leaky ". However, if the recharge ability of a fault is relatively much larger than the pumping rate, the fault may act very much like an infinitely leaky fault. It can be seen on the three

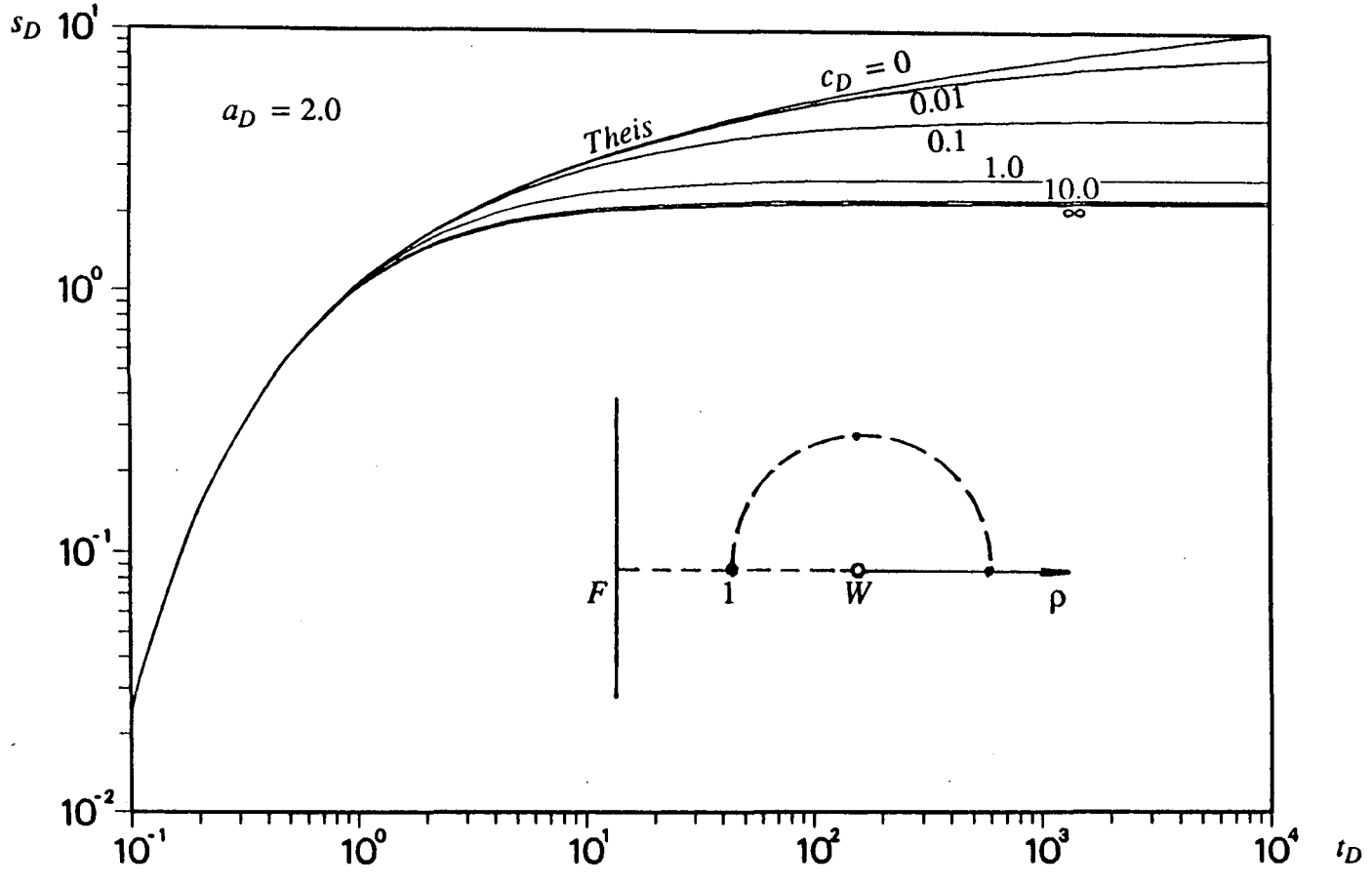

Figure 2.3A Type curves for six values of c_D at Point #1 ($\theta=\pi$).

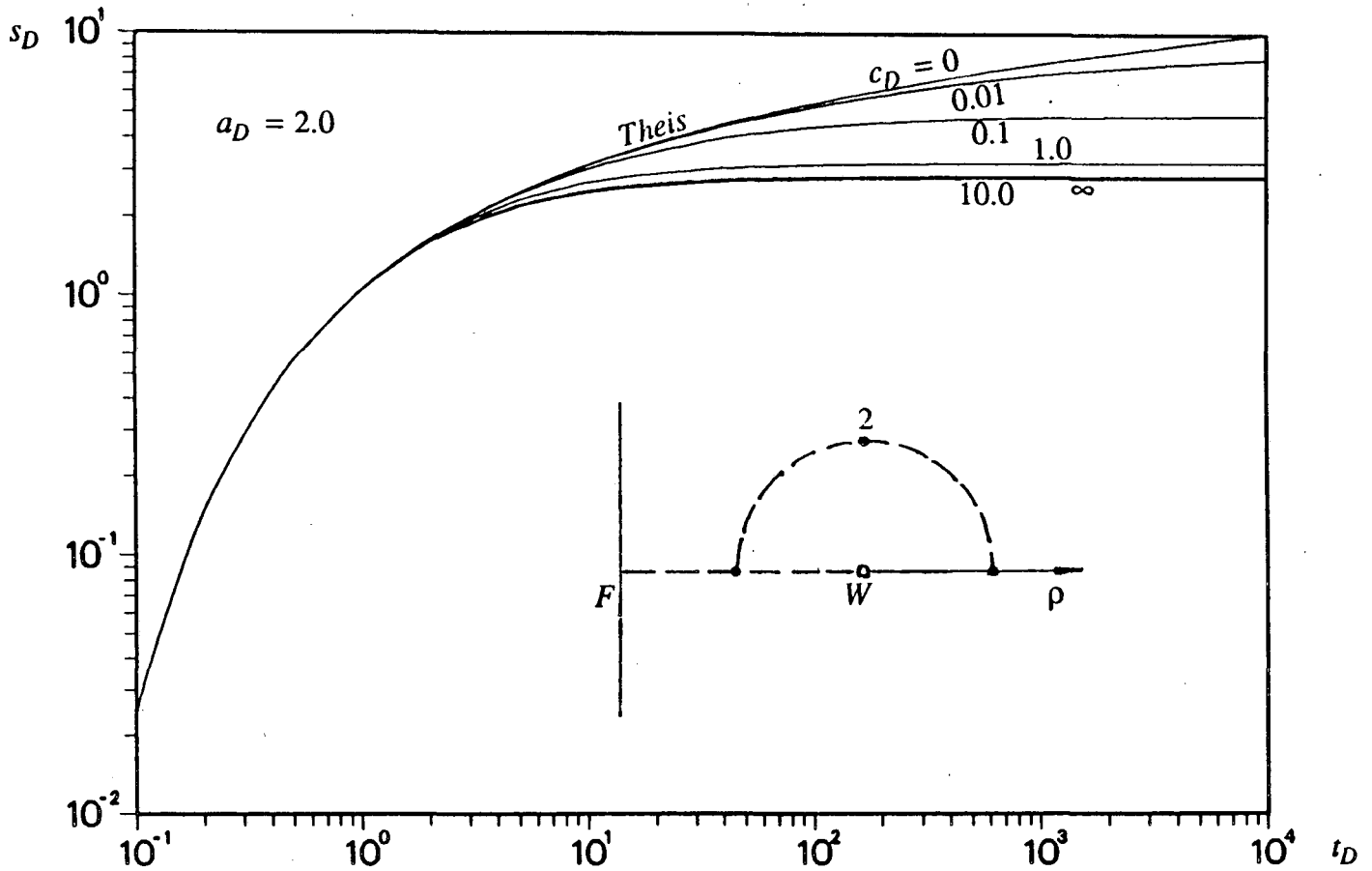

Figure 2.3B Type curves for six values of c_D at Point #2 ($\theta=\pi/2$).

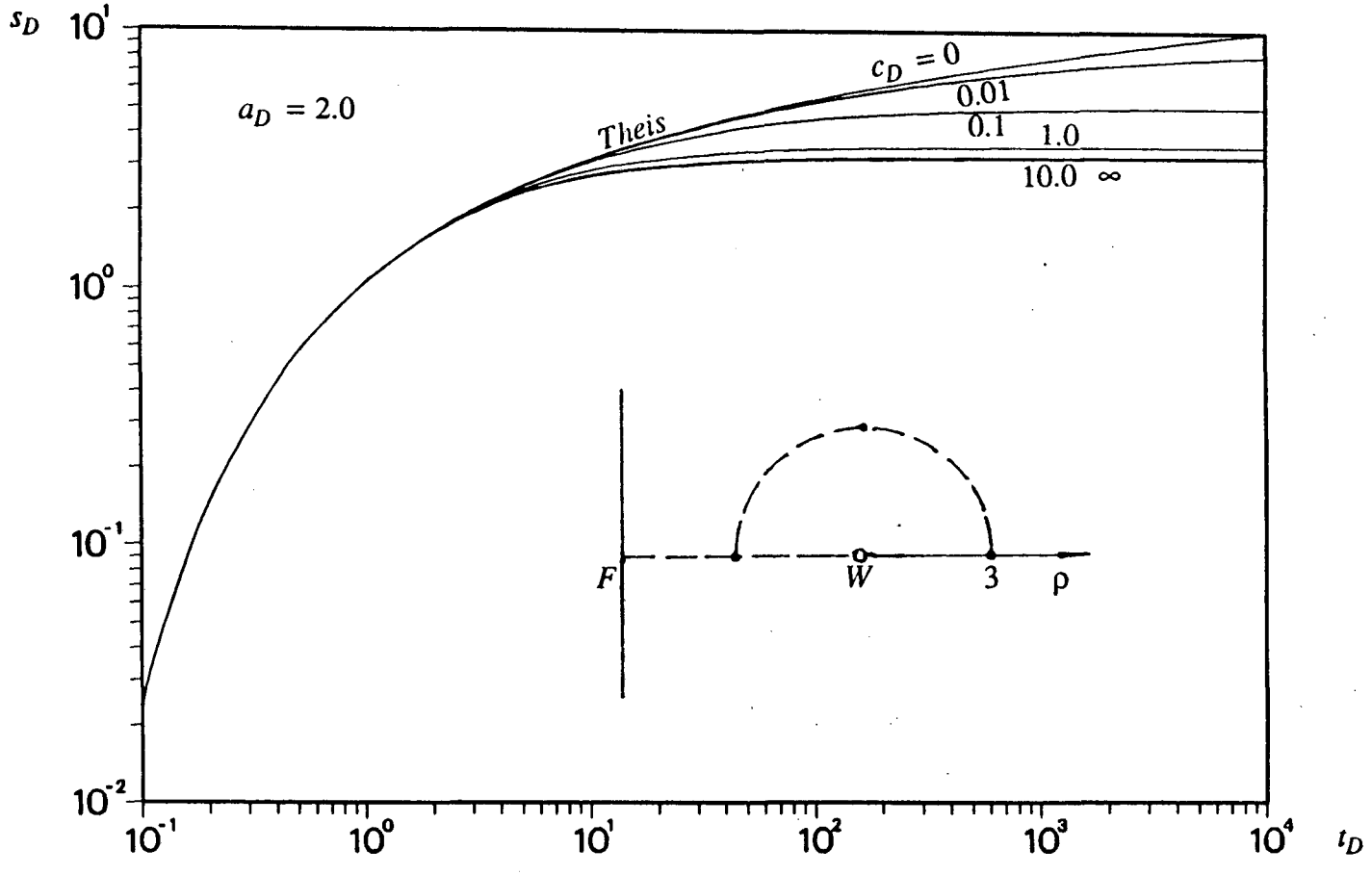

Figure 2.3C Type curves for six values of c_D at Point #3 (θ=0).

figures that the curves corresponding to $c_D = 10$ are always very close to the curves corresponding to $c_D = \infty$. Further studies show that different values of a_D require different values of c_D to get this same result. A series of case calculations suggest that $c_D \cdot a_D \geq 20$ may roughly be taken as the criterion for an " infinitely leaky " fault. In Figure 2.4, Point #1 ($\theta = \pi$) is chosen to be the calculation point. The solid lines are the type curves for different values of a_D corresponding to $c_D = \infty$ (constant-head fault); the dots are calculated data points corresponding to $c_D = 20/a_D$. The mechanism is that the product of c_D and a_D is equal to $(T_f a)/(2T_a L)$. A larger product implies that the fault is more transmissible and / or that the recharge path is shorter. As a result, the head in the fault may remain approximately constant. The reason for choosing Point #1 is that the other points can give a better match than this point, which is the closest point to the fault on the circle. One can check this by comparing Figure 2.3A with Figures 2.3B and 2.3C.

The shape of the type curves is similar to that of the leaky aquifer solution. However, there is a big difference between them. The leaky aquifer problem is axisymmetric and thus has a solution independent of θ; while the leaky fault problem is non-axisymmetric and thus has a θ dependent solution. If the curves for three observation wells are plotted on the same paper (Figure 2.5), the effect of θ is quite clear. The point of $\theta = \pi$ (Point #1) is the closest point on the circle to the fault, therefore the effect of recharge from the fault is more pronounced at this point. As a result, drawdown at this point is the least. On the contrary, the point of $\theta = 0$ (Point #3) is the farthest point from the fault, and the effect of the fault at this point is the weakest of all. As a result, the drawdown at this point is the largest. Two common

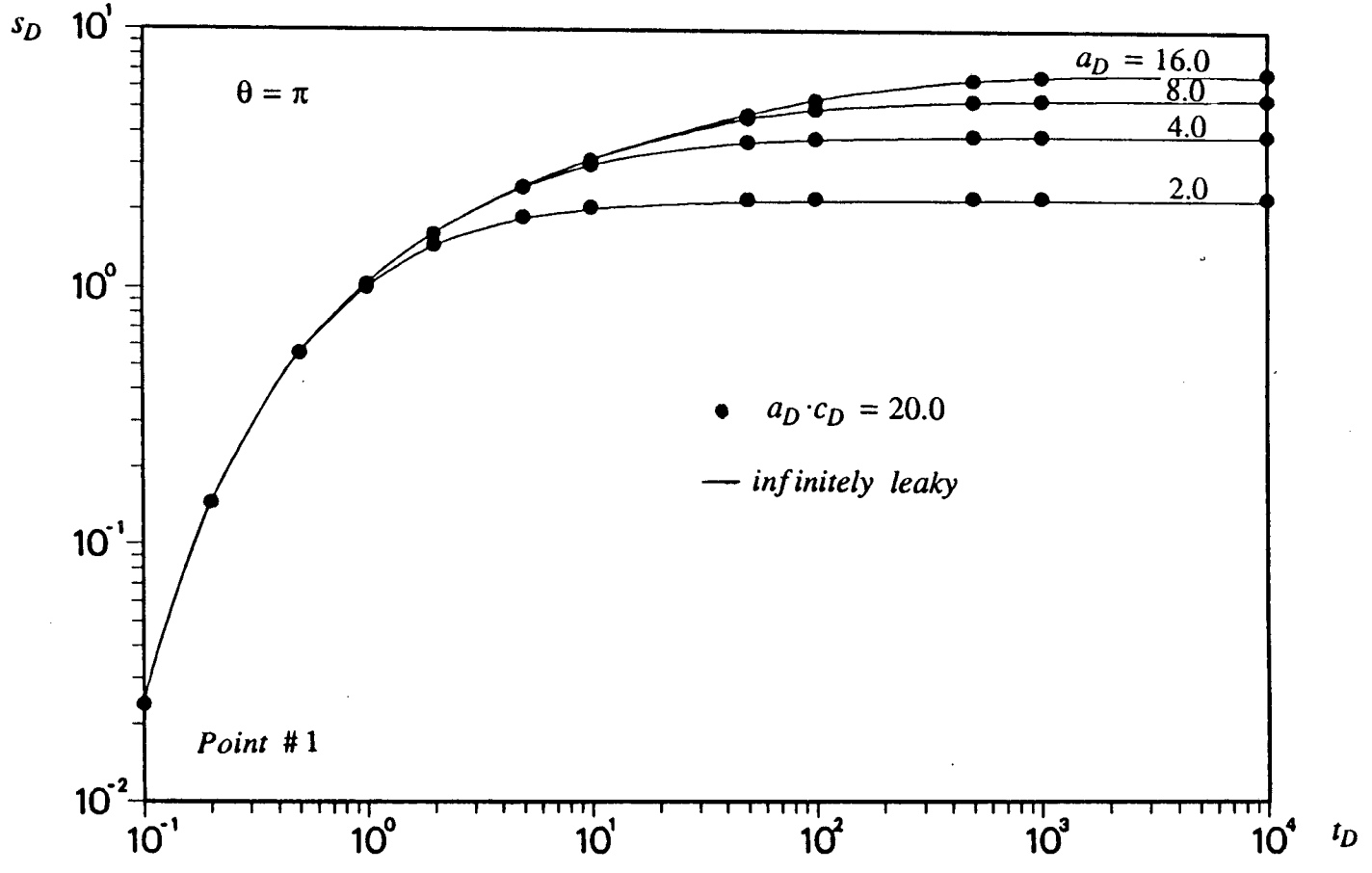

Figure 2.4 Approximation to a constant-head fault.

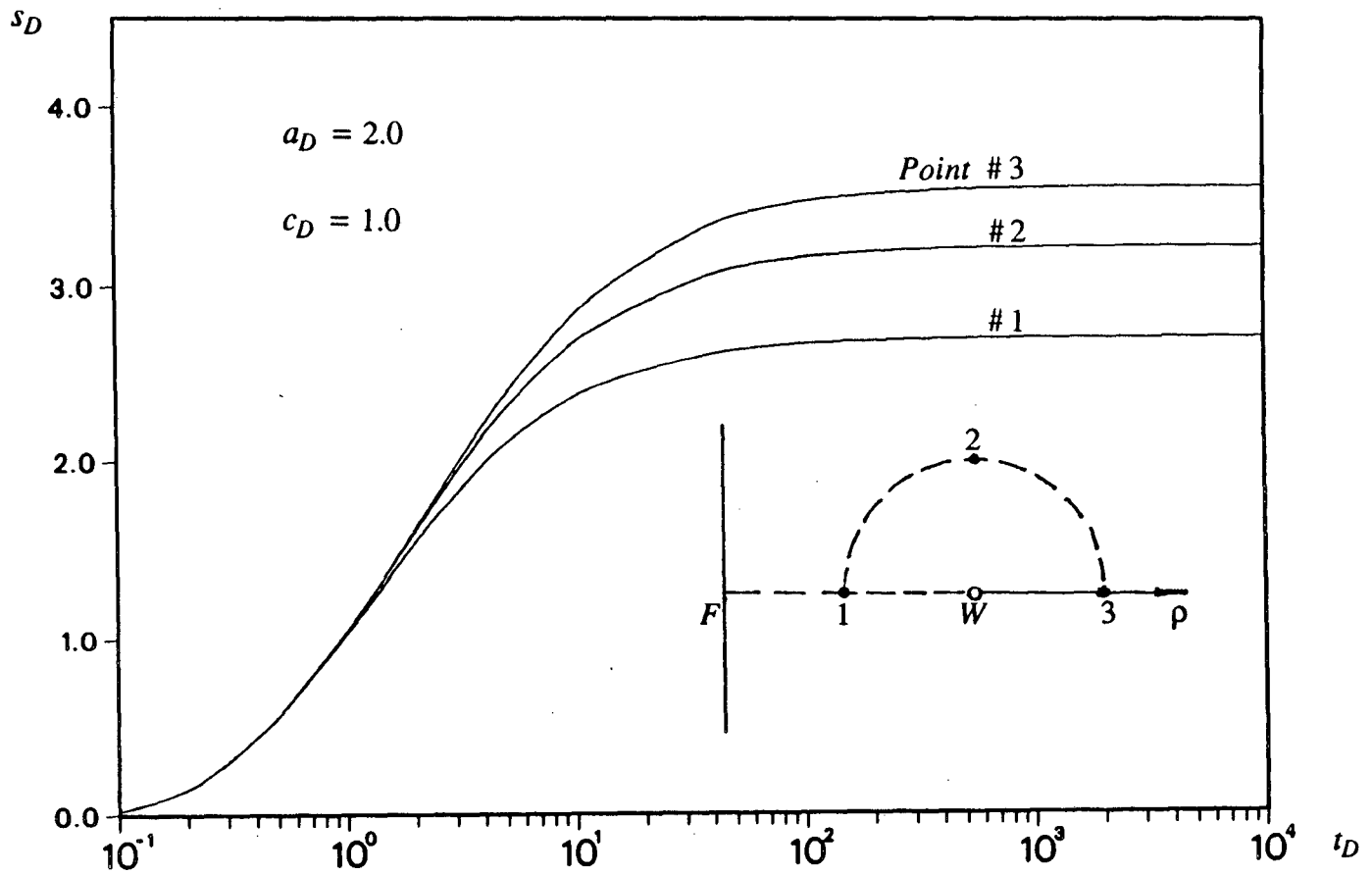

Figure 2.5 Effects of polar angles (θ) on dimensionless drawdown (s_D).

characteristics can be summarized from these type curves. The one is that all curves overlap with the Theis curve, s_T - t_D, at early time and then gradually deviate from it. The other is that all curves sooner or later tend to be horizontal.

Recalling that the total drawdown, s_D, is equal to the Theis drawdown, s_T, minus a component due to the recharge from the fault to the aquifer, s_F, it is necessary to study the behavior of variations of s_F versus t_D. Figure 2.6 is a semilog plot of two drawdown components, s_T and s_F as a function of dimensionless time, t_D, at Point #1. It is found that the s_F curve always starts from zero at early time, becomes non-zero later and eventually becomes parallel to the s_T curve (Theis curve), no matter how small c_D is. This provides a very good explanation for the shape of the type curves.

Actually, the most important and the most useful characteristic of the type curves is that the overall drawdown, s_D eventually becomes a constant. This is not only because the constant drawdown can easily be obtained from field data, but also because a study of this behavior can lead to some practical methods of determining the parameter of most interest, c_D.

2.3.4 Recharge Rate from Fault

The only possibility for drawdown in the aquifer tending to become constant (or flow in the whole system approaching steady state) is that the overall recharge rate from the fault to the aquifer, Q_r becomes equal to that of the pumping rate, Q. To give a proof analytically, it is better to evaluate the recharge rate first. The overall recharge rate, Q_r, is obviously the integration of the recharge flux, q_r given in (2-9), over total length of the fault.

$$Q_r = 2\int_0^\infty q_r\,dy = \frac{2T_f}{L}\int_0^\infty s_{a_1}|_{x=0}\,dy = \frac{2T_f}{L}\cdot(I_1 - I_2) \qquad (2\text{-}47)$$

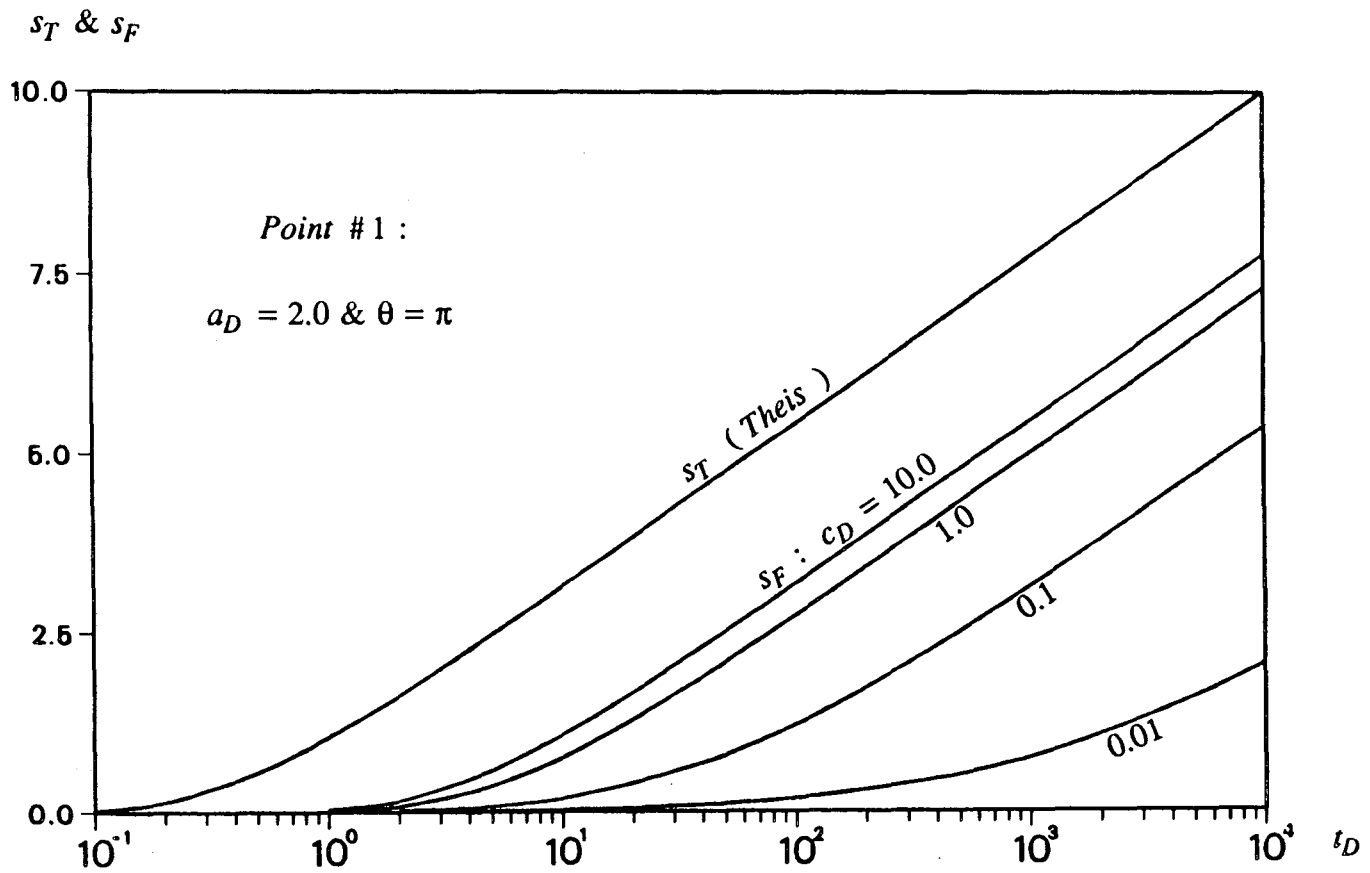

Figure 2.6 Comparison between two drawdown components at Point #1 (θ=π) for four different values of c_D.

where $s_{a_1}|_{x=0}$ can be obtained from (2-36); I_1 and I_2 are two components of the integration defined as:

$$I_1 = \frac{Q}{4\pi T_a}\int_0^{\infty} W\left[\frac{a^2+y^2}{4\alpha_a t}\right] dy \tag{2-48}$$

$$I_2 = \frac{Qc\sqrt{\alpha_a}e^{ca}}{4\sqrt{\pi}T_a}\int_0^{t}\frac{e^{c^2\alpha_a\tau}}{\sqrt{\tau}}\cdot erfc\left[\frac{a}{2\sqrt{\alpha_a\tau}}+c\sqrt{\alpha_a\tau}\right]d\tau\int_0^{\infty}e^{-y^2/(4\alpha_a\tau)}dy \tag{2-49}$$

Noting that,

$$\int_0^{\infty}e^{-y^2/(4\alpha_a\tau)}dy = 2\sqrt{\alpha_a\tau}\int_0^{\infty}e^{-u^2}du = \sqrt{\pi\alpha_a\tau}\cdot erf(\infty) = \sqrt{\pi\alpha_a\tau} \tag{2-50}$$

the double integration in (2-49) can be reduced to:

$$I_2 = \frac{Qc\,\alpha_a e^{ca}}{4T_a}\int_0^{t}e^{c^2\alpha_a\tau}\cdot erfc\left[\frac{a}{2\sqrt{\alpha_a\tau}}+c\sqrt{\alpha_a\tau}\right]d\tau \tag{2-51}$$

In (2-50), $u = y/(2\sqrt{\alpha_a\tau})$ is simply a change of variable and $erf(x) = \frac{2}{\sqrt{\pi}}\int_0^{x}e^{-u^2}du$ is the error function which is equal to 1 as $x = \infty$.

By integrating by parts and interchanging the integration order, the final solution for the overall recharge rate is:

$$Q_r = Q\left[erfc\left[\frac{a}{2\sqrt{\alpha_a t}}\right] - e^{ca+c^2\alpha_a t}\cdot erfc\left[\frac{a}{2\sqrt{\alpha_a t}}+c\sqrt{\alpha_a t}\right]\right] \tag{2-52}$$

Applying equations (2-43) and (2-44), the dimensionless recharge rate, $\overline{Q_r} = Q_r/Q$ is equal to:

$$\overline{Q_r} = erfc\left[\frac{a_D}{2\sqrt{t_D}}\right] - e^{c_D a_D + c_D^2 t_D}\cdot erfc\left[\frac{a_D}{2\sqrt{t_D}}+c_D\sqrt{t_D}\right] \tag{2-53}$$

Apparently, if $c_D = 0$, then from (2-53) $\overline{Q_r} = 0$. For any $c_D \neq 0$, by means of the rule of L'Hospital it is easy to prove that:

$$\lim_{t_D \to \infty} \overline{Q_r} = 1 - 0 = 1 \tag{2-54}$$

This result shows that the recharge rate, Q_r, indeed tends to become equal to the pumping rate, Q, as time becomes large. Figure 2.7 gives a set of $\overline{Q_r}$ - t_D curves. For any fixed value of a_D (here a_D = 2), a larger value of c_D can cause the recharge rate, Q_r, to approach the pumping rate, Q more rapidly. This is reasonable because a larger c_D means that the transmissivity of the fault, T_f, is larger or the recharge path, L, is shorter or both. As a result, it is easier for the source to compensate for the pumping rate earlier.

The effect of the dimensionless distance, a_D can also be studied. As shown on Figure 2.8, by fixing c_D to some value (c_D = 1 here) while changing a_D, one can see that the shapes of all curves are similar to each other. In other words, the variation of a_D only causes a time lag in the curve of $\overline{Q_r}$ - t_D. The farther the pumping well is from the fault, the longer the time will be for the flow field to achieve steady-state.

The above study on recharge rate reveals the mechanism of the important characteristics of the type curves. In the following, the applications of the solution will be discussed.

2.3.5 Determination of Parameters

The dimensionless solution (2-45) together with (2-46) can be used in engineering practice. Both the type curve studies and the recharge rate evaluation are in fact a kind of application with a common condition that all parameters (θ, a_D and c_D) are assumed to be known. This kind of application is rather straightforward and is classified as the " direct problem ". There is, however, another kind of problem to be handled. Conversely, the drawdown data (s_{a_1} vs. t) is obtained from a pumping test

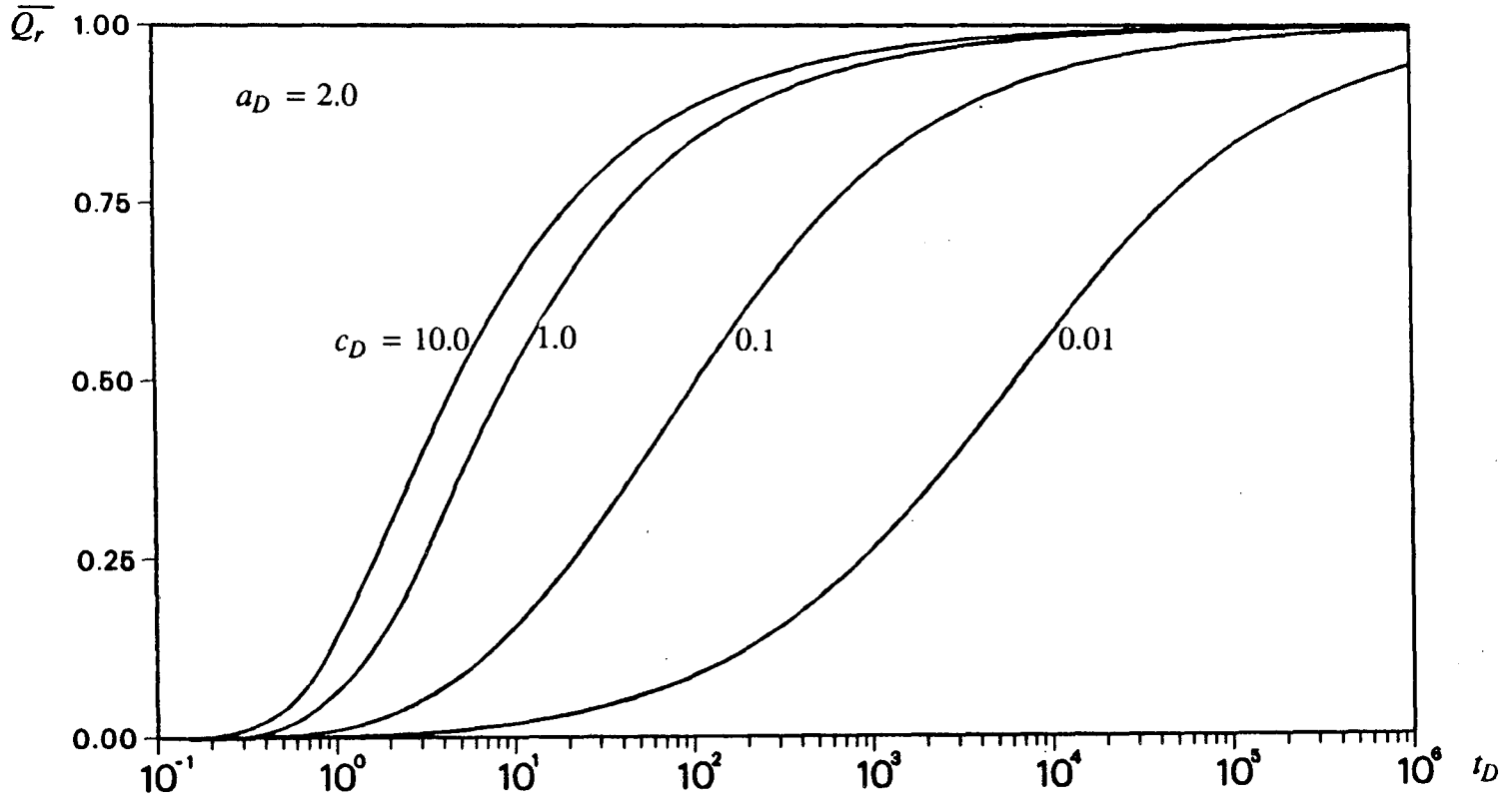

Figure 2.7 Effect of c_D on recharge rate from the fault to the aquifer.

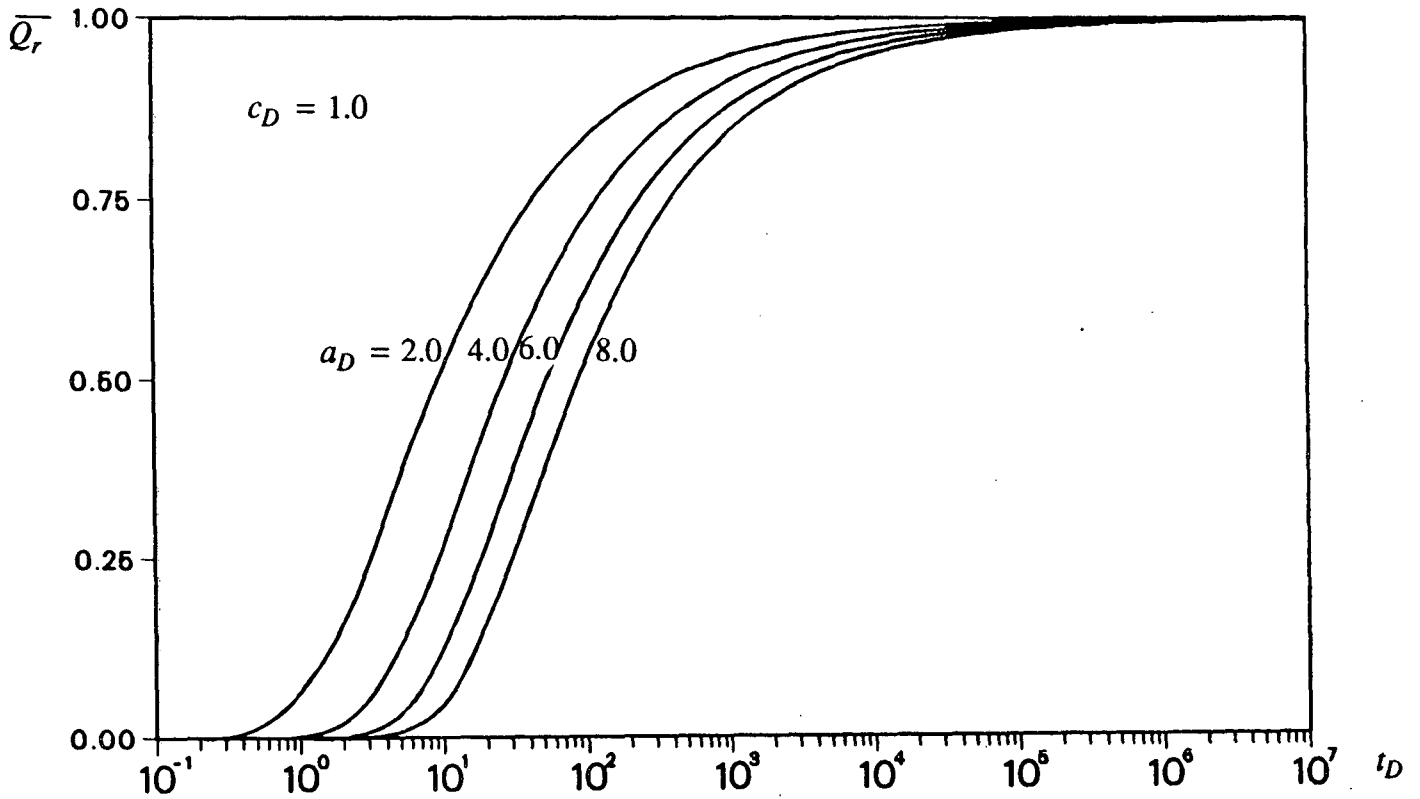

Figure 2.8 Effect of a_D on recharge rate from the fault to the aquifer.

and properties of the fault are to be determined. This is called the "inverse problem" and is of more interest in practice.

Recalling that all drawdown curves will overlap with the Theis curve at some early time, the hydraulic properties of the aquifer, K_a and S_{sa}, may be obtained by means of the conventional curve matching method without any difficulty. Among the other three parameters, c_D (or c) is probably the most difficult to determine. This is because a_D and θ can usually be obtained during geological investigations. Therefore, the major task of this problem is to find a practical way to determine the parameter c. If c is determined, the transmissivity of the fault, T_f can easily be computed using (2-23). Because the parameter c appears only in the second component of the solution, it seems that an analysis of this component is both important and necessary.

For convenience, an observation well at Point #1 ($\theta = \pi$) is first taken into consideration. Upon substitution of $\sin\theta = 0$ and $\cos\theta = -1$ into (2-45) and (2-46), the drawdown component due to fault recharge at Point #1 is:

$$s_{F_1} = \sqrt{\pi}\, c_D\, e^{2c_D \bar{d}} \int_0^{t_D} \frac{e^{c_D{}^2 \tau}}{\sqrt{\tau}} \cdot erfc\left[\frac{\bar{d}}{\sqrt{\tau}} + c_D\sqrt{\tau}\right] d\tau \qquad (2\text{-}55)$$

where $\bar{d}$ is a new dimensionless distance introduced for convenience.

$$\bar{d} = a_D - \frac{1}{2} \qquad (2\text{-}56)$$

Although it is difficult to integrate (2-55) precisely, it is easy to evaluate that approximately for the purposes of application. One of the methods to approximate (2-55) is based on a series expansion of the complementary error function and is described in Appendix C. With the approximation formulae available, two practical methods can be developed as follows.

Method 1. Time-Intersect Method

In groundwater literature, the so called " semilog " method is very effective in determining aquifer properties (such as the transmissivity T and the specific storage S_s) by means of a pumping test. Here, a similar method can also be developed. If a curve of s_F versus t_D is plotted on a semi-log paper (see Figure 2.9), the equation of straight line section of this curve for large values of t_D may be approximated by (C-9). Therefore, one can obtain an expression for t_{D_0}, the intersect time, by setting $s_{F_1}^{(0)} = 0$, which leads to:

$$e^X \cdot W(X) = \ln(0.562\, t_{D_0}/\bar{d}^2) \qquad or:$$

$$t_{D_0} = 1.78\bar{d}^2 e^{W(c_D \bar{d}) e^{c_D \bar{d}}} \tag{2-57}$$

This equation offers a way to determine c_D without using the method of type curve matching (the log-log method). To check the accuracy of this method, let us examine Figure 2.9. Based on the parameters used in this figure, $\bar{d}$ can be calculated from (2-56) to be equal to 1.5. Using (2-57) would yield a value of t_{D_0} which is equal to 6.3. The value of t_{D_0} obtained from Figure 2.9 reads 6.6. One may recall that (2-57) was derived by considering only one term of (C-4). A more accurate solution can be obtained by taking more terms in (C-4) and the determination of X will be based on the method of trial and error. In process of determining X, one needs to calculate $e^X \cdot W(X)$. Pagurova (1961) has given some of its values for $0.01 \le X \le 20.0$. For X out of this range, the value can easily be calculated by numerical integration. If a better accuracy is required, a plot of $Y = e^X W(X)$ should be carefully prepared in advance. Figure 2.10 gives part of the plot in the region of $0.1 \le X \le 3.0$, which can give a better result than that obtained from linear interpolation.

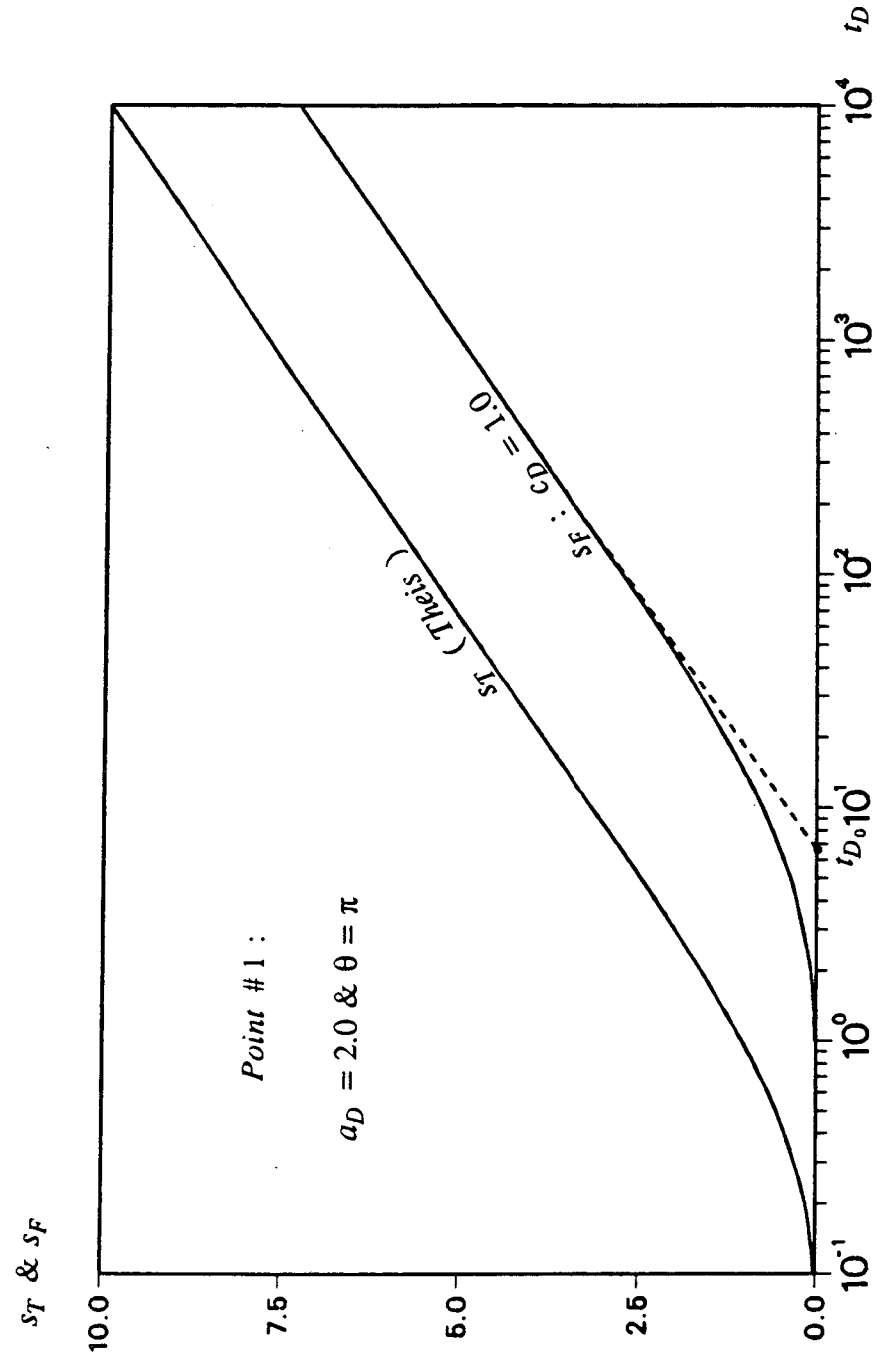

Figure 2.9 Dimensionless time-intersect, t_{D_0}.

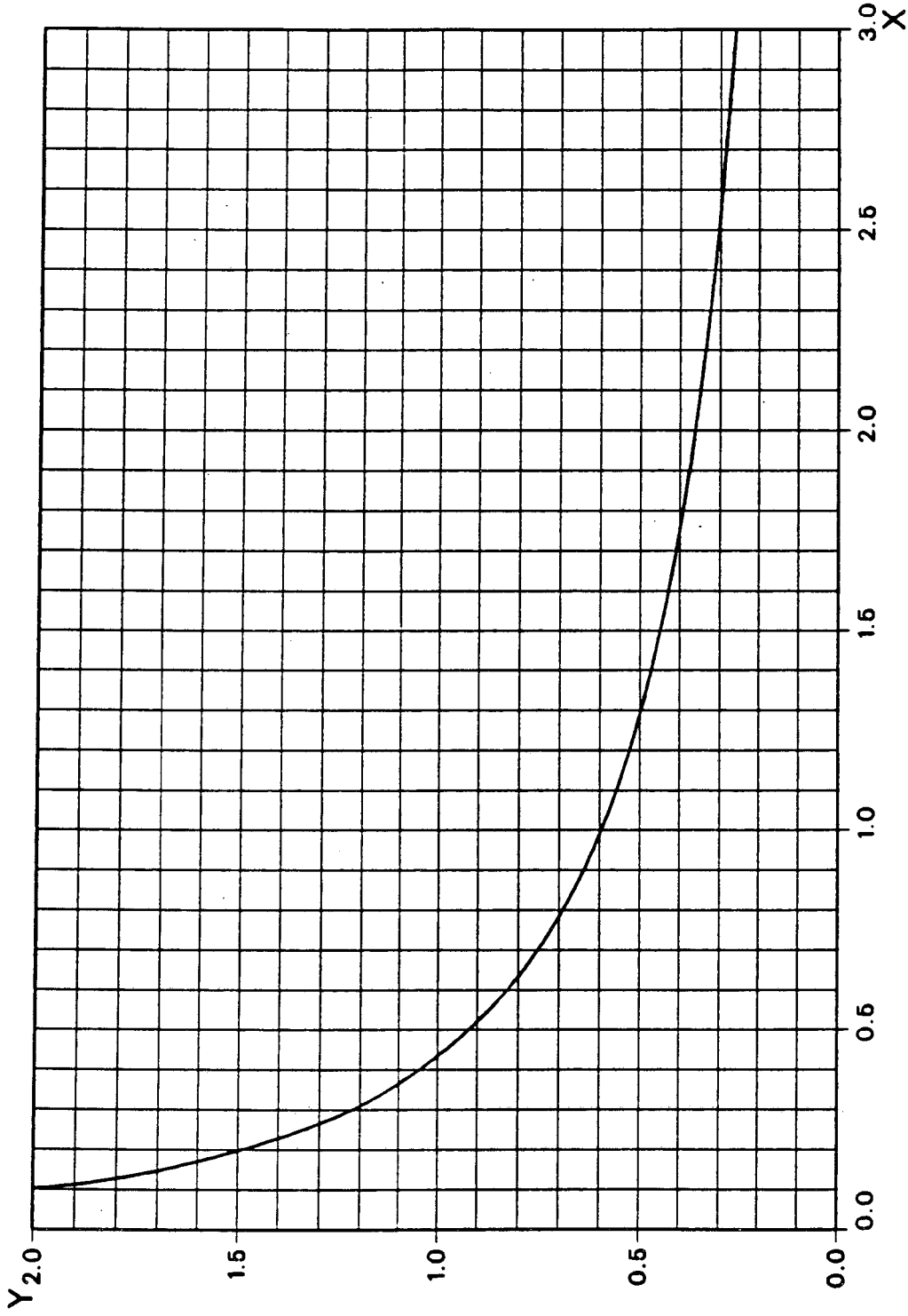

Figure 2.10 Curve of $Y = e^{X} \cdot W(X)$.

Method 2. Drawdown-Limit Method

As mentioned above, the drawdown, s_D at any given point in the aquifer that is recharged by a leaky fault, will always tend to a constant value, which can easily be obtained from field data if the pumping test lasts long enough. This constant value can be called the drawdown-limit. If the drawdown at Point #1 is represented by s_{D_1}, then:

$$s_{D_1} = s_{T_1} - s_{F_1} \tag{2-58}$$

where s_{T_1} is the Theis drawdown at Point #1 and is independent of θ. At large time, its approximate expression can be given by:

$$s_{T_1} \approx -0.5772 - ln(\frac{1}{4t_D}) \tag{2-59}$$

The approximate expression for s_{F_1} at large time can be obtained by adding (C-9), (C-13) and (C-15). If this sum and (2-59) are substituted into (2-58), one can get a set of approximate equations:

One Term:

$$s_{D_1} \approx 2\,ln(2\bar{d}) + e^X \cdot W(X) \tag{2-60}$$

Two Terms:

$$s_{D_1} \approx 2\,ln(2\bar{d}) - \frac{1}{4} + \frac{1}{4X} + (1 + \frac{X}{4})e^X \cdot W(X) \tag{2-61}$$

Three Terms:

$$s_{D_1} \approx 2ln(2\bar{d}) - \frac{X}{32} - \frac{11}{32} + \frac{5}{16X} - \frac{1}{16X^2} + (1 + \frac{3X}{8} + \frac{X^2}{32})e^X \cdot W(X) \tag{2-62}$$

Because $\bar{d}$ and s_{D_1} are some known values, it is easy to get X (and thus c_D) using trial and error. There is no need to give examples of the calculation. However,

it is necessary to evaluate the errors for different cases caused by the above approximations. This can be achieved by calculating the dimensionless drawdown, s_{D_1}, for both the exact solution (2-45) (represented by (E) in the table) and the approximate solutions (2-60) through (2-62) (represented by (A) and (1), (2) and (3) correspondingly), and then compare the results. Table 2.2 shows the magnitude of errors calculated from incorporation of one, two or three terms of (2-45) for two values of X.

Table 2.2 Drawdown–Limit at Point #1

a_D	$\bar{d}=a_D-0.5$	c_D	$X=c_D\cdot\bar{d}$	$s_{D_1}(E)$	$s_{D_1}(A)$	*error*
2.0	1.5	1.0	1.5	2.721	(1) 2.6455 (2) 2.7302 (3) 2.7191	-2.8% +0.3% -0.07%
2.0	1.5	0.1	0.15	4.462	(1) 3.8987 (2) 5.3792 (3) 2.9527	-16.0% +15.9% -36.4%

More calculations have shown that the larger the X is, the better the result will be. It is therefore desirable for the observation well to be drilled close to the pumping well (to get a small r and thus a large X).

It has been pointed out that the above equations are derived at Point #1 ($\theta = \pi$). However, this method is valid for any arbitrary point. In fact, a formula which is quite similar to (C-8) can be obtained for arbitrary values of θ in the same way. The result is:

$$s_F^{(0)} = W\left[\frac{\overline{d_1}^2}{t_D}\right] - e^{\overline{d_2}c_D} \cdot W\left[\frac{\overline{d_1}^2}{t_D} + \overline{d_2}c_D\right] \tag{2-63}$$

where the new parameters, $\overline{d_1}$ and $\overline{d_2}$ are defined as:

$$\overline{d_1} = \sqrt{a_D{}^2 + a_D\cos\theta + 1/4} \quad \& \quad \overline{d_2} = \frac{a_D{}^2 + a_D\cos\theta + 1/4}{a_D + \cos\theta/2} \tag{2-64}$$

One can see that as $\theta = \pi$, $\overline{d_1} = \overline{d_2} = \overline{d}$ and thus (2-63) is reduced to (C-8). Another special case is at Point #3. At this point, $\theta = 0$ and $\cos\theta = 1$. Substituting these values into (2-64) leads to: $\overline{d_1} = \overline{d_2} = \overline{d'} = a_D + 1/2$. Obviously, (2-63) will give exactly the same form as that of (C-8). Therefore, all the above discussion and results for Point #1 can be applied to Point #3 by simply changing the subscript, 1 to 3 and using $\overline{d'}$ instead of $\overline{d}$. Estimation of the errors due to the approximations in the results at Point #3 are shown on Table 2.3.

Table 2.3 Drawdown–Limit at Point #3

a_D	$\overline{d'} = a_D + 0.5$	c_D	$X = c_D \cdot \overline{d'}$	$s_{D_3}(E)$	$s_{D_3}(A)$	*error*
2.0	2.5	1.0	2.5	3.560	(1) 3.5224 (2) 3.5621 (3) 3.5594	-1.1% +0.2% -0.01%
2.0	2.5	0.1	0.25	5.065	(1) 4.5598 (2) 5.3936 (3) 4.5865	-10.0% +6.5% -9.4%

Comparison between the results of Tables 2.2 and 2.3 shows that the calculation at Point #3 can give a higher accuracy. The reason is that X is always larger at Point

#3 than that at Point #1. Thus, another recommendation is that it is better to drill the observation well at Point #3.

It is apparent from the tables 2.2 and 2.3 that the error introduced by this method decreases as X becomes larger than 0.25, while it increases as X becomes smaller than 0.25. Furthermore, as the value of X is much larger than 0.25 (for example, $X = 1.5$), this method can give a very good result even for a one-term approximation. Recalling that the value of X is related to a and r through the formula, $X = c \cdot (a \pm \frac{r}{2})$ at Point #3 and Point #1, it is always possible to choose suitable values of a and r such that the above methods may be applied. For a given aquifer and a leaky fault, the value of c is independent of the locations of pumping and observation wells relative to the fault. Therefore, one should choose the location of the wells in such a way to maximize the magnitude of X. However, the larger the value of X, the longer pumping time will be required for the recharge effect of the fault to reach the observation well. Therefore, the choice of a and r may be restricted by the time of test.

2.3.6 Requirements of Time

(a) Time of Separation

It has been pointed out that all type curves overlap with the Theis curve at early time and then branch out, which means that there exists an instant of time when the curves separate. According to the solution, this corresponds to the instant when the drawdown component due to fault recharge, s_F becomes larger than zero. Theoretically speaking, s_F is always larger than zero as $t > 0$ (or $t_D > 0$). However, its value is too small to be detected at early time. Assuming the detectable drawdown difference is Δs_D and the time of separation is t_{D_s}, then, t_{D_s} is a function of c_D, a_D, θ

and Δs_D. Although there is no explicit expression for this functional relationship, an implicit formula can be derived from (2-45) and (2-46), that is:

$$\Delta s_D = \sqrt{\pi}\, c_D\, e^{c_D(2a_D+\cos\theta)} \int_0^{t_{D_s}} \frac{e^{c_D{}^2\tau - \sin^2\theta/(4\tau)}}{\sqrt{\tau}} \cdot erfc\left[\frac{2a_D+\cos\theta}{2\sqrt{\tau}} + c_D\sqrt{\tau}\right] d\tau \qquad (2\text{-}65)$$

For a given value of $\Delta s_D = 0.1$, Figure 2.11 gives the plots of t_{D_s} as a function of c_D and a_D at Points #1 and #3 (the data points are calculated using (2-65) and the method of trial and error). It may be seen that for very small values of c_D (for example, $c_D = 10^{-5}$), the time of separation is less affected by a_D or θ.

(b) Time of Constant Drawdown

It has also been pointed out that the drawdown at any given point in the aquifer will always tend to a constant value as time becomes large. In practice, it is impossible to continue a pumping test forever; nevertheless, in most cases, the increase in drawdown in an observation well will become too small to be measured as the length of the test increases. Similarly, a criterion for the time of constant drawdown can be set up in such a way that the drawdown, s_D will be said to have reached a constant value if the gradient of variation, $\frac{ds_D}{dt_D}$ becomes less than some certain value, say, $s_D{}'$. If the corresponding time is represented by t_{D_c}, then from (2-45) and (2-46), one can obtain:

$$\frac{ds_D}{dt_D} = \frac{e^{-1/(4t_D)}}{t_D} - \sqrt{\pi}\, c_D\, e^{c_D(2a_D+\cos\theta)} \frac{e^{c_D{}^2 t_D - \sin^2\theta/(4t_D)}}{\sqrt{t_D}} \cdot erfc\left[\frac{2a_D+\cos\theta}{2\sqrt{t_D}} + c_D\sqrt{t_D}\right] \quad or:$$

$$s_D{}' = \frac{e^{-1/(4t_{D_c})}}{t_{D_c}} - \sqrt{\pi} c_D\, e^{c_D(2a_D+\cos\theta)} \frac{e^{c_D{}^2 t_{D_c} - \sin^2\theta/(4t_{D_c})}}{\sqrt{t_{D_c}}} \cdot erfc\left[\frac{2a_D+\cos\theta}{2\sqrt{t_{D_c}}} + c_D\sqrt{t_{D_c}}\right] \qquad (2\text{-}66)$$

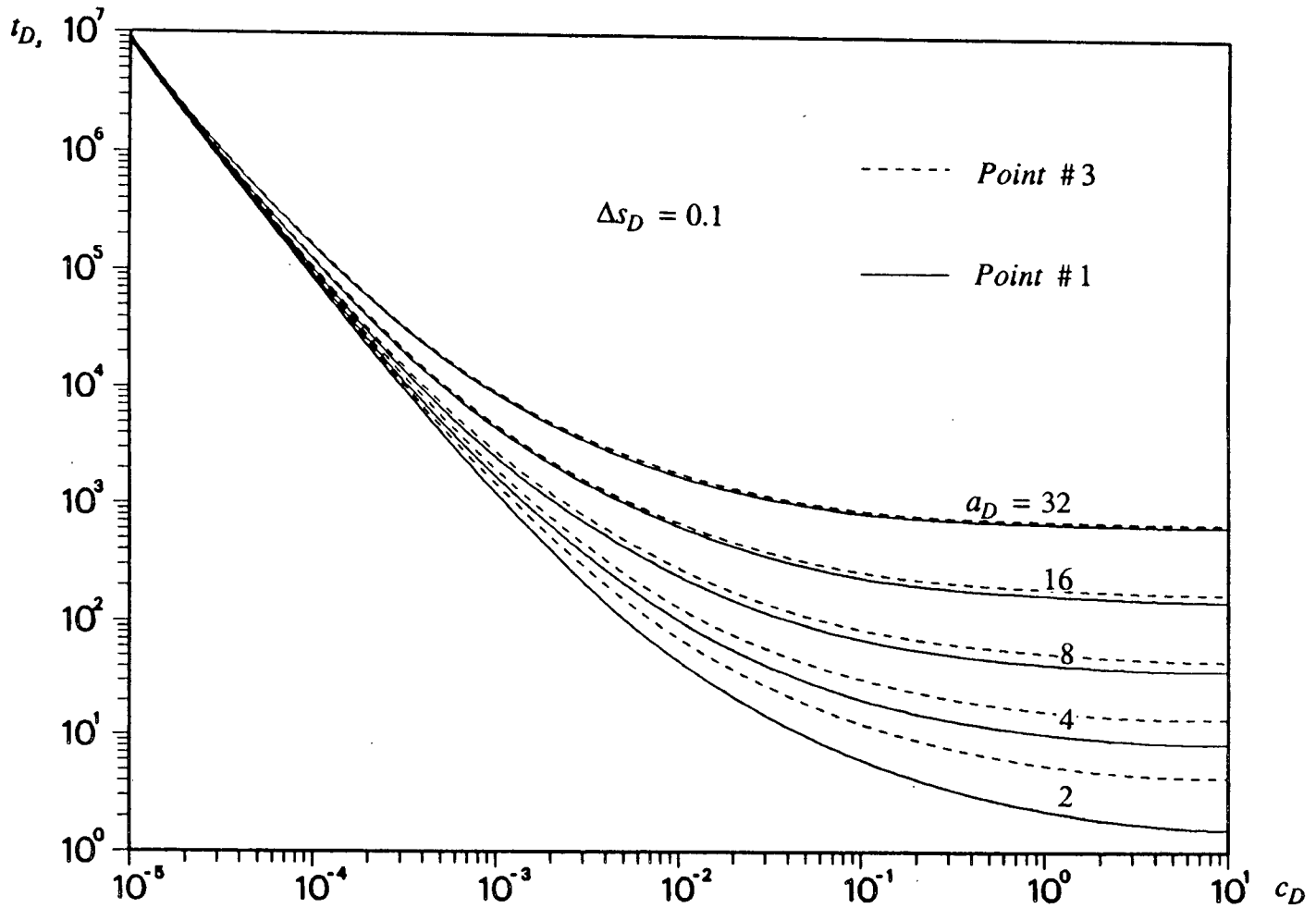

Figure 2.11 Time of separation (t_{D_s}) as a function of c_D and a_D.

At Point #1 and #3, for a given value of s_D', the time of constant drawdown, t_{D_c} can be plotted as a function of c_D and a_D as shown in Figure 2.12.

2.4 Case 2: Variable-Head at the Other End of the Fault

The above solutions are based on the assumption that head at the other end of the fault remains constant (or approximately constant) during the pumping test. In some cases, if the leaky fault cuts through several aquifers and if drawdowns in the unpumped aquifers are not negligibly small, then one needs to consider the effects of drawdowns in the unpumped aquifers as well. Apparently, this will make the whole problem much more complicated. As an example, a two-aquifer system will be investigated here.

Figure 2.13 shows a schematic view of the problem. In this figure, water is pumped from the lower aquifer at a constant rate, Q; and the z axis is chosen to be vertically upward. If on the other hand water is pumped from the upper aquifer, then the z axis would be downward. For purposes of identification, the subscript, u will be used to represent all variables and parameters related to the the unpumped aquifer while all the old notations will keep the same meaning as before. As shown on the figure, the selected coordinates are the same as that for the previous case, i.e., setting the y axis along the fault and the x axis perpendicular to the fault while passing through the well. In the unpumped aquifer, by the virtue of symmetry, only one half of the aquifer needs to be taken into consideration (in the following, the half corresponding to $x \leq 0$ will be used for convenience). Leakage from the fault is assumed to be proportional to the head difference between pumped and unpumped aquifers. Based on these analyses, the governing equations can be written down

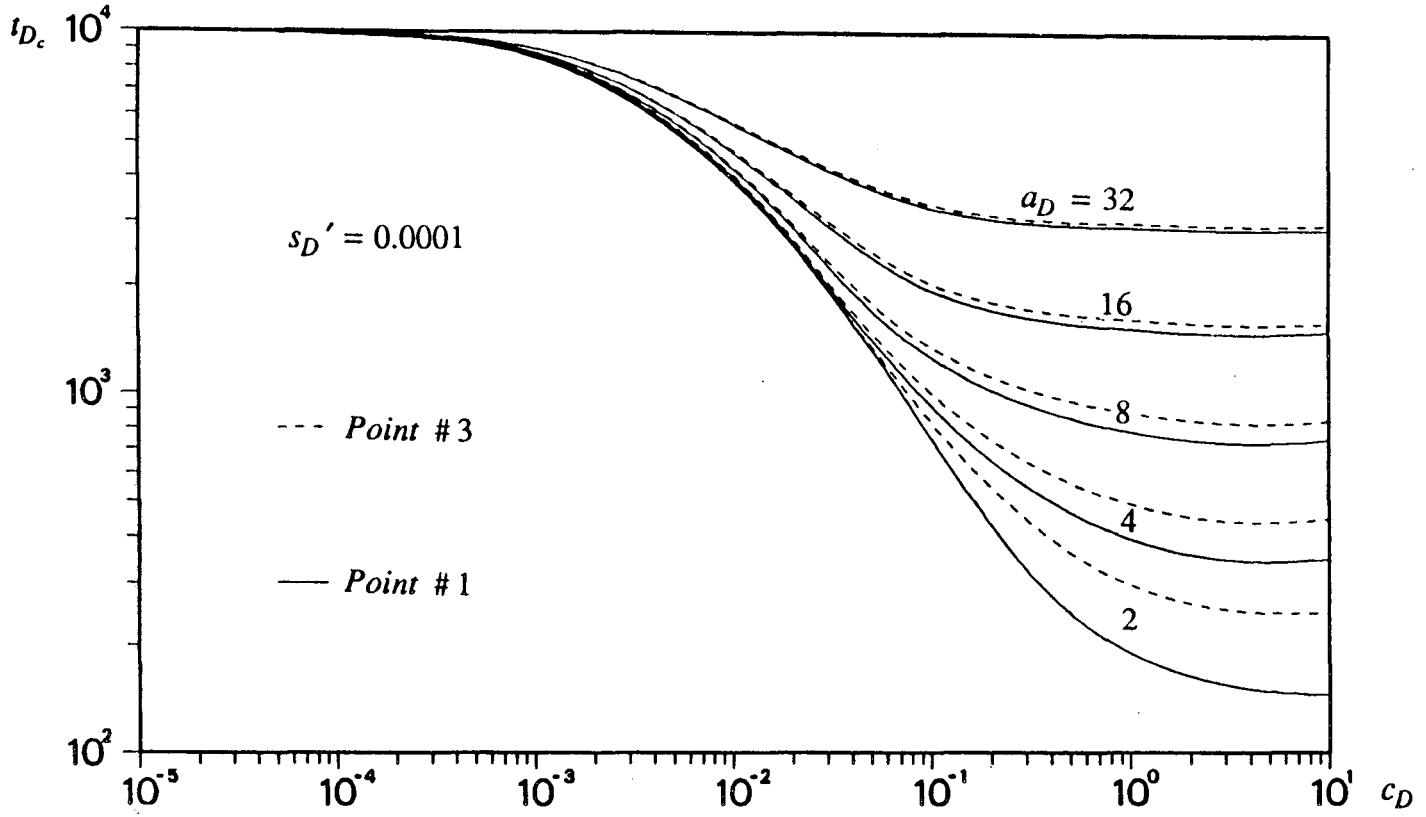

Figure 2.12 Time of constant-drawdown (t_{D_c}) as a function of c_D and a_D.

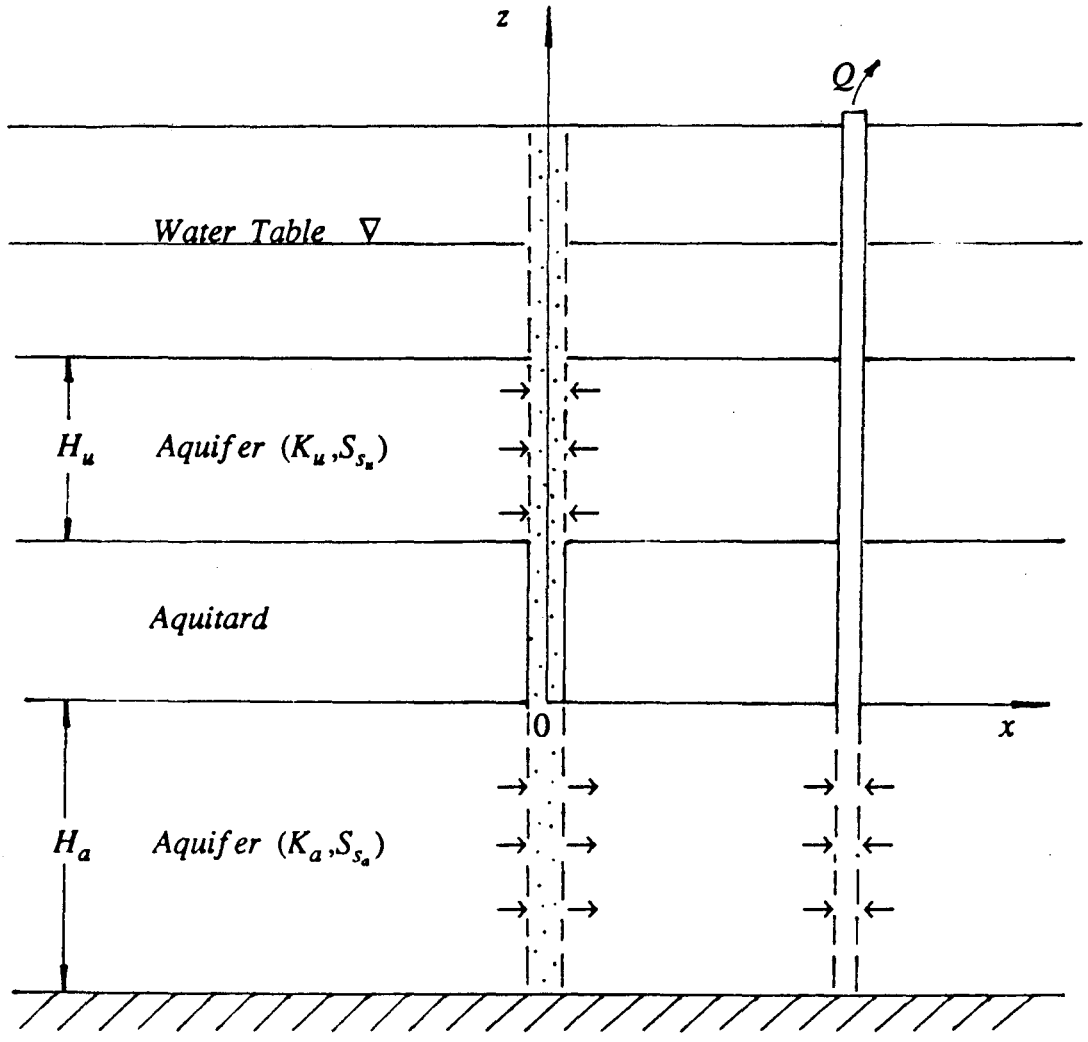

Figure 2.13 Schematic cross-section of an aquifer-fault-aquifer system.

directly from the previous section:

$$\frac{\partial s_{a_1}}{\partial t} = \alpha_a \left[\frac{\partial^2 s_{a_1}}{\partial x^2} + \frac{\partial^2 s_{a_1}}{\partial y^2} \right] + \frac{\alpha_a Q}{T_a} \cdot \delta(x-a) \cdot \delta(y) \qquad (x \geq 0) \tag{2-1}$$

$$\frac{\partial s_{a_2}}{\partial t} = \alpha_a \left[\frac{\partial^2 s_{a_2}}{\partial x^2} + \frac{\partial^2 s_{a_2}}{\partial y^2} \right] \qquad (x \leq 0) \tag{2-2}$$

$$\frac{\partial s_u}{\partial t} = \alpha_u \left[\frac{\partial^2 s_u}{\partial x^2} + \frac{\partial^2 s_u}{\partial y^2} \right] \qquad (x \leq 0) \tag{2-67}$$

It is convenient to have the equation for the unpumped aquifer in a similar form to that for the pumped aquifer in Region II.

The initial condition is very similar to (2-4):

$$s_{a_1} = s_{a_2} = s_u = 0 \quad at \quad t = 0 \tag{2-68}$$

Again, the boundary conditions for this case are similar to those for the previous case:

$$s_{a_1} = 0 \quad at \quad x \to +\infty \quad or \quad y \to \pm\infty \tag{2-5}$$

$$s_u = s_{a_2} = 0 \quad at \quad x \to -\infty \quad or \quad y \to \pm\infty \tag{2-69}$$

$$s_{a_1}|_{x=0} = s_{a_2}|_{x=0} \tag{2-7}$$

$$T_a \left[\frac{\partial s_{a_1}}{\partial x} \right]_{x=0} = T_a \left[\frac{\partial s_{a_2}}{\partial x} \right]_{x=0} + T_f \frac{s_{a_1}|_{x=0} - s_u|_{x=0}}{L} \tag{2-70}$$

$$T_u \left[\frac{\partial s_u}{\partial x} \right]_{x=0} = 0.5\, T_f \frac{s_{a_1}|_{x=0} - s_u|_{x=0}}{L} \tag{2-71}$$

The solution process is very similar to that in the previous case. After taking the Laplace transform, (2-10) and the Fourier transform, (2-11), the governing equations for the pumped aquifer parts and the unpumped aquifer are simply,

$$\frac{d^2 w_{a_1}}{dx^2} - A^2 w_{a_1} = -\frac{Q \cdot \delta(x-a)}{T_a} \cdot \frac{1}{p} \qquad (x \geq 0) \tag{2-14}$$

$$\frac{d^2 w_{a_2}}{dx^2} - A^2 w_{a_2} = 0 \qquad (x \leq 0) \tag{2-15}$$

$$\frac{d^2 w_u}{dx^2} - A_u{}^2 w_u = 0 \qquad (x \le 0) \tag{2-72}$$

where the definition for A_u is similar to that for A defined by (2-16):

$$A_u = \sqrt{p/\alpha_u + \rho^2} \tag{2-73}$$

The unused boundary conditions in the transformed domain are as follows:

$$w_{a_1} = 0 \quad at \quad x \to +\infty \tag{2-17}$$

$$w_u = w_{a_2} = 0 \quad at \quad x \to -\infty \tag{2-74}$$

$$w_{a_1}|_{x=0} = w_{a_2}|_{x=0} \tag{2-19}$$

$$T_a \left[\frac{dw_{a_1}}{dx}\right]_{x=0} = T_a \left[\frac{dw_{a_2}}{dx}\right]_{x=0} + T_f \frac{w_{a_1}|_{x=0} - w_u|_{x=0}}{L} \tag{2-75}$$

$$T_u \left[\frac{dw_u}{dx}\right]_{x=0} = 0.5\, T_f \frac{w_{a_1}|_{x=0} - w_u|_{x=0}}{L} \tag{2-76}$$

The solutions which can satisfy the governing equations and the boundary conditions, (2-17) and (2-74) are as follows:

$$w_{a_1} = \frac{Q}{2T_a} \cdot \frac{e^{-|x-a|A}}{pA} + k_1 e^{-xA} \qquad (x \ge 0) \tag{2-77}$$

$$w_{a_2} = k_2 e^{xA} \qquad (x \le 0) \tag{2-78}$$

$$w_u = k_u e^{xA_u} \qquad (x \le 0) \tag{2-79}$$

Substituting the solutions into the remaining boundary conditions, (2-19), (2-75) and (2-76), and then solving the three equations about k_1, k_2 and k_u simultaneously, one can get:

$$k_1 = -\frac{Q}{2T_a} \cdot \frac{A_u}{A} \cdot \frac{e^{-aA}}{p} \cdot \frac{1}{A/T_D + A_u + A \cdot A_u / c} \tag{2-80}$$

$$k_2 = \frac{Q}{2T_a} \cdot \frac{e^{-aA}}{p} \cdot \frac{1/T_D + A_u/c}{A/T_D + A_u + A \cdot A_u / c} \tag{2-81}$$

$$k_u = \frac{Q}{2T_a} \cdot \frac{e^{-aA}}{p} \cdot \frac{1/T_D}{A/T_D + A_u + A \cdot A_u / c} \tag{2-82}$$

where c has been defined by (2-23) and the new parameter T_D is the transmissivity

ratio of the unpumped aquifer to the pumped aquifer, i.e.,

$$T_D = \frac{T_u}{T_a} \tag{2-83}$$

These coefficients are then substituted into solutions (2-77) through (2-79). The drawdowns, s_{a_1}, s_{a_2} and s_u in the transformed domain are:

$$w_{a_1} = \frac{Q}{2T_a}\left[\frac{e^{-|x-a|A}}{pA} - \frac{A_u}{A}\cdot\frac{e^{-(x+a)A}}{p}\cdot\frac{1}{A/T_D + A_u + A\cdot A_u/c}\right] \tag{2-84}$$

$$w_{a_2} = \frac{Q}{2T_a}\cdot\frac{e^{-(a-x)A}}{p}\cdot\frac{1/T_D + A_u/c}{A/T_D + A_u + A\cdot A_u/c} \tag{2-85}$$

$$w_u = \frac{Q}{2T_a}\cdot\frac{e^{-aA+xA_u}}{p}\cdot\frac{1/T_D}{A/T_D + A_u + A\cdot A_u/c} \tag{2-86}$$

The inversion for the first term in (2-84) has already been worked out in (2-32). The inversions for the other terms will be developed for different possibilities.

2.4.1 Possibility 1: Equal Aquifer-Diffusivities

This implies that $\alpha_u = \alpha_a = \alpha$. Under this condition, the above solutions can be greatly simplified by means of the substitution of $A_u = A$:

$$w_{a_1} = \frac{Q}{2T_a}\left[\frac{e^{-|x-a|A}}{pA} - \frac{e^{-(x+a)A}}{p}\cdot\frac{1}{A(A/c+1/T_D+1)}\right] \tag{2-87}$$

$$w_{a_2} = \frac{Q}{2T_a}\cdot\frac{e^{-(a-x)A}}{p}\cdot\frac{1/T_D + A/c}{A(A/c+1/T_D+1)}$$

$$= \frac{Q}{2T_a}\left[\frac{e^{-(a-x)A}}{pA} - \frac{e^{-(a-x)A}}{p}\cdot\frac{1}{A(A/c+1/T_D+1)}\right] \tag{2-88}$$

$$w_u = \frac{Q}{2T_a}\cdot\frac{e^{-(a-x)A}}{p}\cdot\frac{1/T_D}{A(A/c+1/T_D+1)} \tag{2-89}$$

In fact, the basic factor in the above solutions can be further decomposed as follows:

$$\frac{1}{A(A/c+1/T_D+1)} = \frac{1}{1/T_D+1}\cdot\left[\frac{1}{A} - \frac{1}{A + c(1/T_D+1)}\right]$$

$$= \frac{c}{c'} \cdot \left(\frac{1}{A} - \frac{1}{A + c'} \right) \tag{2-90}$$

where the newly introduced parameter c' is a constant which is equal to:

$$c' = c \cdot (1/T_D + 1) = c \cdot k \tag{2-91}$$

where $k \geq 1$ is a new constant which is very important in the double-aquifer problem. Its significance will be discussed later.

This decomposition is very convenient because one can use the available inversion formulae, (2-32) and (2-34) in this analysis. It is very easy to write down the final solutions:

$$s_{a_1} = \frac{Q}{4\pi T_a} W\left[\frac{(x-a)^2 + y^2}{4\alpha_a t} \right] - \frac{Qc\sqrt{\alpha_a} e^{c'(a+x)}}{4\sqrt{\pi} T_a} \int_0^t g'_1(\tau) d\tau$$

$$(x \geq 0) \tag{2-92}$$

$$s_{a_2} = \frac{Q}{4\pi T_a} W\left[\frac{(x-a)^2 + y^2}{4\alpha_a t} \right] - \frac{Qc\sqrt{\alpha_a} e^{c'(a-x)}}{4\sqrt{\pi} T_a} \int_0^t g'_2(\tau) d\tau$$

$$(x \leq 0) \tag{2-93}$$

$$s_u = \frac{1}{T_D} \cdot \frac{Qc\sqrt{\alpha_a} e^{c'(a-x)}}{4\sqrt{\pi} T_a} \int_0^t g'_2(\tau) d\tau \qquad (x \leq 0) \tag{2-94}$$

where the two integrands, $g'_1(\tau)$ and $g'_2(\tau)$, are similarly defined as that in (2-35) except c' will be used for c.

The unified solution for any value of x can easily be written for drawdowns in both aquifers:

$$s_a = \frac{Q}{4\pi T_a} W\left[\frac{(x-a)^2 + y^2}{4\alpha_a t} \right] - \frac{Qc\sqrt{\alpha_a} e^{c'(|x|+a)}}{4\sqrt{\pi} T_a} \int_0^t g'(\tau) d\tau \tag{2-95}$$

$$s_u = \frac{1}{T_D} \cdot \frac{Qc\sqrt{\alpha_a} e^{c'(|x|+a)}}{4\sqrt{\pi} T_a} \int_0^t g'(\tau) d\tau \tag{2-96}$$

where $g'(\tau)$ can be obtained by replacing c by c' in (2-39).

If the transmissivity of the unpumped aquifer is much larger than that of the pumped aquifer (possibly due to the large difference of thickness), or in other words, if the transmissivity ratio, T_D, is very large, then the definition given by (2-91) can lead to: $k \simeq 1.$ and $c' \simeq c$. Under this condition, the drawdown in the unpumped aquifer will be negligibly small, and the solution of the drawdown in the pumped aquifer is reduced to the solution for the previous case, i.e., (2-38).

The non-dimensionalization of these solutions can be accomplished in a manner similar to that of the solutions in the previous section. For example, by applying the dimensionless formulae (2-43) and (2-44), the dimensionless solution of (2-92) is similar to that of (2-36):

$$\begin{aligned} s_D &= s_T - s_F \\ &= W\left[\frac{1}{4t_D}\right] - \frac{1}{k}\cdot\sqrt{\pi}\, c'_D\, e^{c'_D(2a_D+\cos\theta)} \int_0^{t_D} g'_1(\tau)\, d\tau \end{aligned} \tag{2-97}$$

where

$$g'_1(\tau) = \frac{e^{c'^2_D\tau - \sin^2\theta/(4\tau)}}{\sqrt{\tau}} \cdot erfc\left[\frac{2a_D+\cos\theta}{2\sqrt{\tau}} + c'_D\sqrt{\tau}\right] \tag{2-98}$$

and $c'_D = c' \cdot r = c_D \cdot k$.

Comparing these two equations with (2-45) and (2-46), respectively, it can easily be found that c_D has been replaced by c'_D. Additionally, there is a coefficient of $\frac{1}{k}$ in front of the second term in (2-97). Type curves for the case of equal-diffusivity can be developed using (2-97).

Figure 2.14A shows the effect of the transmissivity ratio, T_D, at Point #1 ($\theta = \pi$). The solid line represents the case of $T_D = \infty$, which is in fact the solution in the previ-

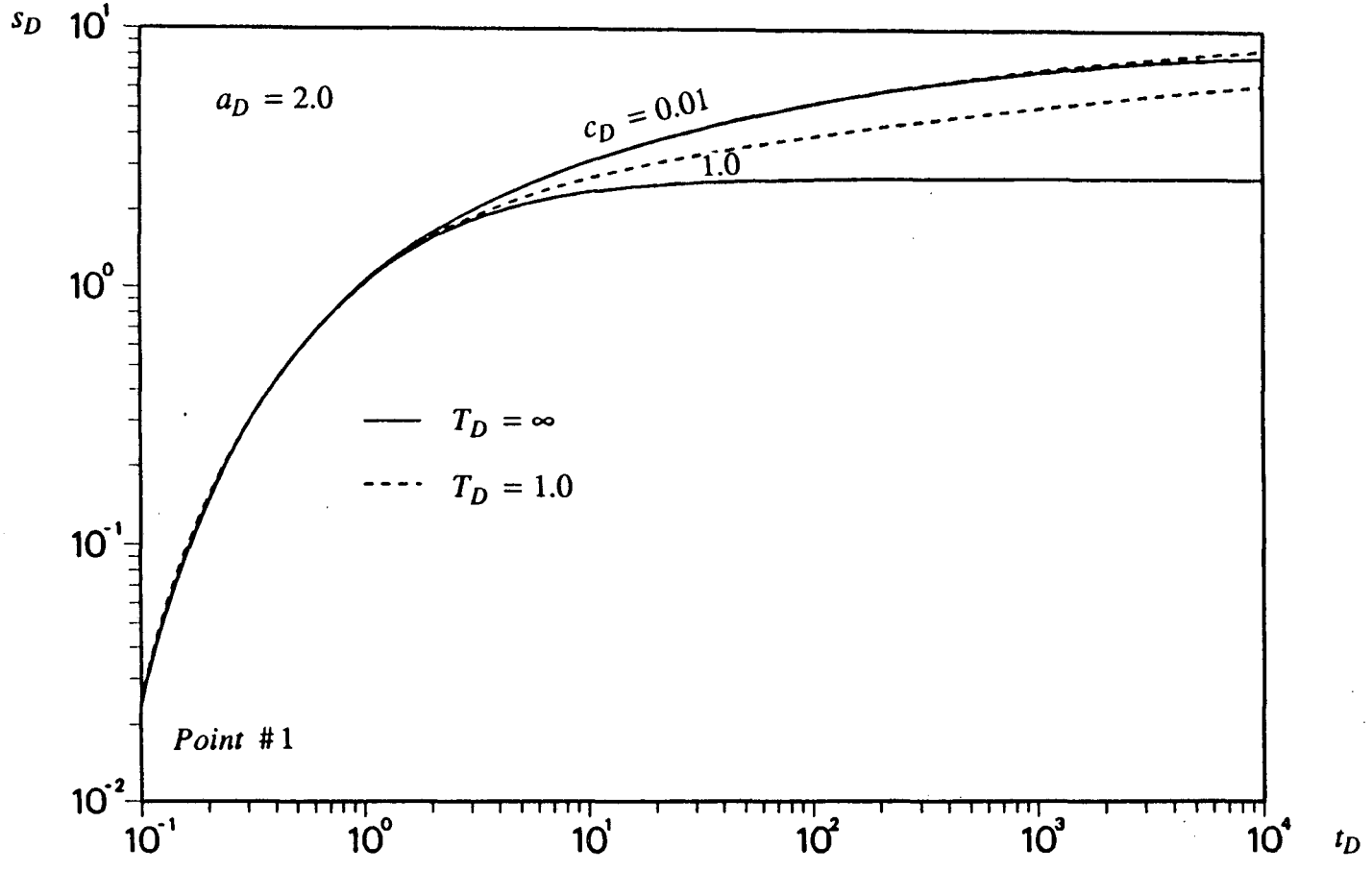

Figure 2.14A Effect of transmissivity ratio (T_D) on dimensionless drawdown (s_D) for two values of c_D, from the equal-diffusivity solution.

ous section. The dashed line represents the case of $T_D = 1.0$, which means that the two aquifers have the same value of transmissivity. For certain values of c_D, the dashed line is always higher than the solid line except at a period of early time when drawdown in the unpumped aquifer is negligibly small. Apparently, the drawdown in the unpumped aquifer has the effect of increasing the drawdown in the pumped aquifer. If $T_D = 0$, the unpumped aquifer can not transfer any water to the pumped aquifer, which means that the solution will reduce to the Theis solution. This can be shown from (2-97) by setting $k = \infty$.

Figure 2.14B is plotted for the purpose of showing that for certain values of T_D (for example, $T_D = 1.0$), the variation of c_D has only a limited effect on the type curves. By definition, increasing the value of c_D will always increase the ability of the fault in conducting water from the unpumped aquifer to the pumped aquifer and therefore will decrease the drawdown in the pumped aquifer. However, as c_D becomes large enough, a further increase in c_D will have less effect in reducing drawdowns in the pumped aquifer. The mechanism is that the amount of water which can be delivered to the pumped aquifer is not only controlled by the transmissivity of the fault (proportional to c_D) but is also controlled by the transmissivity of the unpumped aquifer (proportional to T_D).

In Figure 2.14C, the type curves at Point #1 are plotted on semilog paper. The main difference between these type curves and the ones presented earlier (Figure 2.5) is that the drawdown curves here will never become horizontal no matter how large a value of c_D is given.

An interesting discovery from the comparison between solutions (2-95) and (2-96)

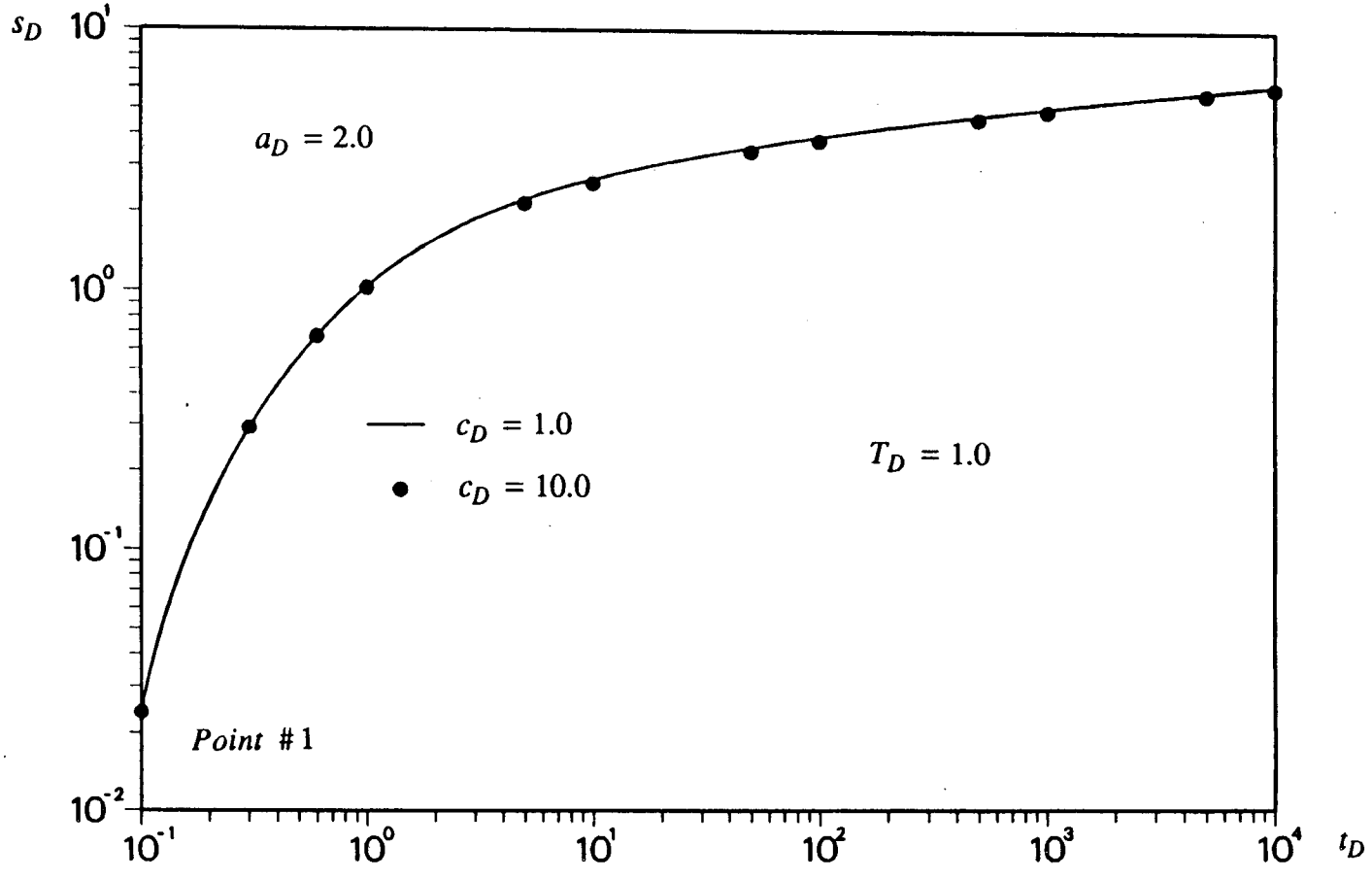

Figure 2.14B Limitation of c_D effect on dimensionless drawdown (s_D) for the case of two identical aquifers.

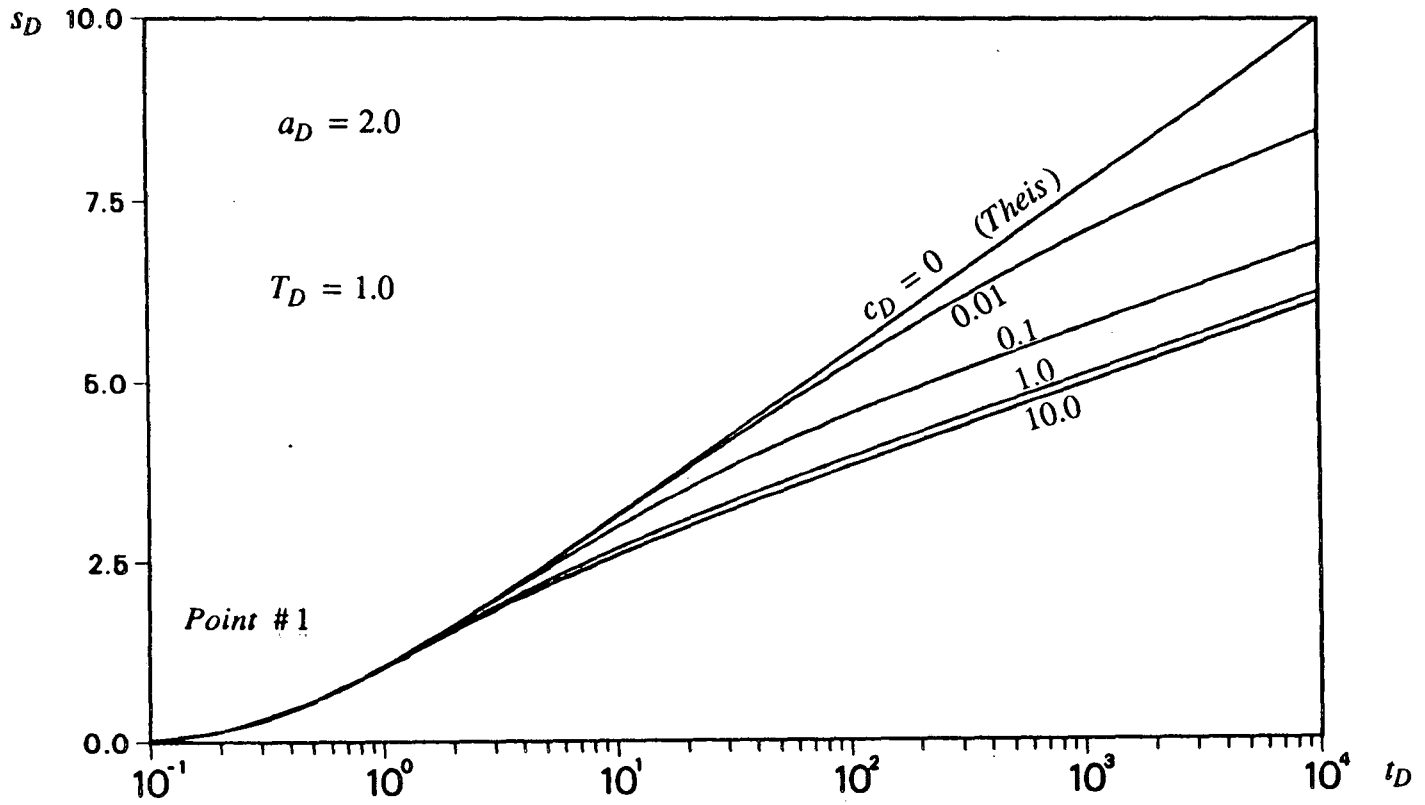

Figure 2.14C Type curves of the equal-diffusivity solution on a semilog paper.

is that there exists a simple relationship between drawdown in the pumped aquifer and drawdown in the unpumped aquifer, i.e.,

$$s_a + T_D \cdot s_u = s_T \tag{2-99}$$

Particularly if $T_D = 1.0$ (for example, for the case of two identical aquifers), we have $s_a + s_u = s_T$, which means that the sum of the drawdowns in the two aquifers is now equal to the Theis drawdown in the pumped aquifer. It seems that due to the connection of the leaky fault, part of the drawdowns at any arbitrary point (x, y) in the pumped aquifer is redistributed to the unpumped aquifer at the same point.

2.4.2 Possibility 2: Different Aquifer-Diffusivities

This implies that $\alpha_u \neq \alpha_a$. For the more general problem, it is probably too difficult to obtain the inversions of (2-84) through (2-86). However, to investigate the effect of the diffusivity of the unpumped aquifer on the drawdown in the pumped aquifer, it is worthwhile to develop some approximate solutions.

Approximate Solution #1

This approximate solution will be obtained by means of a series expansion. To do this, it is necessary to rewrite the important common factor into:

$$\frac{1}{A/T_D + A_u + A \cdot A_u / c} = \frac{c}{A \cdot A_u} \cdot \frac{1}{1+\varepsilon} \tag{2-100}$$

where the new parameter ε is defined as:

$$\varepsilon = c \cdot \left(\frac{1}{A} + \frac{1}{T_D A_u} \right) \tag{2-101}$$

Quantitatively speaking, c is usually very small in practice. If c is so small that we can assume $\varepsilon \ll 1$, then the approximation of $\frac{1}{1+\varepsilon} \approx 1 - \varepsilon$ can be applied without introducing any significant error. This approximation can change (2-84)

through (2-86) into much simpler forms:

$$w_{a_1} = \frac{Q}{2T_a}\left[\frac{e^{-|x-a|A}}{pA} - c\cdot\frac{e^{-(x+a)A}}{pA^2}\cdot\left(1-\frac{c}{T_D A_u}-\frac{c}{A}\right)\right] \tag{2-102}$$

$$w_{a_2} = \frac{Q}{2T_a}\left[\frac{e^{-(a-x)A}}{pA} - c\cdot\frac{e^{-(a-x)A}}{pA}\cdot\left(\frac{1}{A}+\frac{c}{T_D AA_u}+\frac{c}{T_D{}^2 A_u{}^2}\right)\right] \tag{2-103}$$

$$w_u = \frac{Q}{2T_a}\cdot\frac{c}{T_D}\cdot\frac{e^{-aA+xA_u}}{pAA_u}\cdot\left(1-\frac{c}{A}-\frac{c}{T_D A_u}\right) \tag{2-104}$$

If the inversion formula (2-25) is applied to (2-102) through (2-104), the final solutions become:

$$s_{a_1} = \frac{Q}{2T_a}[s^{(1)} - c\cdot s^{(2)} + \frac{c^2}{T_D}\cdot s^{(3)} + c^2\cdot s^{(4)}] \tag{2-105}$$

$$s_{a_2} = \frac{Q}{2T_a}[s^{(1)} - c\cdot s^{(2)} - \frac{c^2}{T_D}\cdot s^{(3)} - \frac{c^2}{T_D{}^2}\cdot s^{(5)}] \tag{2-106}$$

$$s_u = \frac{Q}{2T_a}\cdot\frac{c}{T_D}\cdot[s^{(6)} - c\cdot s^{(7)} - \frac{c}{T_D}\cdot s^{(8)}] \tag{2-107}$$

where the components, $s^{(i)}$ $(i = 1, 2, \cdots 8)$, are given in Appendix D.

The final solutions can also be written in dimensionless form. For example, the drawdown in Region I of the pumped aquifer, i.e., s_{a_1} will have its dimensionless form as:

$$s_D = s_{D_1} + s_{D_2} + s_{D_3} + s_{D_4} \tag{2-108}$$

where the dimensionless drawdown components are defined by:

$$s_{D_1} = W\left(\frac{1}{4t_D}\right) \tag{2-109}$$

$$s_{D_2} = -\sqrt{\pi}c_D\int_0^{t_D}\frac{e^{-y_D{}^2/(4\tau)}}{\sqrt{\tau}}erfc\left(\frac{x_D+a_D}{2\sqrt{\tau}}\right)d\tau \tag{2-110}$$

$$s_{D_3} = \frac{\sqrt{\alpha_D}}{T_D}c_D{}^2\int_0^{t_D}d\tau\int_0^{\tau}\frac{e^{-y_D{}^2/[4(\tau+\alpha_D u-u)]}}{\sqrt{u(\tau+\alpha_D u-u)}}erfc\left(\frac{x_D+a_D}{2\sqrt{\tau-u}}\right)du \tag{2-111}$$

$$s_{D_4} = c_D{}^2\left\{2t_D \cdot e^{-\frac{(x_D+a_D)^2+y_D{}^2}{4t_D}} - \frac{(x_D+a_D)^2+y_D{}^2}{2} W\left[\frac{(x_D+a_D)^2+y_D{}^2}{4t_D}\right]\right\}$$

$$-\sqrt{\pi}(x_D+a_D)c_D{}^2\int_0^{t_D}\frac{e^{-y_D{}^2/(4\tau)}}{\sqrt{\tau}} erfc\left[\frac{x_D+a_D}{2\sqrt{\tau}}\right]d\tau \qquad (2\text{-}112)$$

In deriving these dimensionless solutions, three new dimensionless parameters have been introduced, i.e. the dimensionless coordinates of the observation well: $x_D = x/r$ & $y_D = y/r$; and the dimensionless diffusivity (or the diffusivity ratio), $\alpha_D = \alpha_u/\alpha_a$. The other dimensionless variables and parameters are still defined by (2-43) and (2-44). In (2-111), u is nothing but a dummy variable of integration.

Calculations for different values of c_D show that the solutions are only valid at a time period, which depends on the value of c_D. The smaller the value of c_D, the longer the valid time period will become. Figure 2.15 gives the type curve for $c_D = 0.01$ at Point #1. By setting $\alpha_D = 1$, the solution for the case of equal-diffusivity can be used as the exact solution (solid line in the figure) to verify the newly obtained approximate solution (dots in the figure). One may note on the figure that the approximate solution matches the exact solution quite well for dimensionless times up to $t_D = 10^3$. The mechanism is that in deriving this set of approximate solutions, it has been assumed that the value of ε is very small, which may not be true when time becomes large. This is because a large value of t corresponds to a small value of p, which implies that both A and A_u could be small so that the assumption of small ε will not be valid. Fortunately, it is usually easy to determine the invalid part by observing the type curve and finding the start of oscillation. For a smaller value of c_D (e.g., $c_D = 0.001$), the solution would be valid for longer times.

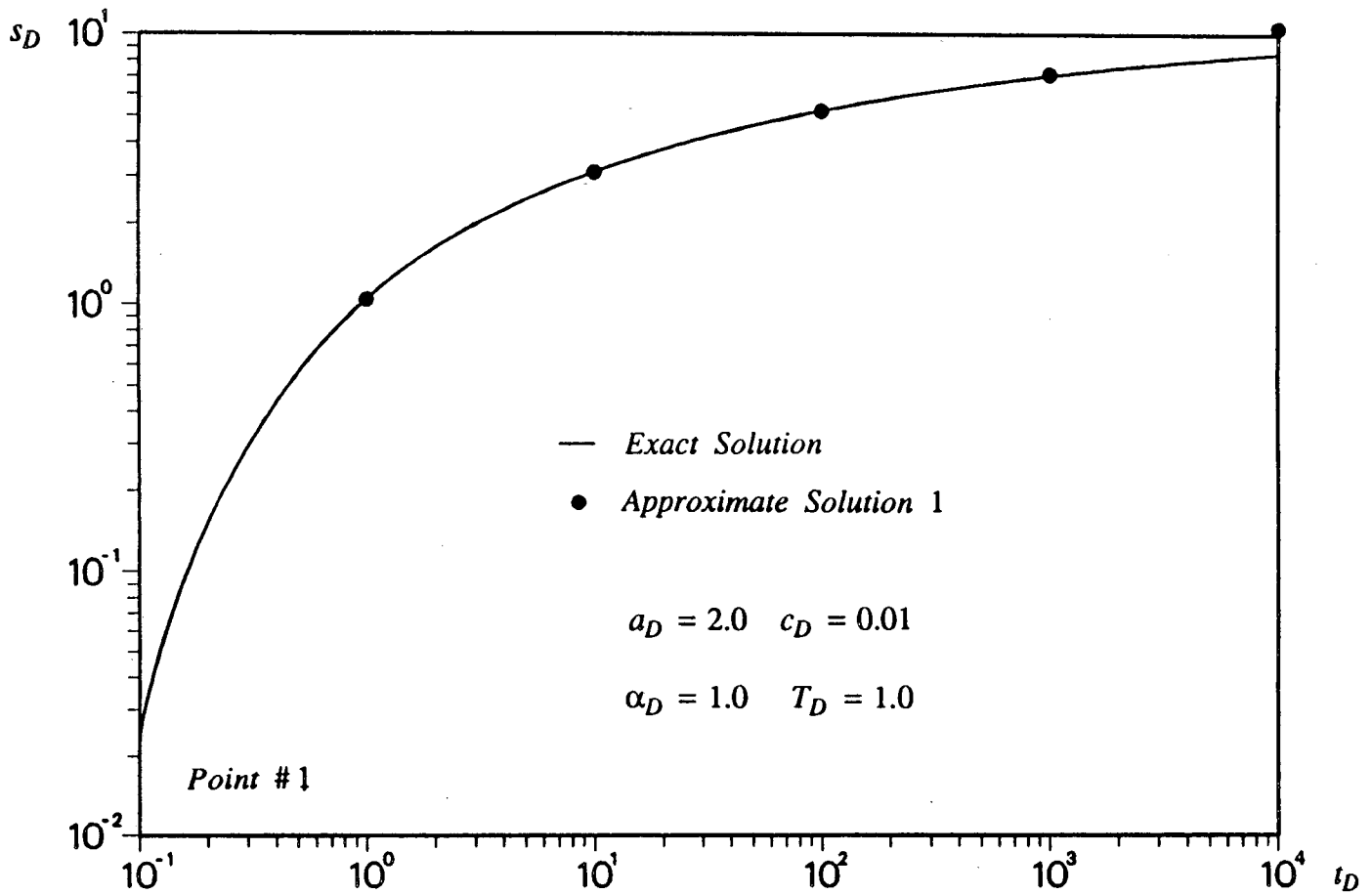

Figure 2.15 Evaluation on Approximate Solution #1 by setting α_D=1.

Approximate Solution #2

Similarly, the common factor in (2-84) through (2-86) needs to be simplified. But different from the method used for obtaining the previous approximate solutions, the following approximate formula is suggested:

$$\frac{1}{A/T_D + A_u + A \cdot A_u / c} = \frac{c}{A \cdot A_u + c \cdot A_u + A \cdot c / T_D}$$
$$\approx \frac{c}{A \cdot A_u + c \cdot A_u + A \cdot c / T_D + c^2 / T_D}$$
$$= \frac{c}{(A + c)(A_u + c / T_D)} \qquad (2\text{-}113)$$

This approximation makes it possible to get solutions without taking the series expansion. The inversion process is given in Appendix E. The dimensionless drawdown in the pumped aquifer at Region I can be written as:

$$s_D = s_T - s_F = s_T - (s_{F_1} + s_{F_2}) \qquad (2\text{-}114)$$

where

$$s_{F_1} = \sqrt{\pi} c_D e^{c_D (x_D + a_D)} \int_0^{t_D} \frac{e^{c_D^2 \tau - y_D^2/(4\tau)}}{\sqrt{\tau}} erfc\left(\frac{x_D + a_D}{2\sqrt{\tau}} + c_D \sqrt{\tau}\right) d\tau \qquad (2\text{-}115)$$

$$s_{F_2} = \frac{\sqrt{\pi \alpha_D} c_D^2}{T_D} e^{c_D (x_D + a_D)} \int_0^{t_D} \left[\frac{c_D \sqrt{\alpha_D}}{T_D} e^{c_D^2 \alpha_D u_D / T_D^2} erfc\left(\frac{c_D \sqrt{\alpha_D u_D}}{T_D}\right) - \frac{1}{\sqrt{\pi u_D}} \right] du_D$$
$$\int_0^{t_D - u_D} \frac{e^{c_D^2 \tau - y_D^2/(4\tau + 4\alpha_D u_D)}}{\sqrt{\tau + \alpha_D u_D}} erfc\left(\frac{x_D + a_D}{2\sqrt{\tau}} + c_D \sqrt{\tau}\right) d\tau \qquad (2\text{-}116)$$

while s_T is the Theis solution which has been defined before.

The dimensionless drawdown in the unpumped aquifer can also be written from Appendix E as follows.

$$s_{D_u} \simeq \frac{c_D\sqrt{\pi\alpha_D}}{T_D}\int_0^{t_D}\left[\frac{e^{-x_D{}^2/(4\alpha_D u_D)}}{\sqrt{\pi u_D}} - \frac{c_D\sqrt{\alpha_D}}{T_D}e^{\frac{c_D|x_D|}{T_D}+\frac{c_D{}^2\alpha_D}{T_D{}^2}u_D}\,erfc\left(\frac{|x_D|}{2\sqrt{\alpha_D u_D}}+\frac{c_D}{T_D}\sqrt{\alpha_D u_D}\right)\right]du_D$$

$$\int_0^{t_D-u_D}\frac{e^{-y_D{}^2/(4\tau+4\alpha_D u_D)}}{\sqrt{\tau+\alpha_D u_D}}\left[\frac{e^{-a_D{}^2/(4\tau)}}{\sqrt{\pi\tau}} - c_D e^{c_D a_D + c_D{}^2\tau}\,erfc\left(\frac{a_D}{2\sqrt{\tau}}+c_D\sqrt{\tau}\right)\right]d\tau \quad (2\text{-}117)$$

Again, if we set $\alpha_D = 1.0$, the problem is reduced to the case of equal diffusivities and thus (2-97) can be used as the exact solution for the purpose of evaluating of Approximate Solution #2. In Figure 2.16A, the dimensionless drawdowns at Point #1 in the pumped aquifer are calculated by both the exact solution (2-97) and the approximate solution (2-114) through (2-116). A comparison of results is given for two values of c_D, i.e. $c_D = 0.01$ and $c_D = 0.1$. Two conclusions can be drawn from this figure: (1) Approximate Solution #2 matches the exact solution very well at early time; and (2) this solution is especially reliable for small values of c_D. The rationale for conclusion (1) is that small values of time, t corresponds to large values of p, which means relatively large values of A and A_u. The rationale for conclusion (2) is that a small value of c_D implies a relatively small value of c^2/T_D. In both cases (early time and small values of c_D), the error resulted from the approximation which is introduced in (2-113) will be negligibly small.

The development of the two approximate solutions differ from each other. In deriving Approximate Solution #1, only one term in the series expansion of the common factor has been used to approximate the original factor; while in deriving Approximate Solution #2, a simple function is used to approximate the common factor. As a result, the first approximate solution has a convergence problem, but the second one does not.

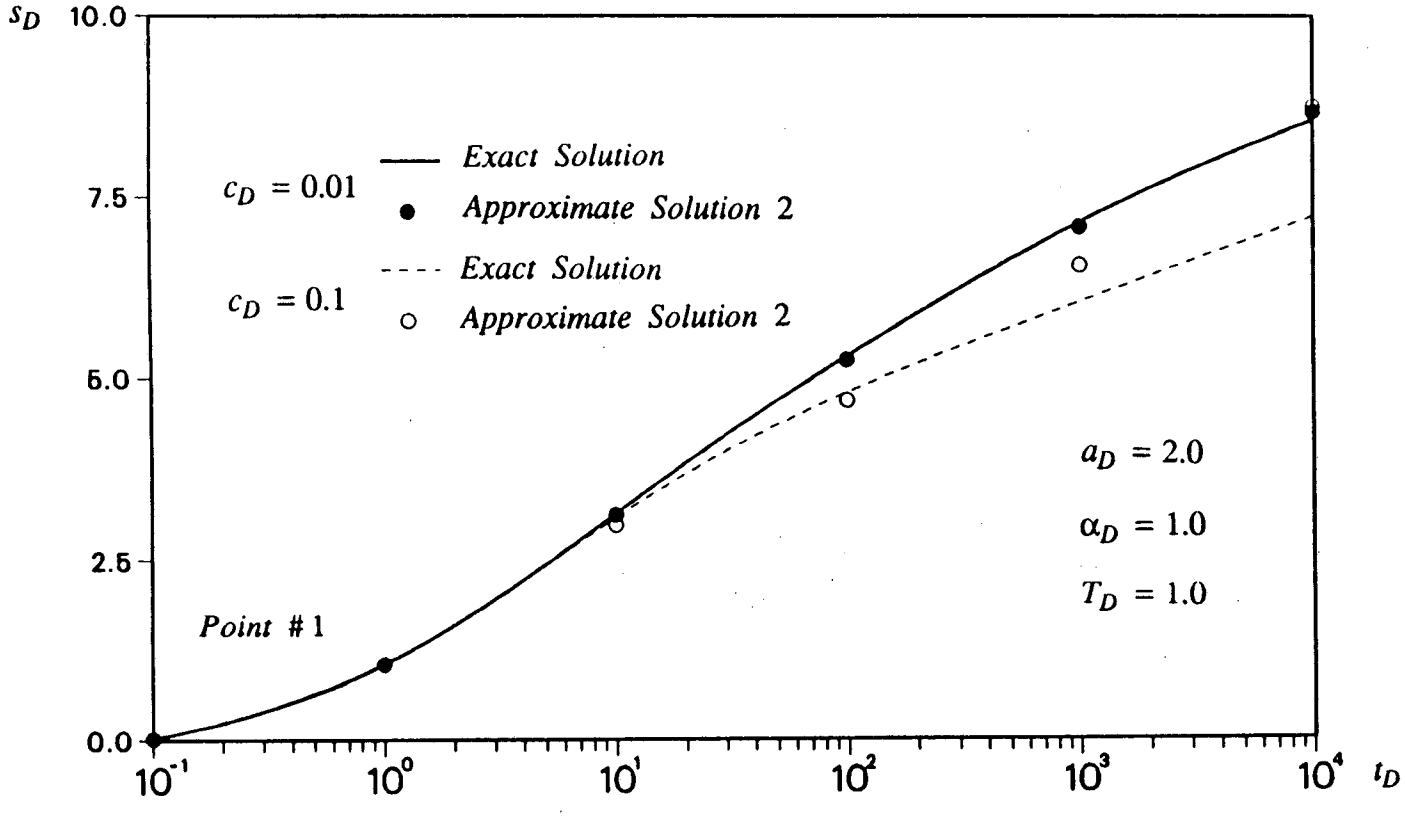

Figure 2.16A Evaluation on Approximate Solution #2 by setting α_D=1.

A comparison of the log-log plot in Figure 2.15 with the semi-log plot in Figure 2.16A for the same case ($c_D = 0.01$) reveals that Approximate Solution #2 is much more reliable. For this reason, it was selected for further study.

The significance of the approximate solutions is that they can take into account the effect of the diffusivity ratio, α_D. However, the quantitative effect of this ratio can only be found by practical calculations and comparison of results. For the particular case of $c_D = 0.01$ and $T_D = 1$, at Point #1, Figures 2.16B and 2.16C show the effect of the diffusivity ratio, α_D, on dimensionless drawdown in the pumped aquifer, s_D and in the unpumped aquifer, s_{D_u}, respectively. As α_D varies from 1 to 100, the dimensionless drawdown in the pumped aquifer increases so little at early time (t_D up to 10^4) that the difference is negligible (Figure 2.16B). On the contrary, the increase of dimensionless drawdown in the unpumped aquifer due to an increase in the diffusivity ratio is large and non-negligible (Figure 2.16C). Although different scales have been used for the two figures, it is still clear that the relative increment of dimensionless drawdown in the unpumped aquifer is much larger than that in the pumped aquifer. The phenomena can be explained as follows. The increase of the diffusivity ratio can be achieved by simply decreasing the specific storage of the unpumped aquifer alone. By definition, a smaller specific storage will definitely cause larger drawdowns in both aquifers. However, the amount of water released from the unpumped aquifer is only a small portion of the whole recharge to the pumped aquifer, especially for small value of c_D and at early time. Figure 2.16B is very important in that it gives the implication of the wide applicability of (2-97) to both equal-diffusivity cases and different-diffusivity cases. It is worthwhile to investigate applications of solution (2-97).

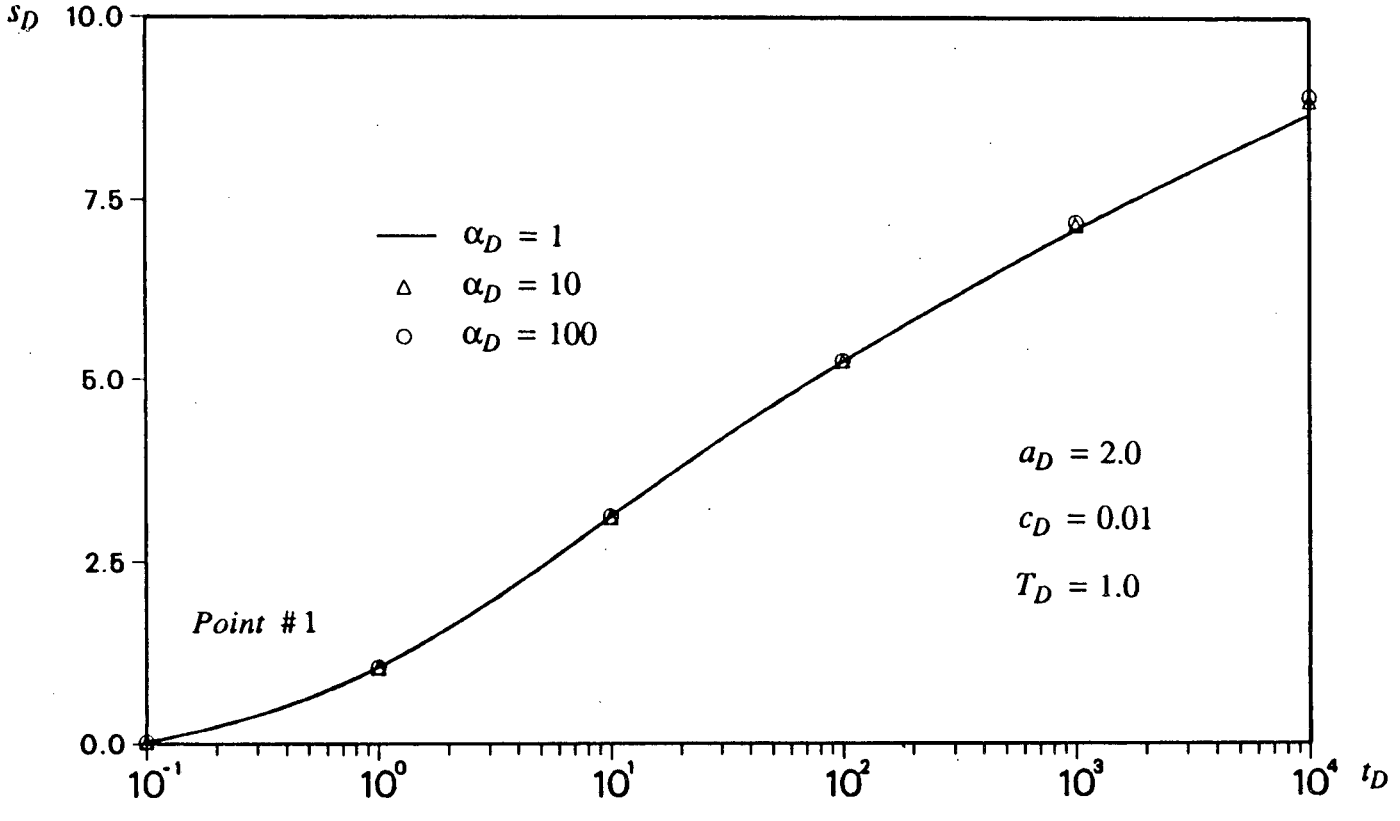

Figure 2.16B Effect of diffusivity ratio (α_D) on dimensionless drawdowns in the pumped aquifer (s_D) for c_D=0.01 and T_D=1.

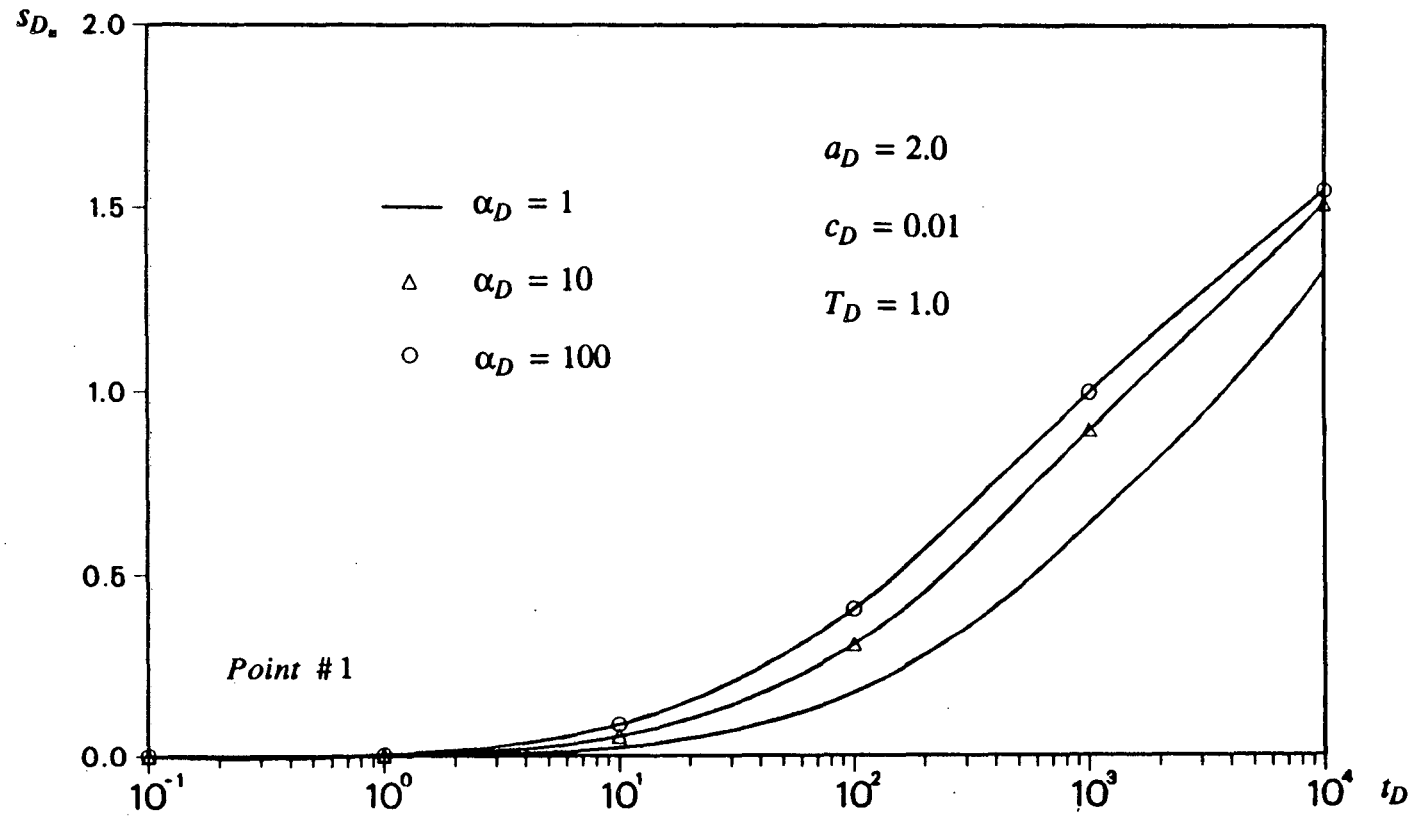

Figure 2.16C Effect of diffusivity ratio (α_D) on dimensionless drawdowns in the unpumped aquifer (s_{D_a}) for c_D=0.01 and T_D=1.

2.4.3 Applications

The application of (2-97) to direct problems has been given in the previous section, where type curves were plotted on Figures 2.14A through 2.14C. Among them, Figures 2.14A and 2.14B can help to show the effects of T_D and c_D; while Figure 2.14C can help to give an idea of how the solution could be used to solve the inverse problem to determine the parameter, c_D.

Although the type curves on the semilog paper do not tend to be horizontal, they do tend to be straight and parallel to each other. This implies that if s_F, the second term in (2-97), is plotted as a function of dimensionless time, t_D, on the semilog paper, there must be a straight line with its tangent independent of c_D. As an example, at Point #1 and for the case of $T_D = 1$, Figure 2.17A shows the Theis solution and the s_F vs. t_D curves for four different values of c_D. It can be found that all s_F curves will sooner or later become straight lines with the same slope. This slope is smaller than that of the Theis line, and the ratio of the two tangents is only dependent on the transmissivity ratio, T_D. Another characteristic of these s_F lines is their intersects with the time axis, which is obviously c_D dependent. A study on how the slope is related to T_D and the intersect for c_D will be helpful in determining these parameters.

In writing down the final dimensionless solution of (2-97), one may have noticed that after c_D is replaced by the new parameter c'_D, there is a coefficient, $\frac{1}{k}$ in front of the second term in s_F. Comparing this solution with (2-45), it is easy to understand that this coefficient, $\frac{1}{k}$, is in fact the ratio of the two slopes between the s_F line and the Theis line. For example, in Figure 2.17A we have $T_D = 1$, then by definition

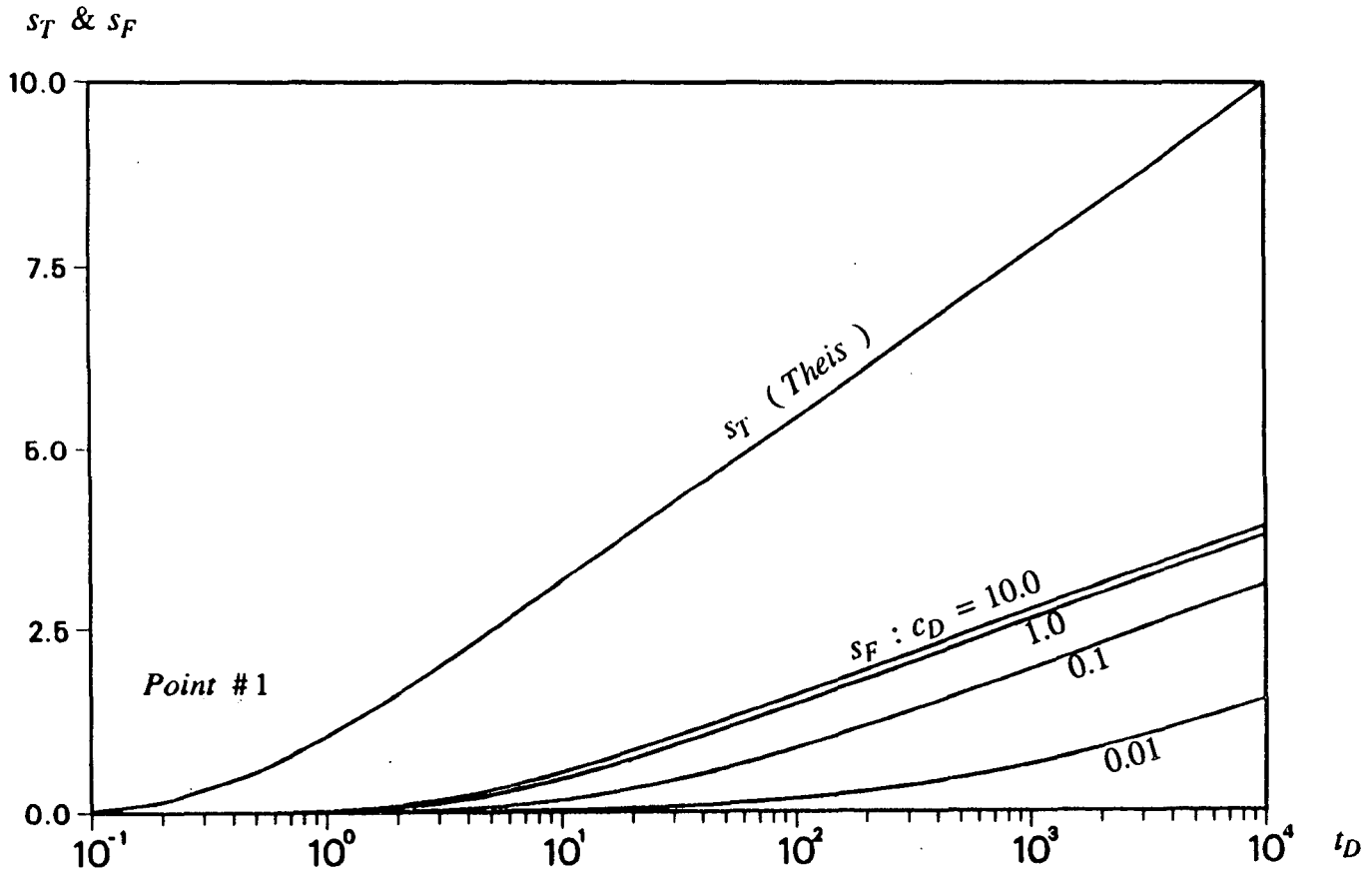

Figure 2.17A Comparison between two drawdown components at Point #1 ($\theta=\pi$) for four different values of c_D and T_D=1.

(2-91), $k = 1/T_D + 1 = 2$; and measurement of the tangents of the lines in this figure indicates that the ratio of the s_F tangent to the s_T tangent is 1/2. Conversely, in practice it is possible to get this ratio from a plot of the pumping test data. Then T_D is easily determined as well as the parameter, k. As T_D tends to infinity (a constant head can be maintained at the unpumped aquifer in this case), k tends to be unity and s_F line will become parallel to the Theis line.

The similarity of solution (2-97) with (2-45) provides great advantages in that all the previous methods and results in applications can be applied to this section as well. The only attention one needs to pay is to change the parameters in (C-3) from c_D to c'_D and from X to X'. Actually, the difference is obtained simply by multiplying them by the factor, k. After that, the process following (C-3) is the same except that c_D should be replaced by c'_D, and X by X'. As an example, let us determine the parameter c_D using the time-intersect. Figure 2.17B gives the s_F line for the case of $c_D = 1.0$. By extrapolating the straight line, its time-intersect can be found to be: $t_{D_0} \approx 5.0$. Recall that at Point #1 we have $\bar{d} = 1.5$, and if these data are substituted into Equation (2-57), the result is $e^{X'} \cdot W(X') \approx 0.2223$. From the tables (Pagurova, 1961), the corresponding X' is about 3.66. Finally, by using the modified formula (C-3), it is easy to get: $c_D = X'/k/\bar{d} = 1.22$. While the exact value of c_D is 1.0, an error of 22% is introduced during the process. In fact, if the time-intersect is read as 5.2 (instead of being 5.0), the calculation can give a result of $c_D = 1.0$. This can be achieved by plotting the s_F line on a larger scale so that the reading of t_{D_0} can be done more accurately. One can conclude that the methods derived in this chapter are very useful in characterizing a leaky fault by means of a pumping test.

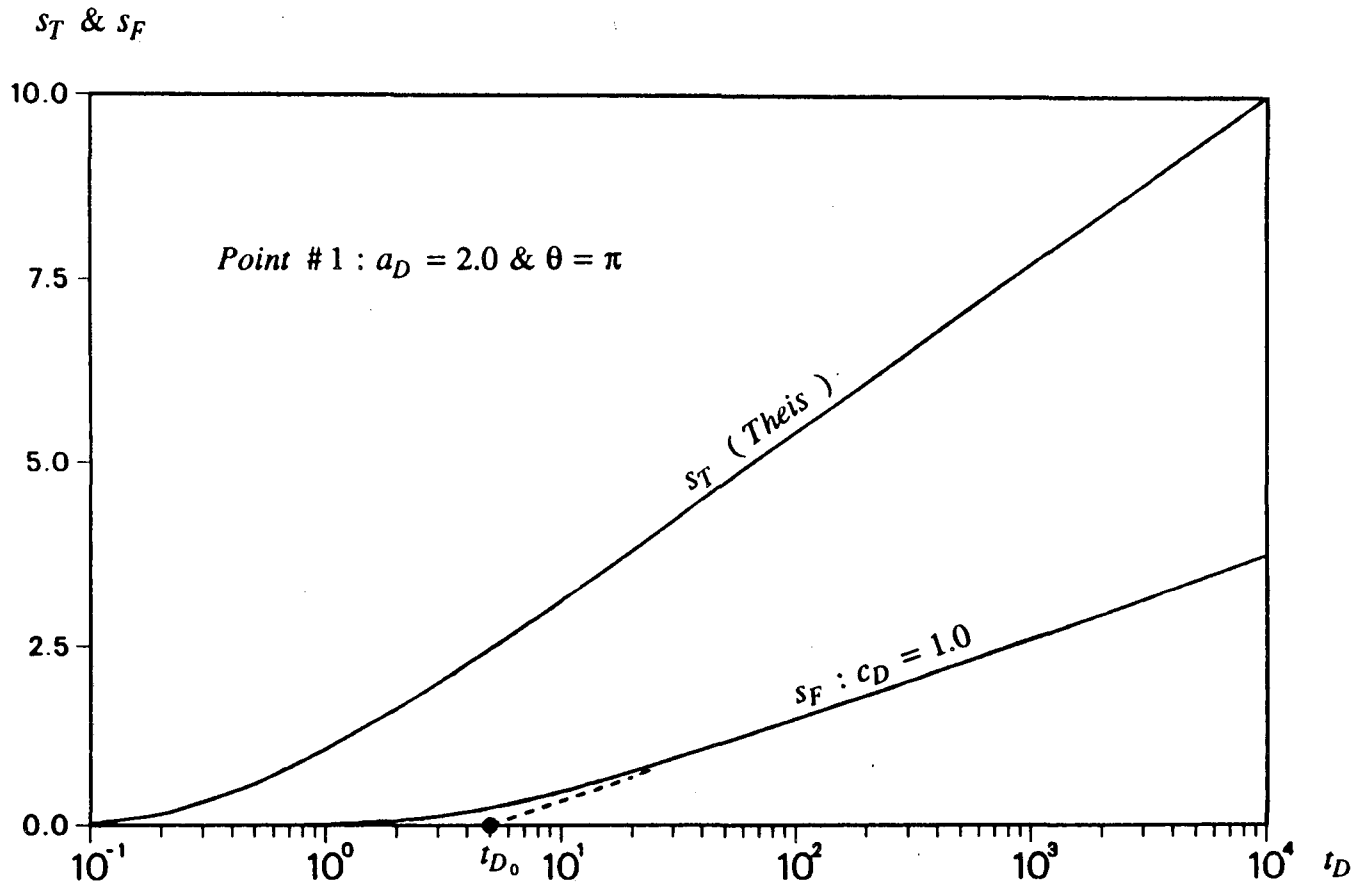

Figure 2.17B Dimensionless time-intersect, t_{D_0} for T_D=1.

CHAPTER 3

CHARACTERIZATION OF LEAKY FAULTS IN THE UNSATURATED ZONE

3.1 Review

Techniques associated with the pumping test is essentially restricted to the saturated media. To characterize leaky faults in the unsaturated zone, where a pumping test is impossible, one has to resort to other types of tests. In this circumstance, a promising way is to analyze the air flow in the unsaturated zone. The idea is that because the fault zone of interest may have a quite different pore structure from that of the surrounding rocks, this could also strongly affect the air flow in the unsaturated zone. If it is possible to find a way to determine the permeability of the fault zone to air, there will be no difficulty in converting the result into hydraulic conductivity in the fully saturated condition.

Movement of air in the unsaturated zone in response to barometric pressure changes was first described and analyzed by Buckingham (1904). He studied the case of a homogeneous layer bounded below by an impermeable boundary and gave the solution of the air pressures at any depth in response to a periodic atmospheric pressure wave at the ground surface. However, the application of studies of air flow in the unsaturated zone was proposed by Stallman at almost six decades later. In 1962, Stallman suggested using the observed air pressure or pneumatic head at depth to determine the permeability of materials in the unsaturated zone (Stallman, written commun., 1962). Several years later, Stallman (1967) and Stallman and Weeks (1969) described

their application of the method at Badger Wash, near Cuba, N. Mex. The data were analyzed based on the assumption that the unsaturated materials comprised a single homogeneous layer bounded below by an impermeable boundary. This assumption was removed by Weeks (1978) a decade later, where he applied the technique for multi-layer problems. Similar research was developed independently by Morris, Snoeberger, Rozsa, Baker, and Morris. Their application was to determine the permeability to air of the materials comprising several nuclear chimneys at the Nevada Test Site.

The theoretical basis for all these applications is the analytical solution of one dimensional diffusion equation, either for a single layer or for the multi-layer problems.

3.2 Theory

If the flow properties of the fault zone are significantly different from the surrounding rock mass, the flow of air in the unsaturated zone becomes much more complicated. The original one-dimensional flow in the vertical direction must now be converted into two-dimensional flow. This effect is very significant in regions close to the fault zone, while negligibly small in regions far from it. In an arid area (for example, Yucca Mountain in the state of Nevada), the dominant movement in the unsaturated zone is usually the gas (or actually, the air) flow. A study of this kind of single-phase flow in the fault-rock system is necessary to determine the hydrologic properties of the leaky faults.

Both the fault zone and the rock mass are treated here as homogeneous and isotropic porous materials with different hydraulic properties. It is well-known that the isothermal gas (air) flow in a porous medium is governed by the following differential

equation (Collins, 1961):

$$\nabla^2 p^2 = \frac{n_a \mu_a}{k_a p} \cdot \frac{\partial p^2}{\partial t'} \tag{3-1}$$

where p represents the air pressure at any arbitrary point; t' denotes time; n_a, μ_a and k_a are the interconnected air-filled porosity, the viscosity of air and the permeability to air, respectively. The sign, ∇ is the Laplacian. In deriving Equation (3-1), it has been assumed that the gravity force and the Klinkenberg effect on air flow are both negligibly small.

It is important to point out that this equation is in a general form for both the rock mass and the fault zone, although they have different values of air-filled porosity and permeability to air. This equation is strongly non-linear. However, if the pressure varies only over a small range during the period of time under investigation, the governing equation can be simplified into:

$$\nabla^2 p^2 = \frac{n_a \mu_a}{k_a \bar{p}} \cdot \frac{\partial p^2}{\partial t'} \tag{3-2}$$

where $\bar{p}$ can be taken as the mean pressure during the process and is thus a known constant.

A similar equation was given in the previous work of Weeks (Equation (2), Weeks, 1978). The only difference is that Weeks used the pneumatic head (ϕ) instead of the air pressure (p) as the dependent variable. This is probably based on the approximation of $p - \overline{\rho_a} g z' \simeq p$, which is acceptable in some cases. Because this treatment will not give any simplifications for the solution process in this study, it will not be adopted here. One may, however, take " p " as the " pneumatic head " in applying the solutions to be derived later on.

The difference between Equations (3-2) and (3-1) is that $\bar{p}$ replaces p in the denominator. Nevertheless, this is an important simplification, because the governing equation becomes linear. This will be apparent if we further introduce:

$$\phi' = p^2 \tag{3-3}$$

$$\alpha' = \frac{k_a \bar{p}}{n_a \mu_a} = \left(\frac{k_a \rho_a g}{\mu_a}\right) / \left(\frac{n_a \rho_a g}{\bar{p}}\right) = \frac{K_a}{S_a} \tag{3-4}$$

where $K_a = \frac{k_a \rho_a g}{\mu_a}$ can be called the " pneumatic conductivity " and $S_a = \frac{n_a \rho_a g}{\bar{p}}$, the " pneumatic specific storage ". These two parameters will be very useful in numerical calculations.

By introducing the new variable and parameter, the governing equation is reduced to the well-known diffusion equation:

$$\nabla^2 \phi' = \frac{1}{\alpha'} \cdot \frac{\partial \phi'}{\partial t'} \tag{3-5}$$

We can refer to α' as the " pneumatic diffusivity ". One may have noticed that several symbols together with their superscripts, $'$, are used to represent some of the dimensioned variables and parameters, whereas these terms without superscripts (for example, ϕ, t and α) represent the corresponding dimensionless variables and parameters. This will be the rule in the following work.

Another simplification given in Weeks' paper (Weeks, 1978) is that he used the pneumatic head to replace its square. To avoid causing any large errors in this treatment, it is necessary to keep the head change within a very small range, e.g., less than one percent of the mean value. Because this assumption makes no difference in solution derivation, it will not be adopted in the present study. However, ϕ' can also be treated as the pneumatic head in applying the results obtained in this study.

For one-dimensional problems with different initial and boundary conditions, analytical solutions of Equation (3-5) have been given in certain books (for example, Carslaw and Jaeger, 1959). However, analytical solutions for two-dimensional flow in a fault-rock system could not be found in the literature.

Figure 3.1 gives the sectional view of the general single layer problem. A vertical fault with a width of $2b'$ cuts through a single layer horizontal rock formation which extends laterally to infinity. The system can be either infinite in depth or bounded by an impermeable boundary at a certain depth, h'. It is easy to see from symmetry that the mid-plane of the fault zone must be a no-flow " boundary ". This is a convenience because we can take only one half of the scheme into consideration. Generally speaking, the half width of the fault zone, b' is always much smaller than the horizontal dimension of the rock mass as well as the depth of the system. This implies that flow through the fault zone can reasonably be assumed as a kind of one-dimensional flow with some lateral recharge from (or discharge to) the rock mass. If the z' axis is chosen to be at the fault-rock contact plane and the x' axis, at the ground surface, based on (3-5), one can write down the governing equations for air flow in the rock mass and in the fault zone in the following forms.

$$\frac{\partial^2 \phi'_r}{\partial z'^2} + \frac{\partial^2 \phi'_r}{\partial x'^2} = \frac{1}{\alpha'_r} \cdot \frac{\partial \phi'_r}{\partial t'} \tag{3-6}$$

$$\frac{\partial^2 \phi'_f}{\partial z'^2} + \frac{k}{b'} \left(\frac{\partial \phi'_r}{\partial x'}\right)_{x'=0} = \frac{1}{\alpha'_f} \cdot \frac{\partial \phi'_f}{\partial t'} \tag{3-7}$$

We will use the subscript " r " to denote all terms which belong to the rock mass, while the subscript " f " refers to the fault zone. The new parameter, k in (3-7) is the permeability ratio defined as,

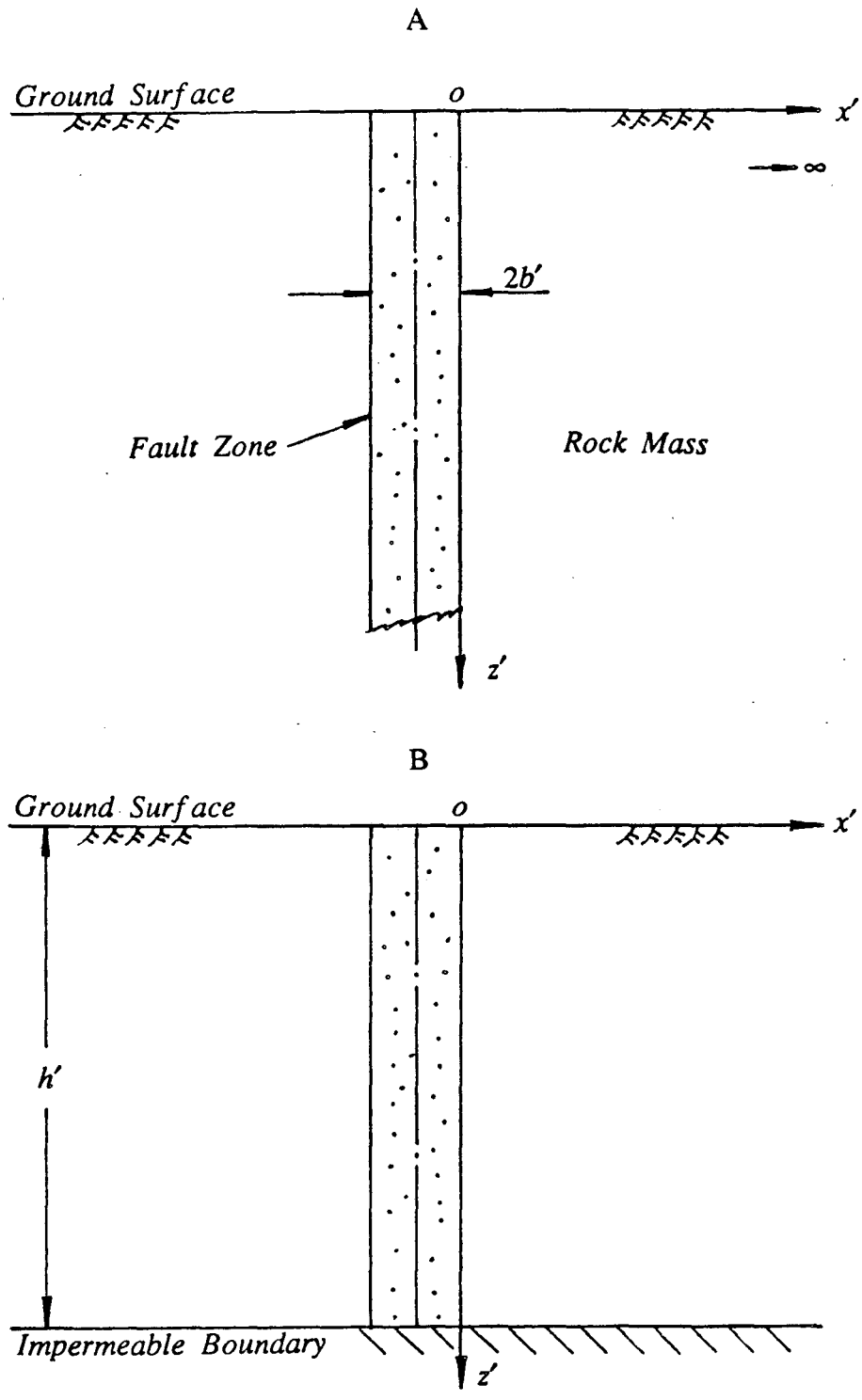

Figure 3.1 Schematic cross section of the fault zone and the surrounding rocks: (A) Infinite in depth; (B) With impermeable boundary at a certain depth.

$$k=\frac{k_r}{k_f} \tag{3-8}$$

where k_r and k_f are the air permeability of the rock mass and the fault zone, respectively.

3.3 Analytical Solutions for Single-Layer Problems

To obtain analytical solutions, it is necessary to limit ourselves to some simple but important basic cases. For the initial condition, it is a convention to assume a uniform distribution over the whole system. In other words, p everywhere is the same at the very beginning ($t' = 0$).

Starting from $t' = 0$, there is an atmospheric pressure fluctuation at the ground surface ($z' = 0$), which causes air to flow into or out of the fault-rock system. The purpose of this study is to obtain the pressure distribution in the fault and the rock for $t' > 0$. Undoubtedly, the actual pressure disturbance at the ground surface will not necessarily be a simple function of time. However, if one can separate these pressures into certain combinations of a series of simple time-dependent functions, the solution can be found by means of superposition of basic solutions (note: the basic equation is linear). Therefore, it is necessary and useful to provide some solutions for some simple but basic boundary conditions.

Two kinds of upper-boundary conditions will be studied in this work: (1) The atmospheric pressure is a step function of time, or in formula, $p\,|_{z'=0} = p_b$ ($p_b \neq p_0$) for $t' > 0$; (2) The atmospheric pressure is a sinusoidal function of time described by $p\,|_{z'=0} = p_0 + p_b \sin\omega' t'$ for $t' > 0$. The newly introduced parameters, p_b and ω' are constants.

Different from the solution process in the previous chapter, here the step of non-dimensionalization can be performed first. The following dimensionless variables and parameters will be applied in all cases.

$$x = \frac{x'}{b'} \qquad z = \frac{z'}{b'} \qquad h = \frac{h'}{b'} \tag{3-9}$$

$$t = \frac{\alpha'_f t'}{b'^2} \tag{3-10}$$

$$\alpha_f = \frac{\alpha'_f}{\alpha'_f} \equiv 1 \qquad \alpha_r = \frac{\alpha'_r}{\alpha'_f} = \alpha \tag{3-11}$$

Because the dimensionless diffusivity of the fault zone is unity, the subscript, r, for dimensionless diffusivity of the rock mass (α_r) can be omitted without causing any confusion. Actually, just as k is the " permeability ratio " of the rock mass to the fault zone, α is the " diffusivity ratio " of the rock mass to the fault zone. One may note that in the above dimensionless formulae, there is no dimensionless formula for the dependent variable, ϕ'. The definition of that is given in case studies.

3.3.1 Case 1: Semi-Infinite Thickness and Step Functional Atmospheric Pressure

For this kind of upper-boundary condition, it is desirable to introduce the following dimensionless formula:

$$\phi = \frac{\phi' - \phi'_0}{\phi'_b - \phi'_0} \tag{3-12}$$

where the initial and boundary values of ϕ' (ϕ'_0 and ϕ'_b) can be easily calculated from the definition formula, (3-3), i.e.,

$$\phi'_0 = p_0^2 \qquad \phi'_b = p_b^2 \tag{3-13}$$

The dimensionless governing equations obtained from substitutions of (3-9) through (3-12) to (3-6) and (3-7) are:

$$\frac{\partial^2 \phi_r}{\partial z^2} + \frac{\partial^2 \phi_r}{\partial x^2} = \frac{1}{\alpha} \cdot \frac{\partial \phi_r}{\partial t} \tag{3-14}$$

$$\frac{\partial^2 \phi_f}{\partial z^2} + k\left(\frac{\partial \phi_r}{\partial x}\right)_{x=0} = \frac{\partial \phi_f}{\partial t} \tag{3-15}$$

The great advantage of (3-12) is that it simplifies the initial and boundary conditions as follows.

$$\phi_r = \phi_f = 0 \quad at \quad t = 0 \tag{3-16}$$

$$\phi_r = \phi_f = 1 \quad at \quad z = 0 \quad for \quad t > 0 \tag{3-17}$$

$$(\phi_r)_{x=0} = \phi_f \tag{3-18}$$

$$\phi_r = \phi_f = 0 \quad at \quad z = \infty \tag{3-19}$$

There are two points to be mentioned here. One is that any boundary conditions between p_r and p_f (or their derivatives) remain similar to the forms for ϕ_r and ϕ_f (or their derivatives) after transformation, because the same transform formulae, (3-3) and (3-12) have been applied to both p_r and p_f. The other is that equating the flux at the fault-rock interface is not required in the boundary conditions because this has already been done in the equation for the fault zone.

With all equations and conditions available, the remaining task is to find the solutions of $\phi_r(x,z,t)$ and $\phi_f(z,t)$ which can satisfy (3-14) through (3-19). Looking at (3-16), an initial condition of zero implies that it is convenient to take the Laplace transform with respect to time, t first:

$$v(s) = L\{\phi(t)\} = \int_0^\infty \phi(t) e^{-st}\, dt \tag{3-20}$$

After the Laplace transform, Equations (3-14) and (3-15) become:

$$\frac{\partial^2 v_r}{\partial z^2} + \frac{\partial^2 v_r}{\partial x^2} = \frac{s}{\alpha} \cdot v_r \tag{3-21}$$

$$\frac{\partial^2 v_f}{\partial z^2} + k\left(\frac{\partial v_r}{\partial x}\right)_{x=0} = s \cdot v_f \tag{3-22}$$

The initial condition (3-16) has been used in this process, while the three boundary conditions (3-17) through (3-19) need to be transformed into the Laplace domain as follows.

$$v_r = v_f = \frac{1}{s} \quad at \quad z = 0 \tag{3-23}$$

$$(v_r)_{x=0} = v_f \tag{3-24}$$

$$v_r = v_f = 0 \quad at \quad z = \infty \tag{3-25}$$

Both v_r and v_f are functions of z which varies from zero to infinity. The two boundary conditions, (3-23) and (3-25) make it possible to perform a Fourier sine transform using:

$$w(\rho) = F_s\{v(z)\} = \int_0^\infty v(z)\sin(\rho z)dz \tag{3-26}$$

The inversion formula for the Fourier sine transform is:

$$v(z) = F_s^{-1}\{w(\rho)\} = \frac{2}{\pi}\int_0^\infty w(\rho)sin(\rho z)d\rho \tag{3-27}$$

The reason for choosing the Fourier sine transform is that it has the important property:

$$F_s\{\frac{d^2v(z)}{dz^2}\} = \rho \cdot v(z)|_{z=0} - \rho^2 \cdot w(\rho) \tag{3-28}$$

in which the factor, $v(z)|_{z=0}$ has a known value of $\frac{1}{s}$ for this problem.

Applying the Fourier sine transform (3-26) to Equations (3-21) and (3-22), utilizing the property (3-28) and boundary conditions (3-23) and (3-25), and rearranging terms, one can get:

$$\frac{d^2w_r}{dx^2} - (\frac{s}{\alpha} + \rho^2)w_r = -\frac{\rho}{s} \tag{3-29}$$

$$w_f = \frac{1}{s+\rho^2}[\frac{\rho}{s} + k \cdot (\frac{dw_r}{dx})_{x=0}] \tag{3-30}$$

Equation (3-29) is a non-homogeneous ordinary differential equation in w_r of second order, which can be solved by means of the method of the variation of parameters (described in Appendix B). Its complete solution is:

$$w_r = C_1 e^{-\sqrt{\frac{s}{\alpha}+\rho^2}x} + C_2 e^{\sqrt{\frac{s}{\alpha}+\rho^2}x} + \frac{\rho}{s(\frac{s}{\alpha}+\rho^2)} \tag{3-31}$$

where C_1 and C_2 are two integral constants. For this practical problem, it is obvious that p_r as well as w_r must be finite at $x \to \infty$, which requires that $C_2 \equiv 0$ in (3-31).

Substituting of (3-31) into (3-30) will give the expression for w_f containing the constant, C_1. If the remaining boundary condition (3-24) in the transformed domain, $(w_r)_{x=0} = w_f$ is applied, C_1 can be easily determined as:

$$C_1 = (\frac{1}{\alpha} - 1) \cdot \frac{\rho}{(\frac{s}{\alpha}+\rho^2)(s+\rho^2+k\sqrt{\frac{s}{\alpha}+\rho^2})} \tag{3-32}$$

Solutions of ϕ_r and ϕ_f in the double-transformed domain are thus obtained, and the next step is to get their inversions. However, it is unnecessary to obtain the inversion of w_f because the solution of ϕ_f can be derived by simply setting $x=0$ in the expression of ϕ_r. Therefore, attention will be concentrated on the inversion process for w_r and recall that:

$$\phi_r = L^{-1}\{F_s^{-1}\{w_r\}\} = F_s^{-1}\{L^{-1}\{w_r\}\} \tag{3-33}$$

where the function to be inverted (w_r) is composed of two components as follows.

$$\begin{aligned} w_r &= w_r^{(1)} + w_r^{(2)} \\ &= \frac{\rho}{s(\frac{s}{\alpha}+\rho^2)} + (\frac{1}{\alpha} - 1) \cdot \frac{\rho e^{-\sqrt{\frac{s}{\alpha}+\rho^2}x}}{(\frac{s}{\alpha}+\rho^2)(s+\rho^2+k\sqrt{\frac{s}{\alpha}+\rho^2})} \end{aligned} \tag{3-34}$$

Therefore, the inversion of w_r can be done term by term, and inversion of the first term can be found directly from tables (Erdelyi, 1954):

$$\begin{aligned}\phi_r^{(1)} &= L^{-1}\{F_s^{-1}\{w_r^{(1)}\}\} \\ &= L^{-1}\{F_s^{-1}\{\frac{1}{s}\cdot\rho/(\rho^2+\frac{s}{\alpha})\}\} \\ &= L^{-1}\{\frac{1}{s}e^{-\sqrt{\frac{s}{\alpha}}z}\} \\ &= erfc(\frac{z}{2\sqrt{\alpha t}})\end{aligned} \tag{3-35}$$

where $erfc(x)$ is the complementary error function.

This is the well-known one-dimensional solution. In fact, as $x \to \infty$, the second term in (3-34) will become zero thus the solution can be reduced to the one-dimensional solution. This agrees with the previous argument that the effect of the fault must be negligibly small at those points very far from the fault zone. This provides a further verification for the final solution.

For finite values of x, there are no direct inversion formulae for the second term in (3-34). However, if the expression of $w_r^{(2)}$ is decomposed into the sum of two terms as follows, a corresponding inversion formula is available using the Laplace transform. Because the order of inversion can be arbitrary, the Laplace inversion can be done first. The process of decomposition is simply,

$$\begin{aligned}w_r^{(2)} &= [(1-\alpha)\rho]\cdot\frac{e^{-\frac{x}{\sqrt{\alpha}}\sqrt{s+\alpha\rho^2}}}{(s+\alpha\rho^2)(\sqrt{s+\alpha\rho^2}+B_1)(\sqrt{s+\alpha\rho^2}+B_2)} \\ &= \frac{(1-\alpha)\rho}{B_1-B_2}\left[\frac{e^{-\frac{x}{\sqrt{\alpha}}\sqrt{s+\alpha\rho^2}}}{(s+\alpha\rho^2)(\sqrt{s+\alpha\rho^2}+B_2)}-\frac{e^{-\frac{x}{\sqrt{\alpha}}\sqrt{s+\alpha\rho^2}}}{(s+\alpha\rho^2)(\sqrt{s+\alpha\rho^2}+B_1)}\right]\end{aligned} \tag{3-36}$$

where B_1 and B_2 are defined as:

$$B_1, B_2 = \frac{1}{2}[\ \frac{k}{\sqrt{\alpha}} \pm \sqrt{\Delta}\ ] \qquad (\Delta>0) \tag{3-37}$$

$$B_1, B_2 = \frac{1}{2}[\ \frac{k}{\sqrt{\alpha}} \pm i\sqrt{-\Delta}\ ] \qquad (\Delta<0) \tag{3-38}$$

with the determinant, Δ defined by:

$$\Delta = \frac{k^2}{\alpha} + 4(\alpha-1)\rho^2 \tag{3-39}$$

In (3-37) and (3-38), the positive sign applies to B_1; while the negative sign applies to B_2.

Although the sign of Δ is important in carrying out the Fourier sine inversion, it can be shown that B_1 and B_2 are always independent of the Laplace transform variable, s. Therefore, the Laplace inversion can be performed without worrying about the expressions for B_1 and B_2.

The first step in the Laplace inversion process is to apply the formula of $L^{-1}\{f(s+b)\} = e^{-bt}L^{-1}\{f(s)\}$ so that the inversion of the two basic terms in (3-36) can be simplified into:

$$L^{-1}\left\{\frac{e^{-\frac{x}{\sqrt{\alpha}}\sqrt{s+\alpha\rho^2}}}{(s+\alpha\rho^2)(\sqrt{s+\alpha\rho^2}+B_i)}\right\} = e^{-\alpha\rho^2 t}\cdot L^{-1}\left\{\frac{e^{-\frac{x}{\sqrt{\alpha}}\sqrt{s}}}{s(\sqrt{s}+B_i)}\right\} \tag{3-40}$$

in which the subscript, i represents both 1 and 2.

In the tables of Laplace transformations, there is an inversion formula for (3-40), that is:

$$L^{-1}\left\{\frac{ae^{-b\sqrt{s}}}{s(\sqrt{s}+a)}\right\} = -e^{ab+a^2t}\cdot erfc(a\sqrt{t}+\frac{b}{2\sqrt{t}}) + erfc(\frac{b}{2\sqrt{t}}) \tag{3-41}$$

By simply substituting $b = \frac{x}{\sqrt{\alpha}}$ and $a = B_1$ & B_2, the application of (3-40) and (3-41) to (3-36) yields:

$$L^{-1}\{w_r^{(2)}\} = (1-\alpha)[f_1(x,\rho,t)+f_2(x,\rho,t)+f_3(x,\rho,t)] \tag{3-42}$$

where the three new functions have the following definitions:

$$f_1(x,\rho,t) = \frac{\rho}{B_1(B_1-B_2)} e^{\frac{x}{\sqrt{\alpha}}B_1+B_1^2t-\alpha\rho^2t} \cdot erfc\left(B_1\sqrt{t}+\frac{x}{2\sqrt{\alpha t}}\right) \tag{3-43}$$

$$f_2(x,\rho,t) = \frac{-\rho}{B_2(B_1-B_2)} e^{\frac{x}{\sqrt{\alpha}}B_2+B_2^2t-\alpha\rho^2t} \cdot erfc\left(B_2\sqrt{t}+\frac{x}{2\sqrt{\alpha t}}\right) \tag{3-44}$$

$$f_3(x,\rho,t) = \frac{\rho}{B_1 \cdot B_2} e^{-\alpha\rho^2t} \cdot erfc\left(\frac{x}{2\sqrt{\alpha t}}\right) \tag{3-45}$$

For both the case of $\Delta>0$ and the case of $\Delta<0$, it will always be true that:

$$B_1 \cdot B_2 = \rho^2(1-\alpha) \tag{3-46}$$

If this is substituted into (3-45), one can see that the function, $f_3(x,\rho,t)$ is independent of B_1 and B_2 and that the third term in (3-42) is always $\frac{e^{-\alpha\rho^2t}}{\rho} \cdot erfc\left(\frac{x}{2\sqrt{\alpha t}}\right)$, which has the following Fourier sine inversion:

$$F_s^{-1}\left\{\frac{e^{-\alpha\rho^2t}}{\rho} \cdot erfc\left(\frac{x}{2\sqrt{\alpha t}}\right)\right\} = erfc\left(\frac{x}{2\sqrt{\alpha t}}\right)\left[F_s^{-1}\left\{\frac{1}{\rho}\right\} - F_s^{-1}\left\{\frac{1-e^{-\alpha\rho^2t}}{\rho}\right\}\right]$$

$$= erfc\left(\frac{x}{2\sqrt{\alpha t}}\right)\left[1-erfc\left(\frac{z}{2\sqrt{\alpha t}}\right)\right] \tag{3-47}$$

In the above process, the inversion of the second term can be obtained directly from tables while the inversion of the first term is derived using inversion formula, (3-27). It may be written as follows.

$$F_s^{-1}\left\{\frac{1}{\rho}\right\} = \frac{2}{\pi}\int_0^\infty \frac{\sin(\rho z)}{\rho} d\rho = \frac{2}{\pi} Si(\infty) = 1 \tag{3-48}$$

where $Si(x) = \int_0^x \frac{\sin\omega}{\omega} d\omega$ is the function of the sine integral. One particular value of this function is: $Si(\infty) = \pi/2$.

Although it is very difficult to get the inversion for the first two terms in (3-42), the solution can still be written in an integral form based on the inversion formula, (3-27).

$$\phi_r^{(2)} = F_s^{-1}\{L^{-1}\{w_r^{(2)}\}\}$$

$$= erfc\left(\frac{x}{2\sqrt{\alpha t}}\right)\left[1 - erfc\left(\frac{z}{2\sqrt{\alpha t}}\right)\right] + \frac{2(1-\alpha)}{\pi}\int_0^\infty (f_1 + f_2)\sin(\rho z)\, d\rho \qquad (3\text{-}49)$$

Combining (3-35) and (3-49), the final solution for the dimensionless ϕ in the rock mass is:

$$\phi_r = erfc\left(\frac{z}{2\sqrt{\alpha t}}\right) + erfc\left(\frac{x}{2\sqrt{\alpha t}}\right) - erfc\left(\frac{z}{2\sqrt{\alpha t}}\right)\cdot erfc\left(\frac{x}{2\sqrt{\alpha t}}\right)$$

$$+ \frac{2(1-\alpha)}{\pi}\int_0^\infty [f_1(x,\rho,t) + f_2(x,\rho,t)]\sin(\rho z)\, d\rho \qquad (3\text{-}50)$$

It is interesting that the first three terms in the final solution are symmetrical in x and z. This is, however, not the case for the fourth term. In the fourth term, the two functions, f_1 and f_2 are given by (3-43) and (3-44), respectively, both are B_1 and B_2 dependent. To calculate the integral in solution (3-50), it is necessary to determine the value of B_1 and B_2 first. There are two formulae for determining B_1 and B_2 given by (3-37) and (3-38), and the question is which one should be used.

Noting that k and α refer to the permeability ratio and the diffusivity ratio of the rock to the fault, respectively, both terms must have some positive values. It is then easy to see that Δ is definitely larger than zero only when $\alpha \geq 1$ and that Δ can be positive, zero or negative when $\alpha < 1$, depending on the value of ρ. Therefore, formula (3-37) can be used for the case of $\alpha \geq 1$ without any problem and the integral term in the final solution can be computed by means of numerical integration without any difficulties. However, this is a rare case in practice, because a value of α which is

larger or equal to unity means that the diffusivity of the rock mass is larger than or equal to the diffusivity of the fault zone. A fault like that is generally impermeable and the problem can be considered as a simple one-dimensional problem. From this point of view, important applications of solution (3-50) are usually for the case of $\alpha < 1$.

As mentioned above, for the case of $\alpha < 1$, both (3-37) and (3-38) will be used in different intervals of the integration on ρ. There is one thing to be pointed out, that is, for certain values of ρ (for example ρ_0), Δ could be zero and $B_1 = B_2 = 0.5k/\sqrt{\alpha}$. The value of ρ_0 can be calculated using the formula:

$$\rho_0 = \frac{k}{2\sqrt{\alpha(1-\alpha)}} \qquad (\alpha < 1) \tag{3-51}$$

At this point (ρ_0), the expression for $w_r^{(2)}$ will be simpler than in (3-36). The reason for not giving the particular expression and its Laplace inversion is that the value of the integrand at a single point (ρ_0) will not make any contribution to the integration (with respect to ρ). It is obvious that $\Delta > 0$ as $\rho < \rho_0$ and that $\Delta < 0$ as $\rho > \rho_0$. Therefore, (3-38) needs to be used in the interval of $\rho_0 < \rho < \infty$ and more work is necessary in calculating the integral term in solution (3-50). Further derivations are given in Appendix F.

3.3.2 Case 2: Finite Thickness and Step Functional Atmospheric Pressure

The governing equations, the initial condition and the boundary conditions are exactly the same as those in Case 1 except that (3-19) needs to be replaced by:

$$\frac{\partial \phi_r}{\partial z} = \frac{\partial \phi_f}{\partial z} = 0 \quad at \quad z = h \tag{3-52}$$

Similarly, if the Laplace transform with respect to t is applied first, the governing

equations and the boundary conditions in the transformed domain are exactly the same as those in Case 1 except that (3-25) needs to be replaced by:

$$\frac{\partial v_r}{\partial z} = \frac{\partial v_f}{\partial z} = 0 \quad at \quad z = h \tag{3-53}$$

In a finite region, $0 \le z \le h$, the Fourier sine transform, (3-26) is no longer applicable. A suitable transform method to this case is the generalized finite Fourier transform:

$$w(n) = F_g\{v(z)\} = \int_0^h v(z)\sin[(n-\frac{1}{2})\frac{\pi z}{h}]dz \tag{3-54}$$

The merit of such kind of transform is that the inversion is directly given by the following formula (Churchill, 1958):

$$v(z) = \frac{2}{h}\sum_{n=1}^{\infty} w(n)\sin[(n-\frac{1}{2})\frac{\pi z}{h}] \tag{3-55}$$

In addition, it is easy to prove that this transform has the following properties:

$$F_g\{c \cdot v(z)\} = c \cdot F_g\{v(z)\} = c \cdot w(n) \tag{3-56}$$

$$F_g\{v''(z)\} = -[(n-\frac{1}{2})\frac{\pi}{h}]^2 w(n) + [(n-\frac{1}{2})\frac{\pi}{h}]v(0) - (-1)^n v'(h) \tag{3-57}$$

where c can be any arbitrary constant; $v''(z)$ represents the second order derivative of $v(z)$ with respect to z, $v'(h)$ is the value of the first order derivative at $z = h$ and $v(0)$ denotes the value of v at $z = 0$. For this problem, (3-23) gives $v(0) = 1/s$ and (3-53) gives $v'(h) = 0$.

For ease in writing the solution process, it is desirable to introduce a new parameter, d, which is a function of n.

$$d = d(n) = (n-\frac{1}{2})\frac{\pi}{h} \tag{3-58}$$

Applying (3-54), (3-56) and (3-57) to (3-21) and (3-22), and using the values of $v(0)$ and $v'(h)$ given by boundary conditions (3-23) and (3-53), the transformed equations after some rearrangement can be written as:

$$\frac{d^2 w_r}{dx^2} - (\frac{s}{\alpha} + d^2) w_r = -\frac{d}{s} \tag{3-59}$$

$$w_f = \frac{1}{s + d^2}[\frac{d}{s} + k \cdot (\frac{dw_r}{dx})_{x=0}] \tag{3-60}$$

Comparing (3-59) with (3-29) and (3-60) with (3-30), it is interesting to find that they are exactly the same except that ρ has been replaced by d. Also, the unused boundary condition (3-24) after transformation is the same as that in Case 1. It is then unnecessary to repeat the same solution process, and the final solution for the rock in the transformed domain can be directly copied from (3-34) by inserting d for ρ.

$$\begin{aligned} w_r &= w_r^{(1)} + w_r^{(2)} \\ &= \frac{d}{s(\frac{s}{\alpha}+d^2)} + (\frac{1}{\alpha} - 1) \cdot \frac{de^{-\sqrt{\frac{s}{\alpha}+d^2}x}}{(\frac{s}{\alpha}+d^2)(s+d^2+k\sqrt{\frac{s}{\alpha}+d^2})} \end{aligned} \tag{3-61}$$

The Laplace inversion for the first term in (3-61) is:

$$\begin{aligned} L^{-1}\{w_r^{(1)}\} &= L^{-1}\left\{\frac{\alpha d}{s(s+\alpha d^2)}\right\} \\ &= L^{-1}\left\{\frac{1}{d}\left[\frac{1}{s} - \frac{1}{s+\alpha d^2}\right]\right\} \\ &= \frac{1 - e^{-\alpha d^2 t}}{d} \end{aligned} \tag{3-62}$$

For the second component, one can use the results of the Laplace inversion in the previous case, that is:

$$L^{-1}\{w_r^{(2)}\} = (1-\alpha)[f_1(x,d,t) + f_2(x,d,t)] + \frac{e^{-\alpha d^2 t}}{d} \cdot erfc(\frac{x}{2\sqrt{\alpha t}}) \tag{3-63}$$

where f_1 and f_2 for this case are similarly defined:

$$f_1(x,d,t) = \frac{d}{B_1(B_1-B_2)} e^{\frac{x}{\sqrt{\alpha}}B_1+B_1^2t-\alpha d^2t} \cdot erfc\left(B_1\sqrt{t}+\frac{x}{2\sqrt{\alpha t}}\right) \qquad (3\text{-}64)$$

$$f_2(x,d,t) = \frac{-d}{B_2(B_1-B_2)} e^{\frac{x}{\sqrt{\alpha}}B_2+B_2^2t-\alpha d^2t} \cdot erfc\left(B_2\sqrt{t}+\frac{x}{2\sqrt{\alpha t}}\right) \qquad (3\text{-}65)$$

The two parameters, B_1 and B_2 are still given by (3-37) and (3-38) but ρ needs to be replaced by d in calculating Δ by means of (3-39).

With these points in mind, all results can be combined to give the solution:

$$\phi_r = \frac{2}{h}\sum_{n=1}^{\infty}\left[\frac{1-e^{-\alpha d^2t}+e^{-\alpha d^2t}\cdot erfc\left(\frac{x}{2\sqrt{\alpha t}}\right)}{d}+(1-\alpha)(f_1+f_2)\right]\sin(dz) \qquad (3\text{-}66)$$

The inversion formula, (3-55) has been used in obtaining (3-66). Actually, this solution can be further simplified. Recalling that the n-dependent variable, d is defined by (3-58), the first term in (3-66) can be calculated as follows.

$$\frac{2}{h}\sum_{n=1}^{\infty}\frac{\sin(dz)}{d} = \frac{2}{h}\sum_{n=1}^{\infty}\frac{\sin[(n-\frac{1}{2})\frac{\pi}{h}z]}{(n-\frac{1}{2})\frac{\pi}{h}}$$

$$= \frac{4}{\pi}\sum_{n=1}^{\infty}\frac{\sin[(2n-1)(\frac{\pi z}{2h})]}{(2n-1)}$$

$$= 1 \qquad (3\text{-}67)$$

The last step of derivation is based on the fact (Gradshteyn and Ryzhik, 1980):

$$\sum_{n=1}^{\infty}\frac{\sin[(2n-1)\cdot X]}{(2n-1)} = \frac{\pi}{4} \qquad (X \neq 0) \qquad (3\text{-}68)$$

If the result of (3-67) is substituted into (3-66), the final solution for Case 2 can

be written as:

$$\phi_r = 1 - \frac{2}{h}[\,1 - erfc(\frac{x}{2\sqrt{\alpha t}})\,]\cdot\sum_{n=1}^{\infty}\frac{e^{-\alpha d^2 t}}{d}\sin(dz)$$
$$+ \frac{2}{h}(1-\alpha)\sum_{n=1}^{\infty}[f_1(x,d,t)+f_2(x,d,t)]\sin(dz) \qquad (3\text{-}69)$$

It can also be found that the second component in solution (3-61) will vanish as x tends to infinity. Applying (3-55) to (3-62) and using the result obtained in (3-67), one can get the one-dimensional solution in the following form:

$$\phi_r(z,t) = 1 - \frac{2}{h}\sum_{n=1}^{\infty}\frac{e^{-\alpha d^2 t}}{d}\sin(dz) \qquad (3\text{-}70)$$

The one-dimensional analytical solution for the same case has been available in literature for a long time (for example, Carslaw and Jaeger, 1959):

$$\phi(z,t) = \sum_{n=0}^{\infty}(-1)^n\{\,erfc[\frac{2(n+1)h-z}{2\sqrt{\alpha t}}]+erfc[\frac{2nh+z}{2\sqrt{\alpha t}}]\,\} \qquad (3\text{-}71)$$

Numerical evaluations of (3-70) and (3-71) give identical results. Therefore, one can see that solutions derived through different ways can have different forms.

3.3.3 Case 3: Semi-Infinite Thickness and Sinusoidal Atmospheric Pressure

In this case, as well as in the next case (Case 4), the pressure square at the ground surface can usually be simplified as:

$$\phi'|_{z'=0} = {p_0}^2 + 2p_0p_b\sin(\omega' t') + {p_b}^2\sin^2(\omega' t')$$
$$\approx {p_0}^2 + 2p_0p_b\sin(\omega' t') \qquad (3\text{-}72)$$

The basis of this simplification is that the magnitude of variation of the atmospheric pressure (p_b) is always much smaller than the absolute value of the basic pressure (p_0). Thus, the third term in above expansion can be neglected without causing any significant error.

Instead of the dimensionless formula, (3-12) used in Case 1 and Case 2, a new dimensionless ϕ is defined for applications in Case 3 and Case 4:

$$\phi = \frac{\phi' - {p_0}^2}{2p_0 p_b} \tag{3-73}$$

By doing so, the dimensionless governing equations for the rock and the fault, the initial and the boundary conditions are exactly the same as those for Case 1 [(3-14) through (3-19)], except the boundary condition, (3-17) needs to be modified into:

$$\phi_r = \phi_f = \sin(\omega t) \quad at \quad z = 0 \quad \text{for} \quad t > 0 \tag{3-74}$$

where the dimensionless frequency, ω is defined as:

$$\omega = \frac{b'^2}{\alpha_f'} \cdot \omega' \tag{3-75}$$

Because this is the only difference, after taking the Laplace transform with respect to t, i.e. applying the transform formula, (3-20), the transformed governing equations and boundary conditions are the same as (3-21) through (3-25) except (3-23) has to be modified into:

$$v_r = v_f = \frac{\omega}{s^2+\omega^2} \quad at \quad z = 0 \tag{3-76}$$

Along the similar process as that given by (3-26) through (3-32), the solution for the rock mass in the transformed domain can be obtained as:

$$w_r = w_r^{(1)} + w_r^{(2)}$$

$$= \frac{\omega\rho}{(s^2+\omega^2)(\frac{s}{\alpha}+\rho^2)} + (\frac{1}{\alpha}-1)\cdot\frac{\omega s}{(s^2+\omega^2)}\cdot\frac{\rho e^{-\sqrt{\frac{s}{\alpha}+\rho^2}x}}{(\frac{s}{\alpha}+\rho^2)(s+\rho^2+k\sqrt{\frac{s}{\alpha}+\rho^2})} \tag{3-77}$$

Comparing this solution with that obtained in Case 1, i.e., (3-34), it is easy to see that they are very similar to each other. If (3-77) is divided by (3-34), the ratio will be, $\frac{\omega}{s^2+\omega^2}:\frac{1}{s}$. This is not strange at all, because a boundary-value problem like that described by (3-21) through (3-25) can always be transformed into the same problem with the boundary value equal to unity. Assuming the boundary value is v_0 (equal to $\frac{1}{s}$ in Case 1 and $\frac{\omega}{s^2+\omega^2}$ in Case 3), if a new variable, $u = v/v_0$ is introduced, then the problems in the two cases have the same governing equations and boundary conditions. Undoubtedly, the solutions for u are the same while the solutions for v are only different by a factor of v_0. Because the process for deriving solution (3-77) is the same as that for deriving solution (3-34), it is understandable why the solutions of v in the Fourier sine domain (w) differ only by a factor of v_0 ($\frac{1}{s}$ and $\frac{\omega}{s^2+\omega^2}$ in this study).

After carefully rechecking the solution (3-77), it is time to do the inversions. The solution of (3-77) contains two components, of which the first component ($w_r^{(1)}$) is the basic one-dimensional solution while the second component ($w_r^{(2)}$) represents the effect of the fault, which is a two-dimensional component.

The inversion of $w_r^{(1)}$ has been found in previous studies (e.g., Carslaw and Jaeger, 1959). It is:

$$\phi_r^{(1)} = e^{-z\sqrt{\frac{\omega}{2\alpha}}}\sin(\omega t - z\sqrt{\frac{\omega}{2\alpha}}) + \frac{2\alpha\omega}{\pi}\int_0^\infty \frac{ue^{-\alpha u^2 t}\sin(uz)}{\omega^2+\alpha^2u^4}du \qquad (3\text{-}78)$$

For inversion of the two-dimensional component, $w_r^{(2)}$, it is still suitable to perform the inverse Laplace transform first. Noting that this is a product of two factors,

the first factor has its familiar Laplace inversion as:

$$L^{-1}\{\frac{\omega s}{s^2+\omega^2}\} = \omega\cdot\cos(\omega t) \tag{3-79}$$

while the Laplace inversion of the second factor has already been given by (3-42) through (3-46). By means of the Duhamel's theorem, the Laplace inversion of the product is:

$$L^{-1}\{w_r^{(2)}\} = (1-\alpha)\omega\int_0^t \cos[\omega(t-\tau)][f_1(x,\rho,\tau)+f_2(x,\rho,\tau)+f_3(x,\rho,\tau)]d\tau \tag{3-80}$$

The second component of the solution can finally be obtained by applying the Fourier sine inversion formula, (3-27) and interchanging the order of integration:

$$\begin{aligned}
\phi_r^{(2)} &= F_s^{-1}\{L^{-1}\{w_r^{(2)}\}\} \\
&= \frac{2}{\pi}\int_0^\infty \{(1-\alpha)\omega\int_0^t \cos[\omega(t-\tau)][f_1+f_2+f_3]d\tau\}\sin(\rho z)d\rho \\
&= \omega\int_0^t \cos[\omega(t-\tau)]d\tau\{\frac{2(1-\alpha)}{\pi}\int_0^\infty [f_1+f_2+f_3]\sin(\rho z)d\rho\} \\
&= \omega\int_0^t erfc(\frac{x}{2\sqrt{\alpha t}})[1-erfc(\frac{z}{2\sqrt{\alpha t}})]\cos[\omega(t-\tau)]d\tau \\
&\quad + \frac{2(1-\alpha)\omega}{\pi}\int_0^\infty \sin(\rho z)d\rho\int_0^t (f_1+f_2)\cos[\omega(t-\tau)]d\tau
\end{aligned} \tag{3-81}$$

In the above derivation, the results in (3-80) and (3-47) have been applied. Combining (3-78) and (3-81), the final solution for the dimensionless ϕ in the rock mass is:

$$\begin{aligned}
\phi_r &= e^{-z\sqrt{\frac{\omega}{2\alpha}}}\sin(\omega t - z\sqrt{\frac{\omega}{2\alpha}}) + \frac{2\alpha\omega}{\pi}\int_0^\infty \frac{ue^{-\alpha u^2 t}\sin(uz)}{\omega^2+\alpha^2u^4}du \\
&\quad + \omega\int_0^t erfc(\frac{x}{2\sqrt{\alpha t}})[1-erfc(\frac{z}{2\sqrt{\alpha t}})]\cos[\omega(t-\tau)]d\tau \\
&\quad + \frac{2(1-\alpha)\omega}{\pi}\int_0^\infty \sin(\rho z)d\rho\int_0^t [f_1(x,\rho,\tau)+f_2(x,\rho,\tau)]\cos[\omega(t-\tau)]d\tau
\end{aligned} \tag{3-82}$$

where $f_1(x,\rho,\tau)$ and $f_2(x,\rho,\tau)$ can be given by (3-43) and (3-44), respectively. The

only requirement is to replace t by τ.

3.3.4 Case 4: Finite Thickness and Sinusoidal Atmospheric Pressure

This case differs from Case 2 only in the upper boundary condition and differs from Case 3 only in the lower boundary condition. If compared with Case 1, the differences are in both. Recall that the transformed solution (w_r) for Case 2 was simply borrowed from that for Case 1. During this process, the only caution is to replace ρ by d. Similarly, the transformed solution for Case 4 can also be copied from that for Case 3, (3-77) as follows.

$$w_r = w_r^{(1)} + w_r^{(2)} = \frac{\omega d}{(s^2+\omega^2)(\frac{s}{\alpha}+d^2)} + (\frac{1}{\alpha}-1)\cdot\frac{\omega s}{(s^2+\omega^2)}\cdot\frac{de^{-\sqrt{\frac{s}{\alpha}+d^2}x}}{(\frac{s}{\alpha}+d^2)(s+d^2+k\sqrt{\frac{s}{\alpha}+d^2})} \tag{3-83}$$

To get the inverse Laplace transform for the first component, we note that it can be rewritten into:

$$w_r^{(1)} = \frac{\omega\alpha d}{(s^2+\omega^2)(s+\alpha d^2)} = \omega\alpha d\cdot\left[\frac{D_1 s}{s^2+\omega^2}+\frac{D_2}{s^2+\omega^2}+\frac{D_3}{s+\alpha d^2}\right] \tag{3-84}$$

where the newly introduced parameters are defined as:

$$D_3,\ D_1 = \pm\frac{1}{\alpha^2 d^4+\omega^2} \qquad D_2 = \frac{\alpha d^2}{\alpha^2 d^4+\omega^2} \tag{3-85}$$

which are all independent of the variable, s.

It is then easy to find that:

$$L^{-1}\{w_r^{(1)}\} = \omega\alpha d\cdot[D_1\cos(\omega t)+\frac{D_2}{\omega}\sin(\omega t)+D_3 e^{-\alpha d^2 t}] \tag{3-86}$$

Further inversion of the first component is simply the application of the inversion

formula, (3-55).

$$\phi_r^{(1)} = F_g^{-1}\{L^{-1}\{w_r^{(1)}\}\} = \frac{2}{h}\sum_{n=1}^{\infty}\omega\alpha d\cdot[D_1\cos(\omega t)+\frac{D_2}{\omega}\sin(\omega t)+D_3e^{-\alpha d^2 t}]\sin(dz)$$

$$= \frac{2\omega}{h}\left[\frac{\sin(\omega t)}{\omega}\sum_{n=1}^{\infty}\frac{d^3\sin(dz)}{d^4+\beta^2}-\frac{\cos(\omega t)}{\alpha}\sum_{n=1}^{\infty}\frac{d\sin(dz)}{d^4+\beta^2}+\frac{1}{\alpha}\sum_{n=1}^{\infty}\frac{de^{-\alpha d^2 t}\sin(dz)}{d^4+\beta^2}\right] \quad (3\text{–}87)$$

where the new constant is defined as:

$$\beta = \omega/\alpha \quad (3\text{-}88)$$

The Laplace inversion of $w_r^{(2)}$ can be directly written down by substitution of ρ by d in (3-80):

$$L^{-1}\{w_r^{(2)}\} = (1-\alpha)\omega\int_0^t\cos[\omega(t-\tau)][f_1(x,d,\tau)+f_2(x,d,\tau)+f_3(x,d,\tau)]d\tau \quad (3\text{-}89)$$

where f_1, f_2 and f_3 can be calculated by (3-43) through (3-45) with the substitution of ρ by d.

After applying the inversion formula, (3-55), the second component in the final solution is simply:

$$\phi_r^{(2)} = \frac{2(1-\alpha)\omega}{h}\sum_{n=1}^{\infty}\sin(dz)\int_0^t\cos[\omega(t-\tau)][f_1(x,d,\tau)+f_2(x,d,\tau)+f_3(x,d,\tau)]d\tau \quad (3\text{–}90)$$

Putting the two components together, the final solution for the dimensionless ϕ in the rock mass is:

$$\phi_r = \frac{2\omega}{h}\left[\frac{\sin(\omega t)}{\omega}\sum_{n=1}^{\infty}\frac{d^3\sin(dz)}{d^4+\beta^2}-\frac{\cos(\omega t)}{\alpha}\sum_{n=1}^{\infty}\frac{d\sin(dz)}{d^4+\beta^2}+\frac{1}{\alpha}\sum_{n=1}^{\infty}\frac{de^{-\alpha d^2 t}\sin(dz)}{d^4+\beta^2}\right]$$

$$+\frac{2(1-\alpha)\omega}{h}\sum_{n=1}^{\infty}\sin(dz)\int_0^t\cos[\omega(t-\tau)][f_1(x,d,\tau)+f_2(x,d,\tau)+f_3(x,d,\tau)]d\tau \quad (3\text{-}91)$$

3.3.5 Applications

The analytical solutions for the single layer problems can be used in characterizing leaky faults. This can be done by means of the method of data matching. In other

words, the measured data for air pressure distribution will be used to match a set of calculated pressure distribution curves. The parameters read from the best matching curve can be taken as the characteristics of the fault zone. Therefore, it is important to show what these solutions look like and how certain parameters (e.g the permeability ratio, k) will affect the solutions. To distinguish which figure is from which solution, a mark of #C1, #C2, #C3 or #C4 is given on the figure obtained from solution for Case #1, Case #2, Case #3 and Case #4, respectively.

Figures 3.2A through 3.2E are calculated by the solution for Case #1, i.e. a semi-infinite thickness and a step function for the atmospheric pressure variation. For fixed values of the permeability ratio $k = 0.02$ and the diffusivity ratio $\alpha = 0.01$, Figure 3.2A shows the variation of dimensionless pressure versus dimensionless depth within the fault zone for three values of dimensionless time. For the same permeability ratio and diffusivity ratio, Figure 3.2B presents the variation of dimensionless pressure in the rock mass versus dimensionless distance from the fault-rock interface for three values of dimensionless time, which are the same as those for Figure 3.2A. This is calculated for a certain dimensionless depth, $z = 20$. The dimensionless pressure distributions for the case of no-fault are also presented on the figure for comparison. Obviously, the difference between the solid line (representing the two-dimensional solution) and the dashed line (representing the one-dimensional solution) is due to the greater permeability of the fault zone and resulting air flux from the fault zone to the rock mass. To show the effect of depth, Figure 3.2C keeps the parameters in Figure 3.2B the same except that $z = 50$. One can see that the response of the pressure variation to the atmospheric pressure disturbance is slower at greater depth. In fact, at $t = 10^3$, the pressure variation at $z = 50$ is approximately zero. Another observation is that the

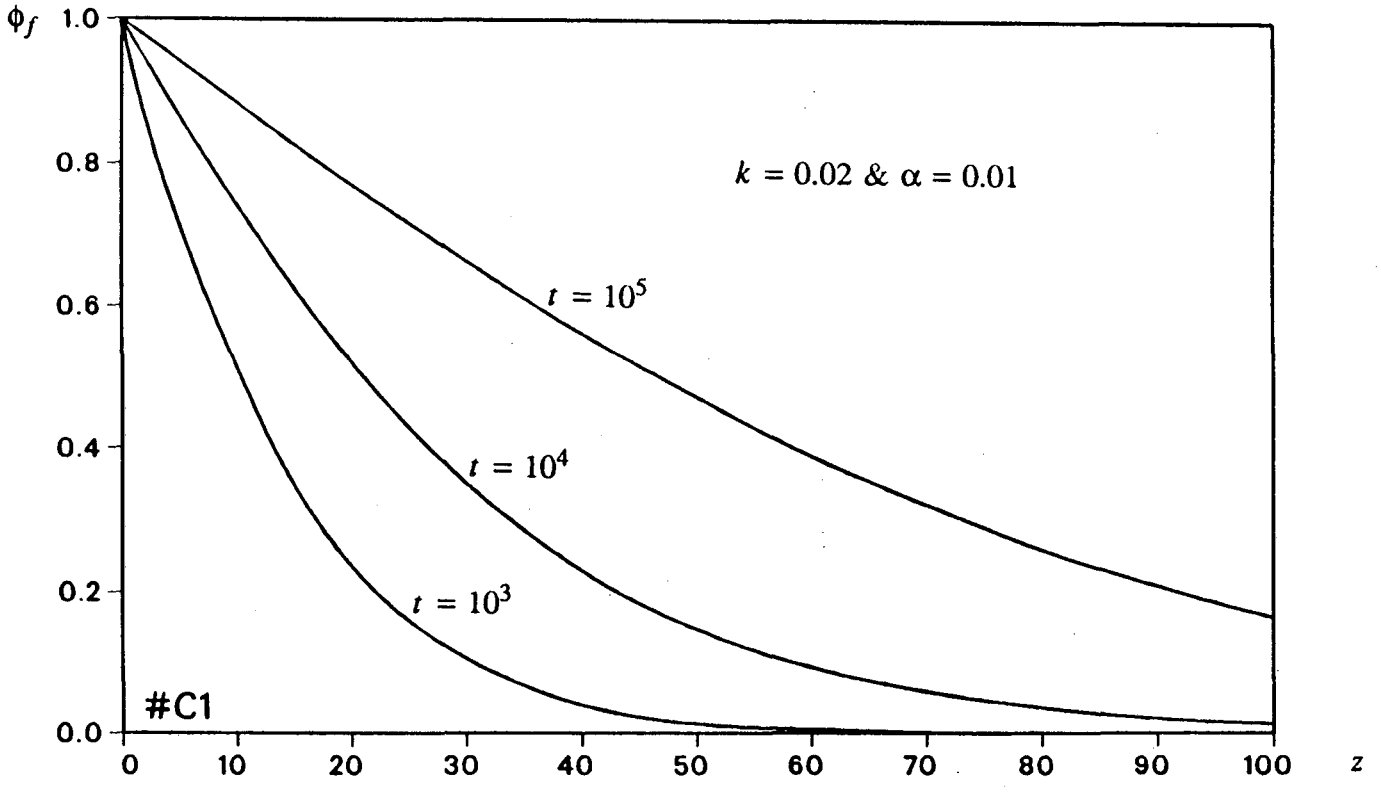

Figure 3.2A Variation of dimensionless pressure versus dimensionless depth within the fault zone for three values of dimensionless time.

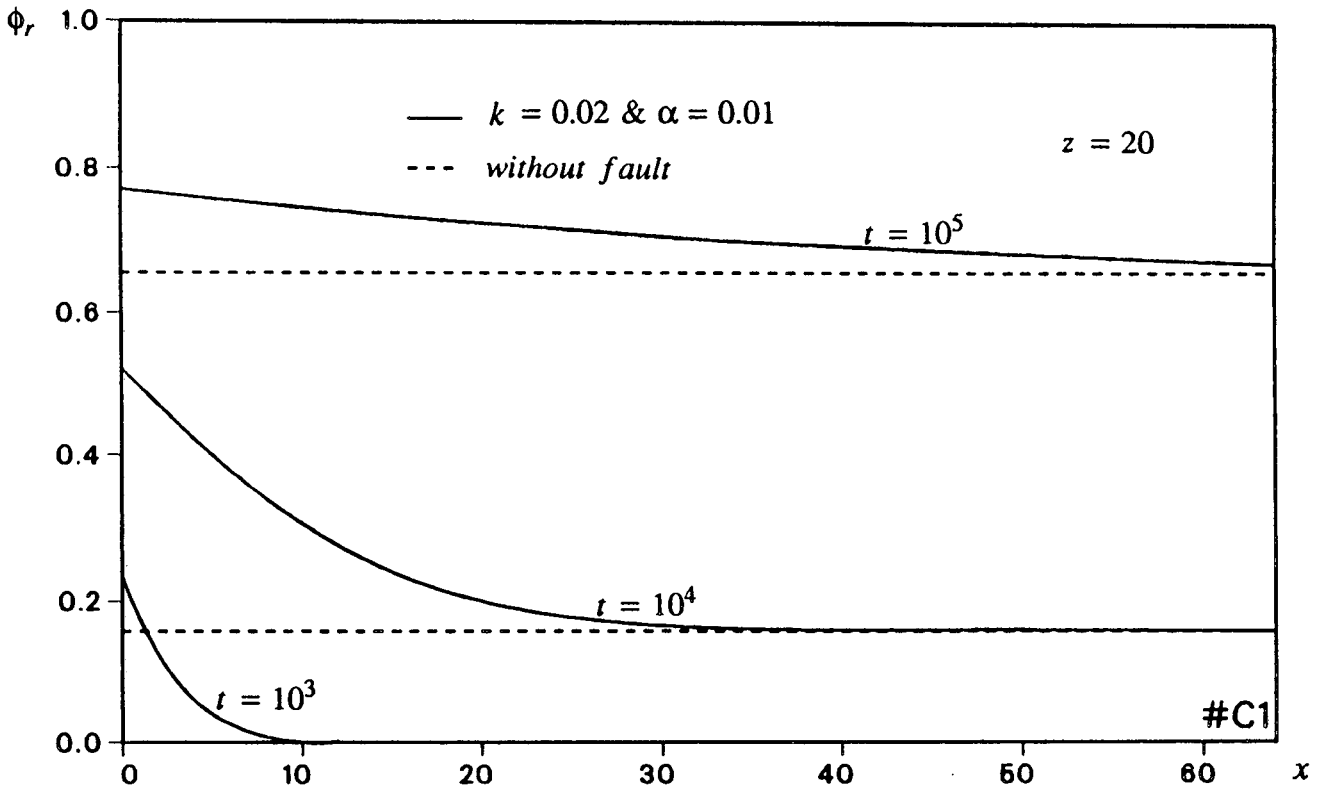

Figure 3.2B Variation of dimensionless pressure versus dimensionless distance from the fault zone at z=20, for three values of dimensionless time.

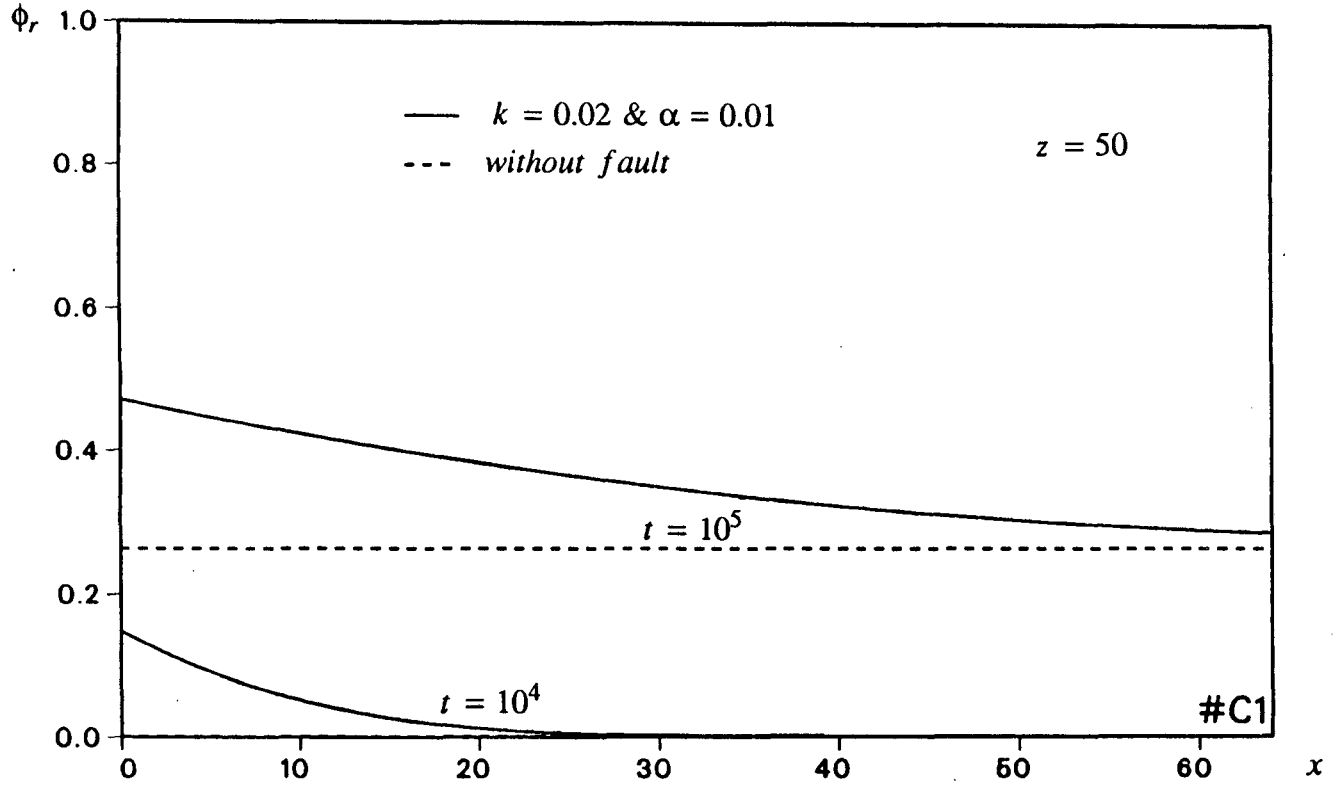

Figure 3.2C Variation of dimensionless pressure versus dimensionless distance from the fault zone at z=50, for two values of dimensionless time.

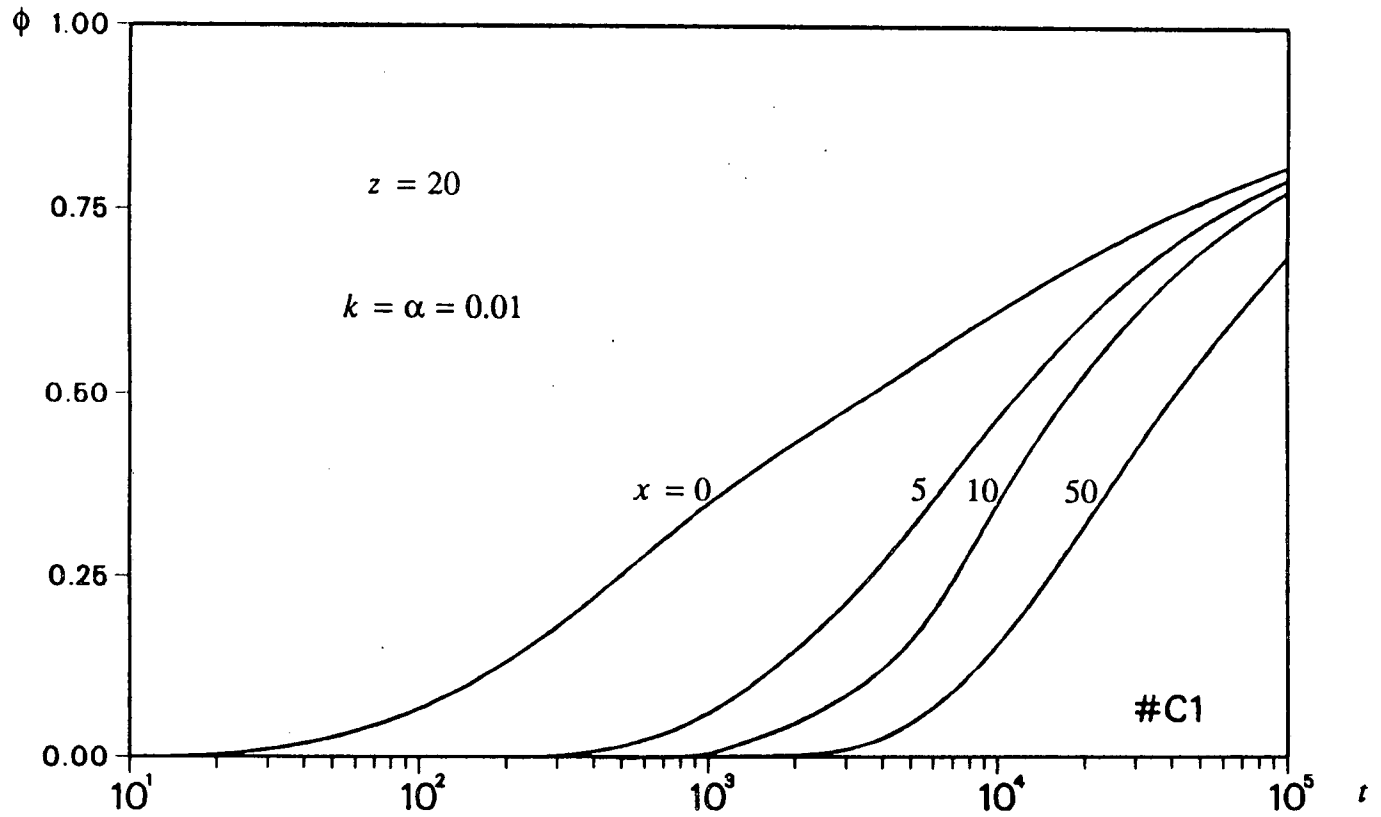

Figure 3.2D Dimensionless pressure versus dimensionless time within the fault zone and three points within the rock mass, at the same depth, for z=20, and k=α=0.01.

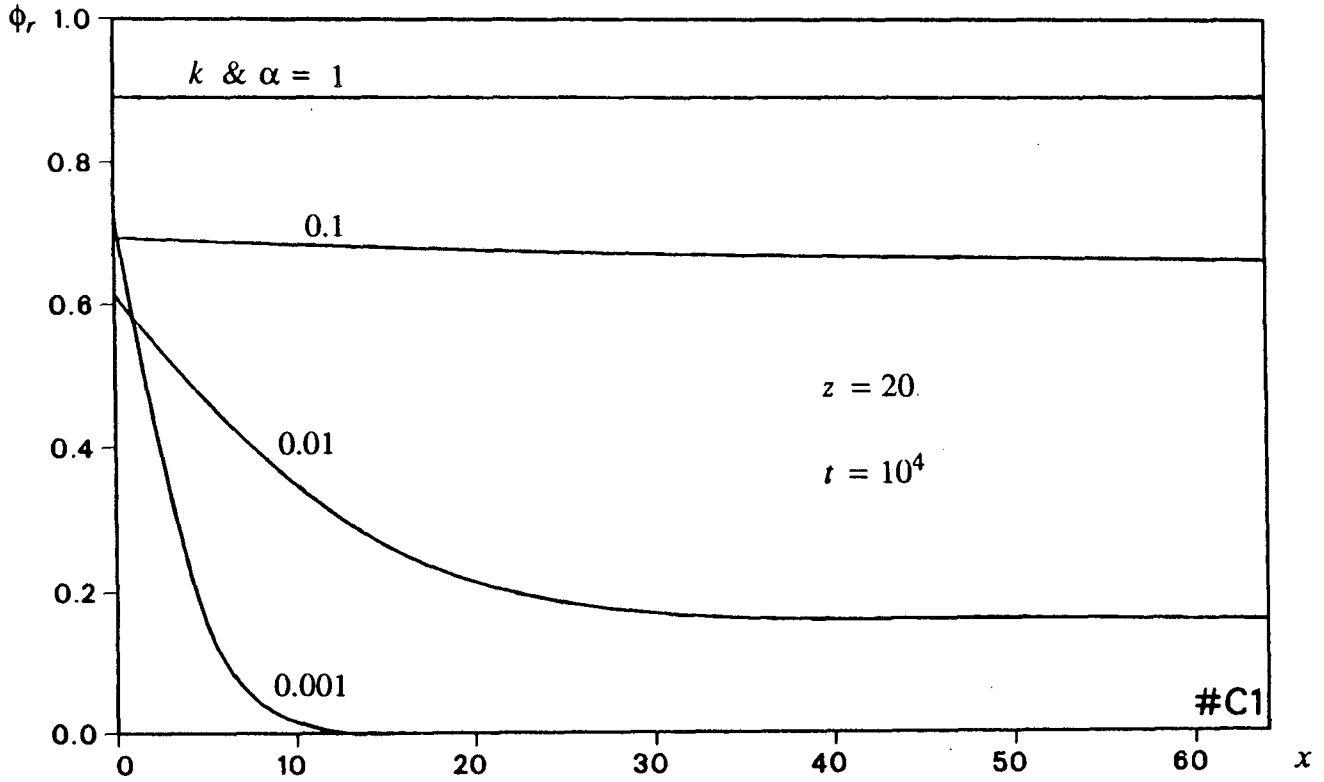

Figure 3.2E Effect of permeability contrast on dimensionless pressure.

largest contrast (of the solid line and the dashed line) appears at different times for different depths. The magnitude of the maximum contrast is also different for different depths. In another manner of plotting, Figure 3.2D shows the time variation of pressure within the fault zone and at three different locations away from the fault at the depth of $z=20$ and $k=\alpha=0.01$. Figure 3.2E presents a snapshot of the dimensionless pressure distribution at $z=20$ in the rock mass for different levels of the permeability ratio. To examine the effect of permeability contrast between the fault zone and the surrounding rocks, the value of $\bar{p}/\mu_a n_a$ has been intentionally kept the same for the two regions. As is apparent in this figure, at any arbitrary time ($t=10^4$ in this figure), the pressure gradient in the horizontal direction increases with the permeability contrast (i.e., decreasing the permeability ratio, k). The gradient, however, decreases with time as shown in Figures 3.2B and 3.2C. A close look at Figure 3.2E indicates that the curve for $k=0.001$ intersects the ones for $k=0.01$ and $k=0.1$ at small values of x. This means that at certain particular times, some points in the vicinity of the fault zone may show higher pressure changes for $k=0.001$ than for larger k values. This phenomenon can be explained by noting that under the two different conditions, the pressure changes at the fault-rock contact (i.e., $x=0$) are identical: (1) when permeability of the rock mass equals the permeability of the fault zone and (2) when the permeability of the rock mass is zero. In both cases, there is no flow across the contact. The first case corresponds to $k=1$ and the second case to $k=0$. When the permeability of the rock mass is less than that of the fault zone, since part of the air entering into the fault zone will flow into the surrounding rock, the pressure increase in the fault zone will be smaller. This is why ϕ_r at $x=0$ for $k=0.1$ and $k=0.01$ become smaller than that for $k=1$. However, when the rock permeability becomes

very small, air flux from the fault zone to the rock mass tends to diminish, and as a result the pressure change in the fault zone increases again.

In the same way, Figures 3.3A through 3.3D are plotted from the solution for Case #2, i.e. finite system thickness and a step functional atmospheric pressure variation. The dimensionless thickness, h, for the four figures is fixed at 100. Again, for fixed values of permeability ratio $k=0.02$ and diffusivity ratio $\alpha=0.01$, Figure 3.3A shows the variation of dimensionless pressure versus dimensionless depth within the fault zone for three values of dimensionless time. For the same permeability ratio and diffusivity ratio, Figure 3.3B presents the variation of dimensionless pressure in the rock mass versus dimensionless distance from the fault-rock interface for three values of dimensionless time, which are the same as those for Figure 3.3A. This is calculated for certain dimensionless depth, $z=20$. The dimensionless pressure distributions for the case of no-fault are also presented on the figure for comparison. To show the effect of depth, Figure 3.3C keeps everything the same as those in Figure 3.3B except $z=50$. One can see that the response of the pressure variation to the atmospheric pressure disturbance is slower at deep point than that at shallow point. In fact, at $t=10^3$, the pressure variation at $z=50$ is approximately zero. Figure 3.3D presents a snapshot of the dimensionless pressure distribution at $z=20$ in the rock mass for different levels of permeability (diffusivity) ratio. Comparing these figures with those plotted from the solution for Case #1, one may find that at early times when the effect of the lower boundary has not been felt the results from both cases are identical. At large values of time, however, results from two cases deviate. For example, the two curves for $t=10^3$ and $t=10^4$ in Figure 3.3A are almost the same as those in Figure 3.2A; but the curve for $t=10^5$ in Figure 3.3A is higher than that in Figure 3.2A. The

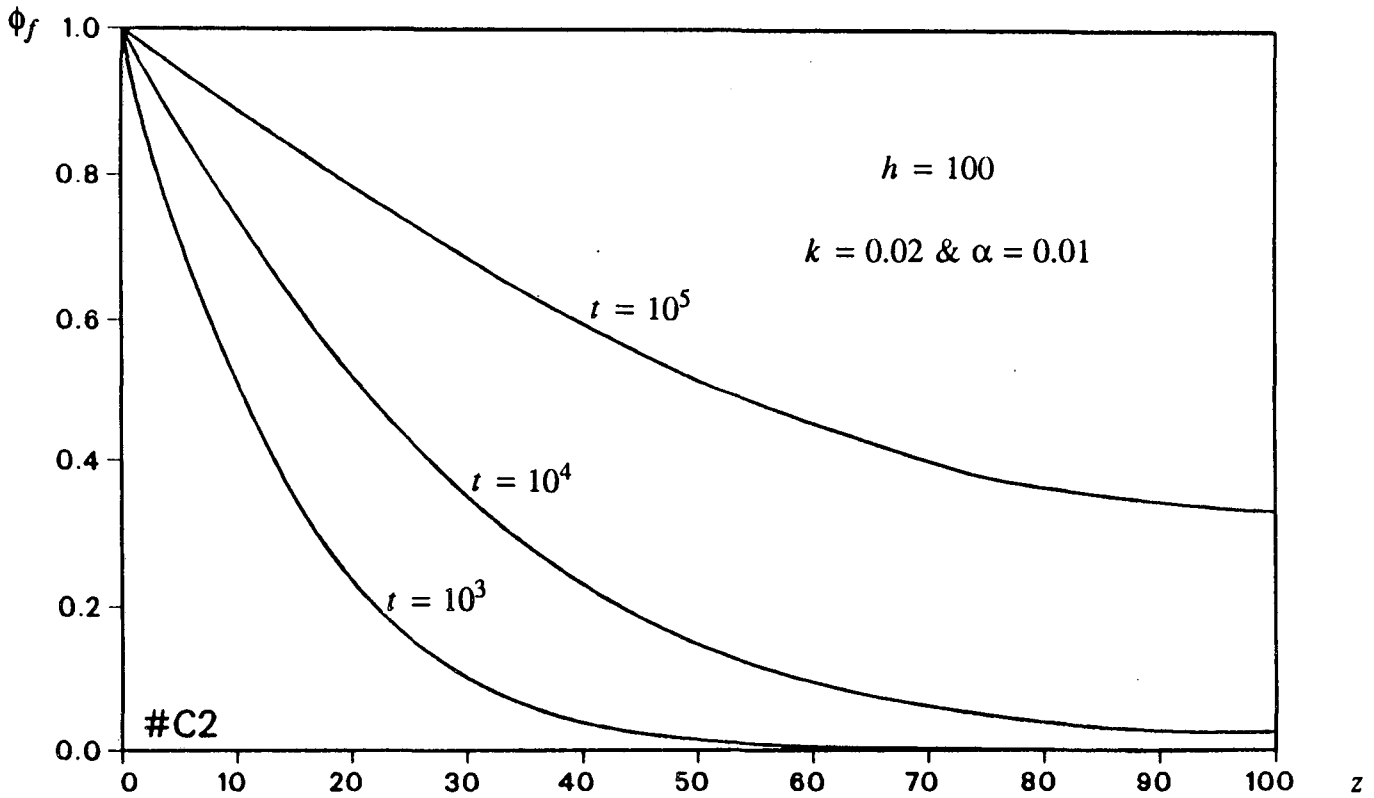

Figure 3.3A Variation of dimensionless pressure versus dimensionless depth within the fault zone for three values of dimensionless time and for the case of dimensionless thickness, h=100.

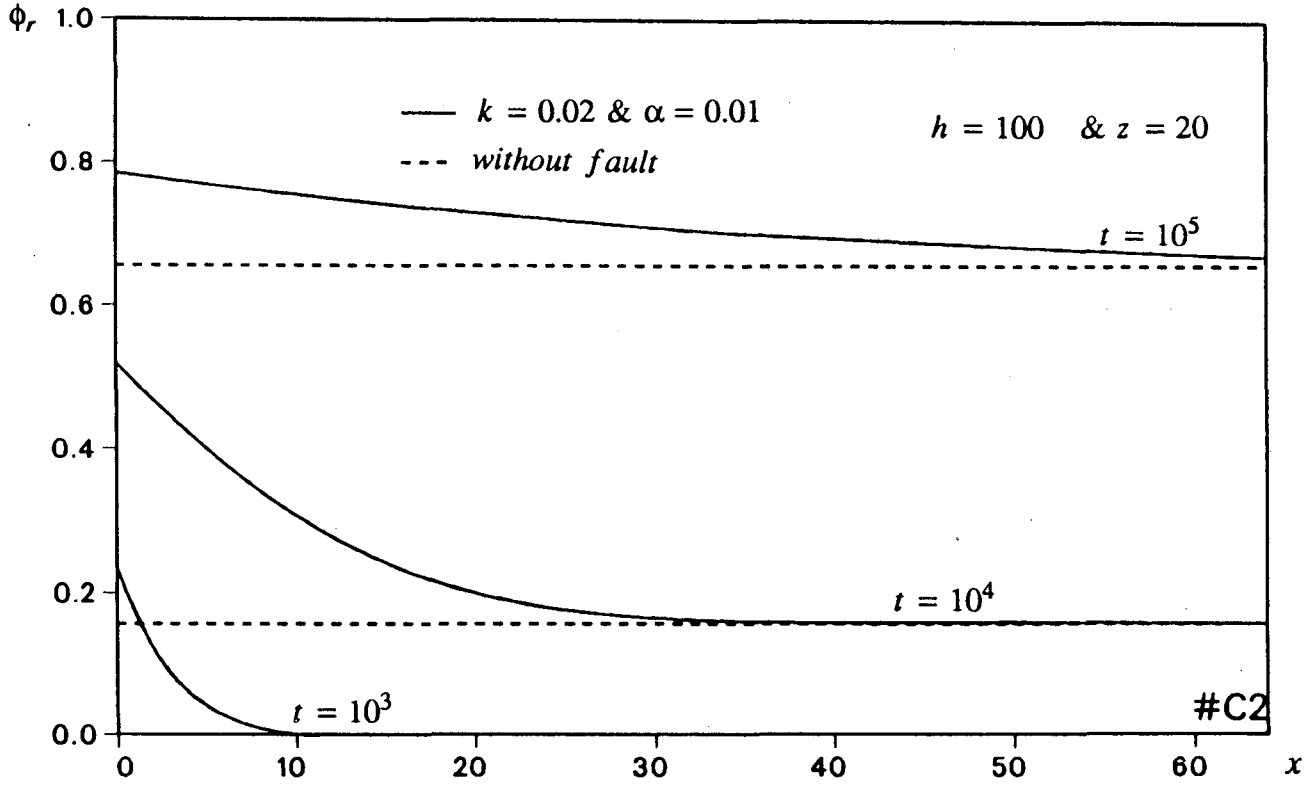

Figure 3.3B Variation of dimensionless pressure versus dimensionless distance from the fault zone at z=20, for three values of dimensionless time and for the case of dimensionless thickness, h=100.

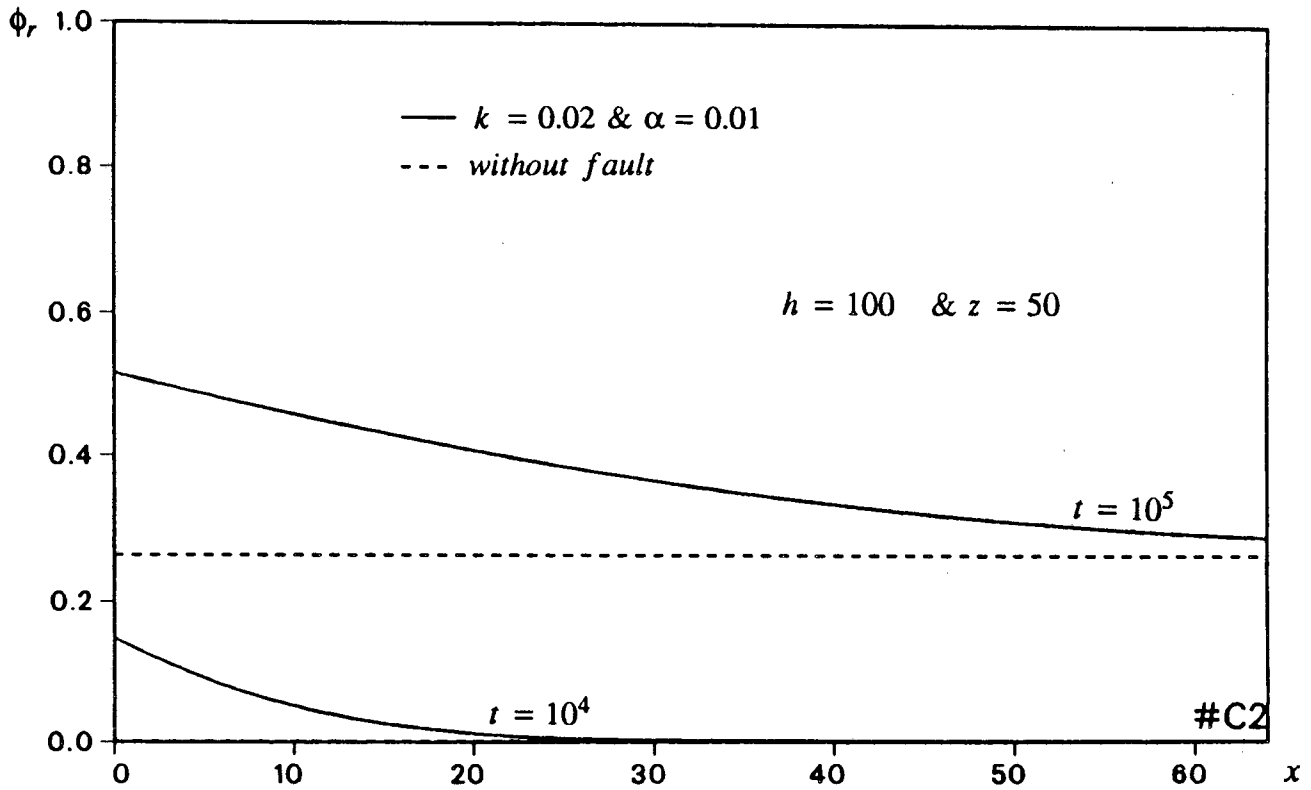

Figure 3.3C Variation of dimensionless pressure versus dimensionless distance from the fault zone at z=50, for two values of dimensionless time and for the case of dimensionless thickness, h=100.

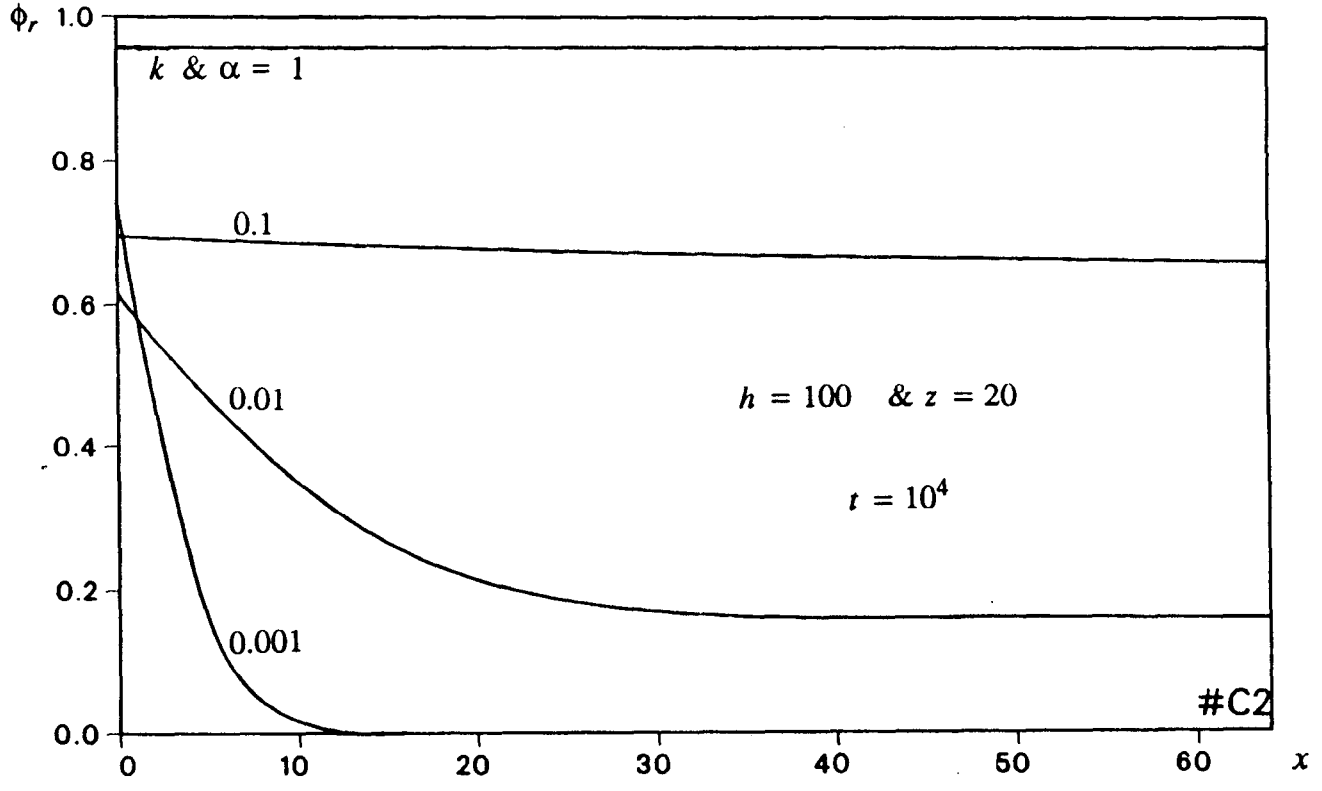

Figure 3.3D Effect of permeability contrast on dimensionless pressure for the case of dimensionless thickness, h=100.

definition of " early time " will depend on the value of dimensionless thickness, h and the depth of the points for measurement. To show this, Figures 3.3E and 3.3F give the comparison of solutions from Case #1 and from Case #2 for two different values of h. At the same depth of measurement ($z = 20$), Figure 3.3E presents the dimensionless pressure distributions for three values of time. The solid line represents the pressure calculated by the solution for the case of semi-infinite thickness (i.e., $h = \infty$); while the dots represent those for the case of finite thickness ($h = 100$). One may find that almost all dots fall on the corresponding solid curve except they are a little bit higher at places close to the fault-rock contact when $t = 10^5$. For this particular case ($h = 100$ and $z = 20$), one may roughly define $t \leq 10^5$ as " early time ". In Figure 3.3F, the impermeable boundary is shifted from $h = 100$ to $h = 50$. Due to this change, a big difference in pressure distribution between the two cases appears at $t = 10^5$. For this particular case ($h = 50$ and $z = 20$), one needs to use $t < 10^4$ as the criterion of " early time ". The above comparisons and analyses can reveal both the applicability of the solution for Case #1 and the necessity of the solution for Case #2. A suitable combination of the applications of the two solutions will be very helpful in practice.

Figures 3.4A through 3.4C present the results obtained from calculation of the solution for Case #3, i.e., semi-infinite system thickness and sinusoidal atmospheric pressure variation. Figure 3.4A shows the time variation of the dimensionless pressure in the fault zone at five different depths for a permeability (diffusivity) ratio of $k = \alpha = 0.01$. As indicated by this figure, there is an attenuation of the amplitude and frequency with depth. It can be expected from the trend of the curves that the time variation of dimensionless pressure will finally overlap with the dashed line at $z = \infty$,

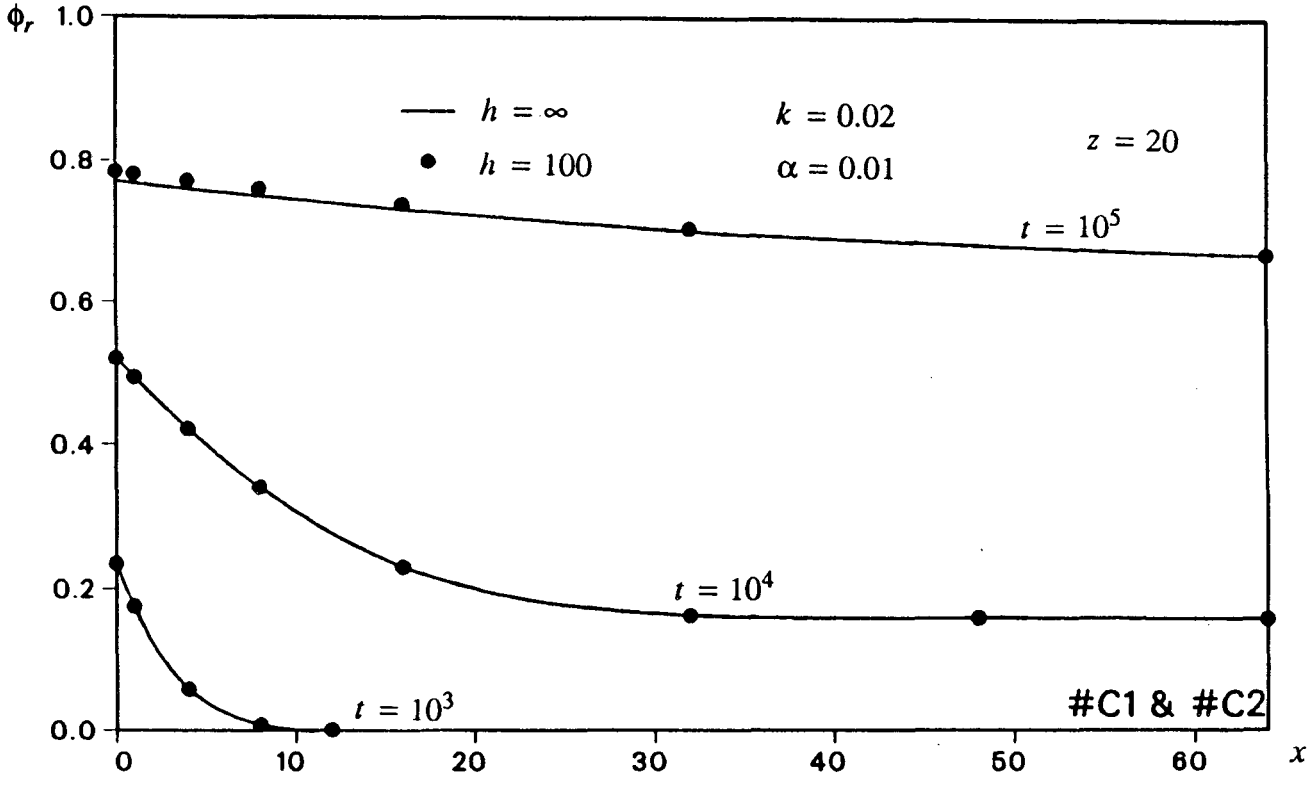

Figure 3.3E Effect of the boundary depth: relative deep (h=100).

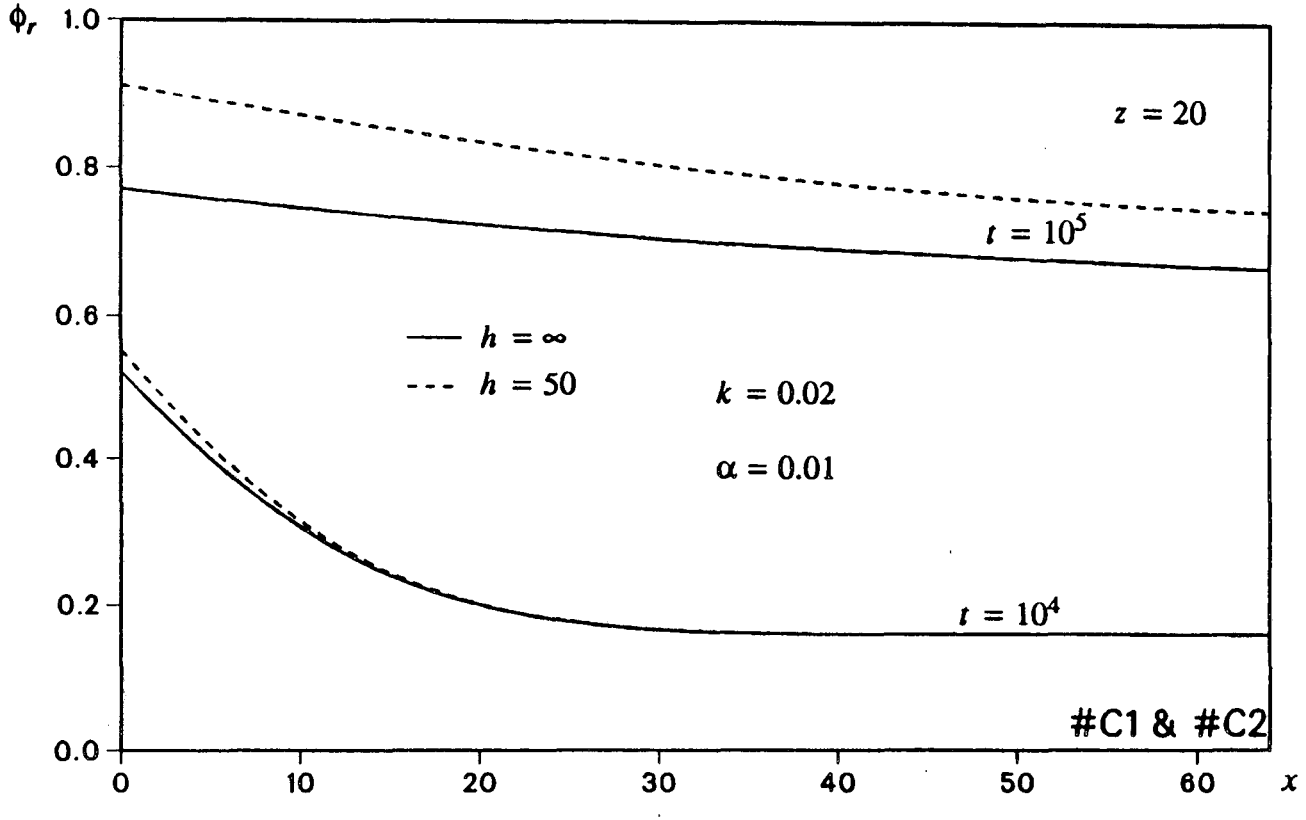

Figure 3.3F Effect of the boundary depth: relative shallow (h=50).

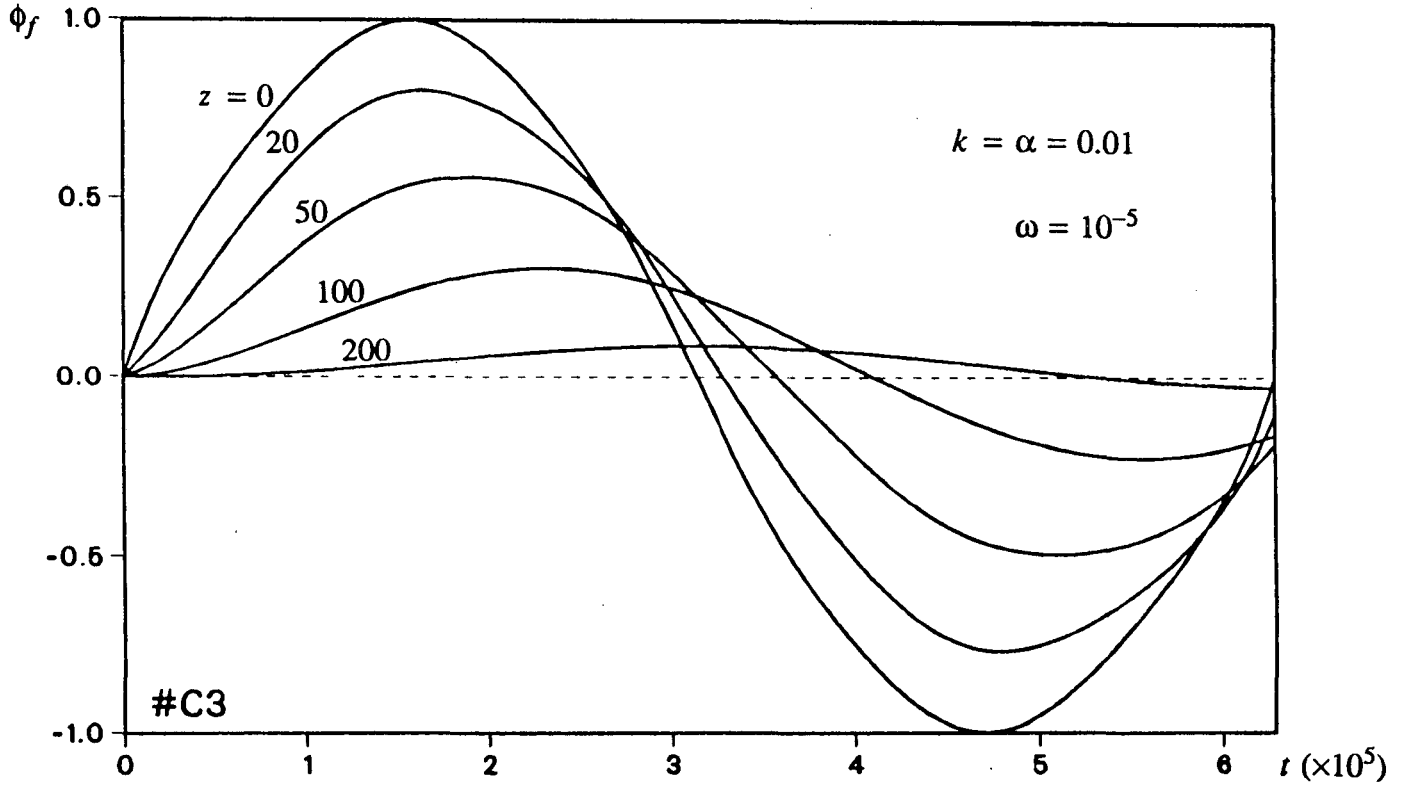

Figure 3.4A Dimensionless pressure versus dimensionless time in the fault zone at five different dimensionless depths (for case of $h=\infty$).

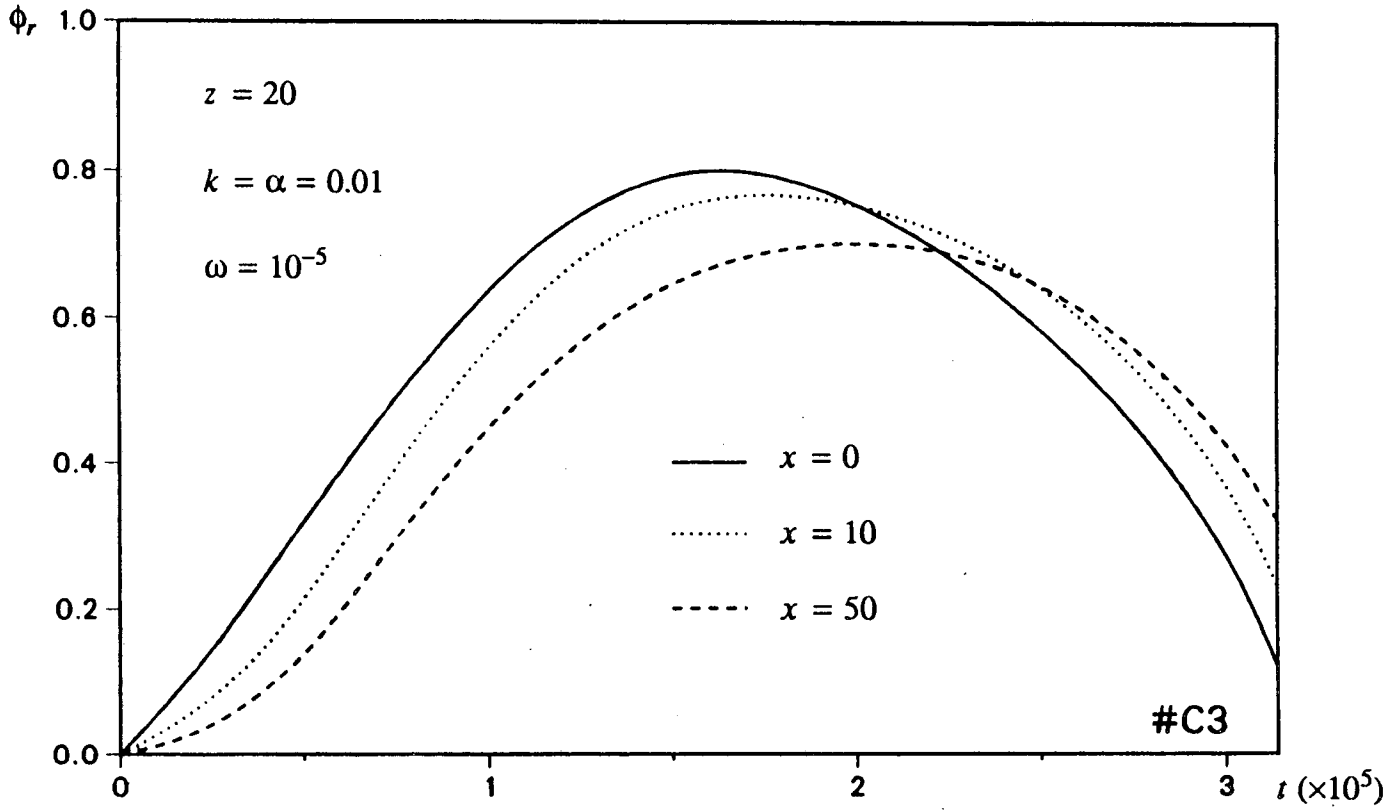

Figure 3.4B Time variation of dimensionless pressure within the fault zone and two other points away from the fault at the same depth, for z=20, and k=α=0.01 (for case of h=∞).

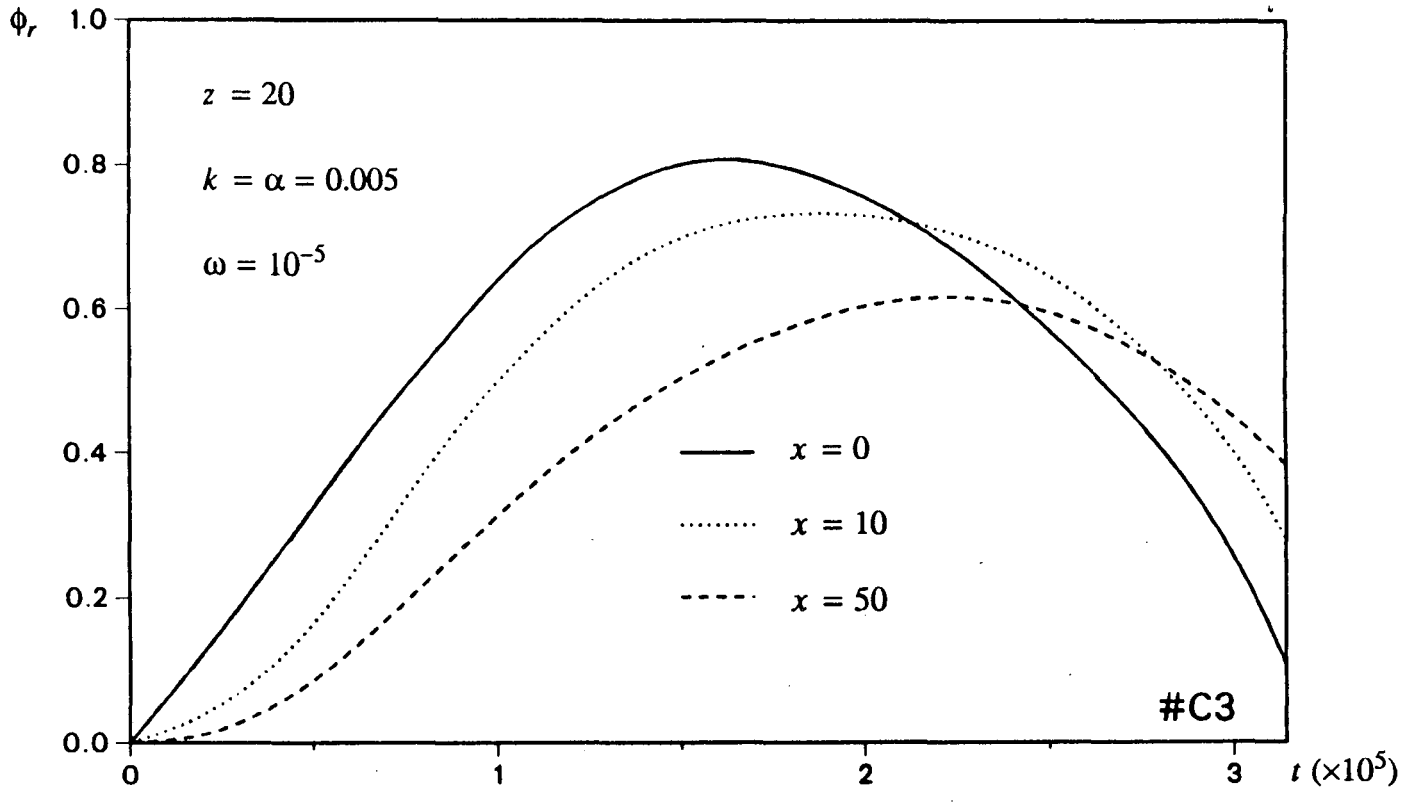

Figure 3.4C Time variation of dimensionless pressure within the fault zone and two other points away from the fault at the same depth, for z=20, and k=α=0.005 (for case of h=∞).

i.e., $\phi_f \equiv 0$. Figure 3.4B illustrates time variation of the dimensionless pressure within the fault zone and at two other points in the rock mass at the same depth, $z = 20$ and for $k = 0.01$. Figure 3.4C shows results for the same set of parameters except for a smaller permeability ratio of $k = 0.005$. The two figures show that when the permeability of the rock adjacent to the fault zone is significantly less than that of the fault zone, points located away from the fault will experience smaller amplitudes. The farther the points, the smaller the amplitudes. Furthermore, there is also a phase lag in the observed pressure changes. The farther the point from the fault, the larger is the lag in the observed pressure changes. Such phenomena seem to be magnified when the permeability contrast increases (i.e., k decreases).

In a similar way, Figures 3.5A through 3.5C are plotted from the results obtained by calculating the solution for Case #4, i.e., finite system thickness and sinusoidal atmospheric pressure variation. The dimensionless thickness in these figures are fixed to be $h = 50$. Figure 3.5A shows the time variation of the dimensionless pressure in the fault zone at three different depths for a permeability (diffusivity) ratio of $k = \alpha = 0.01$. Comparing this figure with Figure 3.4A, it is very clear that the attenuation of the amplitude with depth is much smaller in this case than that in Case #3. This is apparently due to the blockade effect of the impermeable boundary. Actually, Figure 3.5B and Figure 3.5C have the same contents as those of Figure 3.4B and Figure 3.4C, respectively, except for the thickness, $h = 50$. Although in this case the amplitude of the variation of dimensionless pressure in the rock gets higher as well as in the fault, the contrast of the time variation curves becomes clearer. Figure 3.5D shows the boundary effect on sinusoidal solutions for the particular case of $h = 50$. At

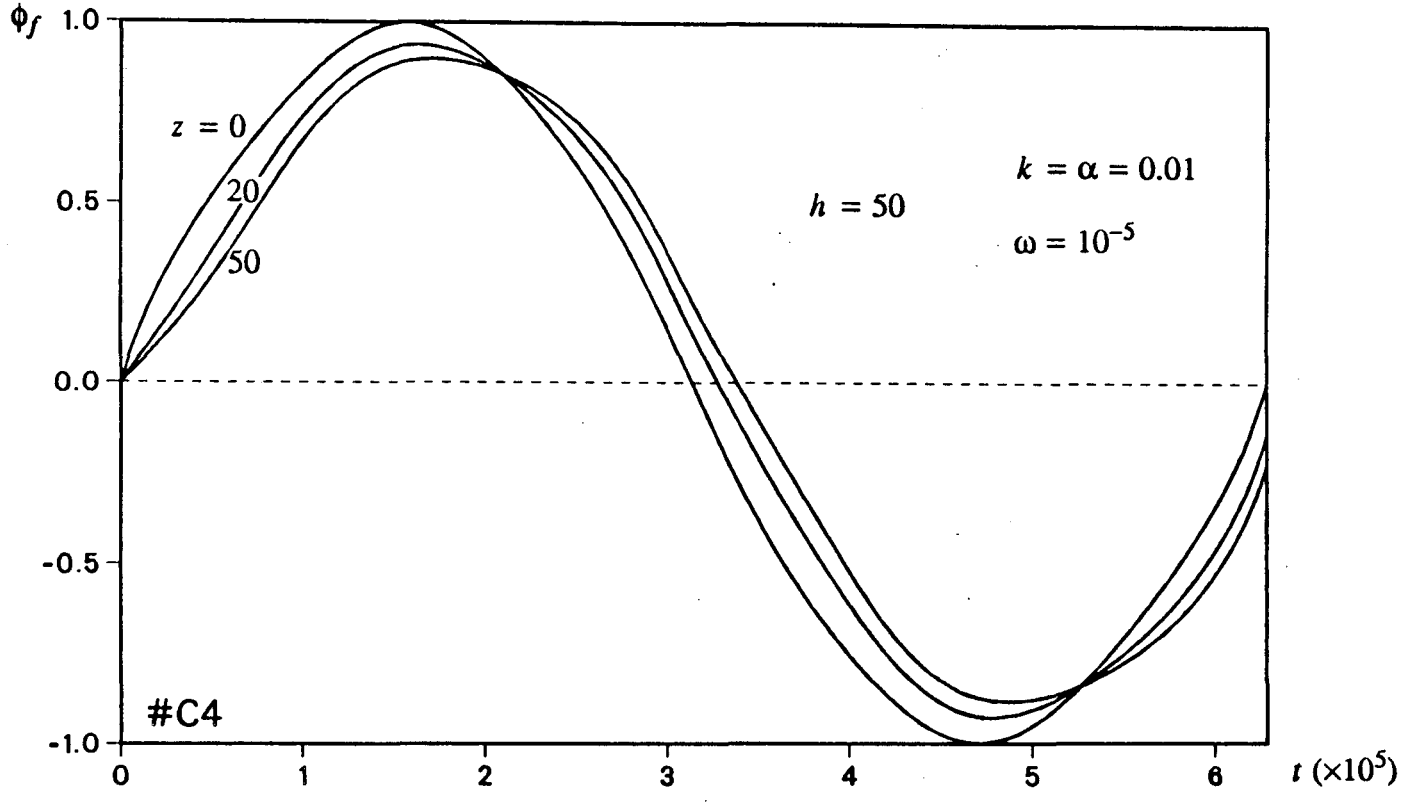

Figure 3.5A Dimensionless pressure versus dimensionless time in the fault zone at three different dimensionless depths (for case of h=50).

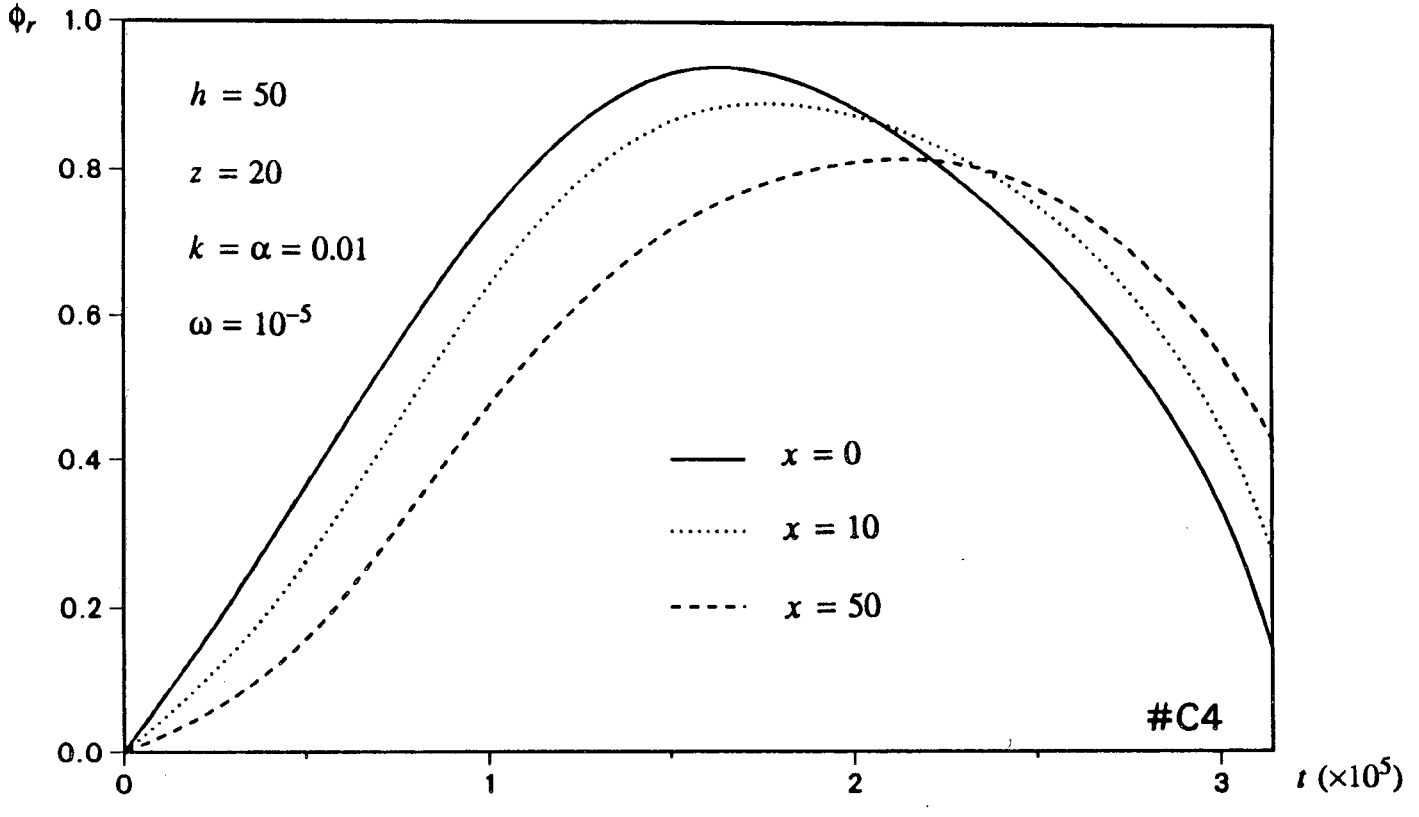

Figure 3.5B Time variation of dimensionless pressure within the fault zone and two other points away from the fault at the same depth, for z=20, and k=α=0.01 (for case of h=50).

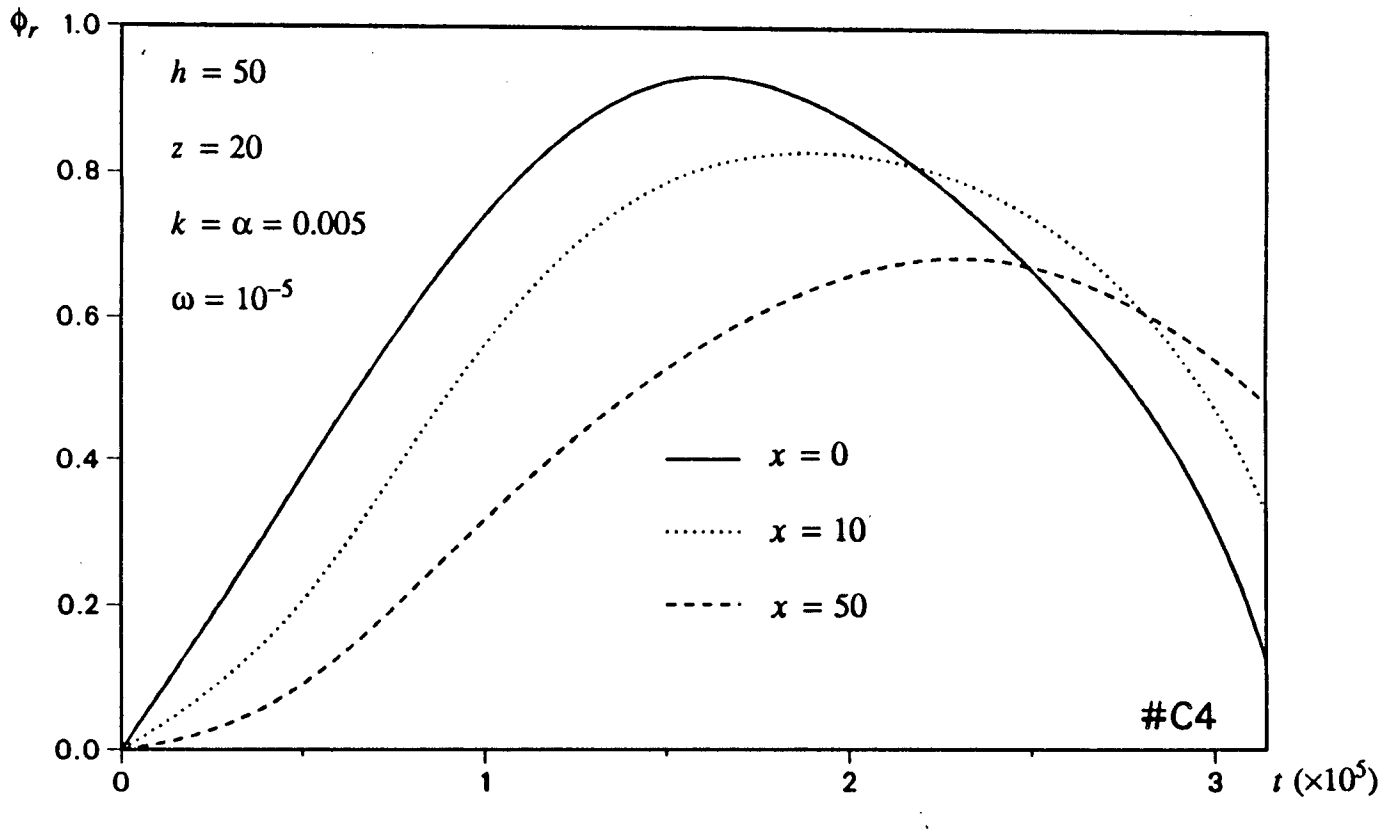

Figure 3.5C Time variation of dimensionless pressure within the fault zone and two other points away from the fault at the same depth, for z=20, and k=α=0.005 (for case of h=50).

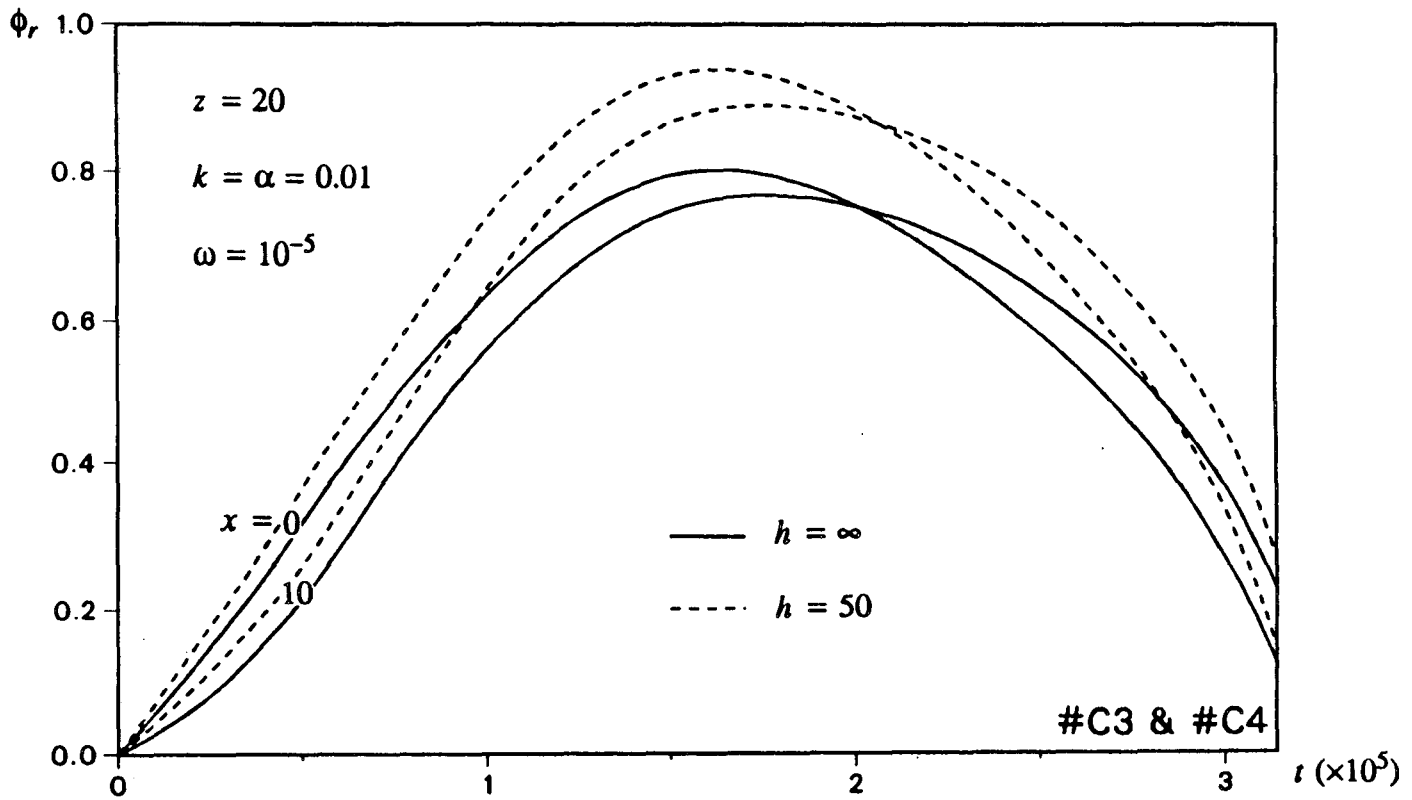

Figure 3.5D Boundary effect on sinusoidal solutions for the case of h=50.

a certain depth, $z = 20$ and for a permeability of $k = 0.01$, the time variation curves in the fault ($x = 0$) and in the rock (for $x = 10$) are plotted for both Case #3 (solid lines) and Case #4 (dashed lines). Generally speaking, the impermeable boundary has the effect of reducing both the attenuation of amplitude and the phase lag.

An examination of Figures 3.2E, 3.3D, 3.4C and 3.5C reveals that when the contrast between permeability of the fault zone and the surrounding rock mass is significant, the spatial pressure variations in the vicinity of the fault zone could be large enough to lend itself to be measured by conventional instruments. Therefore, air pressure data from isolated intervals in horizontal or inclined boreholes drilled through the fault zone and the rock mass may be analyzed to obtain the permeability ratio between the rock mass and the fault zone. An example of solution application is given in the following.

Example: Assuming that the rock-fault system has a thickness of $h' = 100m$ and that the pneumatic specific storage of the fault zone and the rock mass are the same: $S_{a_f} = S_{a_r} = 10^{-5}m^{-1}$. The initial pressure is $p_0 = 1atm. = 10^5 Pa$. The pressure variation at the ground surface ($z' = 0$) is roughly $p = p_0 + p_b \sin(\omega' t')$. Normally, this fluctuation will have a period of 24 hours, which implies that $\omega' = 2\pi/24/3600 \simeq 7.27 \times 10^{-5} s^{-1}$. For this example, it is assumed that the amplitude of the variation is $p_b = 1000Pa$, which is one percent of the mean pressure. Four groups of parameters including the half width of the fault zone (b') and the pneumatic conductivities of the rock and the fault (K_{a_r} and K_{a_f}) are given in Table 3.1. For each case, determine the pressure variation at the depth of $z' = 50m$.

Table 3.1 Parameters for Calculating Pressure Effects

Number	$b'(m)$	$K_{a_f}(m\cdot s^{-1})$	$K_{a_r}(m\cdot s^{-1})$
#1	10	10^{-3}	10^{-5}
#2	10	10^{-3}	10^{-4}
#3	10	10^{-4}	10^{-5}
#4	1	10^{-3}	10^{-5}

Solution:

The related dimensionless parameters for each case are given in Table 3.2.

Table 3.2 Dimensionless Parameters for Calculating Pressure Effects

Number	h	z	$k(\alpha)$	ω
#1	10	5	0.01	7.27×10^{-5}
#2	10	5	0.1	7.27×10^{-5}
#3	10	5	0.1	7.27×10^{-4}
#4	100	50	0.01	7.27×10^{-7}

For any given value of time, (3-91) gives the dimensionless pressure, ϕ. By definition formulae (3-3) and (3-73), $p=\sqrt{\phi'}=\sqrt{p_0^2+2p_0p_b\cdot\phi}$. We define $\Delta p = p - p_0$ as the 'pressure increment'.

Figures 3.5E through 3.5H present the distribution of the pressure increments within 10 meters from the fault-rock contact, at $t = 1\,hour$, $6\,hours$ and $12\,hours$ for each of the four cases. One can find that when $t = 1\,hour$ or $12\,hours$, except for the case of #2 (Figure 3.5F) there is a big pressure difference of about 20 to 40 Pa within 10 meters of distance from the fault. Because the accuracy of the pressure measurement in field tests is usually less than 1 Pa (e.g., 0.3Pa. Weeks, 1978.), the characteristic curves of the pressure increment can be used to help determine the permeability ratio of the rock-fault system, especially when the permeability contrast between the rock mass and the fault zone is large (e.g., $k = 0.01$ in this example). Comparing Case #2 with Case #3, it is interesting to find that although the permeability ratios are the same (0.1), the results are quite different due to the orders of difference between the corresponding pneumatic conductivities in two cases. Figures 3.5G and 3.5H are similar because Cases #2 and #3 have the same transmissivity in the fault zone.

All these analytical solutions derived in this study are, of course, valid only for a single layer problem. For multi-layer problem, the theoretical pressure distribution curves may be calculated by numerical methods.

3.4 Numerical Solutions for Multi-Layer Problems

A numerical code, TRUMP was used to solve the multi-layer problems with more complicated boundary conditions. This program was written by Edwards (1972) for transient and steady-state temperature distributions in multi-dimensional systems. The similarity of our problem to the problem of heat transfer enables us to apply this program without difficulties. Before applying it to solve the multi-layer problems, it is better to verify the code against the analytical solutions obtained in this chapter.

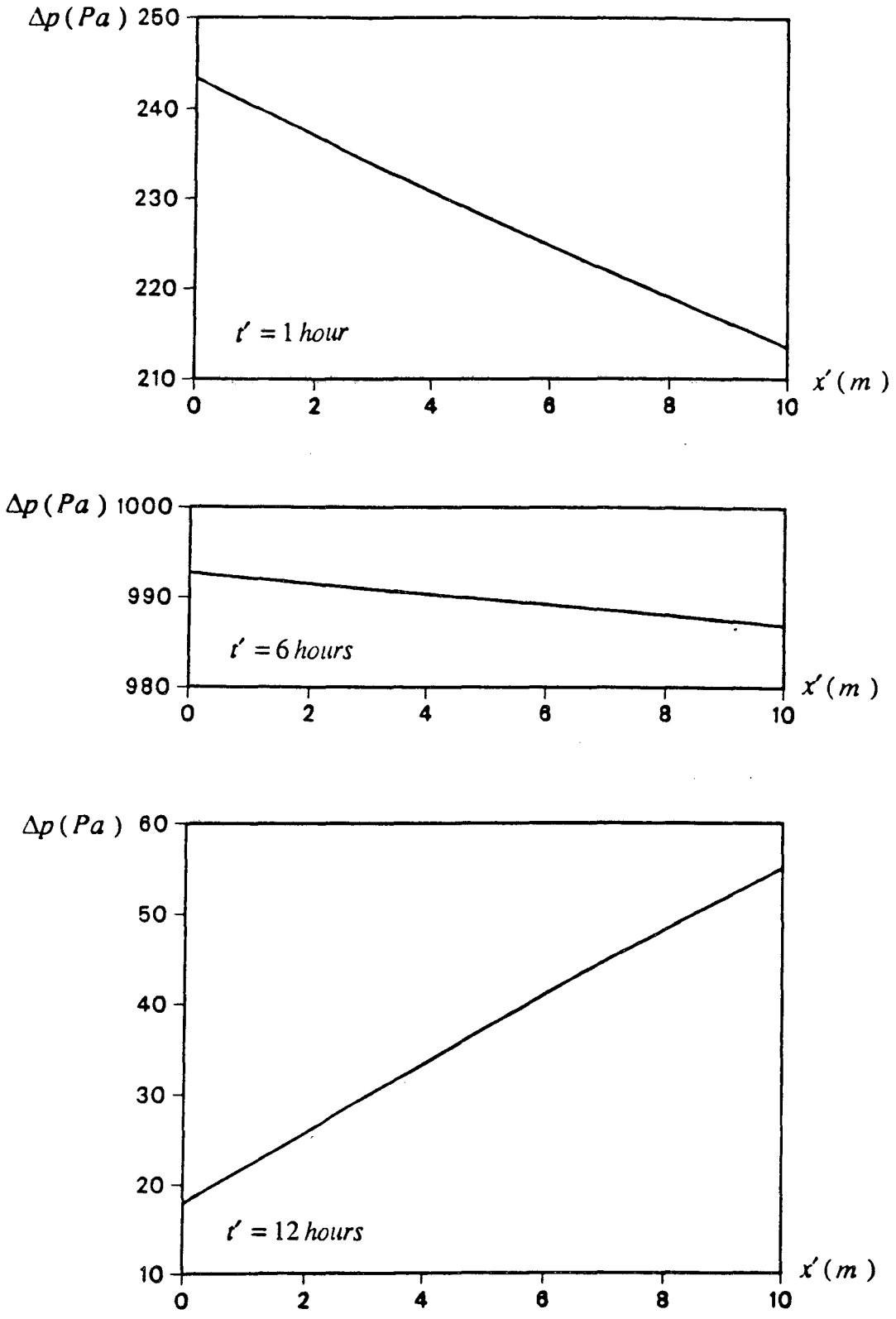

Figure 3.5E Distribution of pressure increment in the rock mass at a depth of $z' = 50m$ and three values of time, for the calculation example #1.

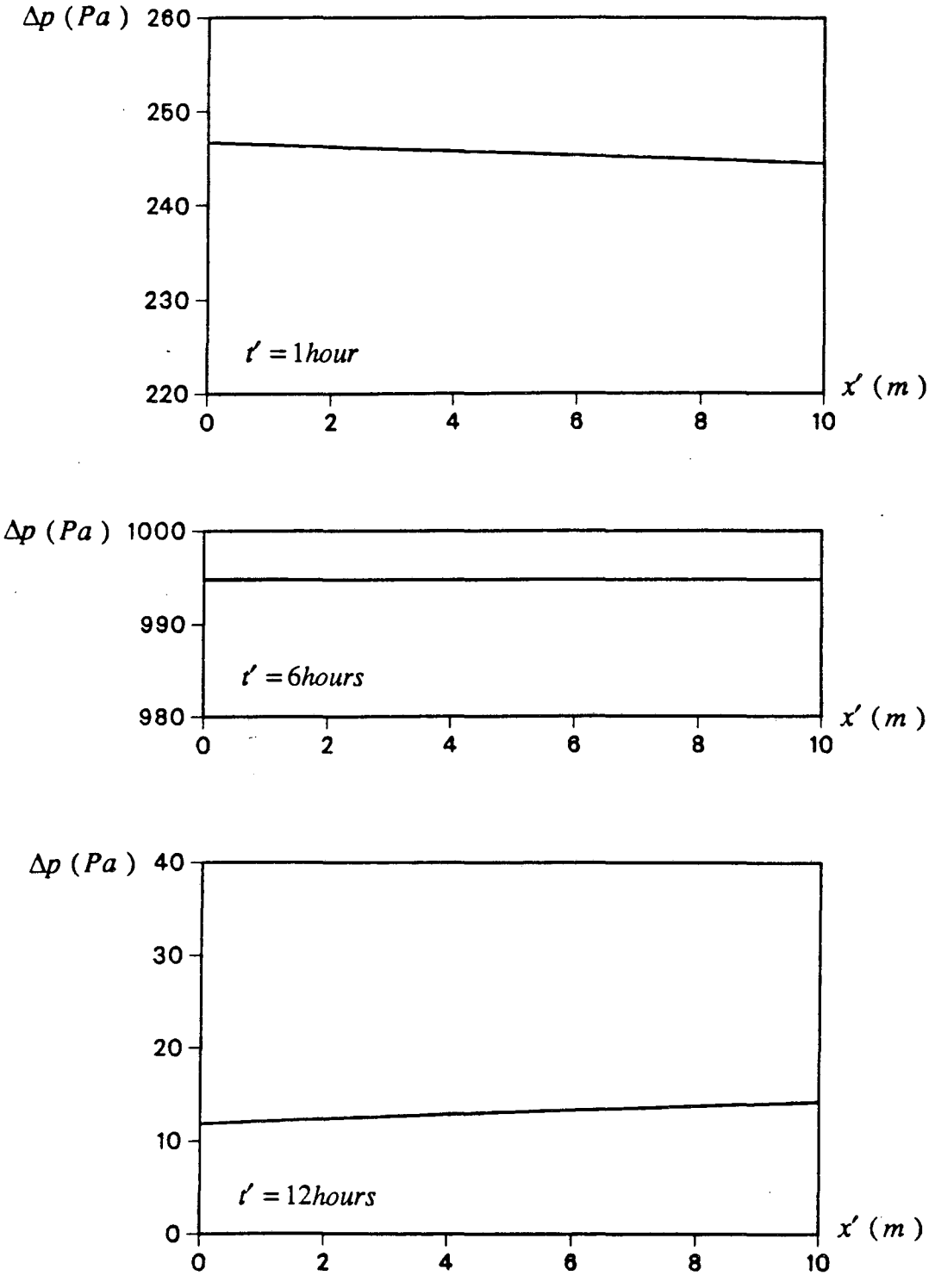

Figure 3.5F Distribution of pressure increment in the rock mass at a depth of $z'=50m$ and three values of time, for the calculation example #2.

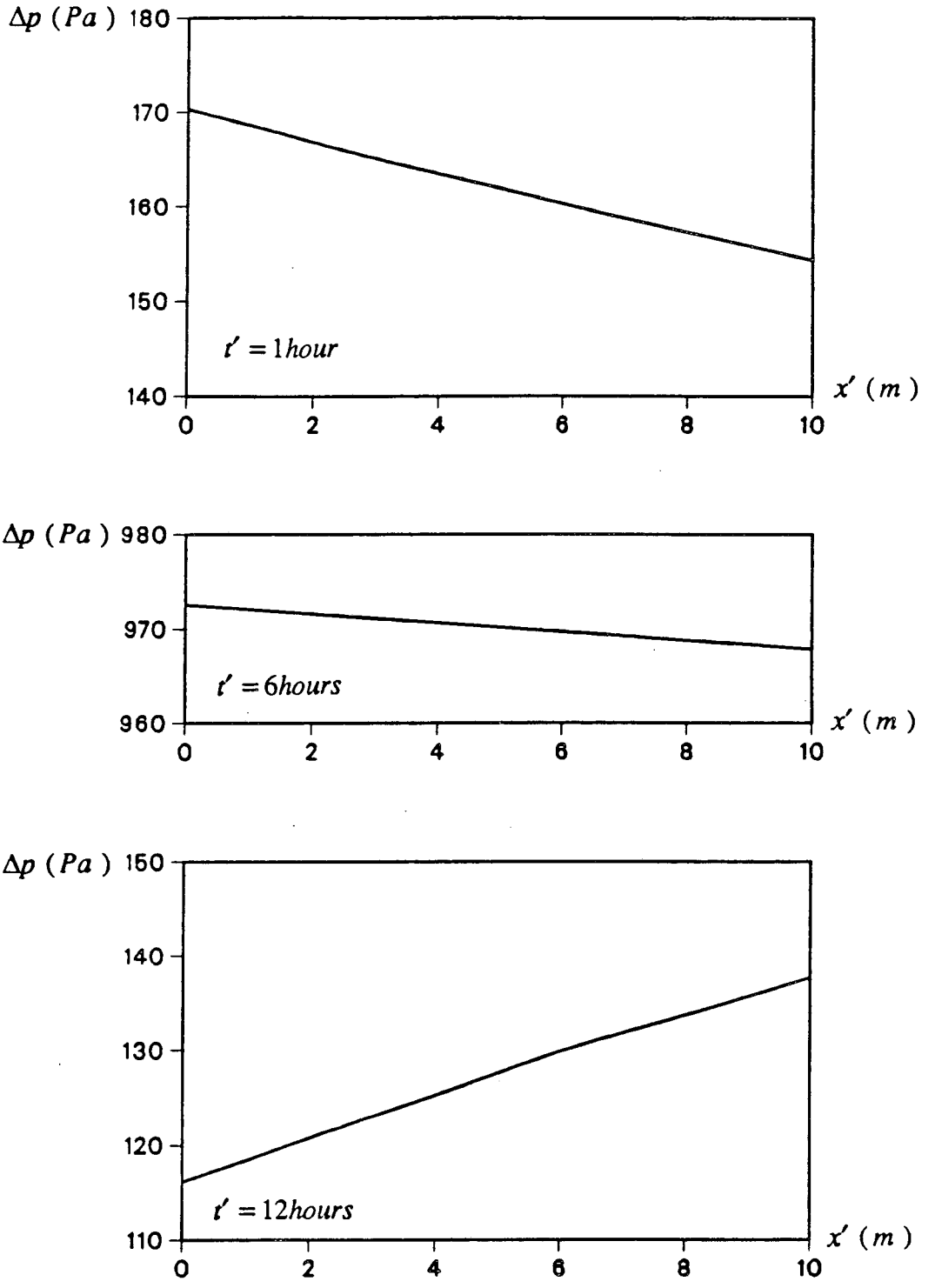

Figure 3.5G Distribution of pressure increment in the rock mass at a depth of z'=50m and three values of time, for the calculation example #3.

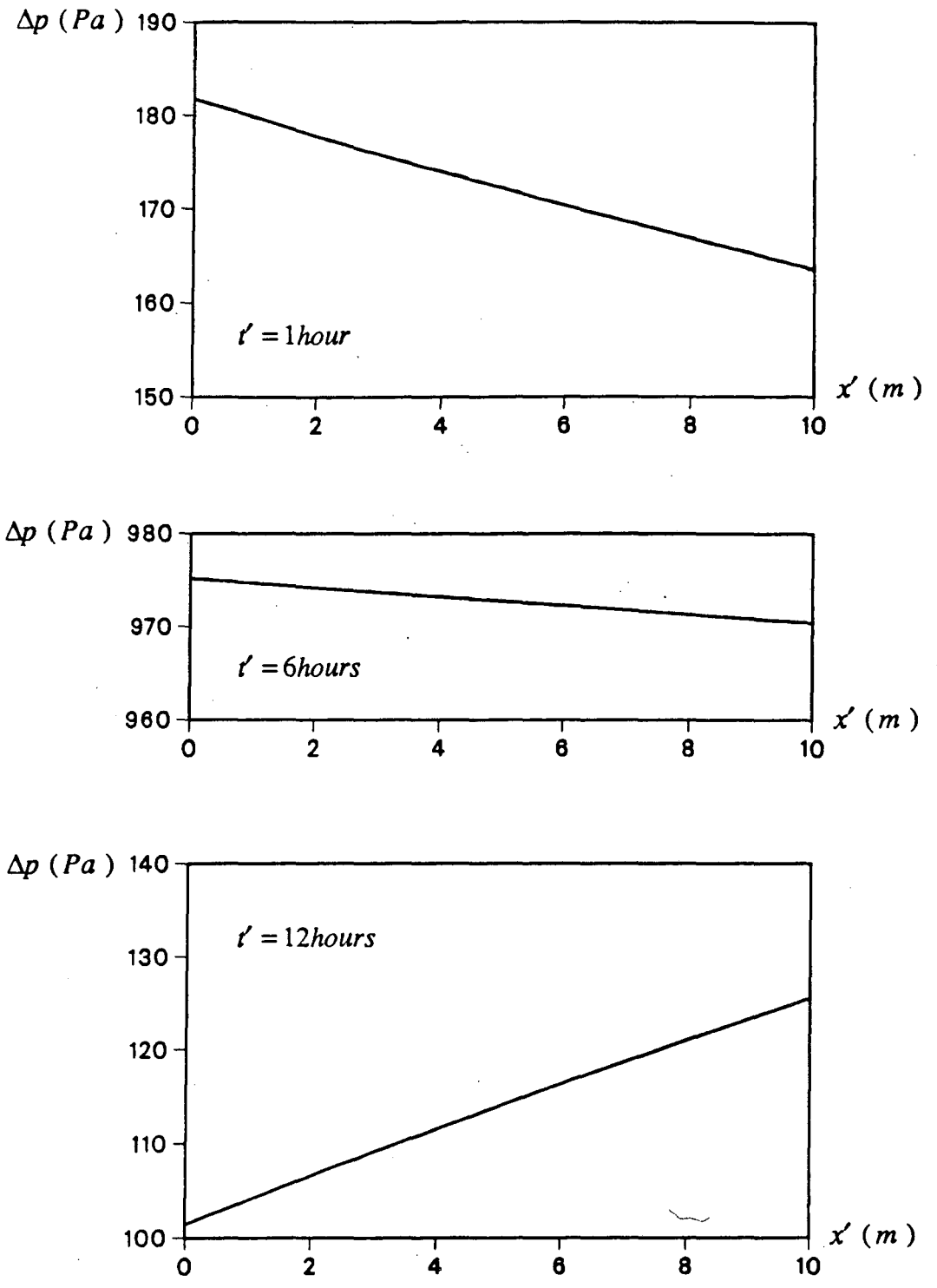

Figure 3.5H Distribution of pressure increment in the rock mass at a depth of z'=50m and three values of time, for the calculation example #4.

3.4.1 Verification of Code

Figures 3.6A through 3.6C provide some verifications on the numerical code, TRUMP. Figure 3.6A represents a study on effect of mesh size during the process of verification. This plot is the dimensionless pressure distribution in the rock mass at a dimensionless depth of $z = 20$ and at the dimensionless time, $t = 10^4$. The other parameters used in the calculations are: $k = 0.02$ and $\alpha = 0.01$. The solid curve in the figure represents the result calculated by the analytical solution for Case #2 with a particular dimensionless thickness of $h = 100$. Three different markers represent numerical solutions obtained by using three different meshes. In all three mesh designs, the width (the dimension in x direction) of the elements was designed to increase by doubling, i.e., 1, 2, 4, 8, 16, 32 and 64, where 1 is the width of all the fault elements and the others are the widths for the rock elements. The thickness of the system, $h = 100$ was divided equally into N parts, with N equal to 25, 50 and 100 in three different meshes. In other words, the heights of all elements in the three different meshes were 4, 2 and 1, respectively. As shown in Figure 3.6A, the results of the numerical solution become closer and closer to that of the analytical solution as the division gets finer and finer. At $N = 100$ (element height equal to unity), the numerical solution is approximately the same as the analytical solution. Further increase of N will have very little effect in improving the match.

In Figures 3.6B and 3.6C, the TRUMP solutions for Case #1 and Case #4 (dots) are compared with their corresponding analytical solutions (solid lines). The meshes used for these numerical calculations are the same as that for Figure 3.6A at $N = 100$. All three figures can show that the numerical code, TRUMP can provide very reliable

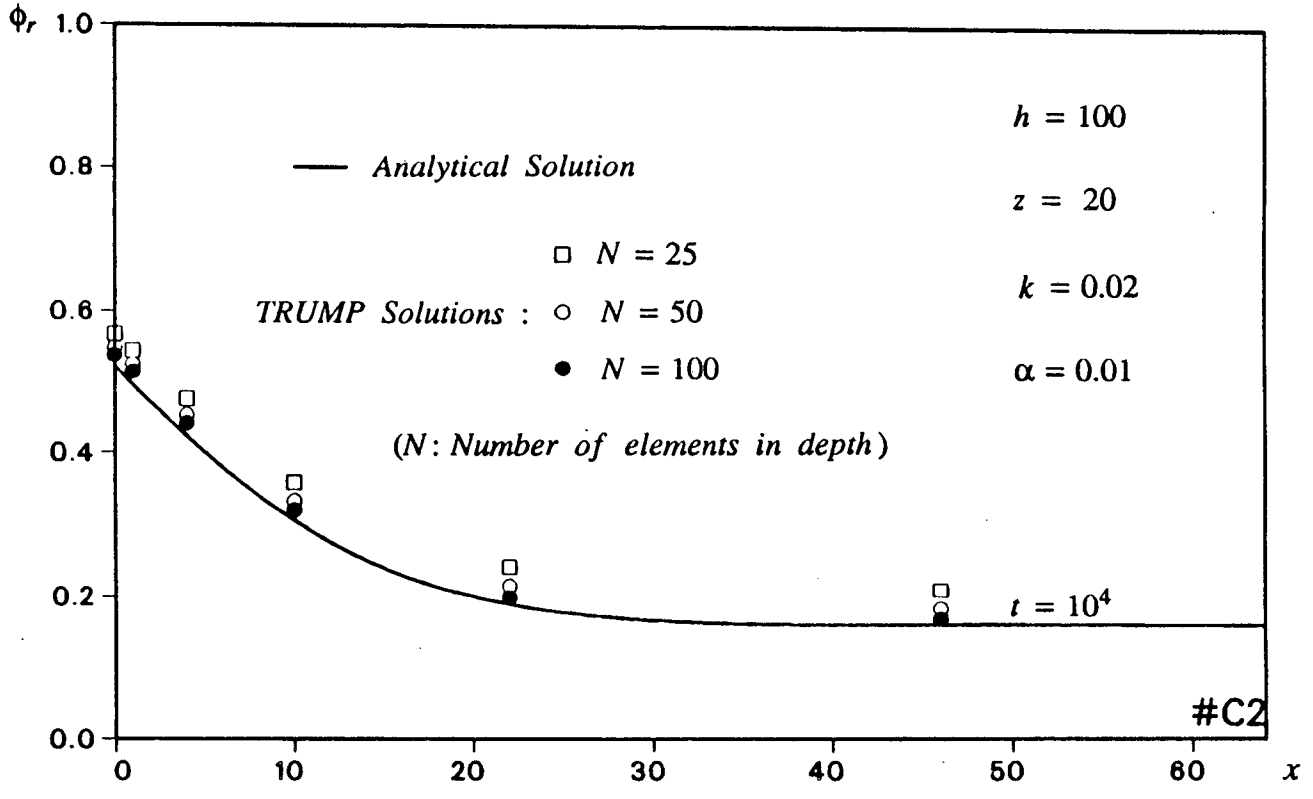

Figure 3.6A Effect of mesh found in verification on numerical code TRUMP.

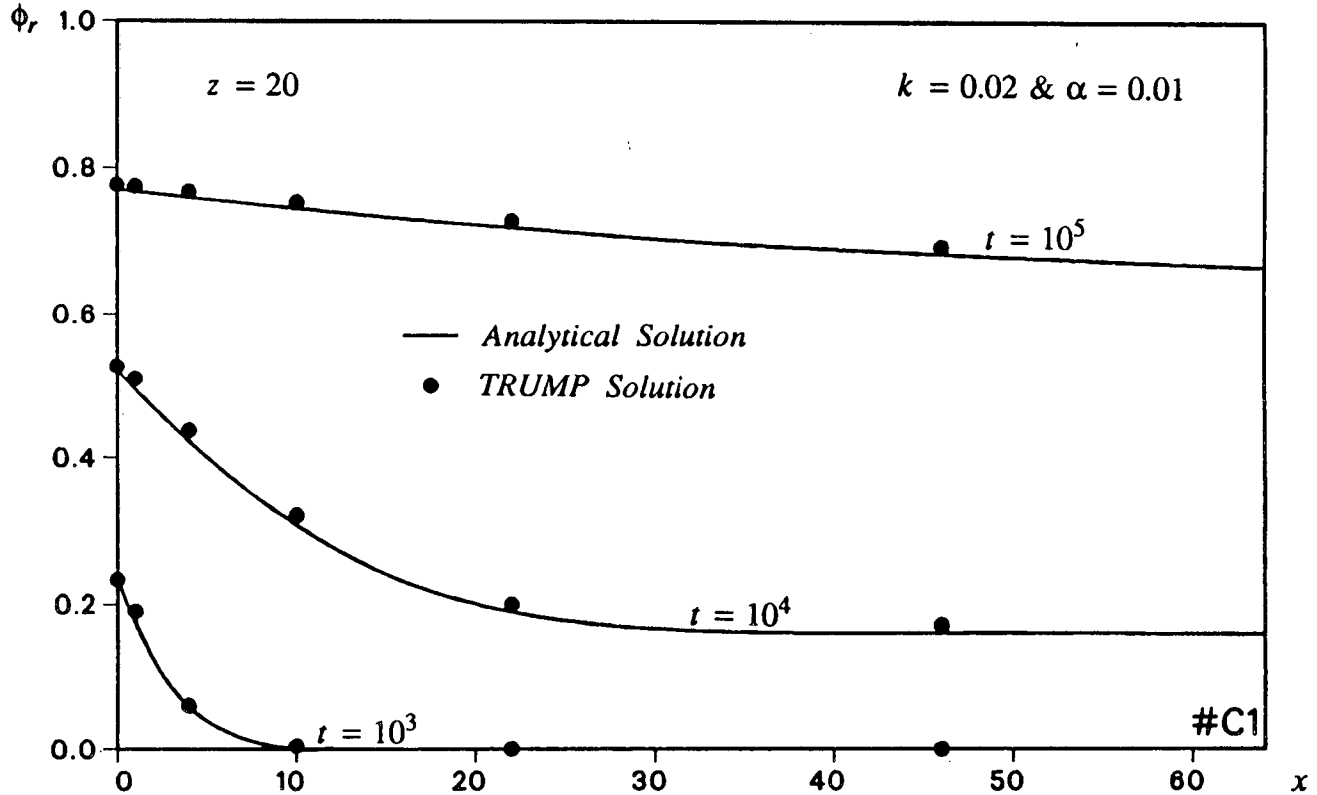

Figure 3.6B Comparison of step function solution with numerical code TRUMP.

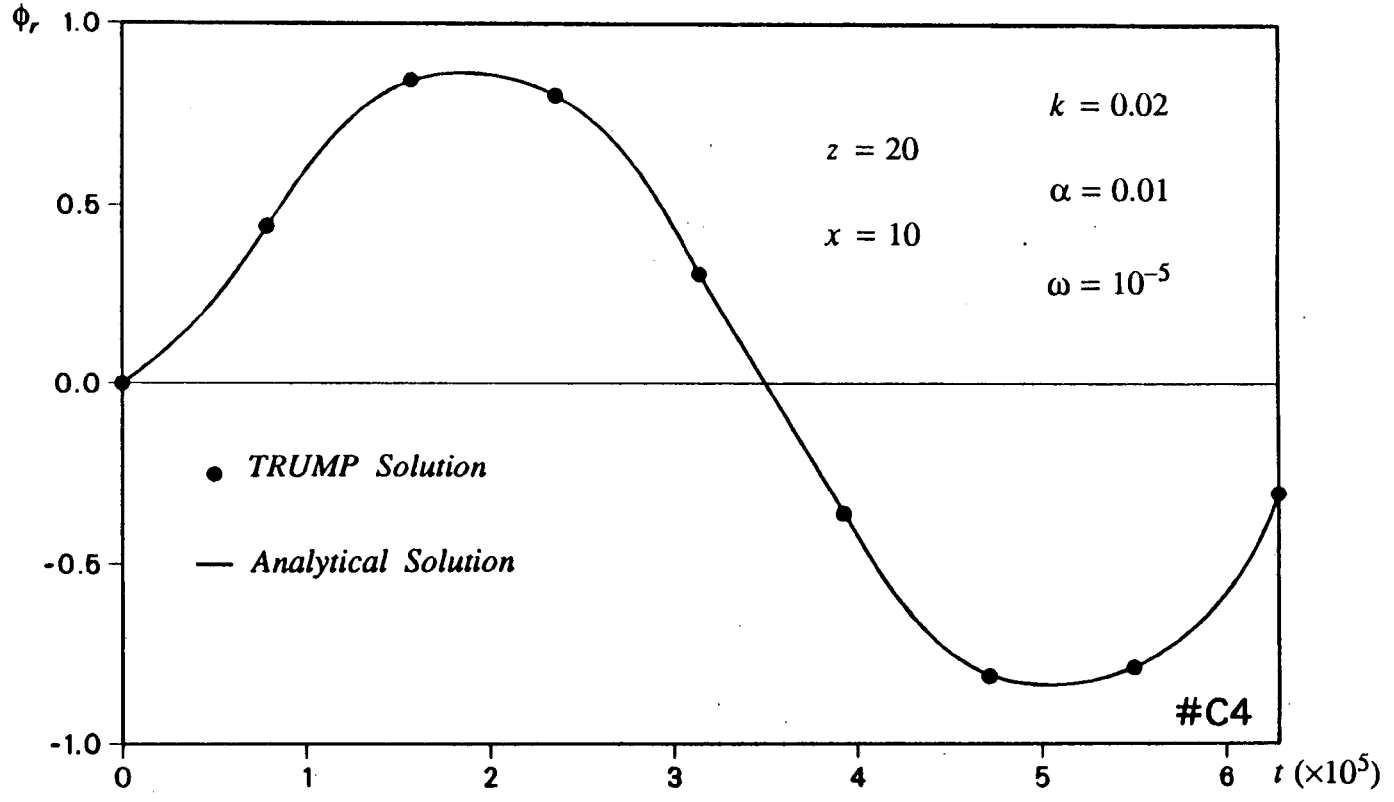

Figure 3.6C Comparison of sinusoidal solution with numerical code TRUMP.

results by using well designed fine meshes.

3.4.2 Check on Assumptions

On the one hand, the analytical solutions can be used to verify the numerical code; on the other hand, the verified code may be used to check the validity of assumptions as the basis for the analytical solutions. An important assumption specifically introduced in this study is the one-dimensional vertical flow in the fault zone. This assumption can be checked by means of TRUMP because as a numerical code, TRUMP can be used to simulate a model that allows two-dimensional flow in both the rock mass and the fault zone. Actually, this can be done by dividing the fault zone into several elements along the horizontal direction (x direction) as well as along the vertical direction (z direction). In this way, the pressure distribution in the fault zone along the horizontal direction will also be calculated.

The results of calculations for a wide range of parameter combinations have revealed that, except for very small values of time and permeability contrast, the assumption of one-dimensional flow in the fault zone is quite reasonable. Two examples are given in Figure 3.7A and Figure 3.7B. Both of them show the dimensionless pressure (ϕ) distribution at certain depth in the whole system (including the rock mass and the fault zone). Figure 3.7A presents the results for a small permeability contrast of $k=0.5$ and a small depth of $z=2$ at small values of time ($t=1, 10$). While Figure 3.7B shows the results for $k=0.01$, $z=20$ and $t=10^3, 10^4$. It is very clear that except for very small values of time and even for small permeability contrasts, the isopotentials in the fault zone are essentially horizontal. In other words, the flow lines in the fault zone are essentially vertical.

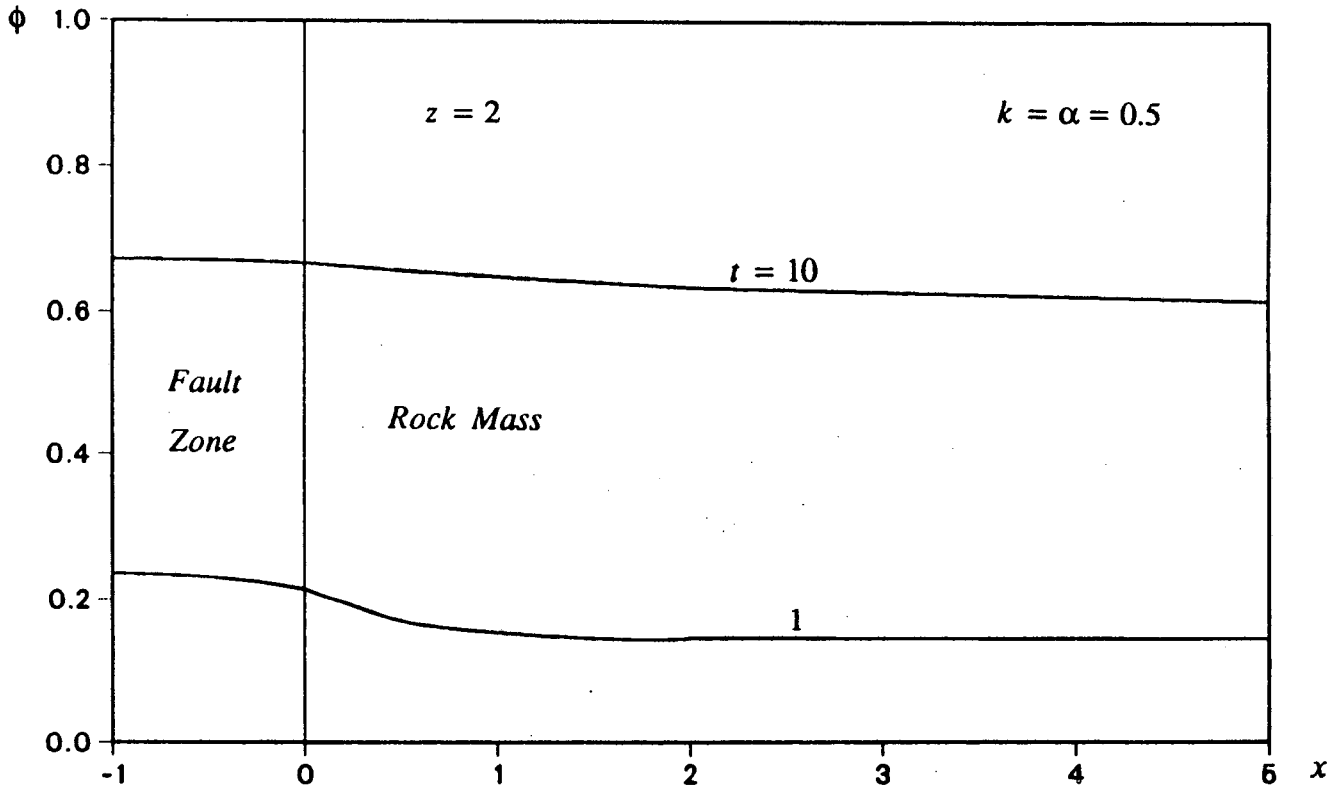

Figure 3.7A Distribution of pressure head in the system at $z=2$ and $k=\alpha=0.5$ at two values of time.

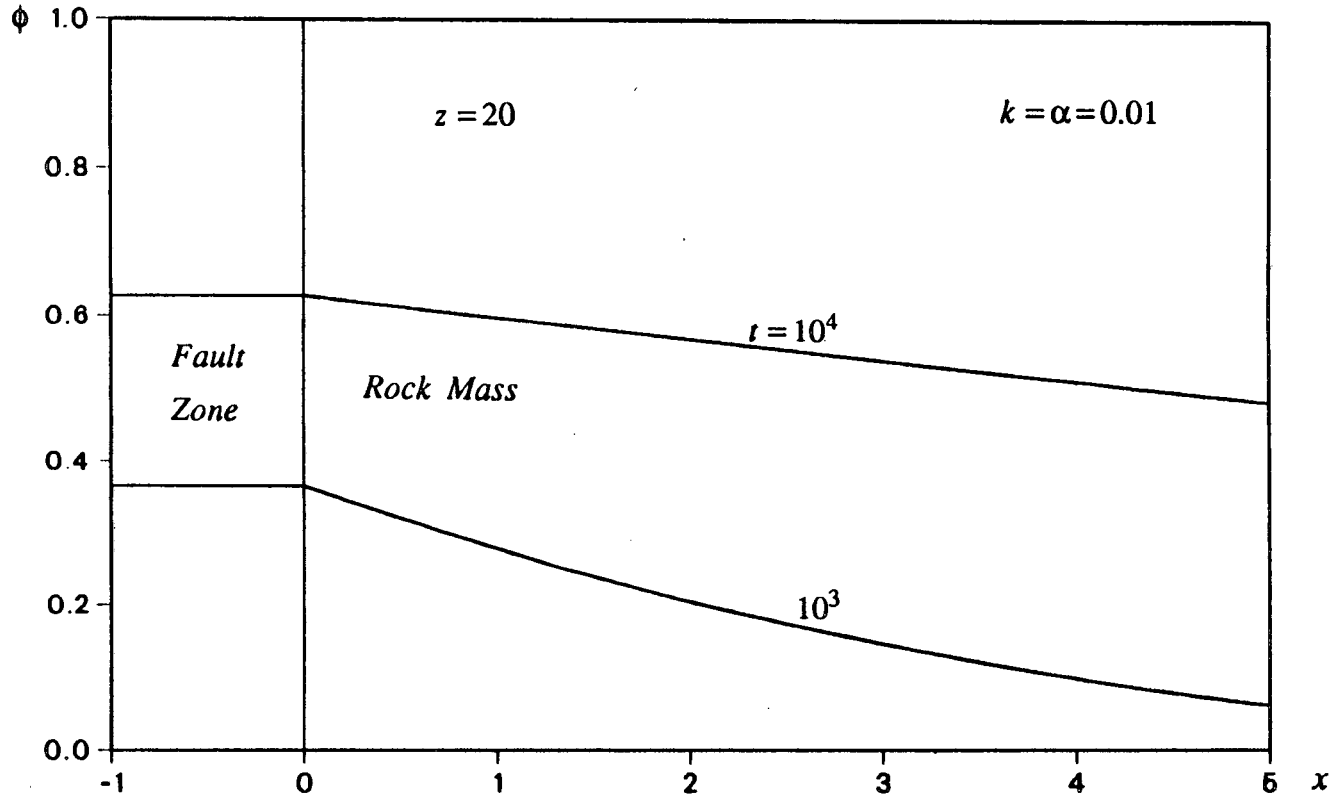

Figure 3.7B Distribution of pressure head in the system at $z=20$ and $k=\alpha=0.01$ at two values of time.

3.4.3 Application Examples of TRUMP

Numerical solutions for the multi-layer problems such as that described in Figure 3.8 can be applied to the field determination of the hydrologic properties of the fault zone. The idea is that if we install a set of instruments at isolated spots of same depth but different distances from the fault zone (they should be close to the fault zone such that the effect of the fault zone can be detected), the air pressure at these points can be measured when atmospheric pressure is changing. If these data are compared with the numerical solutions of TRUMP, it should be possible to determine the air permeability of the fault zone by means of the method of trial and error. The permeability to air may in turn be converted to an equivalent hydraulic conductivity for the fault zone if this zone is not structurally affected by wetting.

In preparing the input data for the TRUMP program, the air filled porosity of the fault zone and all related rock layers, and the air permeability of each rock layer are assumed to be known. The former values can be obtained from other sources such as the sample tests in the laboratory. While the latter values may be determined by applying the method proposed by Stallman (1967) and practised by Weeks (1978). It is worthwhile to point out that the piezometer nest for determining the air permeabilities of the rock layers should be constructed at a distance far away from the fault zone such that the model of one-dimensional flow still holds at the test site. By simply adjusting the air permeability of the fault zone, one can get a result which best matches the field data. The corresponding value of the input data is the proposed air permeability of the fault zone.

As two examples of applications, the air pressure variations in the rock units due

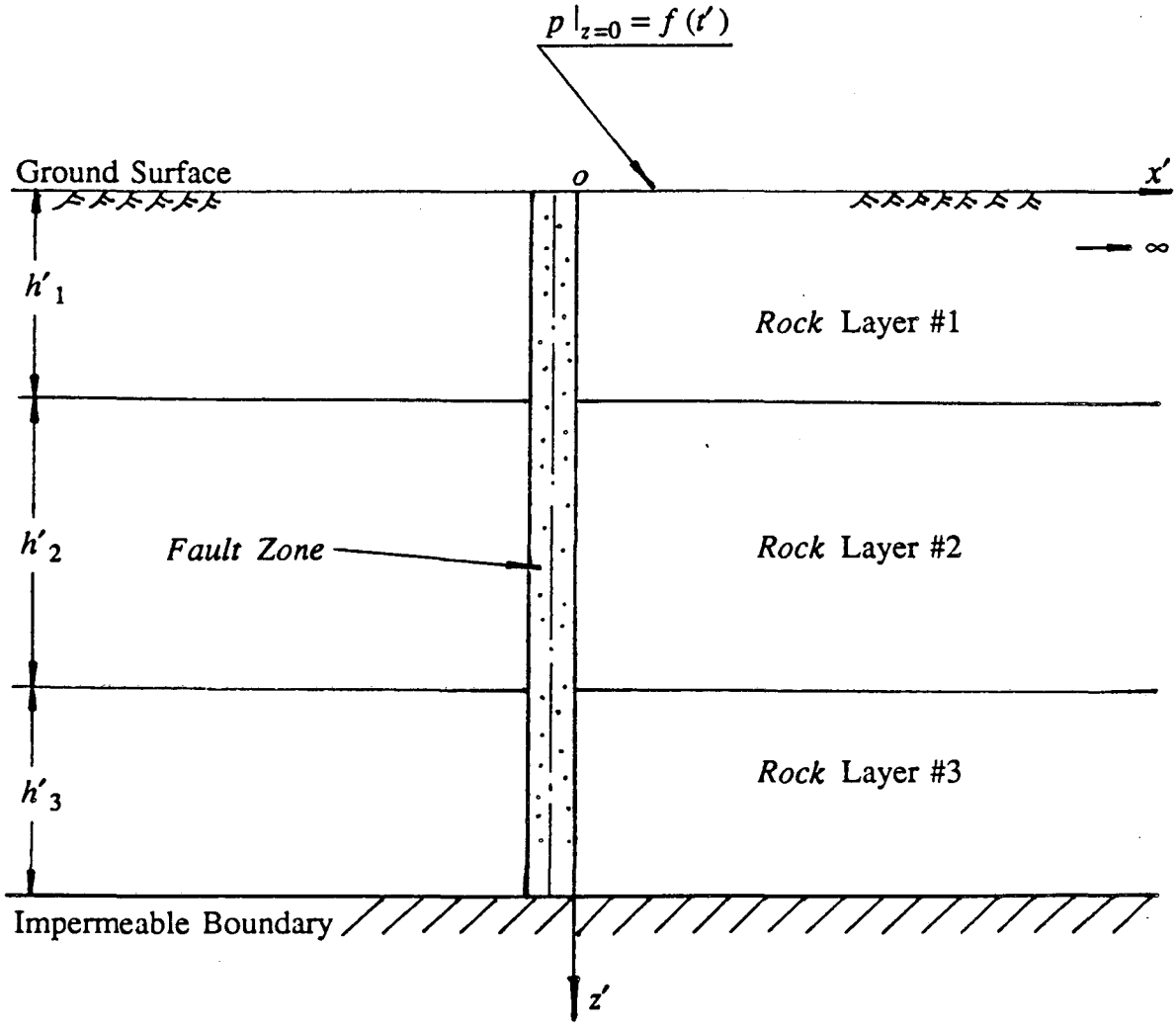

Figure 3.8 Schematic cross section of the fault zone and the surrounding rocks for multi-layer problem.

to actual atmospheric pressure changes have been computed by TRUMP for proposed parameters. The computations are performed for two cases. Each represents a simplified model of the Solitario Canyon Fault and the Ghost Dance Fault at the Yucca Mountain in Nevada.

Figure 3.9 is a cross-section of the Yucca Crest. The two fault zones and the rock units above the water table are simplified within the dashed line frames. Numerical grids used to compute the two faults are given in Figure 3.10A and Figure 3.10B, respectively. This time, the x' axis is set to be on the water table while the z' axis is still along the fault-rock contact but pointing *upwards*. Elements height is 10 meters everywhere while their lengths change from column to column. For the rock mass, it increases in a doubling manner, starting with 2 meters for the first column right adjacent to the fault zone (dotted elements in these figures) and ending with 256 meters for the eighth column. For some cases, if the fault zone is extremely permeable, additional columns could be added to minimize the effect of the boundary. However, this is unnecessary in the following case studies. In other words, eight columns of elements in the rock mass are good enough for these calculations. For the fault zone, because the half width (b') is an unknown, the lengths of the fault elements are subject to change. For example, in the following case studies if $b' = 2\,m$, there will be two equal columns for the fault zone, each column with a length of 1 meter; if $b' = 10\,m$, we will divide the fault zone into five columns with the lengths of 3, 3, 2, 1 and 1 meters sequentially so that the column adjacent to the rock column has a length of 1 meter; if $b' = 100\,m$, the fault zone could have seven columns with the lengths of 37, 32, 16, 8, 4, 2 and 1 meters sequentially so that the column adjacent to the rock column has a length of 1 meter. The three hydrogeologic units of the rock layers are

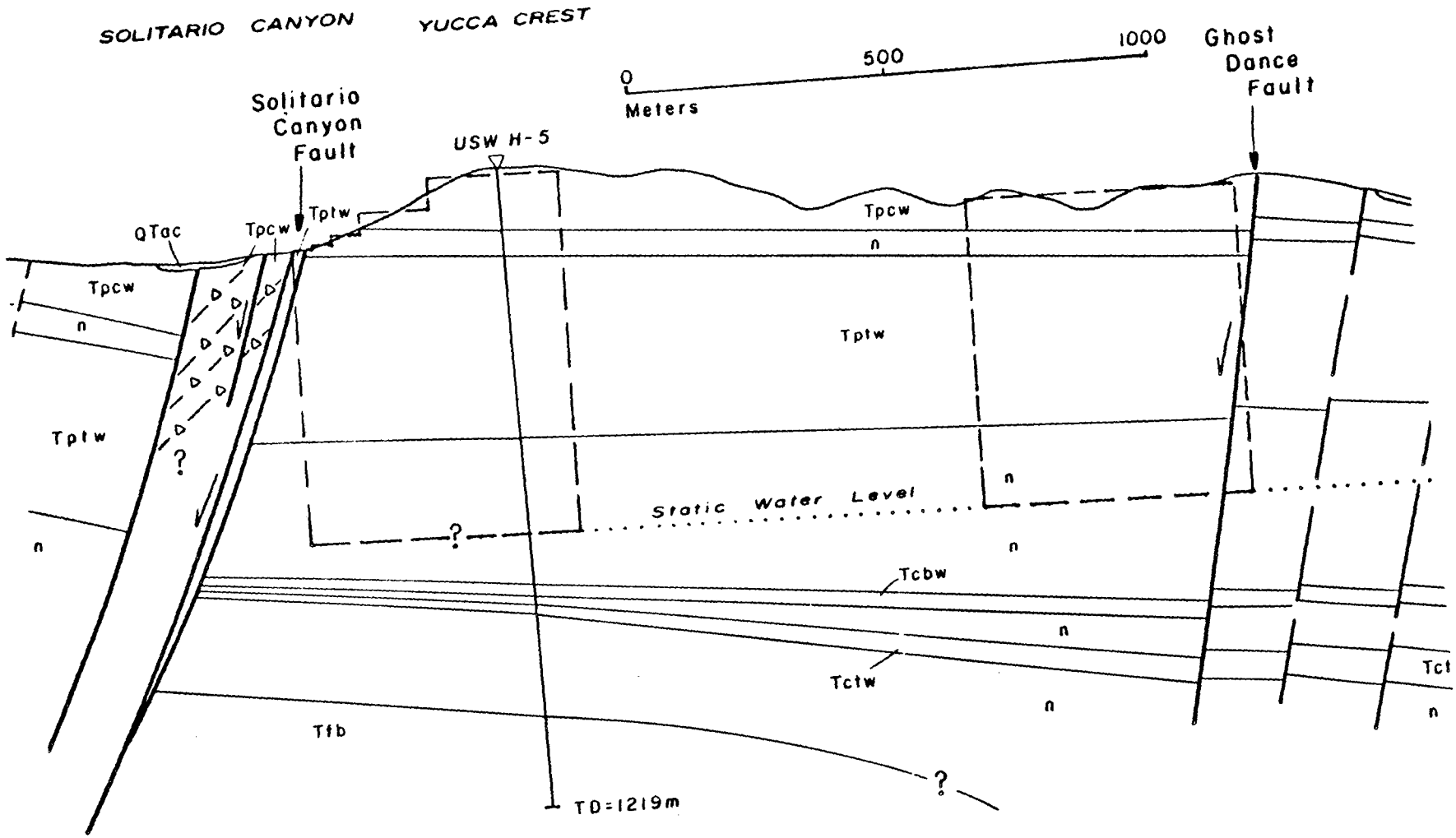

Figure 3.9 Cross-section of the Yucca Crest and adjacent fault zones (modified from Scott and Bonk, 1981).

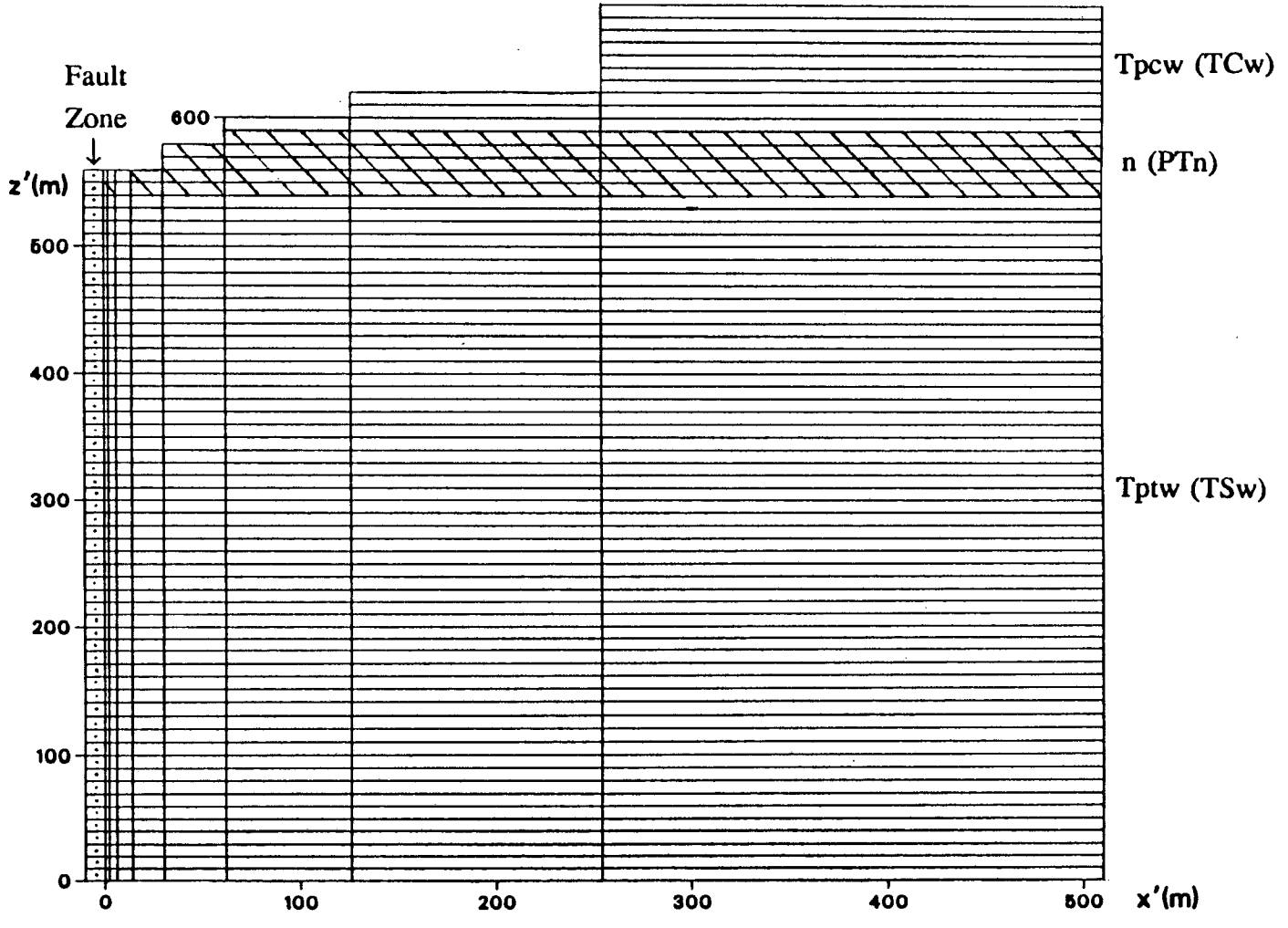

Figure 3.10A Numerical grid used to compute the Solitario Canyon Fault.

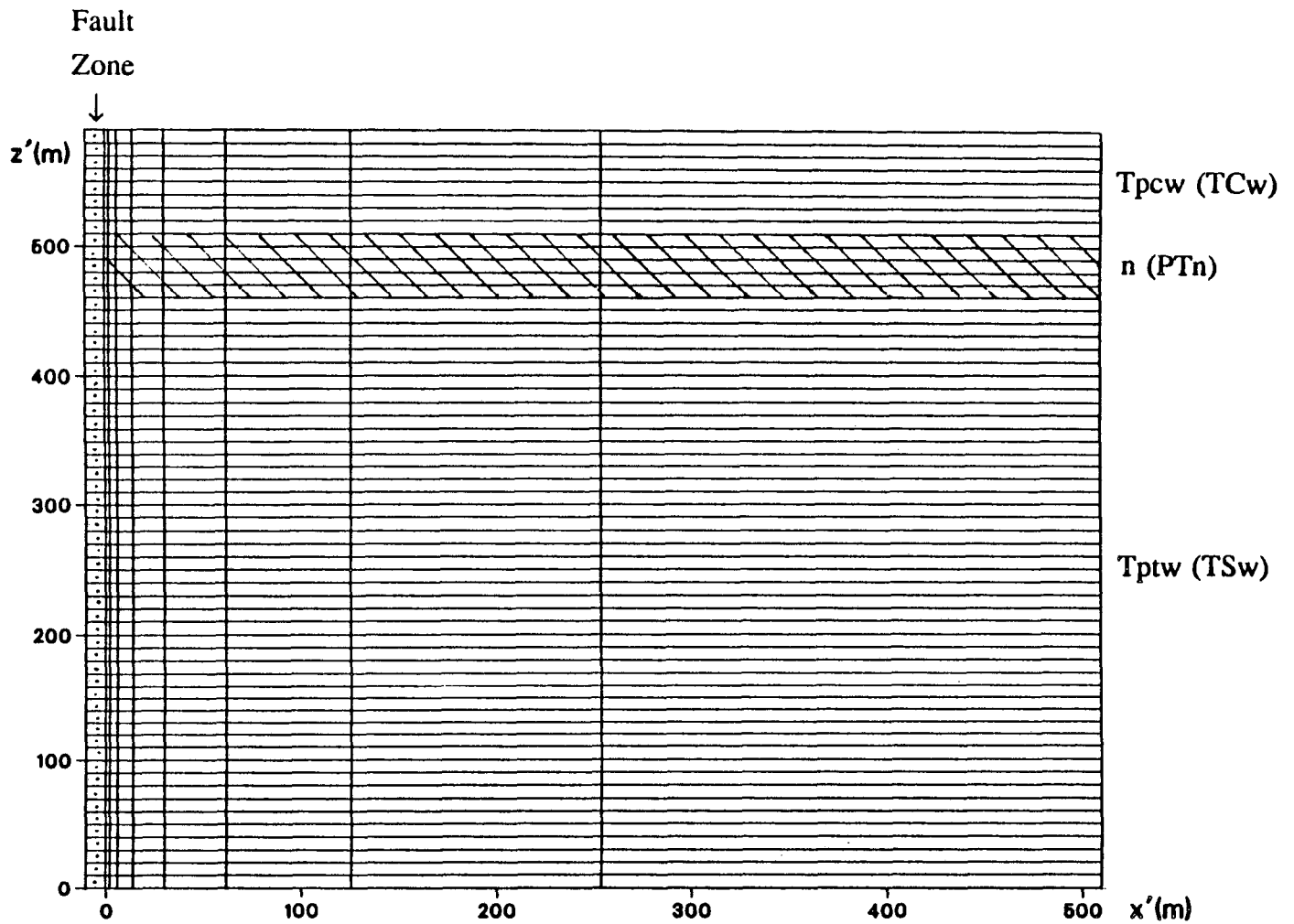

Figure 3.10B Numerical grid used to compute the Ghost Dance Fault.

represented by TCw (Tiva Canyon welded unit), PTn (Paintbrush nonwelded unit) and TSw (Topopah Spring welded unit), respectively. For purposes of simplification, part of the nonwelded unit above the groundwater table and below the TSw unit (Figure 3.9) is also considered as the TSw unit. Hopefully, this treatment will not cause any significant errors in the pressure calculation at places high above this region.

In preparing the input data for TRUMP, we need to give the values of heat capacity and thermal conductivity for all the materials. In our problem, the two parameters correspond to the pneumatic specific storage (S_a) and the pneumatic conductivity (K_a), respectively. The ranges of these two parameters for three different hydrogeologic units are available from Montazer et al. (1988). All these data for the rocks will be treated as definitely known values and thus kept as constants in the case studies. Table 3.3 gives the constant parameters used in the following calculation.

Table 3.3 Calculation Parameters of Three Rock Units

Rock Unit	n_a	$S_{a_r}(m^{-1})$	$K_{a_r}(m \cdot s^{-1})$
TCw	0.15	1.8×10^{-5}	10^{-5}
PTn	0.25	3.0×10^{-5}	10^{-7}
TSw	0.05	0.6×10^{-5}	10^{-5}

For the input data in the fault zones, we have three unknowns, i.e., the width of the fault elements (b'), the pneumatic conductivity (K_{a_f}) and the pneumatic specific storage (S_{a_f}). Because the conductivity of the fault zone is of most interest, we can select a reasonable value for the pneumatic specific storage and keep it unchanged in

all studies. The value to be used in this study is $S_{a_f} = 10^{-5} m^{-1}$. By doing so, we can concentrate on studying the effect of the conductivity of the fault zone. Three values of different order were used in the calculations. They are: $K_{a_f} = 10^{-4}$, 10^{-3}, $10^{-2}\,(m/s)$, which are one, two and three orders of magnitude higher than that of the TCw (or TSw) unit, respectively. To study the effect of the width of the fault zone, two values were assumed for each fault zone. For the Salitario Canyon Fault, b' was assigned with two values: 10m and 100m; for the Ghost Dance Fault, it was assumed to be equal to 10m or 2m.

The atmospheric pressure variation in twelve hours from 6 p.m. January 15, 1982 to 6 a.m. the next morning recorded at a station in Yucca Mountain area was taken as the input boundary conditions at the ground surface. The atmospheric pressure records at every one hour during the time interval are given in Table 3.4, and the variation can be shown in Figure 3.11.

Table 3.4 Input Data of Atmospheric Pressure

$t'\,(hour)$	1	2	3	4	5	6
$p\,(Pa)$	85047	85173	85263	85357	85440	85523
$t'\,(hour)$	7	8	9	10	11	12
$p\,(Pa)$	85573	85623	85653	85713	85777	85840

From Figure 3.11 it is found that the atmospheric pressure in the previous two hours before the beginning ($t' = 0$) approximately remained a constant of $p_0 = 84933\,Pa$. We will take this value as the initial pressure in the system.

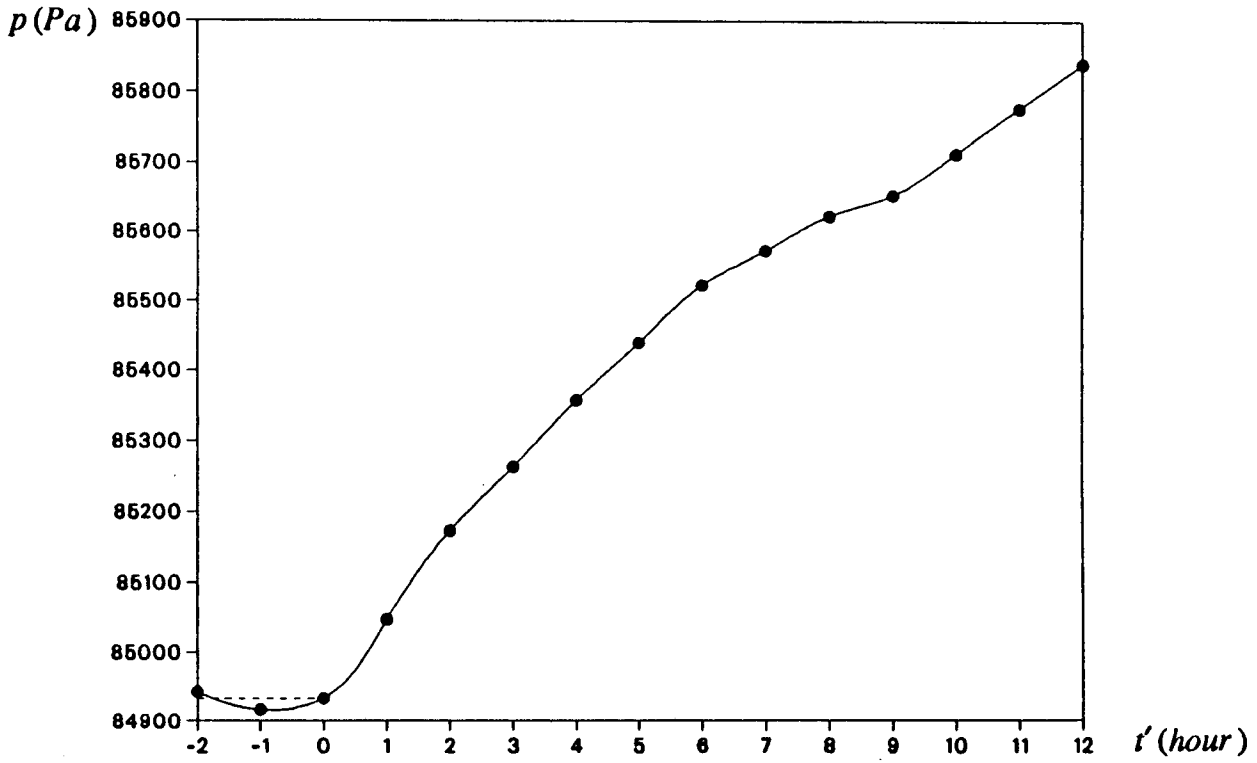

Figure 3.11 Atmospheric pressure used for computation.

Again, it is convenient to study the pressure increment, $\Delta p = p - p_0$ as a function of space and time. Figures 3.12A through 3.12D present the pressure increment distributions along the horizontal direction in two different rock units (PTn and TSw) close to the Solitario Canyon Fault. Figures 3.13A through 3.13F present the pressure increment distributions along the horizontal direction in three different rock units (TCw, PTn and TSw) close to the Ghost Dance Fault. The ten figures are all plotted at time $t' = 6\,hours$ and $t' = 12\,hours$.

Several points can be interpreted from these figures: (1) the large difference in permeability between the fault zone and the rock layer results in a significant pressure difference in the horizontal direction. The greatest pressure difference occurs in the PTn unit which has the largest permeability contrast with respect to the fault zone; (2) the greatest effect of an increase in fault zone conductivity and an increase in fault zone width can be found in the TSw unit because it is the deepest unit such that its air flux is mainly derived through the fault zone; (3) the topography does affect the air pressure variation in the rock units, especially the PTn unit, where the curves have a deflection in Figure 3.12A due to the sudden change of the thickness of the PTn unit in the Solitario Canyon Fault region; and (4) the PTn unit can have the effect of blockading the air flux downwards in the TCw unit such that there is air flux from the TCw unit to the fault zone in some cases. However, at early time when the boundary effect is very small, the air is always flowing from the fault zone to the TCw unit. This can be shown by Figure 3.13G, where the pressure increment distributions in the TCw unit at $t' = 1\,hour$ is plotted for the case of $b' = 2\,m$ in the Ghost Dance Fault region.

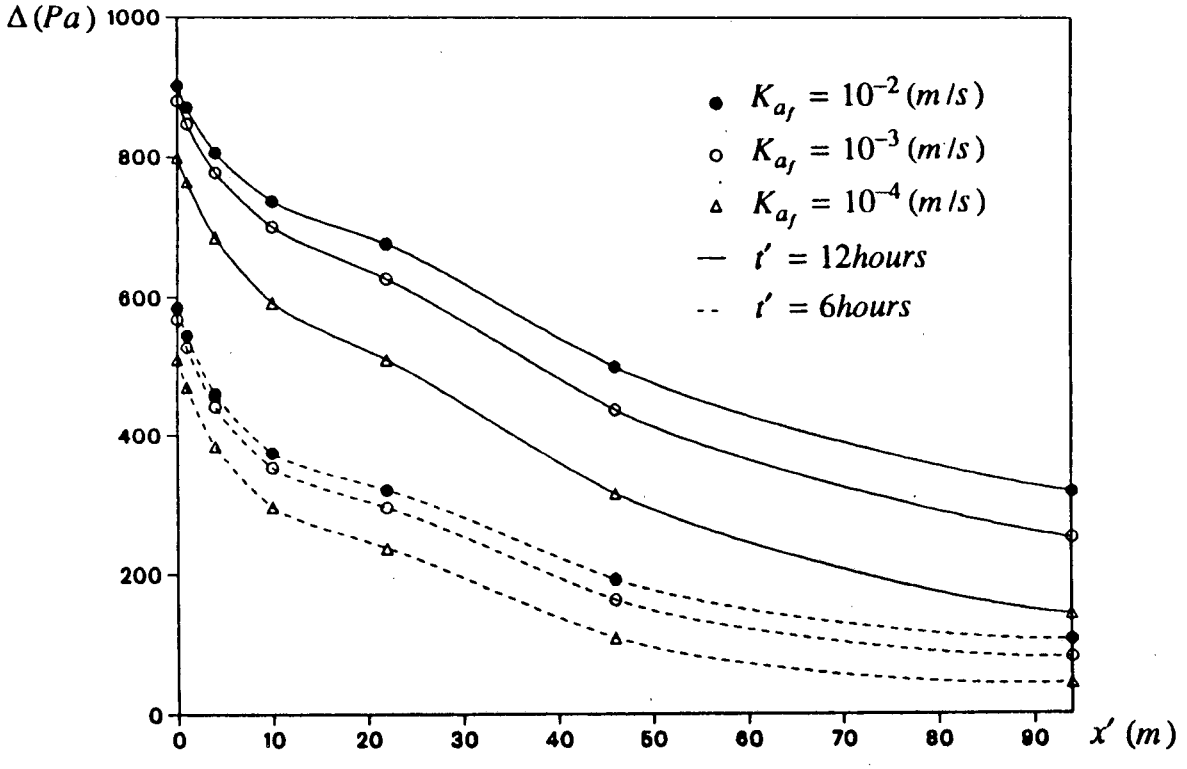

Figure 3.12A Pressure increment distribution at z'=545m (in PTn unit) close to the Solitario Canyon Fault for the case of b'=10m.

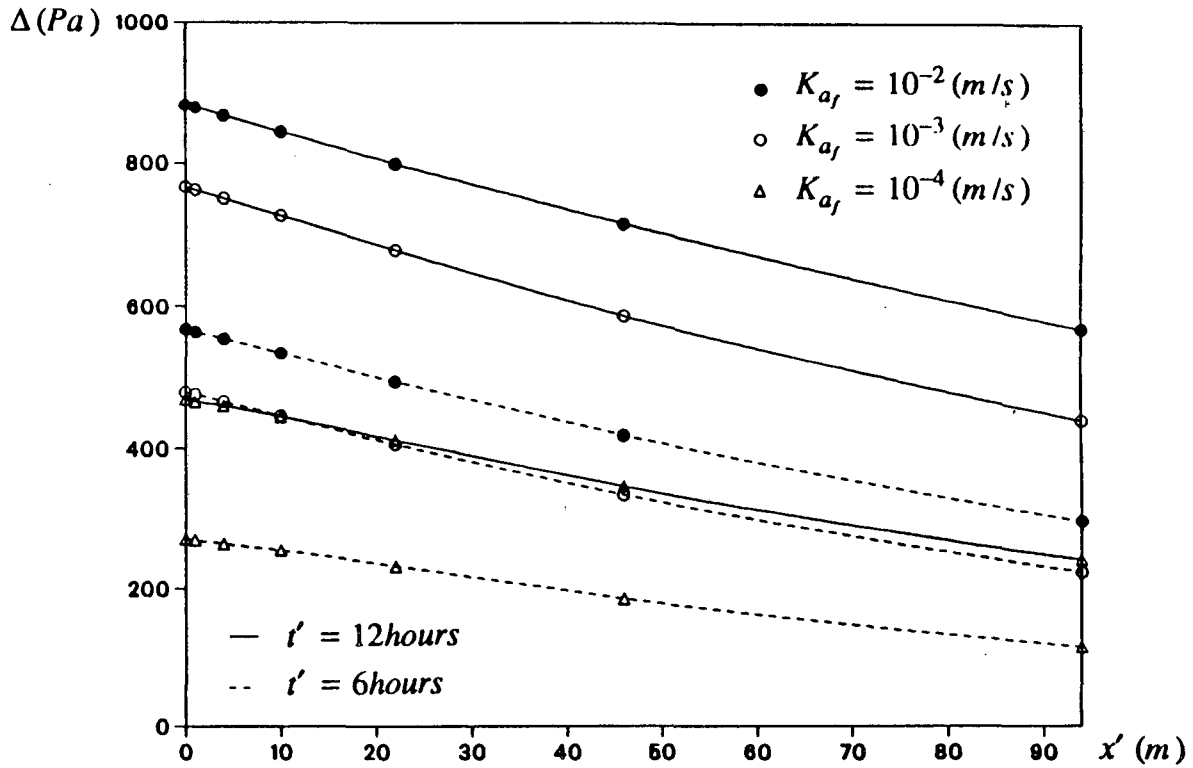

Figure 3.12B Pressure increment distribution at z'=495m (in TSw unit) close to the Solitario Canyon Fault for the case of b'=10m.

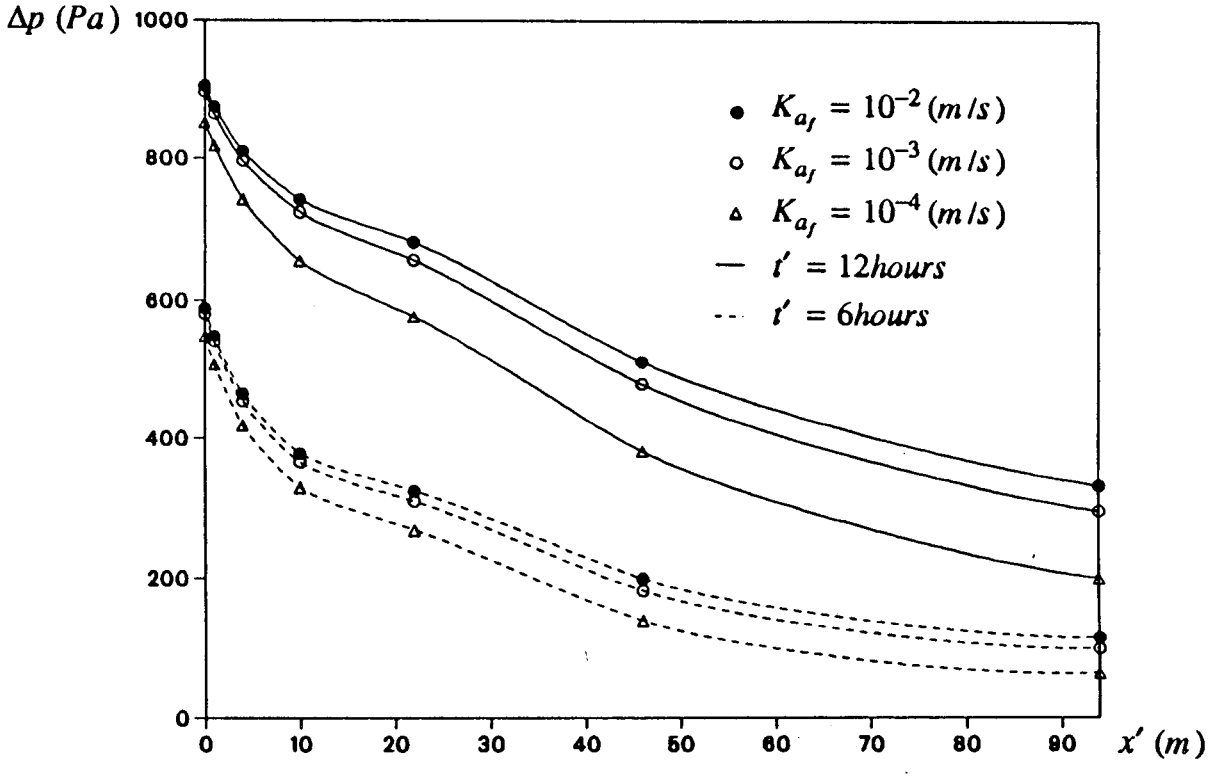

Figure 3.12C Pressure increment distribution at z'=545m (in PTn unit) close to the Solitario Canyon Fault for the case of b'=100m.

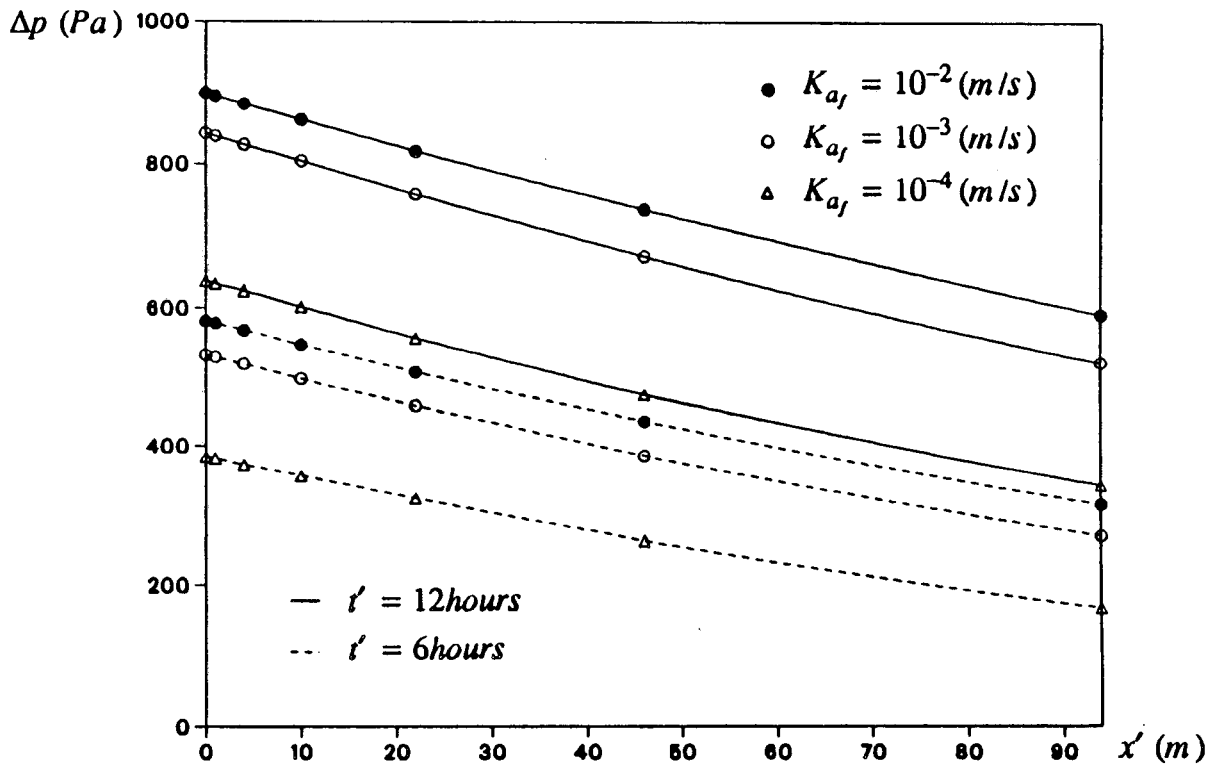

Figure 3.12D Pressure increment distribution at z'=495m (in TSw unit) close to the Solitario Canyon Fault for the case of b'=100m.

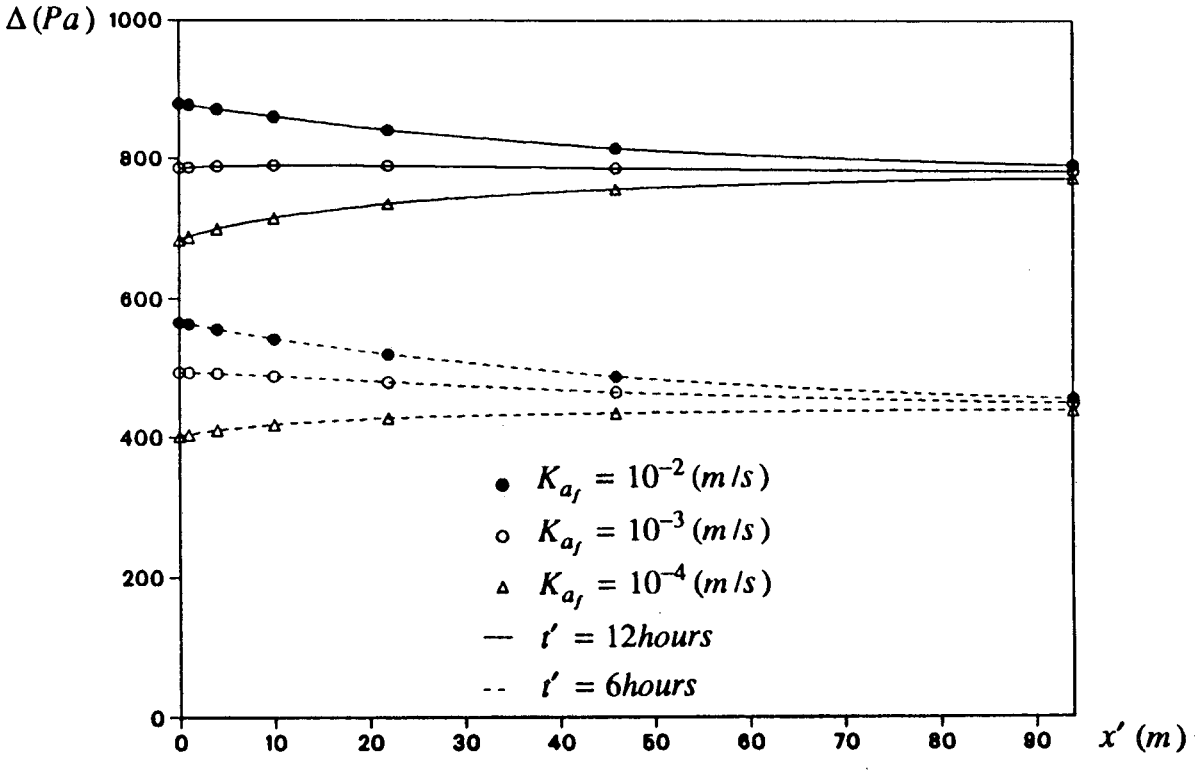

Figure 3.13A Pressure increment distribution at z'=515m (in TCw unit) close to the Ghost Dance Fault for the case of b'=10m.

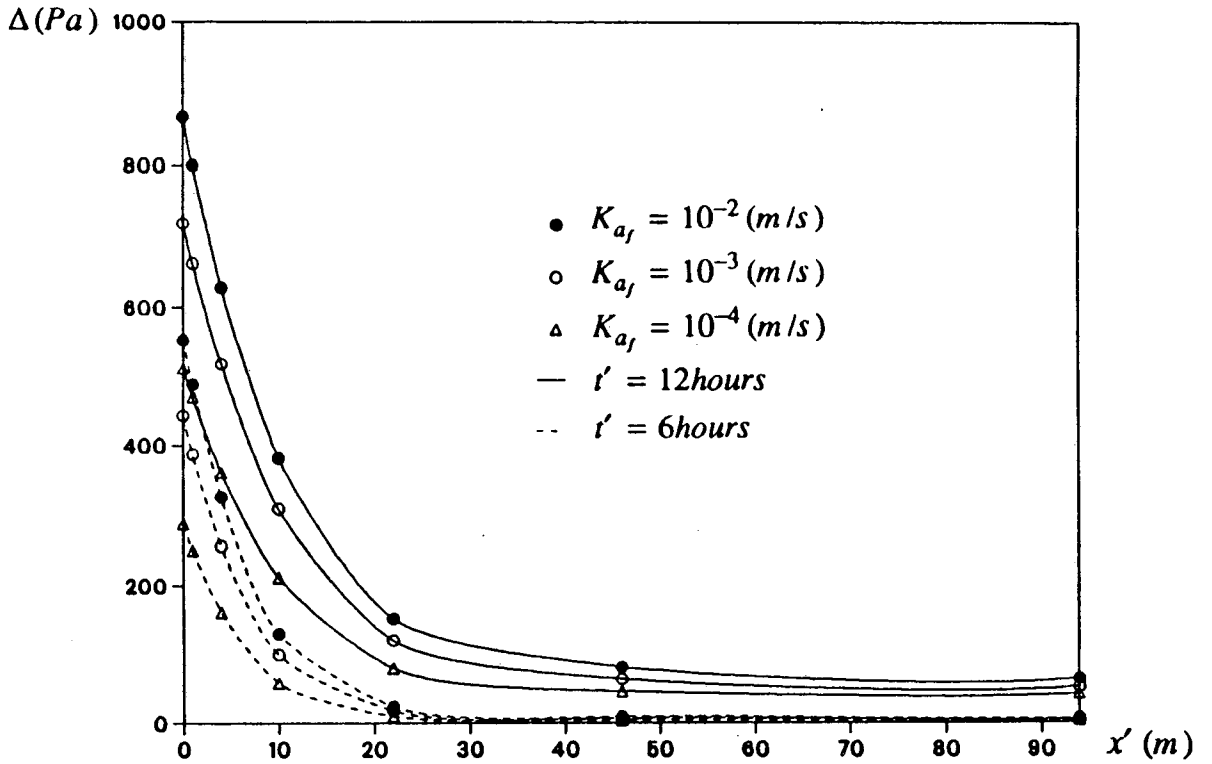

Figure 3.13B Pressure increment distribution at z'=485m (in PTn unit) close to the Ghost Dance Fault for the case of b'=10m.

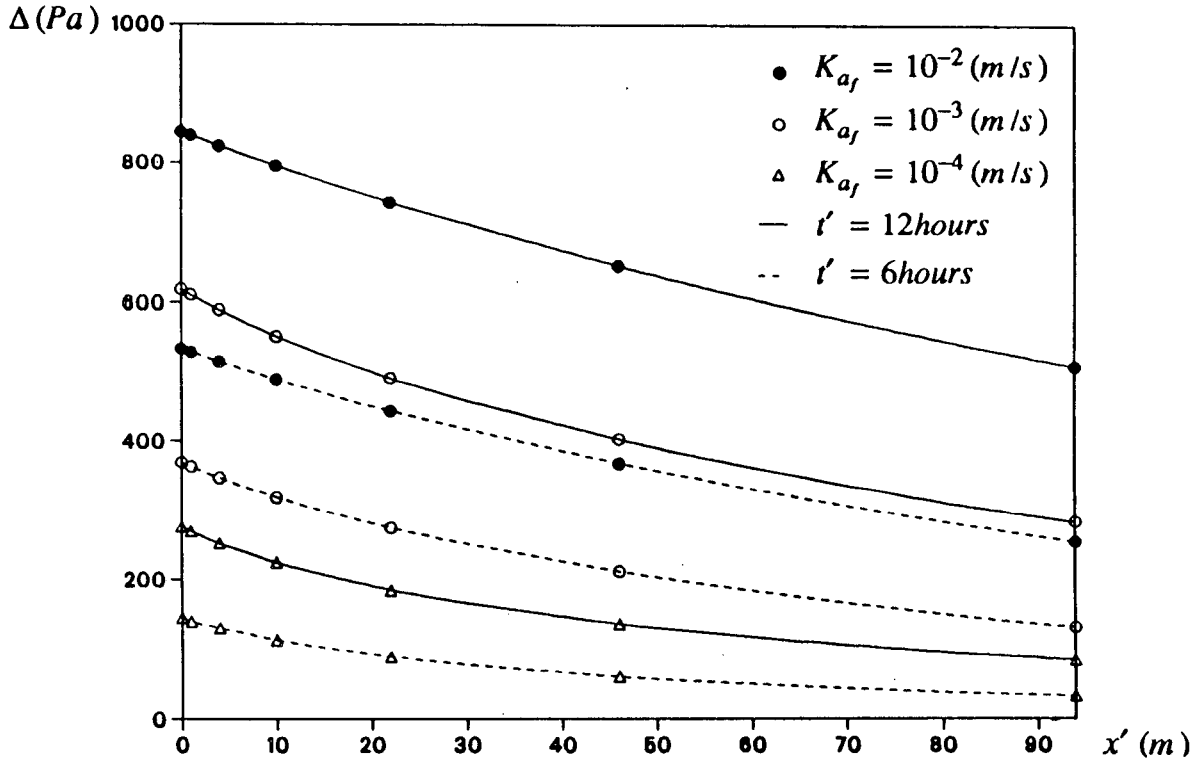

Figure 3.13C Pressure increment distribution at z'=455m (in TSw unit) close to the Ghost Dance Fault for the case of b'=10m.

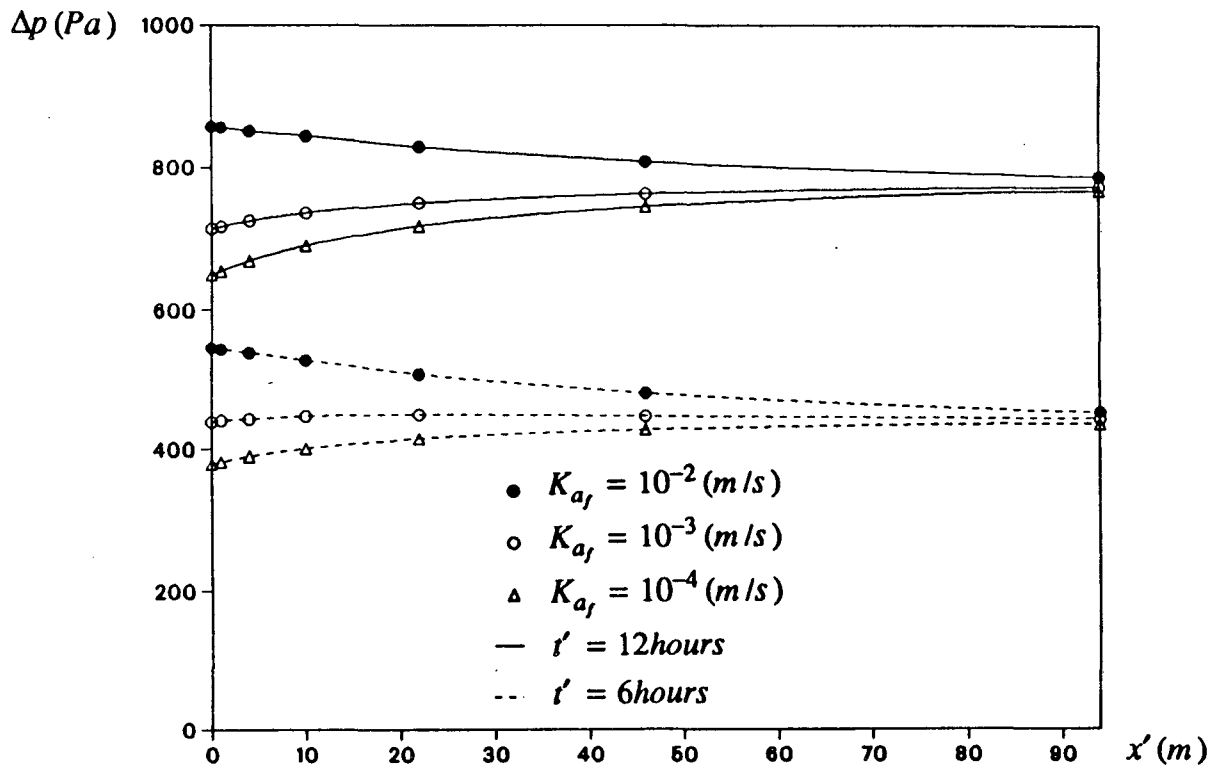

Figure 3.13D Pressure increment distribution at z'=515m (in TCw unit) close to the Ghost Dance Fault for the case of b'=2m.

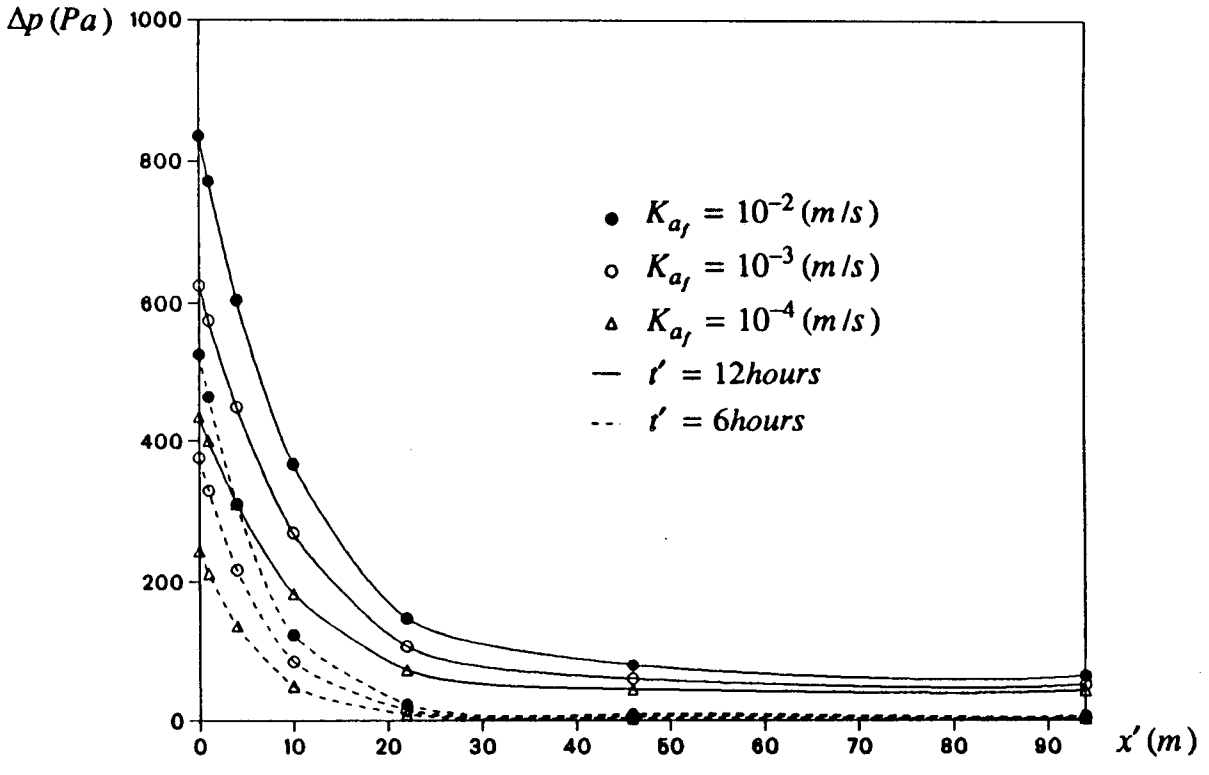

Figure 3.13E Pressure increment distribution at z'=485m (in PTn unit) close to the Ghost Dance Fault for the case of b'=2m.

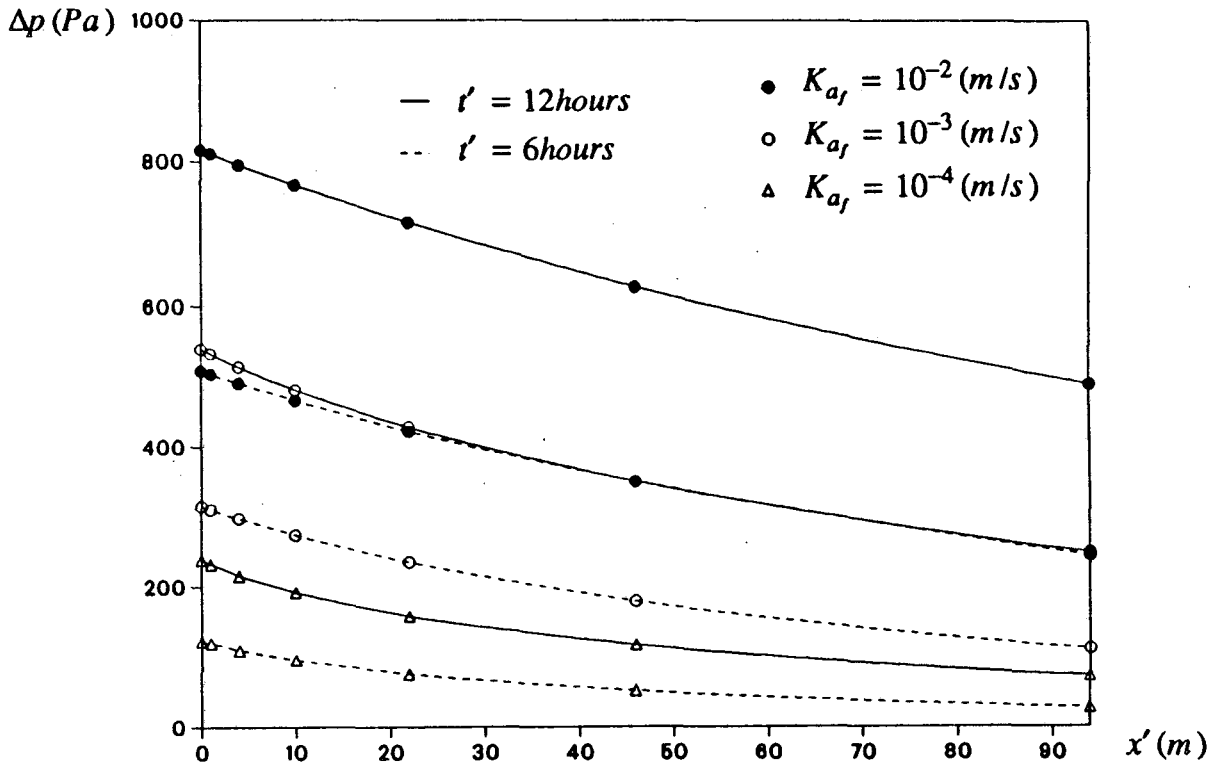

Figure 3.13F Pressure increment distribution at z'=455m (in TSw unit) close to the Ghost Dance Fault for the case of b'=2m.

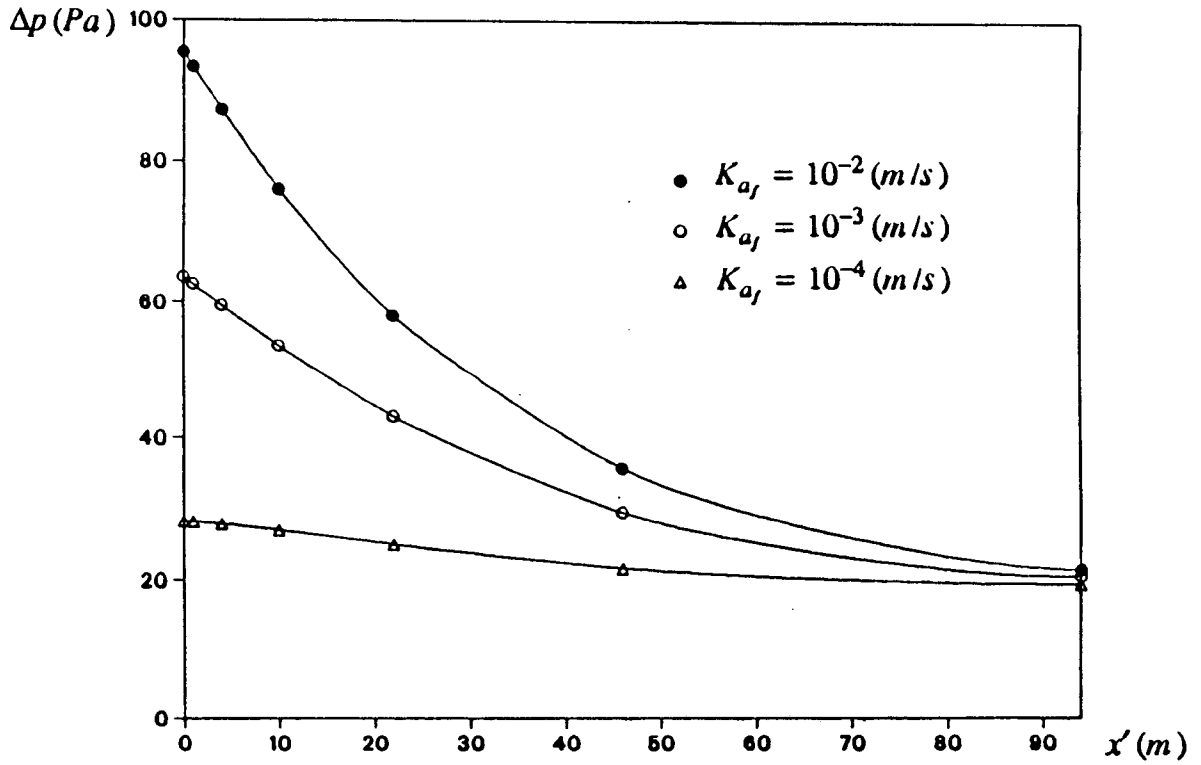

Figure 3.13G Pressure increment distribution at z'=515m (in TCw unit) close to the Ghost Dance Fault for the case of b'=2m at t'=1hour.

To get a clear view about the pressure difference at the same elevation quantitatively, it is necessary to calculate the difference between two fixed points, e.g., between the point at the fault-rock contact face ($x' = 0m$) and the point which is 10 meters away from the contact ($x' = 10m$). For an easier description, we define: $\delta_{10} = p\,|_{x'=0m} - p\,|_{x'=10m}$ at a certain elevation, z' and a certain time, t'. Some of the values of δ_{10} are calculated and listed in Tables 3.5 through 3.8.

These tables demonstrate that except for TCw unit there will always be a pressure difference of several tens to several hundreds pascals between the point at the contact plane and another point which is 10 meters away from the contact. Such a difference in pressure is surely detectable in field tests. It is therefore concluded that the method developed in this chapter should be useful in determining the permeability of a fault zone by means of air pressure measurements in the unsaturated zone.

Table 3.5 $\delta_{10}(Pa)$ *at* t'=6 *hours in Solitario Canyon Fault Region*

$b'(m)$	10	10	100	100
K_{a_f} \ $z'(m)$	545_{PTn}	495_{TSw}	545_{PTn}	495_{TSw}
$10^{-4}(m \cdot s^{-1})$	217	17	220	28
$10^{-3}(m \cdot s^{-1})$	217	33	215	35
$10^{-2}(m \cdot s^{-1})$	212	35	211	34

Table 3.6 $\delta_{10}(Pa)$ at t'=12 hours in Solitario Canyon Fault Region

$b'(m)$	10	10	100	100
K_{a_f} \ $z'(m)$	545_{PTn}	495_{TSw}	545_{PTn}	495_{TSw}
$10^{-4}(m \cdot s^{-1})$	206	24	196	36
$10^{-3}(m \cdot s^{-1})$	182	41	173	40
$10^{-2}(m \cdot s^{-1})$	167	38	165	37

Table 3.7 $\delta_{10}(Pa)$ at t'=6 hours in Ghost Dance Fault Region

$b'(m)$	10	10	10	2	2	2
K_{a_f} \ $z'(m)$	515_{TCw}	485_{PTn}	455_{TSw}	515_{TCw}	485_{PTn}	455_{TSw}
$10^{-4}(m \cdot s^{-1})$	−16	230	32	−22	195	28
$10^{-3}(m \cdot s^{-1})$	6	342	50	−8	292	43
$10^{-2}(m \cdot s^{-1})$	24	423	45	18	404	43

Table 3.8 $\delta_{10}(Pa)$ at t'=12 hours in Ghost Dance Fault Region

$b'(m)$	10	10	10	2	2	2
K_{a_f} \ $z'(m)$	515_{TCw}	485_{PTn}	455_{TSw}	515_{TCw}	485_{PTn}	455_{TSw}
$10^{-4}(m \cdot s^{-1})$	−30	298	53	−40	253	46
$10^{-3}(m \cdot s^{-1})$	−4	408	67	−22	357	59
$10^{-2}(m \cdot s^{-1})$	19	484	51	13	469	49

CHAPTER 4

CONCLUSIONS AND RECOMMENDATIONS

4.1 Summary and Conclusions

The objective of this study is to provide some practical methods for determining the hydrogeologic properties of a leaky fault, particularly, the permeability (or the hydraulic conductivity) of the fault zone. Based on the results obtained in this work, this goal has been attained.

The basic idea for developing research in this field is that a leaky fault can have quite different hydrologic properties from those of the surrounding rocks or aquifers. As a result, the fluid flow (water or air flow) close to the fault zone may behave quite differently. For example, the variation of water head in the aquifer or air pressure in the unsaturated rocks will be different from that to be expected without considering the existence of the leaky fault. The flow field close to the fault zone will be greatly affected by the fault properties, or in other words, the abnormal head (or pressure) distribution will mainly depend on how permeable the fault zone is. There must exist certain kinds of relationship between the water pressure in the aquifer (or the air pressure in the unsaturated rocks) and the hydrologic properties of the nearby fault zone. Once this relationship is found, one can analyze the hydrologic properties (particularly the permeability) of the fault zone by measuring of the water head in the aquifer (or the air pressure in the unsaturated rocks).

Based on this concept, two kinds of flow have been studied. One is the flow of water in a confined aquifer-fault system and the other is the flow of air in an unsaturat-

ed rock-fault system.

Water flow in the confined aquifer is assumed to be caused by a constant rate pumping (or injection) test. This study which is given in Chapter 2 contains two parts. In the first part, we consider the case of a negligibly small head variation at the fault top (or in the unpumped aquifer); while in the second part we take consideration of the head variation in the unpumped aquifer.

The confined aquifer is assumed to be horizontal, homogeneous, isotropic, uniform in thickness and infinite in horizontal extent. The same assumptions apply to the fault zone except that it is vertical and infinite in lateral extent. The governing equations are written down for two regions of the pumped aquifer and the fault zone separately. The boundary conditions at the connecting faces are chosen such that they satisfy the head continuity and mass conservation. Flow in the fault zone is assumed to be one-dimensional in the vertical direction. Such assumption helps the derivation of the analytical solution for drawdown in the pumped aquifer. To make sure that the assumption of one-dimensional vertical flow is valid in most cases, the solution was checked against an exact solution for some simple cases. The dimensionless solution was used to calculate type curves of drawdown as a function of time. The final solution is composed of two components, with the first one being exactly the Theis solution and the second is a negative component, which represents the recharge effect of the leaky fault. In addition to dimensionless time, three other dimensionless parameters are involved in the second component of the dimensionless drawdown. Represented by θ, a_D and c_D, they have the meaning of the polar angle of the observation well, the relative distance between the pumping well and the fault, and the relative transmis-

sivity of the fault zone, respectively.

It has been shown that the new analytical solution can be reduced to the Theis solution when the fault is impermeable and to the constant-head fault solution when the fault is infinitely permeable. This provides a verification for the solution. Further studies on the second component have provided a formula to evaluate the rate of recharge from the fault zone to the aquifer, and more importantly, practical methods for determining the transmissivity of the fault zone. The method of constant-drawdown and the method of time-intersect are both simple and effective. Examples have been given for both methods with satisfactory results.

In the second part of Chapter 2, analytical solutions have been derived for the case of an aquifer-fault-aquifer system, where the drawdown in the unpumped aquifer is non-negligibly small. The solution for the case of 'equal aquifer-diffusivity' has been proved to be universally applicable, and a similar method for the time-intersect has been developed to determine the transmissivity of the fault zone under the falling head condition.

Air flow in the unsaturated rock-fault system is assumed to be caused by a natural variation in atmospheric pressure. An analysis of the effects is given in Chapter 3 and also contains two parts. The first part gives the analytical solutions for a single layer rock-fault system with specified boundary conditions. The second part uses a numerical code, TRUMP to solve the multi-layer problem with more realistic boundary conditions.

To obtain analytical solutions for the single layer problem, the air pressure variation at the ground surface is assumed to be either a step function or a sinusoidal func-

tion of time. The fault is assumed to be vertical and the ground surface horizontal. The system can be either semi-infinite in thickness or bounded by some impermeable boundary at certain depth. The combination of the upper boundary and lower boundary conditions leads to four case studies. In each case, the same model has been used, i.e., in the vertical section we have two-dimensional air flow in the rock mass and one-dimensional air flow in the fault zone. The interaction between the fault zone and the rock mass is considered by including a flux term in the governing equation of the fault zone. By means of integral transforms, analytical solutions have been obtained for all four cases. The significance of these analytical solutions lies not only in that they can be used to determine the permeability of the fault zone in some cases but also they can be used to verify numerical codes for other cases. Examples of the application of these solutions have been worked out to demonstrate their usefulness.

In the second part, a well developed numerical code, TRUMP, is used to solve multi-layer problems with more realistic boundary conditions. This program was first verified against the analytical solutions for single layer problems and then used to check the important assumption of one-dimensional vertical flow model in the fault zone. TRUMP was then used to solve a multi-layer problem somewhat similar to the case at the Yucca Mountain site. Two fault-rock systems, i.e., the Solitario Canyon Fault and the Ghost Dance Fault have been analyzed. Simplified vertical cross-sections based on geologic maps for the Yucca Mountain area were used. The hydrologic properties for the three different hydrogeologic units were obtained directly from previous studies. The atmospheric pressure variation was selected from records of real data. By assigning possible values to the width of the fault zone as well as the pneumatic conductivity of the fault zone, the air pressure distribution in the whole system

was computed for different times. The results are very encouraging in that at the same elevation, a detectable pressure difference would be measured within a small distance from the fault zone.

The results obtained in this study make it possible to characterize a leaky fault either by measuring drawdowns in the confined aquifer during a pumping test, or by measuring air pressure variations in the unsaturated rocks during some time period when atmospheric pressure is changing significantly.

4.2 Recommendations

There are two basic ways to determine the hydrologic properties of a fault zone. If it is possible to conduct a water pumping test, this is recommended as the first priority. The methods provided in this study for analyzing flow in a confined aquifer are simpler than that of air pressure measurement. Apart from this, the unsaturated regions may be too moist, so that solutions for the air flow may not be applicable. The solutions for air flow in an unsaturated rock-fault system are most applicable in arid regions, where the moisture content is so small that its movement is insignificant and the permeability to air will not be affected. The method developed in this study needs measurements of air pressure only for short periods of about 12 hours. Where a water pumping test is rather difficult, as in an arid region, then the method using air pressure measurement is recommended. With the latter method, the trial and error technique must be applied to obtain the best result. Therefore, the two tools have different advantages and different applicabilities.

In all of these solutions, the fault zone is always assumed to be homogeneous, which may not be true in practice. It is quite possible that the fault zone will also be

divided into layers with different properties. However, this will make the problem much more complicated. It can probably be handled using numerical methods. To do this, one may need to determine the properties of the fault zone layer by layer. Nevertheless, the methods presented in this study can still provide the mean (or 'equivalent') permeability of the fault zone, which may be very useful in engineering problems.

The present study is concentrated only on flow problems, hopefully, it can be extended to transport problems in the future.

REFERENCES

Abramowitz, M., and I. A. Stegun: *Handbook of mathematical functions*, U. S. Govt. Off., Washington, 1964.

Birkeland, P. W., and E. E. Larson: *Putnam's geology*, 3rd. ed., Oxford Univ., New York, 1978.

Bixel, H. C., B. K. Larkin, and H. K. Van Poollen: Effect of linear discontinuities on pressure build-up and drawdown behavior, *J. Petro. Technol.*, 885-895, August, 1963.

Buckingham, Edgar: Contributions to our knowledge of the aeration of soils, *U. S. Dept. Agriculture Soils Bur. Bull.*, (25), 1904.

Carslaw, H. S., and J. C. Jaeger: *Conduction of heat in solids*, Oxford, London, 1959.

Churchill, R. V.: Temperature distribution in a slab of two layers, *Duke Math. J.*, (2), 405-414, 1936.

Churchill, R. V.: *Operational mathematics*, 2nd. ed. McGraw-Hill, New York, 1958.

Collins, R. E.: *Flow of fluids through porous materials*, Reinhold, New York, 1961.

Davis, E. Grady Jr., and M. F. Jr. Hawkins: Linear fluid-barrier detection by well pressure measurements, *J. Petro. Technol.*, 1077-1079, October, 1963.

Dolan, J. P., C. A. Einarsen, and G. A. Hill: Special applications of drillstem test pressure data, *Trans., AIME*, 210, 318-324, 1957.

Edwards, A. L., *TRUMP: A computer program for transient and steady state temperature distributions in multi-dimensional system*, Rep. 14754, Rev. 3, Livermore, CA, Lawrence Livermore Nat. Lab., 1972.

Erdélyi, A.: *Tables of integral transforms*, McGraw-Hill Book Company, Inc., New York, 1954.

Ferris, J. G., D. B. Knowles, R. H. Browne, and R. W. Stallman: Theory of aquifer tests, *U.S. Geol. Surv. Water-Supply Paper*, 1536-E, 1962.

Freeze, R. A., and J. A. Cherry: *Groundwater*, Prentice-Hall, Inc., Englewood Cliffs, N.J.07632, 1979.

Gradshteyn, I. S., and I. M. Ryzhik: *Table of integrals, series, and products*, Academic Press, New York and London, 1965.

Hantush, M. S.: Hydraulics of wells, *Adv. Hydrosci.*, (1), 281-432, 1964.

Hantush, M. S.: Analysis of data from pumping tests in leaky aquifers, *Trans. Amer. Geophys. Union*, 37, 702-714, 1956.

Horner, D. R.: Pressure buildup in wells, *Proc., Third World Pet. Cong.*, The Hague, Sec. II, 503, 1951.

Huang, S. C., and Y. P. Chang: Heat conduction in unsteady, periodic, and steady states in laminated composites, *Transactions of the ASME*, Vol. 102, 742-748, 1980.

Jaeger, J. C., and N. G. W. Cook: *Fundamentals of rock mechanics*, 3rd. ed., Chapman and Hall, New York, 1979.

Jaeger, J. C.: Conduction of heat in composite slabs, *Trans. Appl. Math.*, (8), 187-198, 1950.

Javandel, I., C. F. Tsang, and P. A. Witherspoon: Hydrologic detection of abandoned wells near proposed injection wells for hazardous waste disposal, *Water Resour.*

Res., 24(2), 261-270, 1988.

Javandel, I., and P. A. Witherspoon: A semianalytical solution for partial penetration in two-layer aquifers, *Water Resour. Res.*, 16(6), 1099-1106, 1980.

Klinkenberg, L. J.: The permeability of porous media to liquids and gases, *Am. Petroleum Inst. Drilling and Production Practice*, 1941.

Montazer, P., E. P. Weeks, Falah Thamir, Dale Hammermeister, S. N. Yard, and Peter B. Hofrichter: Monitoring the vadose zone in fractured tuff, *GWMR*, 72-88, Spring 1988.

Morris, G. A., and D. F. Snoeberger: Calculations of pressure change at depth in a nuclear chimney following atmospheric pressure change, *Lawrence Livermore Lab. Report*, UCID-15963, 1971.

Muskat, Morris: *Flow through porous media*, McGraw-Hill, New York, 1946.

Neuman, S. P., and P. A. Witherspoon: Theory of flow in a confined two-aquifer system, *Water Resour. Res.*, (5), 803-816, 1969a.

Neuman, S. P., and P. A. Witherspoon: Applicability of current theories of flow in leaky aquifers, *Water Resour. Res.*, (5), 817-829, 1969b.

Overpeck, A. C., and W. R. Holden: Well imaging and fault detection in anisotropic reservoirs, *J. Petro. Technol.*, 1317-1325, October, 1970.

Prasad, Raj K.: Pressure transient analysis in the presence of two intersecting boundaries, *J. Petro. Technol.*, 89-96, January, 1975.

Pagurova, V. I.: *Tables of the exponential integral*, U.S.S.R. Academy of Sciences Computing Centre, Pergamon Press, New York · Oxford · London · Paris, 1961.

Rosza, R. B., D. F. Snoeberger, and J. Baker: Permeability of a nuclear chimney and surface alluvium, Area 2, ERDANTS, *Lawrence Livermore Lab. Report*, UCID-16722, 11p, 1975.

Scott, R. B., and J. Bonk: Preliminary geologic map of Yucca Mountain with geologic sections, Nye County, Nevada, *U.S. Geological Survey, Open-File Report*, 84-494, Scale 1:12000, 1981.

Snoeberger, D. F., C. J. Morris, and J. Baker: Chimney permeability by atmospheric pressure change-instruments and data handling, *Lawrence Livermore Lab. Report*, UCID-16154, 14p, 1972.

Stallman, R. W.: Flow in the zone of areation, *Advances in Hydroscience*, (4), 151-195, 1967.

Stallman, R. W., and E. P. Weeks: The use of atmospherically induced gas-pressure fluctuations for computing hydraulic conductivity of the unsaturated zone (abs.), *Geol. Soc. America Abs. with Programs*, 1969.

Stewart, G., A. Gupta, and P. Westaway: The interpretation of interference tests in a reservoir with sealing and partially communicating faults, paper SPE 12967 presented at the *1984 SPE European Petroleum Conference, London*, October 1984.

Theis, C. V.: The relation between the lowering of the piezometric surface and the rate and duration of discharge of a well using groundwater storage, *Trans. Amer. Geophys. Union*, (2), 519-524, 1935.

Tiab, D., and Anil Kumar: Application of p'_D function to interference analysis, *J. Pet. Tech.*, 1465-1470, August, 1980.

U.S. Environmental Protection Agency: Report to congress on injection of hazardous waste, *EPA 570/9-85-003*, Office of Drinking Water, Washington D.C., 1985.

Weeks, E. P.: Field determination of vertical permeability to air in the unsaturated zone, *USGS professional paper*, No. 1051, 1978.

Witherspoon, P. A., I. Javandel, S. P. Neuman and R. A. Freeze: *Interpretation of aquifer gas storage conditions from water pumping tests*, American Gas Association, New York, 1967.

Wylie, C. R., and L. C. Barrett: *Advanced engineering mathematics*, 5th. ed. McGraw-Hill, New York, 1982.

Yaxley, L. M.: Effect of a partially communicating fault on transient pressure behavior, *SPE Formation Evaluation*, 590-598, December, 1987.

APPENDIX A

VALIDATION OF THE ASSUMPTION

There is a major assumption in Chapter 2, i.e., the recharge rate from the fault to the aquifer is proportional to the head difference between the two ends of the vertical fault. By adopting this assumption, we have obtained the analytical solution for drawdowns in the aquifer without solving the differential equation for the fault zone.

Although this assumption is generally acceptable in practice, it is better to validate the solution. Apparently, the best way to do this is to get certain exact solution (even if it is only for some special case), and then compare the solution obtained in Chapter 2 with the exact solution.

In the case of a constant head at the other end of the fault, the governing equations for two parts of the aquifer are given by (2-1) and (2-2):

$$\frac{\partial s_{a_1}}{\partial t} = \alpha_a \left[\frac{\partial^2 s_{a_1}}{\partial x^2} + \frac{\partial^2 s_{a_1}}{\partial y^2} \right] + \frac{\alpha_a Q}{T_a} \cdot \delta(x-a) \cdot \delta(y) \qquad (x \geq 0) \qquad (2\text{-}1)$$

$$\frac{\partial s_{a_2}}{\partial t} = \alpha_a \left[\frac{\partial^2 s_{a_2}}{\partial x^2} + \frac{\partial^2 s_{a_2}}{\partial y^2} \right] \qquad (x \leq 0) \qquad (2\text{-}2)$$

To obtain an exact solution, we need to consider the governing equation for the fault zone as well:

$$\frac{\partial s_f}{\partial t} = \alpha_f \left[\frac{\partial^2 s_f}{\partial z^2} + \frac{\partial^2 s_f}{\partial y^2} \right] \qquad (0 \leq z \leq L) \qquad (A\text{-}1)$$

In deriving the exact solution, the drawdown in the fault (s_f) is an unknown function of y, z and t, which is to be determined. Therefore, the initial condition including s_f becomes:

$$s_{a_1} = s_{a_2} = s_f = 0 \quad at \quad t = 0 \tag{A-2}$$

and the boundary conditions are:

$$s_{a_1} = 0 \quad at \quad x \to +\infty \quad or \quad y \to \pm\infty \tag{2-5}$$

$$s_{a_2} = 0 \quad at \quad x \to -\infty \quad or \quad y \to \pm\infty \tag{2-6}$$

$$s_f = 0 \quad at \quad z = L \quad or \quad y \to \pm\infty \tag{A-3}$$

$$s_{a_1}|_{x=0} = s_{a_2}|_{x=0} = s_f|_{z=0} \tag{A-4}$$

$$T_a \left[\frac{\partial s_{a_1}}{\partial x}\right]_{x=0} = T_a \left[\frac{\partial s_{a_2}}{\partial x}\right]_{x=0} - T_f \left[\frac{\partial s_f}{\partial z}\right]_{z=0} \tag{A-5}$$

Through the same transform process as that given by (2-10) through (2-13), the governing equations in the transformed domain are:

$$\frac{d^2 w_{a_1}}{dx^2} - A^2 w_{a_1} = -\frac{Q \cdot \delta(x-a)}{pT_a} \qquad (x \geq 0) \tag{2-14}$$

$$\frac{d^2 w_{a_2}}{dx^2} - A^2 w_{a_2} = 0 \qquad (x \leq 0) \tag{2-15}$$

$$\frac{d^2 w_f}{dz^2} - A_f{}^2 w_f = 0 \qquad (0 \leq z \leq L) \tag{A-6}$$

where $A_f = \sqrt{\rho^2 + p/\alpha_f}$ is similar to the definition for A, (2-16).

The unused boundary conditions are:

$$w_{a_1} = 0 \quad at \quad x \to +\infty \tag{2-17}$$

$$w_{a_2} = 0 \quad at \quad x \to -\infty \tag{2-18}$$

$$w_f = 0 \quad at \quad z = L \tag{A-7}$$

$$w_{a_1}|_{x=0} = w_{a_2}|_{x=0} = w_f|_{z=0} \tag{A-8}$$

$$T_a \left[\frac{dw_{a_1}}{dx}\right]_{x=0} = T_a \left[\frac{dw_{a_2}}{dx}\right]_{x=0} - T_f \left[\frac{ds_f}{dz}\right]_{z=0} \tag{A-9}$$

Applying the method of the variation of parameters and determining all integral constants, the solutions satisfying the governing equations and the boundary conditions are as follows.

$$w_{a_1} = w_{a_1}^{(1)} + w_{a_1}^{(2)}$$

$$= \frac{Q}{2T_a}\frac{e^{-|x-a|A}}{pA} + C_1 \cdot e^{-Ax} \qquad (x \geq 0) \tag{A-10}$$

$$w_{a_2} = C_2 \cdot e^{Ax} \qquad (x \leq 0) \tag{A-11}$$

$$w_f = C_3 \cdot e^{A_f z} + C_4 \cdot e^{-A_f z} \qquad (0 \leq z \leq L) \tag{A-12}$$

The four integral constants are determined by using the boundary conditions.

$$C_1 = T_f A_f (1 + e^{2A_f L}) \cdot D \tag{A-13}$$

$$C_2 = 2T_a A (1 - e^{2A_f L}) \cdot D \tag{A-14}$$

$$C_3 = 2T_a A \cdot D \tag{A-15}$$

$$C_4 = -2T_a A e^{2A_f L} \cdot D \tag{A-16}$$

where D is a common factor which is equal to:

$$D = \frac{[Q/(2T_a pA)]e^{-aA}}{2T_a A (1 - e^{2A_f L}) - T_f A_f (1 + e^{2A_f L})} \tag{A-17}$$

The inversion of $w_{a_1}^{(1)}$ has been given in (2-36), while it is probably too difficult to get the inversions for the other terms. However, the purpose of this appendix is to evaluate the reliability of the solution obtained in Chapter 2. This implies that an exact solution for any special case will be good enough for verification. Recall that the solution obtained in Chapter 2 is based on the assumption of a large fault-diffusivity, it is important to know how good the solutions will be if the fault-diffusivity is small, for example, equal to the diffusivity of the aquifer.

Under this condition, it is obvious that $\alpha_f = \alpha_a = \alpha$ and $A_f = A$. Solutions in the transformed domain can be simplified to:

$$w_{a_1}^{(2)} = C_1 \cdot e^{-xA} \tag{A-18}$$

$$w_{a_2} = C_2 \cdot e^{xA} \tag{A-19}$$

$$w_f = C_3 \cdot e^{zA} + C_4 \cdot e^{-zA} \tag{A-20}$$

where the four constants can be written as:

$$C_1 = -\left[\frac{QT_f}{2T_a(2T_a+T_f)}\right]\frac{e^{-aA}}{pA}\cdot\frac{e^{2LA}+1}{e^{2LA}-\xi}$$

$$= -\left[\frac{QT_f}{2T_a(2T_a+T_f)}\right]\frac{e^{-aA}}{pA}\cdot\left[1+\frac{(\xi+1)e^{-2LA}}{1-\xi e^{-2LA}}\right] \tag{A-21}$$

$$C_2 = \left[\frac{Q}{2T_a+T_f}\right]\frac{e^{-aA}}{pA}\cdot\frac{e^{2LA}-1}{e^{2LA}-\xi}$$

$$= \left[\frac{Q}{2T_a+T_f}\right]\frac{e^{-aA}}{pA}\cdot\left[1+\frac{(\xi-1)e^{-2LA}}{1-\xi e^{-2LA}}\right] \tag{A-22}$$

$$C_3 = -\left[\frac{Q}{2T_a+T_f}\right]\frac{e^{-aA}}{pA}\cdot\frac{e^{-2LA}}{1-\xi e^{-2LA}} \tag{A-23}$$

$$C_4 = \left[\frac{Q}{2T_a+T_f}\right]\frac{e^{-aA}}{pA}\cdot\frac{1}{1-\xi e^{-2LA}} \tag{A-24}$$

where ξ is defined as:

$$\xi = \frac{2T_a - T_f}{2T_a + T_f} \tag{A-25}$$

Obviously, $|\xi| \le 1$ and $0 < e^{-2LA} < 1$, which implies that the following series expansion is always convergent.

$$\frac{1}{1-\xi e^{-2LA}} = \sum_{n=0}^{\infty}\xi^n\cdot e^{-2nLA} \tag{A-26}$$

If this expansion is substituted into the above solutions, the inversions can be easily written down by means of (2-32), i.e.

$$s_{a_1} = \frac{Q}{4\pi T_a}\left\{W\left[\frac{(x-a)^2+y^2}{4\alpha_a t}\right] - \xi_1\cdot W\left[\frac{(x+a)^2+y^2}{4\alpha_a t}\right] - \xi_2\cdot\sum_{n=1}^{\infty}\xi^{n-1}W\left[\frac{(x+a+2nL)^2+y^2}{4\alpha_a t}\right]\right\} \tag{A-27}$$

$$s_{a_2} = \frac{Q}{4\pi T_a}\left\{\xi_3\cdot W\left[\frac{(-x+a)^2+y^2}{4\alpha_a t}\right] - \xi_2\cdot\sum_{n=1}^{\infty}\xi^{n-1}W\left[\frac{(-x+a+2nL)^2+y^2}{4\alpha_a t}\right]\right\} \tag{A-28}$$

$$s_f = \frac{Q}{4\pi T_a}\xi_3\cdot\sum_{n=0}^{\infty}\xi^n\left\{W\left[\frac{(z+a+2nL)^2+y^2}{4\alpha_a t}\right] - W\left[\frac{[-z+a+2(n+1)L]^2+y^2}{4\alpha_a t}\right]\right\} \tag{A-29}$$

where the three new constants have the following definitions:

$$\xi_1 = \frac{T_f}{2T_a+T_f} \tag{A-30}$$

$$\xi_2 = \frac{4T_a T_f}{(2T_a + T_f)^2} \tag{A-31}$$

$$\xi_3 = \frac{2T_a}{2T_a + T_f} \tag{A-32}$$

With the exact solution, the verification of the solution obtained in Chapter 2 can easily be given. In Figure A.1 the dots represent drawdown components, s_F, computed from (2-45) while the solid lines represent the same components computed from (A-27). Although the previous solution is based on the assumption of a large fault-diffusivity, comparison shows that it is also valid even if the diffusivity of the fault is equal to that of the aquifer, as long as the relative transmissivity of the fault is not too small (e.g. $c_D = 0.001$).

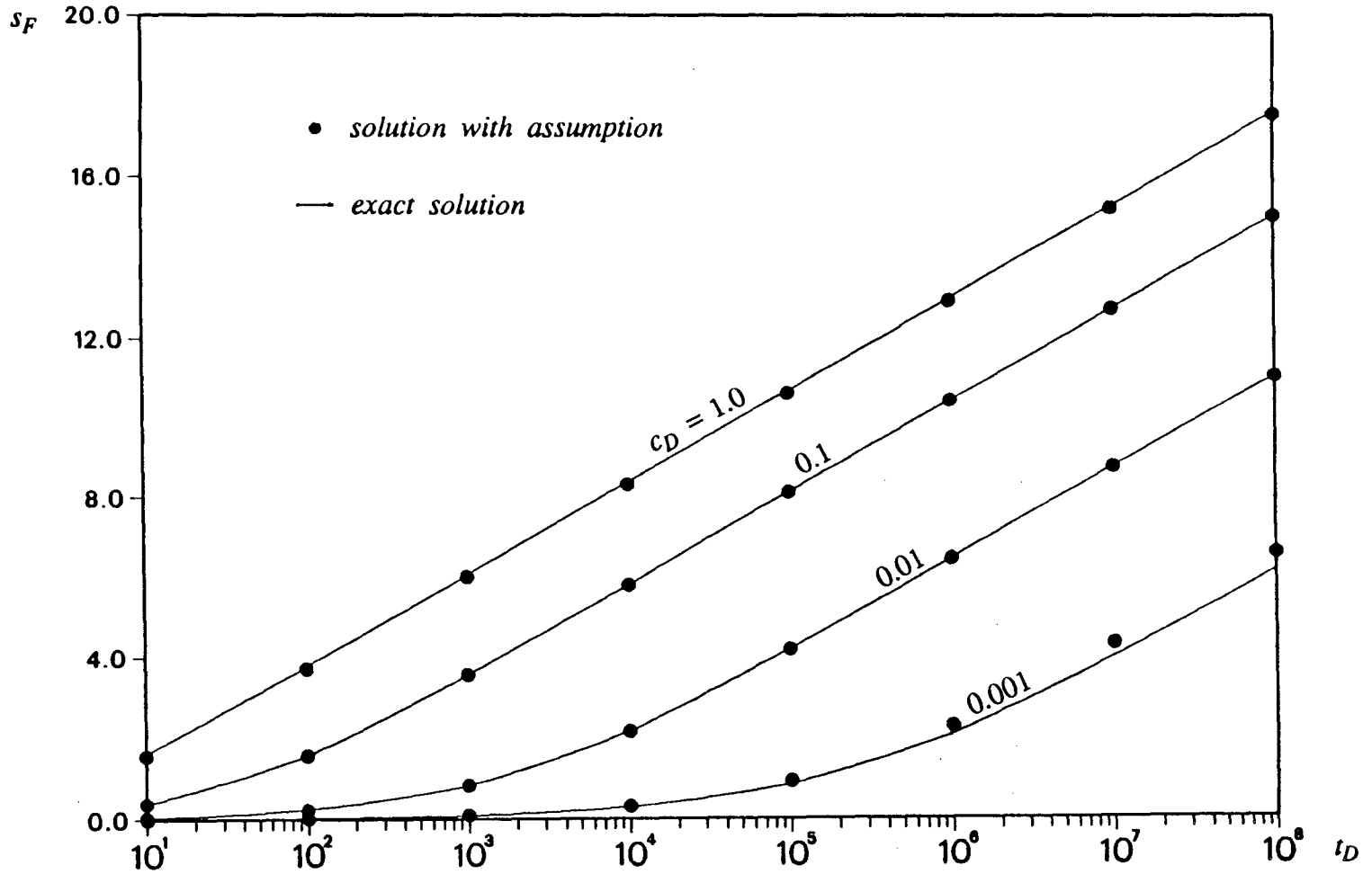

Figure A.1 Evaluation on the validity of the assumption of one-dimensional flow in the fault zone for four values of c_D.

APPENDIX B

SOLUTION DERIVATION

Equations (2-14) and (2-15) are two ordinary differential equations of the second order. While (2-15) is homogeneous, (2-14) is nonhomogeneous. The only difference between them is that (2-14) has a non-zero term on the right-hand side of the equation. The homogeneous equation has two particular integrals, i.e., e^{Ax} and e^{-Ax}. Therefore, the general solution for (2-15) is:

$$w_{a_2} = C_1 e^{Ax} + C_2 e^{-Ax} \tag{B-1}$$

To satisfy the boundary condition of (2-18), we must have $C_2 = 0$. The solution for w_{a_2} is reduced to:

$$w_{a_2} = C_1 e^{Ax} \tag{B-2}$$

where C_1 is an integral constant to be determined.

The solution for Equation (2-14) can be obtained by applying the method of variation of parameters. This method is described as follows (Wylie and Barrett, 1982, pp 82-83):

The solution for a general second-order ordinary differential equation,

$$a_0(x)y'' + a_1(x)y' + a_2(x)y = f(x) \tag{B-3}$$

can be expressed by:

$$y = u_1 y_1 + u_2 y_2 \tag{B-4}$$

where y_1 and y_2 represent the two particular integrals of the corresponding homogeneous equation of (B-3); u_1 and u_2 are functions of x, which have the following derivatives:

$$u'_1 = -\frac{y_2}{y_1 y'_2 - y_2 y'_1} \cdot \frac{f(x)}{a_0(x)} \tag{B-5}$$

$$u'_2 = \frac{y_1}{y_1 y'_2 - y_2 y'_1} \cdot \frac{f(x)}{a_0(x)} \tag{B-6}$$

For Equation (2-14), we have: $a_0(x) = 1$ and $f(x) = -\frac{Q}{pT_a} \cdot \delta(x-a)$. The two particular integrals are:

$$y_1 = e^{Ax} \qquad y_2 = e^{-Ax} \tag{B-7}$$

Substituting all these into (B-5) and (B-6) can lead to:

$$u'_1 = -\frac{Q}{2pAT_a} e^{-Ax} \delta(x-a) \tag{B-8}$$

$$u'_2 = \frac{Q}{2pAT_a} e^{Ax} \delta(x-a) \tag{B-9}$$

One of the theorems in calculus tells that an indefinite integral can be written as the sum of a corresponding definite integral and an arbitrary constant, i.e.,

$$\int f(x)dx = \int_0^x f(t)dt + C \tag{B-10}$$

Therefore, we can get:

$$u_1 = -\frac{Q}{2pAT_a} \int_0^x e^{-At} \delta(t-a)dt + C_3 \tag{B-11}$$

$$u_2 = \frac{Q}{2pAT_a} \int_0^x e^{At} \delta(t-a)dt + C_4 \tag{B-12}$$

where C_3 and C_4 are two integral constants to be determined, and t is a dummy variable in the range between 0 and x.

The property of the Dirac δ function gives:

$$\int_0^x f(t)\delta(t-a)dt = f(a) \cdot u(x-a) \tag{B-13}$$

where $u(x-a)$ is the unit step function which equals to 0 for $x < a$ and 1 for $x \geq a$.

Applying (B-13) to (B-11) and (B-12), we can get:

$$u_1 = -\frac{Q}{2pAT_a}e^{-Aa}\cdot u(x-a) + C_3 \tag{B-14}$$

$$u_2 = \frac{Q}{2pAT_a}e^{Aa}\cdot u(x-a) + C_4 \tag{B-15}$$

For our problem, y in (B-4) should be replaced by w_{a_1}. Applying the results in (B-7), (B-14) and (B-15) to (B-4) gives:

$$w_{a_1} = [-\frac{Q}{2pAT_a}e^{-Aa}\cdot u(x-a)+_3]e^{Ax}+[\frac{Q}{2pAT_a}e^{Aa}\cdot u(x-a)+C_4]e^{-Ax} \tag{B-16}$$

The boundary condition (2-17) requires that w_{a_1} be zero at x equal to infinity, which means that we must have:

$$C_3 = \frac{Q}{2pAT_a}e^{-Aa} \tag{B-17}$$

The other two boundary conditions, (2-19) and (2-20) equate the drawdown and flux at $x=0$, respectively. At $x=0$, the unit step function is always zero. Therefore, (B-16) can be simplified to:

$$w_{a_1} = C_3e^{Ax} + C_4e^{-Ax} \tag{B-18}$$

If (B-2) and (B-18) are substituted into (2-19) and (2-20), we can get the following two equations:

$$C_3 + C_4 = C_1 \tag{B-19}$$

$$T_aA(C_3 - C_4) = T_aAC_1 + \frac{T_f}{L}(C_3 + C_4) \tag{B-20}$$

Solving the two equations simultaneously and expressing C_4 and C_1 in C_3 as that given in (B-17), we can get:

$$C_4 = \frac{-c}{A + c}C_3 \tag{B-21}$$

$$C_1 = \frac{A}{A + c} C_3 \tag{B-22}$$

where c is a modified transmissivity ratio defined by:

$$c = T_f / (2T_a L) \tag{B-23}$$

Substituting (B-22) together with (B-17) into (B-2) leads to:

$$w_{a_2} = \frac{Q}{2T_a} \cdot \frac{e^{-(a-x)A}}{p(A + c)} \tag{B-24}$$

Substituting (B-17) and (B-21) into (B-16), we can obtain:

$$w_{a_1} = \frac{Q}{2T_a pA} \left[e^{-(a-x)A} - \frac{c e^{-(x+a)A}}{(A + c)} \right] \qquad \text{for } x < a \tag{B-25}$$

$$w_{a_1} = \frac{Q}{2T_a pA} \left[e^{-(x-a)A} - \frac{c e^{-(x+a)A}}{(A + c)} \right] \qquad \text{for } x \geq a \tag{B-26}$$

Finally, the expression for w_{a_1} can be written in the following unified form:

$$w_{a_1} = \frac{Q}{2T_a} \left[\frac{e^{-|x-a|A}}{pA} - \frac{c e^{-(x+a)A}}{pA(A + c)} \right] \tag{B-27}$$

APPENDIX C

APPROXIMATION FOR (2-55)

Although it is difficult to integrate (2-55) precisely, it is easy to evaluate that approximately for the purposes of application. It can be shown that, if the independent variable, x is some large value, the complementary error function, $erfc(x)$ has the following series expansion which converges very rapidly (Carslaw and Jaeger, 1959).

$$erfc(x) = \frac{1}{\sqrt{\pi}} e^{-x^2} \sum_{m=0}^{\infty} (-1)^m \cdot x^{-(2m+1)} \cdot \frac{1 \cdot 3 \cdots (2m-1)}{2^m} \tag{C-1}$$

For this problem, because both $\frac{\bar{d}}{\sqrt{\tau}}$ and $c_D \sqrt{\tau}$ have positive values at $t > 0$, it is easy to prove that,

$$\frac{\bar{d}}{\sqrt{\tau}} + c_D \sqrt{\tau} \geq 2\sqrt{c_D \cdot \bar{d}} > 1.0 \qquad \text{for} \qquad X > 0.25 \tag{C-2}$$

where

$$X = c_D \cdot \bar{d} \tag{C-3}$$

It is better to point out that to guarantee the convergence of the expansion (C-1) in the region of $0 \leq \tau \leq t_D$, a condition of $X > 0.25$ should be kept in mind and must be checked at the end of calculation. When $X \gg 0.25$, it is possible to obtain a good approximation by taking only the first term in the expansion.

Under these conditions, if the expansion formula (C-1) is applied to solution (2-55), the result will be:

$$s_{F_1} = \sum_{m=0}^{\infty} s_{F_1}^{(m)} \tag{C-4}$$

where the arbitrary term in (C-4) can be written as:

$$s_{F_1}^{(m)} = (-1)^m \cdot \frac{1\cdot 3\cdots(2m-1)}{2^m} \cdot c_D \int_0^{t_D} \frac{e^{-\bar{d}^2/\tau}}{\sqrt{\tau}(\bar{d}/\sqrt{\tau} + c_D\sqrt{\tau})^{2m+1}} d\tau \qquad \text{(C-5)}$$

Introducing a new variable z and a new parameter u defined as:

$$z = \bar{d}^2/\tau \qquad \& \qquad u = \bar{d}^2/t_D \qquad \text{(C-6)}$$

the above expression can finally be simplified to:

$$s_{F_1}^{(m)} = (-1)^m \cdot \frac{1\cdot 3\cdots(2m-1)}{2^m} \cdot X \int_u^{\infty} \frac{z^{m-1}\cdot e^{-z}}{(z+X)^{2m+1}} dz \qquad \text{(C-7)}$$

Although it may be possible to derive a general expression a step further from (C-7), a practical problem probably requires only the first few terms to achieve a good approximation. From this point of view, one may work on (C-7) term by term. The following gives the results for $m = 0$, $m = 1$ and $m = 2$. There are no difficulties in obtaining the other terms.

(1) $m = 0$

Substituting $m = 0$ into (C-7) and noting that $(-1)^m \cdot 1\cdot 3\cdots(2m-1)/2^m = 1$, one can obtain a simple integral and work out a better expression step by step as follows.

$$\begin{aligned} s_{F_1}^{(0)} &= \int_u^{\infty} \frac{e^{-z}}{z(z/X+1)} dz \\ &= \int_u^{\infty} e^{-z} dz \left[\frac{1}{z} - \frac{1}{z+X}\right] \\ &= \int_u^{\infty} \frac{e^{-z}}{z} dz - e^X \cdot \int_u^{\infty} \frac{e^{-(z+X)}}{(z+X)} d(z+X) \\ &= W(u) - e^X \cdot W(u+X) \end{aligned} \qquad \text{(C-8)}$$

With a table of exponential integrals, (C-8) can be calculated by hand. However, the behavior of the component s_{F_1} is of most interest at large time. As $t \to \infty$, $u = \bar{d}^2/t_D \to 0$ and the approximation for $s_{F_1}^{(0)}$ is:

$$s_{F_1}^{(0)} \approx -0.5772 - ln\left(\frac{\overline{d}^2}{t_D}\right) - e^X \cdot W(X)$$

$$\approx 2.3 \log\left[\frac{0.562\, t_D}{\overline{d}^2} \cdot e^{-e^X \cdot W(X)}\right] \qquad \text{(C-9)}$$

(2) $m = 1$

Very straightforwardly, (C-7) gives:

$$s_{F_1}^{(1)} = -\frac{X}{2}\int_u^\infty \frac{e^{-z}}{(z+X)^3}dz \qquad \text{(C-10)}$$

There is a suitable formula in the integral tables (Gradshteyn and Ryzhik, 1965):

$$\int_u^\infty \frac{e^{-z}}{(z+X)^n}dz = e^{-u}\sum_{k=1}^{n-1}\frac{(k-1)!(-1)^{n-1-k}}{(n-1)!(u+X)^k} + \frac{(-1)^{n+1}}{(n-1)!}e^X \cdot W(u+X)$$

$$[\, n \geq 2 \quad \& \quad |arg(u+X)| < \pi \,] \qquad \text{(C-11)}$$

Here, $n = 3$. Therefore, (C-10) can be further integrated into:

$$s_{F_1}^{(1)} = \frac{X}{4}\{\, e^{-u}\,[(u+X)^{-1} - (u+X)^{-2}] - e^X \cdot W(u+X)\,\} \qquad \text{(C-12)}$$

Again, because $u \to 0$ as $t \to \infty$, (C-12) at large time becomes:

$$s_{F_1}^{(1)} \approx \frac{1}{4} - \frac{1}{4X} - \frac{X}{4} \cdot e^X W(X) \qquad \text{(C-13)}$$

(3) $m = 2$

Substituting this m value into (C-7) gives:

$$s_{F_1}^{(2)} = \frac{3X}{4}\int_u^\infty \frac{z \cdot e^{-z}}{(z+X)^5}dz$$

$$= \frac{3X}{4}\int_u^\infty e^{-z}\left[\frac{1}{(z+X)^4} - \frac{X}{(z+X)^5}\right]dz \qquad \text{(C-14)}$$

Applying (C-11) and letting $t \to \infty$ will finally lead to:

$$s_{F_1}^{(2)} \approx \frac{X}{32} + \frac{3}{32} - \frac{1}{16X} + \frac{1}{16X^2} - \left(\frac{X}{8} + \frac{X^2}{32}\right)e^X W(X) \qquad \text{(C-15)}$$

APPENDIX D

DETERMINATION OF COMPONENTS

(1) Determination of $s^{(1)}$

This can be obtained by means of (2-32):

$$s^{(1)} = F^{-1}\left\{L^{-1}\left\{\frac{e^{-|x-a|A}}{pA}\right\}\right\} = \frac{1}{2\pi}\cdot W\left[\frac{(x-a)^2+y^2}{4\alpha_a t}\right] \tag{D-1}$$

(2) Determination of $s^{(2)}$

It is necessary to point out that from this part on, the inversion formulae (2-26) through (2-29) will be used frequently. In addition, the following four inversion formulae are also required:

$$L^{-1}\{\frac{1}{\sqrt{p}}\} = \frac{1}{\sqrt{\pi t}} \tag{D-2}$$

$$L^{-1}\{\frac{e^{-k\sqrt{p}}}{p}\} = erfc(\frac{k}{2\sqrt{t}}) \tag{D-3}$$

$$L^{-1}\{\frac{e^{-k\sqrt{p}}}{p\sqrt{p}}\} = 2\sqrt{\frac{t}{\pi}}\cdot e^{-k^2/(4t)} - k\cdot erfc(\frac{k}{2\sqrt{t}}) \tag{D-4}$$

$$F_c\{e^{-k\rho^2}\} = \frac{1}{2}\sqrt{\frac{\pi}{k}}\cdot e^{-y^2/(4k)} \tag{D-5}$$

Noting that,

$$L^{-1}\left\{\frac{e^{-(x+a)A}}{A^2}\right\} = \alpha_a L^{-1}\left\{\frac{e^{-[(x+a)/\sqrt{\alpha_a}]\sqrt{p+\alpha_a\rho^2}}}{p+\alpha_a\rho^2}\right\}$$

$$= \alpha_a e^{-\alpha_a\rho^2 t}\cdot erfc\left[\frac{x+a}{2\sqrt{\alpha_a t}}\right] \tag{D-6}$$

By formula (2-28), it is easy to see:

$$L^{-1}\left\{\frac{e^{-(x+a)A}}{pA^2}\right\} = \alpha_a\int_0^t e^{-\alpha_a\tau\rho^2}\cdot erfc\left[\frac{x+a}{2\sqrt{\alpha_a\tau}}\right]d\tau \tag{D-7}$$

Because $(x+a)$ for $x>0$ and $a-x$ for $x<0$ can be written in a unified form of $(|x|+a)$, one can get:

$$s^{(2)} = F^{-1}\left\{L^{-1}\left\{\frac{e^{-(|x|+a)A}}{pA^2}\right\}\right\}$$
$$= \frac{\alpha_a}{\pi}\int_0^t F_c\left\{e^{-\alpha_a\tau\rho^2}\right\}\cdot erfc\left[\frac{|x|+a}{2\sqrt{\alpha_a\tau}}\right]d\tau$$
$$= \frac{\sqrt{\alpha_a}}{2\sqrt{\pi}}\int_0^t \frac{e^{-y^2/(4\alpha_a\tau)}}{\sqrt{\tau}}\cdot erfc\left[\frac{|x|+a}{2\sqrt{\alpha_a\tau}}\right]d\tau \qquad \text{(D-8)}$$

(3) Determination of $s^{(3)}$

Similarly, the inverse Laplace transform is carried out:

$$L^{-1}\left\{\frac{e^{-(x+a)A}}{A^2A_u}\right\} = \alpha_a\sqrt{\alpha_u}L^{-1}\left\{\frac{e^{-[(x+a)/\sqrt{\alpha_a}]\sqrt{p+\alpha_a\rho^2}}}{(p+\alpha_a\rho^2)\sqrt{p+\alpha_u\rho^2}}\right\}$$
$$= \alpha_a\sqrt{\alpha_u}e^{-\alpha_a\rho^2t}\cdot L^{-1}\left\{\frac{e^{-[(x+a)/\sqrt{\alpha_a}]\sqrt{p}}}{p\sqrt{p+(\alpha_u-\alpha_a)\rho^2}}\right\}$$
$$= \alpha_a\sqrt{\alpha_u}e^{-\alpha_a\rho^2t}\cdot\int_0^t \frac{e^{-(\alpha_u-\alpha_a)\rho^2\tau}}{\sqrt{\pi\tau}}erfc\left[\frac{x+a}{2\sqrt{\alpha_a(t-\tau)}}\right]d\tau \qquad \text{(D-9)}$$

In the last step of above derivations, two basic inversion formulae, (D-2) and (D-3), have been used, and the theory of convolution has been applied. If (2-28) and (2-26) are further applied one by another, it is easy to get the final solution in a double integral form:

$$s^{(3)} = F^{-1}\left\{L^{-1}\left\{\frac{e^{-(|x|+a)A}}{pA^2A_u}\right\}\right\}$$
$$= \frac{\alpha_a\sqrt{\alpha_u}}{2\pi}\int_0^t d\tau\int_0^\tau \frac{e^{-y^2/4[\alpha_u u+\alpha_a(\tau-u)]}}{\sqrt{u[\alpha_u u+\alpha_a(\tau-u)]}}\cdot erfc\left[\frac{|x|+a}{2\sqrt{\alpha_a(\tau-u)}}\right]du \qquad \text{(D-10)}$$

(4) Determination of $s^{(4)}$

Applying (2-27) and (D-4), one can obtain:

$$L^{-1}\left\{\frac{e^{-(x+a)A}}{A^3}\right\} = \alpha_a\sqrt{\alpha_a}e^{-\alpha_a\rho^2 t}\cdot L^{-1}\left\{\frac{e^{-[(x+a)/\sqrt{\alpha_a}]\sqrt{p}}}{p\sqrt{p}}\right\}$$

$$= \alpha_a\sqrt{\alpha_a}e^{-\alpha_a\rho^2 t}\left[2\sqrt{\frac{t}{\pi}}e^{-(x+a)^2/(4\alpha_a t)} - \frac{x+a}{\sqrt{\alpha_a}}erfc\left(\frac{x+a}{2\sqrt{\alpha_a t}}\right)\right] \qquad \text{(D-11)}$$

Further application of (2-28) and (2-26) leads to:

$$F^{-1}\left\{L^{-1}\left\{\frac{e^{-(x+a)A}}{pA^3}\right\}\right\} = \frac{\alpha_a\sqrt{\alpha_a}}{\pi}\int_0^t F_c\{e^{-\alpha_a\tau\rho^2}\}\left[2\sqrt{\frac{\tau}{\pi}}e^{-(x+a)^2/(4\alpha_a\tau)} - \frac{x+a}{\sqrt{\alpha_a}}erfc\left(\frac{x+a}{2\sqrt{\alpha_a\tau}}\right)\right]d\tau$$

$$= \frac{\alpha_a}{\pi}\int_0^t e^{-\frac{(x+a)^2+y^2}{4\alpha_a\tau}}d\tau - \frac{\sqrt{\alpha_a}(x+a)}{2\sqrt{\pi}}\int_0^t\frac{e^{-y^2/(4\alpha_a\tau)}}{\sqrt{\tau}}erfc\left(\frac{x+a}{2\sqrt{\alpha_a\tau}}\right)d\tau \qquad \text{(D-12)}$$

The first term in the solution can be integrated by parts and the solution becomes:

$$s^{(4)} = \frac{\alpha_a t}{\pi}e^{-\frac{(x+a)^2+y^2}{4\alpha_a t}} - \frac{(x+a)^2+y^2}{4\pi}W\left[\frac{(x+a)^2+y^2}{4\alpha_a t}\right]$$

$$-\frac{\sqrt{\alpha_a}(x+a)}{2\sqrt{\pi}}\int_0^t\frac{e^{-y^2/(4\alpha_a\tau)}}{\sqrt{\tau}}erfc\left(\frac{x+a}{2\sqrt{\alpha_a\tau}}\right)d\tau \qquad \text{(D-13)}$$

(5) Determination of $s^{(5)}$

By applying inversion formula (2-29) and the theory of convolution, we can obtain:

$$L^{-1}\left\{\frac{e^{-(a-x)A}}{AA_u^2}\right\} = \alpha_u\sqrt{\alpha_a}e^{-\alpha_a\rho^2 t}\cdot L^{-1}\left\{\frac{e^{-[(a-x)/\sqrt{\alpha_a}]\sqrt{p}}}{\sqrt{p}\,[p+(\alpha_u-\alpha_a)\rho^2]}\right\}$$

$$= \alpha_u\sqrt{\alpha_a}e^{-\alpha_a\rho^2 t}\int_0^t e^{-(\alpha_u-\alpha_a)\rho^2\tau}\frac{e^{-\frac{(a-x)^2}{4\alpha_a(t-\tau)}}}{\sqrt{\pi(t-\tau)}}d\tau \qquad \text{(D-14)}$$

Very similar to the derivation for $s^{(3)}$, the final expression for $s^{(5)}$ is:

$$s^{(5)} = F^{-1}\left\{L^{-1}\left\{\frac{e^{-(a-x)A}}{pAA_u^{\,2}}\right\}\right\}$$
$$= \frac{\alpha_u\sqrt{\alpha_a}}{2\pi}\int_0^t d\tau\int_0^\tau \frac{e^{-y^2/4[\alpha_u u+\alpha_a(\tau-u)]-(a-x)^2/[4\alpha_a(\tau-u)]}}{\sqrt{(\tau-u)[\alpha_u u+\alpha_a(\tau-u)]}}du \qquad \text{(D-15)}$$

(6) Determination of $s^{(6)}$

The following derivation is based on inversion formula (2-29) and the theory of convolution:

$$L^{-1}\left\{\frac{e^{-aA+xA_u}}{AA_u}\right\} = \frac{\sqrt{\alpha_a\cdot\alpha_u}}{\pi}\int_0^t e^{-\alpha_a\rho^2\tau-\alpha_u\rho^2(t-\tau)}\frac{e^{-\frac{a^2}{4\alpha_a\tau}-\frac{x^2}{4\alpha_u(t-\tau)}}}{\sqrt{\tau(t-\tau)}}d\tau \qquad \text{(D-16)}$$

The inversion theorem (2-28) leads to:

$$L^{-1}\left\{\frac{e^{-aA+xA_u}}{pAA_u}\right\} = \frac{\sqrt{\alpha_a\alpha_u}}{\pi}\int_0^t d\tau\int_0^\tau e^{-[\alpha_a u+\alpha_u(\tau-u)]\rho^2}\frac{e^{-\frac{a^2}{4\alpha_a u}-\frac{x^2}{4\alpha_u(\tau-u)}}}{\sqrt{u(\tau-u)}}du \qquad \text{(D-17)}$$

Therefore, the solution of $s^{(6)}$ can be obtained by applying the conversion formula (2-26) and the inversion formula (D-5):

$$s^{(6)} = F^{-1}\left\{L^{-1}\left\{\frac{e^{-aA+xA_u}}{pAA_u}\right\}\right\}$$
$$= \frac{\sqrt{\alpha_a\alpha_u}}{2\pi\sqrt{\pi}}\int_0^t d\tau\int_0^\tau \frac{e^{-\frac{a^2}{4\alpha_a u}-\frac{x^2}{4\alpha_u(\tau-u)}-\frac{y^2}{4[\alpha_a u+\alpha_u(\tau-u)]}}}{\sqrt{u(\tau-u)[\alpha_a u+\alpha_u(\tau-u)]}}du \qquad \text{(D-18)}$$

(7) Determination of $s^{(7)}$

It is easy to get:

$$L^{-1}\left\{\frac{e^{-aA}}{A^2}\right\} = \alpha_a e^{-\alpha_a\rho^2 t}erfc\left(\frac{a}{2\sqrt{\alpha_a t}}\right) \qquad \text{(D-19)}$$

Similarly, the Laplace inversion can be processed as follows.

$$L^{-1}\left\{\frac{e^{-aA+xA_u}}{A^2A_u}\right\} = \frac{\alpha_a\sqrt{\alpha_u}}{\sqrt{\pi}}\int_0^t e^{-\alpha_u\rho^2\tau-\alpha_a\rho^2(t-\tau)}\frac{e^{-\frac{x^2}{4\alpha_u\tau}}}{\sqrt{\tau}}erfc\left[\frac{a}{2\sqrt{\alpha_a(t-\tau)}}\right]d\tau \qquad \text{(D-20)}$$

$$L^{-1}\left\{\frac{e^{-aA+xA_u}}{pA^2A_u}\right\}=\frac{\alpha_a\sqrt{\alpha_u}}{\sqrt{\pi}}\int_0^t dT\int_0^T e^{-[\alpha_u\tau+\alpha_a(T-\tau)]\rho^2}\frac{e^{-\frac{x^2}{4\alpha_u\tau}}}{\sqrt{\tau}}erfc\left[\frac{a}{2\sqrt{\alpha_a(T-\tau)}}\right]d\tau \tag{D-21}$$

Very similar to the previous derivations, one can get:

$$\begin{aligned}s^{(7)}&=F^{-1}\left\{L^{-1}\left\{\frac{e^{-aA+xA_u}}{pA^2A_u}\right\}\right\}\\&=\frac{\alpha_a\sqrt{\alpha_u}}{2\pi}\int_0^t d\tau\int_0^\tau\frac{e^{-\frac{x^2}{4\alpha_u u}-\frac{y^2}{4[\alpha_u u+\alpha_a(\tau-u)]}}}{\sqrt{u[\alpha_u u+\alpha_a(\tau-u)]}}erfc\left[\frac{a}{2\sqrt{\alpha_a(\tau-u)}}\right]du\end{aligned} \tag{D-22}$$

(8) Determination of $s^{(8)}$

By exchanging the positions of $-a$ and x as well as α_a and α_u, the solution for $s^{(8)}$ can be copied from that for $s^{(7)}$:

$$\begin{aligned}s^{(8)}&=F^{-1}\left\{L^{-1}\left\{\frac{e^{-aA+xA_u}}{pAA_u^2}\right\}\right\}\\&=\frac{\alpha_u\sqrt{\alpha_a}}{2\pi}\int_0^t d\tau\int_0^\tau\frac{e^{-\frac{a^2}{4\alpha_a u}-\frac{y^2}{4[\alpha_a u+\alpha_u(\tau-u)]}}}{\sqrt{u[\alpha_a u+\alpha_u(\tau-u)]}}erfc\left[\frac{|x|}{2\sqrt{\alpha_u(\tau-u)}}\right]du\end{aligned} \tag{D-23}$$

APPENDIX E

PROCESS OF INVERSION

Upon substitution of (2-113) into (2-85), the solution for Region II is reduced to (2-22) with its inversion given by (2-37). This simple form is, of course, caused by approximation.

For (2-84), the inversion of the first term is the Theis solution. The substitution of (2-113) can change the second term in (2-84) to a product of two factors, $\frac{ce^{-(x+a)A}}{pA(A+c)}$ and $\frac{A_u}{A_u+c/T_D}$. By applying (2-27), it is easy to get:

$$L^{-1}\left\{\frac{e^{-(x+a)A}}{A(A+c)}\right\} = \alpha_a e^{-\alpha_a \rho^2 t} \cdot L^{-1}\left\{\frac{e^{-\frac{x+a}{\sqrt{\alpha_a}}\sqrt{p}}}{\sqrt{p}\,(\sqrt{p}+c\sqrt{\alpha_a})}\right\}$$

$$= \alpha_a e^{-\alpha_a \rho^2 t} \cdot e^{c(x+a)+c^2\alpha_a t}\, erfc\left(\frac{x+a}{2\sqrt{\alpha_a t}} + c\sqrt{\alpha_a t}\right) \qquad \text{(E-1)}$$

By applying (2-28), we can write:

$$L^{-1}\left\{\frac{c\cdot e^{-(x+a)A}}{p\cdot A(A+c)}\right\} = c\,\alpha_a e^{c(x+a)} \int_0^t e^{-\alpha_a \rho^2 \tau} \cdot e^{c^2\alpha_a \tau}\, erfc\left(\frac{x+a}{2\sqrt{\alpha_a \tau}} + c\sqrt{\alpha_a \tau}\right) d\tau \qquad \text{(E-2)}$$

The Laplace inversion for the other factor is:

$$L^{-1}\left\{\frac{A_u}{A_u + c/T_D}\right\} = e^{-\alpha_u \rho^2 t} \cdot L^{-1}\left\{\frac{\sqrt{p}}{\sqrt{p}+b}\right\}$$

$$= e^{-\alpha_u \rho^2 t} \cdot L^{-1}\left\{1 - \frac{b}{\sqrt{p}+b}\right\}$$

$$= e^{-\alpha_u \rho^2 t}\left\{\delta(t) - b\left[\frac{1}{\sqrt{\pi t}} - be^{b^2 t}\, erfc(b\sqrt{t})\right]\right\} \qquad \text{(E-3)}$$

where the parameter, b is defined by:

$$b = \frac{c\sqrt{\alpha_u}}{T_D} \tag{E-4}$$

By using the theorem of convolution, the inversion of the product is:

$$L^{-1}\left\{\frac{ce^{-(x+a)A}}{pA(A+c)}\cdot\frac{A_u}{A_u+c/T_D}\right\} = c\alpha_a e^{c(x+a)}\int_0^t e^{-\alpha_u\rho^2 u}\left\{\delta(u) - b[\frac{1}{\sqrt{\pi u}} - be^{b^2u}erfc(b\sqrt{u})]\right\}du$$
$$\int_0^{t-u} e^{-\alpha_a\rho^2\tau}\cdot e^{c^2\alpha_a\tau}erfc(\frac{x+a}{2\sqrt{\alpha_a\tau}} + c\sqrt{\alpha_a\tau})d\tau \tag{E-5}$$

For the Dirac δ function, there is the formula:

$$\int_0^t f(u)\delta(u)du = f(0) \tag{E-6}$$

If this is applied to (E-5), the result is reduced to:

$$L^{-1}\left\{\frac{ce^{-(x+a)A}}{pA(A+c)}\cdot\frac{A_u}{A_u+c/T_D}\right\} = c\alpha_a e^{c(x+a)}\{\int_0^t e^{-\alpha_a\rho^2\tau}\cdot e^{c^2\alpha_a\tau}erfc(\frac{x+a}{2\sqrt{\alpha_a\tau}} + c\sqrt{\alpha_a\tau})d\tau$$
$$- b\int_0^t[\frac{1}{\sqrt{\pi u}} - be^{b^2u}erfc(b\sqrt{u})]du$$
$$\int_0^{t-u} e^{-(\alpha_a\tau+\alpha_u u)\rho^2}\cdot e^{c^2\alpha_a\tau}erfc(\frac{x+a}{2\sqrt{\alpha_a\tau}} + c\sqrt{\alpha_a\tau})d\tau\ \} \tag{E-7}$$

Finally, by using (2-26) and (2-31), we can get:

$$F^{-1}\left\{L^{-1}\left\{\frac{ce^{-(x+a)A}}{pA(A+c)}\cdot\frac{A_u}{A_u+c/T_D}\right\}\right\} =$$
$$\frac{c\sqrt{\alpha_a}e^{c(x+a)}}{2\sqrt{\pi}}\int_0^t\frac{e^{c^2\alpha_a\tau - y^2/(4\alpha_a\tau)}}{\sqrt{\tau}}erfc(\frac{x+a}{2\sqrt{\alpha_a\tau}} + c\sqrt{\alpha_a\tau})d\tau$$
$$- \frac{bc\alpha_a e^{c(x+a)}}{2\sqrt{\pi}}\int_0^t[\frac{1}{\sqrt{\pi u}} - be^{b^2u}erfc(b\sqrt{u})]du$$
$$\int_0^{t-u}\frac{e^{c^2\alpha_a\tau - y^2/(4\alpha_a\tau+4\alpha_u u)}}{\sqrt{\alpha_a\tau+\alpha_u u}}erfc(\frac{x+a}{2\sqrt{\alpha_a\tau}} + c\sqrt{\alpha_a\tau})d\tau \tag{E-8}$$

With the second term inverted, the solution for s_{a_1} is then completely determined.

The inversion of w_u can be performed in the same way. Upon substitution of (2-113) into (2-86), the expression for w_u becomes:

$$w_u \approx \frac{Qc}{2T_u} \cdot \frac{e^{-aA}}{p(A+c)} \cdot \frac{e^{xA_u}}{A_u + c/T_D} \tag{E-9}$$

Noting that for w_u, x is always negative or zero, therefore, the last factor in above equation is in fact similar to the second factor except the absence of p in the denominator. In the derivation process of (2-34), it has been shown that:

$$L^{-1}\left\{\frac{e^{-aA}}{A+c}\right\} = \sqrt{\alpha_a}\, e^{-\alpha_a \rho^2 t}\left[\frac{e^{-a^2/4\alpha_a t}}{\sqrt{\pi t}} - c\sqrt{\alpha_a}\, e^{ca+c^2\alpha_a t}\, erfc\left(\frac{a}{2\sqrt{\alpha_a t}} + c\sqrt{\alpha_a t}\right)\right] \tag{E-10}$$

By applying (2-28) and the theorem of convolution, the Laplace inversion of the product is:

$$L^{-1}\left\{\frac{e^{-aA}}{p(A+c)} \cdot \frac{e^{xA_u}}{A_u + c/T_D}\right\} = \sqrt{\alpha_a \alpha_u} \cdot$$

$$\int_0^t e^{-\alpha_u \rho^2 u}\left[\frac{e^{-x^2/(4\alpha_u u)}}{\sqrt{\pi u}} - \frac{c\sqrt{\alpha_u}}{T_D} e^{-\frac{cx}{T_D} + \frac{c^2\alpha_u}{T_D^2}u}\, erfc\left(\frac{-x}{2\sqrt{\alpha_u u}} + \frac{c}{T_D}\sqrt{\alpha_u u}\right)\right] du$$

$$\int_0^{t-u} e^{-\alpha_a \rho^2 \tau}\left[\frac{e^{-a^2/(4\alpha_a \tau)}}{\sqrt{\pi\tau}} - c\sqrt{\alpha_a}\, e^{ca+c^2\alpha_a \tau} erfc\left(\frac{a}{2\sqrt{\alpha_a \tau}} + c\sqrt{\alpha_a \tau}\right)\right] d\tau \tag{E-11}$$

Finally, by using the Fourier inversion formulae (2-26) and (2-31), the drawdown in the unpumped aquifer is:

$$s_u \approx \frac{Qc\sqrt{\alpha_a \alpha_u}}{4\sqrt{\pi} T_u} \cdot \int_0^t \left[\frac{e^{-x^2/(4\alpha_u u)}}{\sqrt{\pi u}} - \frac{c\sqrt{\alpha_u}}{T_D} e^{-\frac{cx}{T_D} + \frac{c^2\alpha_u}{T_D^2}u}\, erfc\left(\frac{-x}{2\sqrt{\alpha_u u}} + \frac{c}{T_D}\sqrt{\alpha_u u}\right)\right] du$$

$$\int_0^{t-u} \frac{e^{-y^2/(4\alpha_a \tau + 4\alpha_u u)}}{\sqrt{\alpha_a \tau + \alpha_u u}}\left[\frac{e^{-a^2/(4\alpha_a \tau)}}{\sqrt{\pi\tau}} - c\sqrt{\alpha_a}\, e^{ca+c^2\alpha_a \tau} erfc\left(\frac{a}{2\sqrt{\alpha_a \tau}} + c\sqrt{\alpha_a \tau}\right)\right] d\tau \tag{E-12}$$

APPENDIX F

CALCULATION OF INTEGRALS

In Chapter 3, there is an integral to be calculated in the region of a real integrand as well as in the region of a complex integrand. This integral appears in (3-50) and can be divided into two parts:

$$\int_0^{\infty}(f_1+f_2)\sin(\rho z)d\rho = \int_0^{\rho_0}(f_1+f_2)\sin(\rho z)d\rho + \int_{\rho_0}^{\infty}(f_1+f_2)\sin(\rho z)d\rho \qquad \text{(F-1)}$$

where the point of separation, ρ_0 can be calculated by (3-51).

For the first part of integral ($\rho < \rho_0$), it is always true that $\Delta > 0$ so that (3-37) can be used for the expressions of B_1 and B_2. As a result, the integrand is a real function and the integral can be computed by numerical integration without any problem.

On the contrary, for the second part of the integral ($\rho > \rho_0$), the integrand will be a complex function due to applying of (3-38). It is shown in the following how the integration of a complex function can be converted to integrations of real functions.

As $\rho > \rho_0$, the substitution of (3-38) into (3-43) and (3-44) leads to:

$$f_1+f_2 = \frac{2\rho}{i}\left[\frac{e^{z_1}erfc(z_2)}{z_3} - \frac{e^{\bar{z}_1}erfc(\bar{z}_2)}{\bar{z}_3}\right] \qquad \text{(F-2)}$$

where $\bar{z}$ and z is a pair of conjugates. In other words, if

$$z = a + ib = re^{i\theta} \qquad \text{(F-3)}$$

then

$$\bar{z} = a - ib = re^{-i\theta} \qquad \text{(F-4)}$$

The expressions for a_i and b_i ($i = 1, 2, 3$) in this particular problem are given as follows:

$$a_1 = \frac{K(x+Kt)}{2\alpha} - t\rho^2 \tag{F-5}$$

$$a_2 = \frac{(x+Kt)}{2\sqrt{\alpha t}} \tag{F-6}$$

$$a_3 = \frac{K}{\sqrt{\alpha}}\sqrt{-\Delta} \tag{F-7}$$

$$b_1 = \frac{(x+Kt)}{2\sqrt{\alpha}}\sqrt{-\Delta} \tag{F-8}$$

$$b_2 = \frac{\sqrt{t}}{2}\sqrt{-\Delta} \tag{F-9}$$

$$b_3 = -\Delta \tag{F-10}$$

To evaluate (F-2), it is better to write:

$$\begin{aligned} e^{z_1} &= e^{a_1+ib_1} \\ &= e^{a_1}(\cos b_1 + i\sin b_1) \\ &= e^{a_1}(A_1 + iB_1) \end{aligned} \tag{F-11}$$

Similarly, one can get:

$$e^{\overline{z_1}} = e^{a_1}(A_1 - iB_1) \tag{F-12}$$

where the newly introduced A_1 and B_1 are equal to:

$$A_1 = \cos b_1 \qquad \& \qquad B_1 = \sin b_1 \tag{F-13}$$

Recall that the error function has the following expansion formula (Abramowitz and Stegun, 1964):

$$erf(z) = \frac{2}{\sqrt{\pi}} \sum_{n=0}^{\infty} \frac{(-1)^n z^{2n+1}}{n!(2n+1)} \tag{F-14}$$

If this expansion formula is applied to $erf(z_2)$, one can obtain:

$$\begin{aligned} erf(z_2) &= \frac{2}{\sqrt{\pi}} \sum_{n=0}^{\infty} \frac{(-1)^n r_2^{2n+1} e^{i(2n+1)\theta_2}}{n!(2n+1)} \\ &= A_2 + iB_2 \end{aligned} \tag{F-15}$$

and similarly:

$$erf(\overline{z_2}) = A_2 - iB_2 \tag{F-16}$$

where A_2 and B_2 are defined as:

$$A_2 = \frac{2}{\sqrt{\pi}} \sum_{n=0}^{\infty} \frac{(-1)^n r_2^{2n+1} \cos[(2n+1)\theta_2]}{n!(2n+1)} \tag{F-17}$$

$$B_2 = \frac{2}{\sqrt{\pi}} \sum_{n=0}^{\infty} \frac{(-1)^n r_2^{2n+1} \sin[(2n+1)\theta_2]}{n!(2n+1)} \tag{F-18}$$

Substituting all expressions into (F-2), we can obtain:

$$\begin{aligned} f_1 + f_2 &= \frac{2\rho e^{a_1}}{i} \left[\frac{(A_1+iB_1)(1-A_2-iB_2)}{a_3+ib_3} - \frac{(A_1-iB_1)(1-A_2+iB_2)}{a_3-ib_3} \right] \\ &= 4\rho e^{a_1} \cdot \frac{(A_2-1)(b_3A_1-a_3B_1) - B_2(a_3A_1+b_3B_1)}{a_3^2 + b_3^2} \end{aligned} \tag{F-19}$$

which is completely a real value.

For purposes of numerical computation, it is necessary to find better expression formulae for A_2 and B_2. Actually, these two terms are the real and imaginary part of $erf(z_2)$, respectively. By definition, one can write:

$$erf(z_2) = \frac{2}{\sqrt{\pi}} \int_0^{z_2} e^{-z^2} dz \tag{F-20}$$

The integrand, $f(z) = e^{-z^2}$, is an analytical function on the complex plane. Therefore, the following integration formula can be applied (Wylie and Barrett, 1982):

$$\int_c f(z)dz = \int_c (u \cdot dx - v \cdot dy) + i \int_c (v \cdot dx + u \cdot dy) \tag{F-21}$$

The integration path, c, can be any arbitrary curve connecting the two limit points; u and v represent the real and imaginary part of $f(z)$, respectively. For this problem, the integrand can also be written as:

$$f(z) = e^{-x^2+y^2} \cdot [\cos(2xy) - i \sin(2xy)] \tag{F-22}$$

which implies that:

$$u = e^{-x^2+y^2}\cdot\cos(2xy) \tag{F-23}$$

$$v = -e^{-x^2+y^2}\cdot\sin(2xy) \tag{F-24}$$

By mathematical theorem, the integration of (F-21) is independent of the integration path. Therefore, we can choose one for convenience. The integral in (F-20) starts from 0 [represented by a point, $O(0,0)$] and ends at z_2 [represented by a point, $Z(a_2,b_2)$]. Another point of $M(a_2,0)$ is employed here, and the integration path is chosen to be $O \rightarrow M \rightarrow Z$. This choice is convenient in that:

On path $O-M$, $y \equiv 0$, $dy \equiv 0$ and x varies from 0 to a_2.

$$u = e^{-x^2} \qquad \& \qquad v = 0 \tag{F-25}$$

On path $M-Z$, $x \equiv a_2$, $dx \equiv 0$ and y varies from 0 to b_2.

$$u = e^{y^2-a_2^2}\cdot\cos(2a_2y) \tag{F-26}$$

$$v = -e^{y^2-a_2^2}\cdot\sin(2a_2y) \tag{F-27}$$

Applying formula (F-21) to (F-20) and substituting all above results, it is easy to get:

$$erf(z_2) = \frac{2}{\sqrt{\pi}}\left[\int_0^{a_2} e^{-x^2}dx + \int_0^{b_2} e^{y^2-a_2^2}\cdot\sin(2a_2y)dy + i\int_0^{b_2} e^{y^2-a_2^2}\cdot\cos(2a_2y)dy\right] \tag{F-28}$$

Through this way, another pair of formulae is obtained for A_2 and B_2 in forms which are much easier for calculation.

$$A_2 = erf(a_2)\frac{2}{\sqrt{\pi}} + \int_0^{b_2} e^{y^2-a_2^2}\cdot\sin(2a_2y)dy \tag{F-29}$$

$$B_2 = \frac{2}{\sqrt{\pi}}\int_0^{b_2} e^{y^2-a_2^2}\cdot\cos(2a_2y)dy \tag{F-30}$$

If (F-29) and (F-30) are substituted into (F-19), we can finally get:

$$\int_{\rho_0}^{\infty}(f_1+f_2)\sin(\rho z)d\rho = I_1+I_2+I_3 \tag{F-31}$$

where

$$I_1 = -4\int_{\rho_0}^{\infty}\frac{b_3A_1-a_3B_1}{a_3^2+b_3^2}\rho\sin(\rho z)e^{a_1}erfc(a_2)d\rho \tag{F-32}$$

$$I_2 = \frac{8}{\sqrt{\pi}}\int_{\rho_0}^{\infty}\frac{b_3A_1-a_3B_1}{a_3^2+b_3^2}\rho\sin(\rho z)e^{a_1-a_2^2}d\rho\int_0^{b_2}e^{y^2}\sin(2a_2y)dy \tag{F-33}$$

$$I_3 = -\frac{8}{\sqrt{\pi}}\int_{\rho_0}^{\infty}\frac{a_3A_1+b_3B_1}{a_3^2+b_3^2}\rho\sin(\rho z)e^{a_1-a_2^2}d\rho\int_0^{b_2}e^{y^2}\cos(2a_2y)dy \tag{F-34}$$

Although these expressions are awful, the integrations can be easily worked out by a computer.

LAWRENCE BERKELEY LABORATORY
UNIVERSITY OF CALIFORNIA
INFORMATION RESOURCES DEPARTMENT
BERKELEY, CALIFORNIA 94720